Studies of the Degradation Behaviour of γ-TiAl and Fe_3Al Intermetallics

Ali Abdulgader ALJARANY
BSc, MSc (Eng)

A thesis submitted in partial fulfilment of the requirements of the University of Northumbria at Newcastle

for the degree of

Doctor of Philosophy

October 2002

Dedication

To my parents, wife and children

Contents

List of Figures

List of Tables

AKNOWLEDGEMENTS

I wish to express my thanks and appreciation to Professor P.K. Datta and Dr. J.S Gray for their supervision and guidance throughout this investigation. The author is also grateful to Dr H. L. Du for his valuable advice provided during my study and in the preparation of this thesis.

The financial support of Biruni research centre – Libya, without which, this research would not have been successful. The continuous supply of the experimental materials from the ABB (Switzerland) and IRC (UK) are also acknowledged.

Thanks are also due to the technical staff and to my colleagues in the mechanical engineering departments, University of Northumbria and Newcastle University for their help in work characterisation.

This study was part of an on-going investigation performed in the Advanced Material Research Institute (AMRI) at the University of Northumbria at Newcastle (UK).

I hereby declare that:

- during the period I have been registered for the degree of PhD, for which this thesis is submitted, I have not been a registered candidate for any other award of the CNAA or of a university.

- that I have attended: selected lectures from the post-Graduate Diploma in offshore Materials and Corrosion Engineering Research Group, Northumbria University; annual symposia of the Institute of Corrosion Science and Technology; presented papers at selected conferences both international and in the UK within the field of high temperature corrosion; published two papers in a selected journals in the area of high temperature materials.; and have followed the course of guided reading laid down by my supervisors.

Ali Abdulgader ALJARANY

ABSTRACT

By Ali ALJARANY

The oxidation behaviour of Fe_3Al intermetallic alloys with and without reactive element (RE) and Ti-46.7Al-1.9W-0.5Si alloy over the temperature ranges of 900 to 1100°C and 750 to 950°C respectively were studied for up to 240h. The isothermal and cyclic oxidation behaviour of Fe_3Al intermetallic materials was studied in static air. The Al_2O_3 adherence of (Y and/or Hf)-doped Fe_3Al alloys was examined using newly developed – by the researcher – cyclic oxidation rig built in AMRI's laboratory. However the oxidation of Ti-46.7Al-1.9W-0.5Si alloy was studied in air and under Ar-O_2 atmospheres of three oxygen partial pressures; pO_2 = (0.05, 0.2 and 0.8) x 10^5 Pa. Isothermal sulphidation/oxidation work of coated – with specially designed single and multi-layer coatings – and uncoated Ti-46.7Al-1.9W-0.5Si alloy was performed in relatively high partial pressure of sulphur (pS_2 = 6.8 x 10^{-1} Pa) and low partial pressure of oxygen (pO_2 = 1.2 x 10^{-15} Pa) at 850° C for up to 240h. Characterisation of the specimens was conducted using SEM, EDX, and XRD techniques. Higher oxidation rates of Ti-46.7Al-1.9W-0.5Si alloy were observed in air than in Ar-20%O_2 at all temperatures. The scale formed in air consisted of $TiO_2/Al_2O_3/TiO_2/TiN/TiAl_2$/substrate, whilst the scale developed in Ar-20%O_2 atmosphere was comprised of $TiO_2/Al_2O_3/TiO_2/Al_2O_3/Ti_3Al$/substrate. The oxidation rates of Ti-46.7Al-1.9W-0.5Si alloy increased with decreasing the oxygen partial pressure in Ar-O_2 atmospheres at the entire range of temperatures. The employment of single AlTiN and CrN single layer coatings improved the sulphidation/oxidation behaviour of Ti-46.7Al-1.9W-0.5Si alloy at 850°C for up to 240h in $H_2/H_2O/H_2S$ gas mixture. However, the use of NbN and CrN diffusion barrier coatings significantly enhanced its corrosion resistance. The scale on uncoated Ti-46.7Al-.9W-0.5Si alloy in sulphidising/oxidising atmosphere consisted of $TiO_2/Al_2O_3/TiS+W/TiAl_3/TiAl_2$/substrate. The reactive element (RE) – Y and/or Hf – addition especially Y significantly improved the oxide adherence of Fe_3Al over the specified range of temperature and exposure time (or cycles). However, higher oxidation rate of Fe_3Al alloys doped with Y was obtained under both isothermal and cyclic oxidation. Although the scale thickness of Hf-doped alloy was always higher than that of Y-doped alloys, the oxidation rate constant of the later is found in some cases to be less than that of the first by one order of magnitude. However, the scale on the Hf-doped alloy is relatively adherent to the substrate if compared with the scale of undoped Fe_3Al alloy even at the areas where oxide pegs were observed on Fe_3Al-Hf alloy. Generally, no conclusion could be taken from the kinetic data of Fe_3Al alloys regarding the reactive element effect (REE) due to the intergranular attack on the Y-containing alloys. Improving the interface properties by RE addition led to a better control of the outward diffusion of aluminium and eliminated the detrimental effect of sulphur (possibly present in the Fe_3Al alloys). However, the presence of the RE in the alloy led to the formation of coherent scales. At 1100°C and after prolonged exposure, the scale of RE-doped alloys was not able to remain in contact with the substrate especially under thermal cycling conditions. The external scale severely cracked especially at places where oxide ridges were formed. The Y-containing Fe_3Al alloys were capable of producing another thin and adherent scale underneath the cracked external scale.

Principal supervisor: Professor Santu Datta
Director of Advanced Materials Research Institute
and
Research associate Dean for school of Engineering at the University of Northumbria at Newcastle

Second supervisor: Dr. J. S. Burnell-Gray
Deputy Director of Advanced Materials Research Institute

CHAPTER ONE

INTRODUCTION

CHAPTER ONE

1. INTRODUCTION

The performance of metals and alloys in high temperature (HT) corrosive environments is dependent upon their ability to promote the formation of adherent and coherent 'protective' scales such as Cr_2O_3 and Al_2O_3. These scales limit the degradation of the base metal or alloy to be employed at HT for long periods of time, thus improving efficiency (for example in power generation plants) and decreasing the maintenance costs [**1**]. At high temperatures where the oxygen activity is high, a protective, mechanically stable external oxide scale is produced on the exposed alloy surface, which normally reduces the subsequent corrosion to acceptable design levels [**2**]. However, under the influence of a second oxidant e.g. sulphur, severe corrosion may occur. In environments of low oxygen and high sulphur activities (sulphidation/oxidation), sulphides formed on certain alloys may offer a moderate measure of protection, in fact analogous to a protective oxide film, but in general, sulphide scales are much more friable and more subject to exfoliation than oxide scales on most HT alloys due to larger Pilling-Bedworth ratios (see **Section 2.4.1**). Furthermore, oxide scales formed on the alloys usually melt at relatively high temperatures, above the melting point of the alloys, whereas sulphides have comparatively low melting points and frequently form low melting point eutectics [**3**]. In addition, the diffusion coefficients of cations in sulphide scales are relatively high because of the greater degree of non-stoichiometry of sulphide structures [**3-5**]. The effects of nitrogen on the corrosion behaviour of HT materials have also been noticed by many researchers [**6-10**]. The nitride formation may prevent the formation of a continuous alumina scale and thus accelerates the weight gain of the alloy after exposure in air. The mechanism of nitride formation and the role of the nitride layer on the corrosion kinetics and scale properties are not quite yet clear.

The development of corrosion resistant alloys depends on the addition of an element, which will oxidise selectively so that it will produce a more protective surface oxide. If alloying elements are added in sufficient quantities, a continuous external oxide layer may be formed. Aluminium is the principal element in common HT alloys designed to provide adequate degrees of corrosion resistance to iron-nickel-cobalt and titanium-based alloys. Alloying elements, such as chromium and silicon, additionally conferring a degree of oxidation and sulphidation (except Cr in sulphur-containing environments) resistance. However, low oxygen activity, coupled with high sulphur activity (for example, pS_2 sufficient to permit the development of sulphides of iron, nickel and cobalt, but not Ti) may have very adverse effects on the corrosion resistance of the alloys since sulphide reaction products rather than oxides might be stable [**11**]. One approach for solving such problems is to subject the alloy to pre-oxidation or pre-sulphidation treatment to form compact, adherent and protective scales that would subsequently act as a barrier to the penetration of reacting species such as sulphur, oxygen or nitrogen from the surrounding environment [**12**]. In essence, such scales formed by pre-oxidation or pre-sulphidation are a type of conversion coating, to be contrasted with a conventional protective extraneous coating that involves the addition of other oxidation/sulphidation resistance materials on the surface. Such surface treatment approach is simple and convenient and probably less costly than extraneous coatings. However, it could be a viable alternative only if an adequate self-healing property of the alloys exists. If the preformed (oxide/sulphide) scale cracked or spalled, accelerated corrosion attack might occur in complex environments where the oxygen or sulphur activity was not sufficient to promote self-healing of the cracked scale. The second approach widely investigated is the use of HT protective coatings on the corrosion resistance alloys. The process of coating indicates that the top surface of the alloy is isolated from the environment by the coated layer(s). The deposited layer(s) is enriched with the desirable elements, which are expected to provide protection of the base alloy from the reacting species of the

surrounding environment at high temperatures. Additional improvement in the corrosion resistance of the chromia-forming and alumina-forming alloys or coating alloys is achieved by additions of rare earth/reactive elements. Reactive elements (REs) such as Y or Hf have been found to be effective in improving corrosion resistance for many HT alloys, however the mechanisms by which the improved performance occurs are not completely understood. It is known that these elements are quite effective when used in alumina-forming structural alloys and coatings in particular, it appears that REs may improve oxide scale adherence. Recent research has shown that noble metal additions may also produce other beneficial effects influencing the selective oxidation of aluminium. It is apparent, therefore, that new alloys or coatings with adequate resistance against environments containing oxygen and sulphur at high temperatures need to be carefully designed. In designing new coatings or alloys, both thermodynamic and kinetic factors (as summarised in **Chapter 2**) that control the formation, growth and stability of the "protective" scale on the alloy surface need to be considered. The environmental parameters – such as gas composition and temperature – influencing high temperatures corrosion properties of alloys must be also investigated.

Over the past 30 years, the bulk of the oxidation/sulphidation work has been given to Fe-Ni- and Co-base alloys without and with ternary element additions. Nowadays there is an increasing interest in understanding the corrosion behaviour of Fe- and Ti-aluminides at high temperatures since they have the potential to replace the higher density Ni-based super-alloys in many industrial applications. These materials possess low density and acceptable mechanical properties at high temperatures. Some progress has been made concerning the understanding of the scaling behaviour of these materials at high temperatures. Several corrosion aspects of these materials still need to be resolved.

Among various types of intermetallics, Fe-Al and Ti-Al alloys are considered as candidate structural and coating materials for industrial and aero-gas turbines respectively. However, these materials have low fracture toughness (K_{Ic}) and relatively poor HT

corrosion resistance. Recently γ-TiAl and Fe_3Al intermetallic alloys in particular are receiving significant attention. The low-density (3.8 g/cm^3) γ-TiAl intermetallics with high specific strength at elevated temperatures are being studied extensively with a view to application in e.g. engine valves, turbine blades, aircraft and automotive engines [**13-18**]. Of major concern of γ-TiAl alloys for structural applications is its low oxidation resistance at high temperatures. The poor high temperature oxidation resistance of Ti-Al intermetallic alloys is due to the fact that they do not form long-lasting protective alumina scales even if they contain a high aluminium concentration close to 50at%. After longer exposure times, the scales initially rich in alumina, deteriorate and scales with a high amount of titania predominate with similar high growth rates as pure titania. According to previous studies, a higher concentration of aluminium is needed to achieve a protective alumina scale. However, the increase of the aluminium concentration is technologically not desired because of loss of ductility by the formation of brittle $TiAl_3$. The high aluminium content of iron aluminides (such as in FeAl and Fe_3Al) allows the formation of relatively protective external alumina layer that improves sulphidation resistance of iron aluminides. Therefore, iron aluminides are particularly suitable in harsh, aggressive and corrosive environments up to 800°C as compared to FeCrAl and FeCrNi alloys. Aluminides based on FeAl exhibit better oxidation and corrosion resistance than Fe_3Al alloys. Both iron-base intermetallic compounds have lower density by as much as 30 to 40% if compared to steels and other commercial iron-based alloys [**19**]. Although FeAl and Fe_3Al intermetallics containing relatively high amount of aluminium, cracking and spallation of their scales under practical conditions at HT is a common problem due to poor adhesion between alumina scale and the iron aluminides. For example, it was reported that alumina scales grown on FeAl containing 40 at%Al spall extensively at 900-1100°C [**20**]. It is also known that addition (by doping or surface implantation) of small amounts of reactive elements (such as yttrium, hafnium, cerium and other rare earth metals) in such alloys can improve their scale spallation

resistance. Also it was found that REs affect other oxidation properties for this class of materials including reaction kinetics and scale morphology. In this context the beneficial role of small additions (~ 1 at%) of reactive elements, has received considerable attention. The RE effects have, in fact, been studied extensively for chromia-forming alloys. However, as maximum use of temperatures could increase to (~ 1200°C), chromia is no longer protective, due to its volatility. At higher temperatures, alumina gives better protection due to its relatively low volatility, slow growing kinetics and chemical inertness. Most of the experimental observations, reported in the literature show an improvement in the oxidation behaviour of RE-doped alloys. However, the exact mechanisms by which a RE addition changes the oxidation behaviour have not been conclusively identified and not fully understood. Various mechanisms have been proposed, but a general agreement is yet not to be reached. Despite all the efforts made, the understanding of HT corrosion processes of γ-TiAl and Fe_3Al intermetallics is still far from complete and requires a more thorough investigations.

There are several important aspects of the HT corrosion behaviour of Ti-aluminides and Fe-aluminides intermetallics that need further attention: the occurrence of multi-layered scales (TiO_2/Al_2O_3), the transition kinetics of γ-TiAl, the effect of nitrogen, the partial pressures of oxygen and sulphur on the scaling behaviour of γ-TiAl, also the mechanism of the internal attack of Fe_3Al and the phase transformation of the formed Al_2O_3 at high temperatures, as well as the mode of Al_2O_3 scale growth and scale breakdown of the Fe_3Al intermetallics – with and without reactive element – in both isothermal and cycling conditions. All of these aspects need to be critically examined and investigated in a wide range of temperatures and exposure time. Based on such background, the present research programme has been undertaken with two main objectives: (1) to provide new experimental HT corrosion data essential for alloy design purposes and (2) to provide new fundamental

information concerning the mode of degradation of (a) un-doped and Y and/or Hf doped Fe_3Al intermetallic materials and (b) uncoated Ti-46.7Al-1.9W-0.5Si alloy and coated with selected single and double layers of coatings.

The research programme focuses on the study of oxidation behaviour of Ti-46.7Al-1.9W-0.5Si alloy within the temperature range (750 - 950°C) and Fe_3Al at (900 - 1100°C). A parallel study has been conducted to examine the HT sulphidation/oxidation behaviour of selected single (CrN and AlTiN) and double (CrN/NbN, AlTiN/NbN and AlTiN/CrN) layers coatings on Ti-46.7Al-1.9W-0.5Si alloy at 850°C. Such studies are of particular importance in elucidating the mechanisms of oxidation and sulphidation of these materials before their practical use.

The oxidation study of Fe_3Al has been extended to assess the role of the RE (Y and/or Hf) in isothermal and cyclic conditions in air. Here the aim has been to assess whether the presence of these rare earth elements influences beneficially or adversely the oxidation behaviour of Fe_3Al in the specified range of temperatures and for long exposure time (up to 240h). The isothermal oxidation study of Ti-46.7Al-1.9W-0.5Si alloy (at 750 - 950°C) was intended to understand the effects of nitrogen and the partial pressure of oxygen on their oxidation behaviour. The isothermal sulphidation/oxidation studies at 850°C of the uncoated and coated Ti-46.7Al-1.9W-0.5Si alloy were attempts to understand the influences of coating on the corrosion behaviour of Ti-46.7Al-1.9W-0.5Si alloy in high pS_2 (~ 6.8×10^{-1} Pa) and low pO_2 (~ 1.2×10^{-15} Pa) atmosphere at 850°C.

The emphasis of this programme of work has been to adopt an integrated approach involving assessment of weight gain data, scaling kinetics and examination of scale formation and development processes. Such information has been needed to identify the mechanisms of the corrosion behaviour of the experimental materials.

This thesis has been structured in eight chapters. An overview of the relevant theoretical aspects of HT corrosion of metals and alloys is presented in **Chapter 2**. Emphasis is placed upon the thermodynamics and kinetics of oxidation and sulphidation of metals and alloys. This chapter also considers the effect of stresses generated within the scales and the basic principles and theories related to the subject. **Chapter 3** critically reviews the relevant literature on the subject of the oxidation/sulphidation behaviour of Fe- and Ti-aluminides. Also, previous work to improve the oxidation and sulphidation resistance of these classes of materials with an emphasis on the modified and non-modified Fe_3Al and γ-TiAl intermetallics are briefly reported. Previous attempts available in the open literature to explain the effects of environmental composition and the reactive element effects on the corrosion behaviour of Ti-Al and Fe-Al systems have been reviewed. An introduction to the present experimental work is outlined in **Chapter 4**. Detailed description of the experimental methodology of this work is given in **Chapter 5**. The oxidation and sulphidation results of the modified and non-modified Ti-46.7Al-1.9W-0.5Si alloy and Fe_3Al alloys are given in **Chapter 6**. General discussion, which outlines the HT oxidation/sulphidation of the experimental materials are included in **Chapter 7**. The behaviour of the un-modified and modified Fe_3Al and Ti-46.7Al-1.9W-0.5Si alloy is compared and highlighted. The high temperature corrosion mechanisms of the experimental materials in oxidising and sulphidising environments are also modelled. **Chapter 8** includes conclusions from the present work and future areas of research based on the outcomes derived from this thesis.

CHAPTER TWO

THEORITICAL ASPECTS OF HIGH TEMPERATURE CORROSION BEHAVIOUR OF METALS AND ALLOYS

CHAPTER TWO

2.0 THEORITICAL ASPECTS OF HIGH TEMPERATURE CORROSION BEHAVIOUR OF METALS AND ALLOYS

2.1 Introduction

High temperature (HT) oxidation involves very basic thermodynamics and kinetics. The aim of corrosion protection is not to prevent the reaction between metals and their working environment (in this chapter exclusively oxygen) but to use the reaction product to inhibit further corrosion. For better protection of the base metal or alloy, the corrosion product must be dense and stable, preferably slow-growing and adherent to the substrate.

This chapter summarises the basic concepts governing the thermodynamics and kinetics of HT corrosion processes of metals and alloys, also it includes important aspects related to defect structures and transport processes associated with scale formation and growth processes.

2.2 Thermodynamics and Kinetics of High Temperature Corrosion

Most metals are unstable at HT and react with environments to form corrosion products. Oxidation reaction begin at the metal/environment interface and, unless the reaction products are volatile, they will result in the formation of an intermediate layer which separates the metal from the environment. The possible forms of this layer are numerous and may alter as the reaction proceeds. Once a complete and compact film covers the metal surface, the reaction may continue only by diffusion of the reactants through the scale film hence, corrosion becomes dependent upon diffusion kinetics [**21**]. For engineering purposes, these characteristics are usually achieved by combining some base element (such as Fe, Ni, Co or Ti) with one or more elements (such as Cr, Al or Si) which form a protective scale.

The formation of a metal oxide may be represented as:

$$xM_{(s)} + \frac{y}{2}O_{2(g)} = M_xO_{y(s)} \quad \text{.....(1)}$$

The mechanisms by which the reactants may penetrate the oxide layer are seen to be an important part of the mechanism by which HT oxidation occurs. Similar principles apply to the formation and growth of sulphide and other similar reaction products.

2.2.1 Thermodynamics of High Temperature Corrosion

The oxidation of alloys involves the same general phenomena as for pure metals but is of course more complex since the components of an alloy has different affinities for oxygen. Owing to the complicated mechanisms involved, it is often difficult to predict the oxidation behaviour of alloys except for relatively simple systems. Thermodynamics allow the prediction of possible corrosion reactions. The overall driving force for metal reaction with the environmental species is the associated reduction in free energy of formation, although this may bear little or no relation to the rates of reaction, which are controlled by kinetic phenomena. **Figure 2-1** shows an Ellingham diagram of the free energies of formation of various oxides, because Al_2O_3 has a lower free energy of formation than FeO and TiO_2, it is thermodynamically more stable. Thus, in equilibrium, Al will oxidise preferentially to Fe or Ti. The change in Gibbs's free energy ΔG for a reaction is given in **equation 2** as:

$$\Delta G - \Delta G^\circ = RT \ln K \quad \text{.....(2)}$$

where, ΔG° is the standard free energy of formation associated with the reaction, R is the gas constant and T, is the reaction temperature in Kelvin. The standard free energy of formation is related to the equilibrium constant, K of the reaction. K is derived from the law

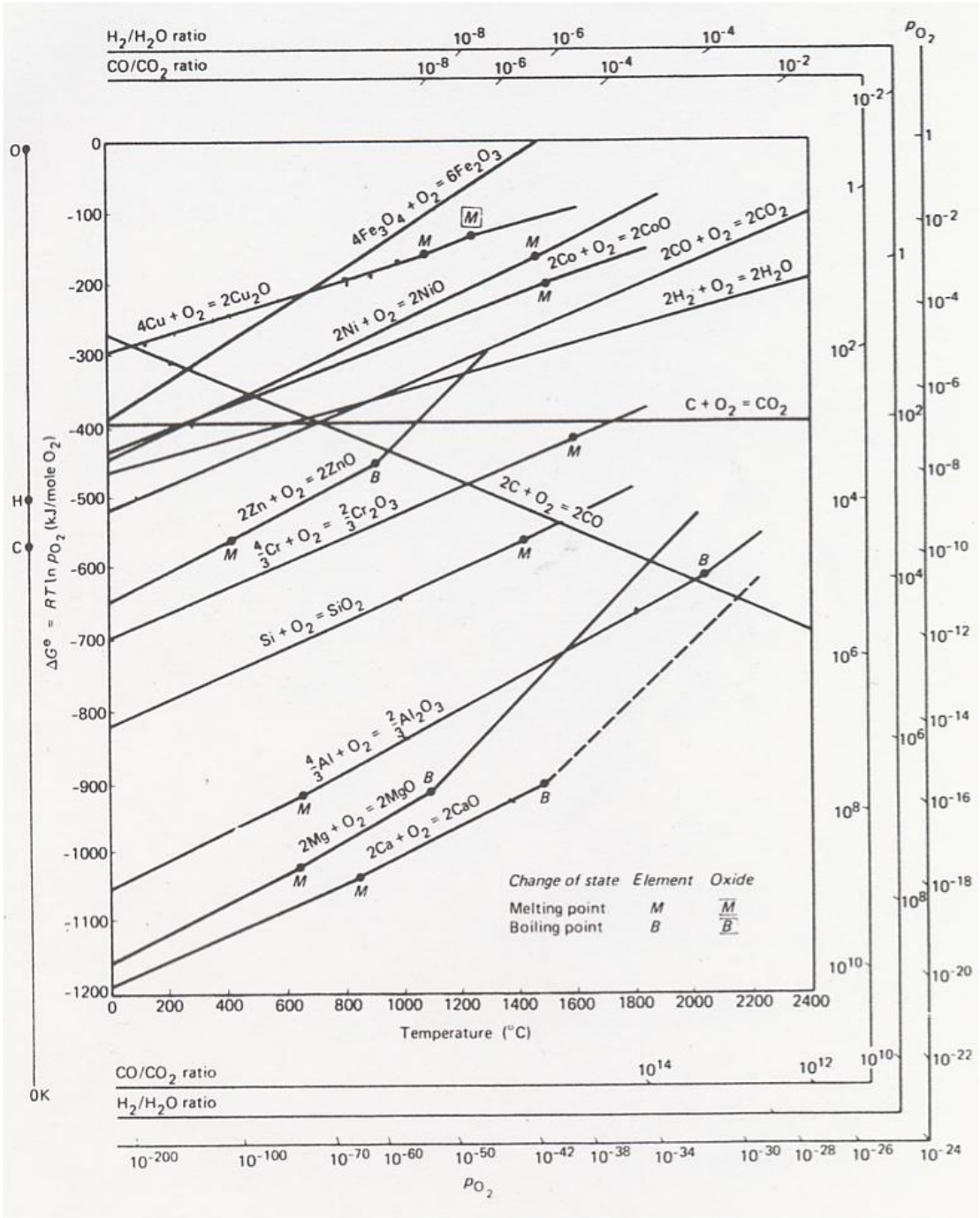

Figure 2-1 Standard free energy of formation of selected oxides as a function of temperature [**22**]

of mass action. Considering **reaction 1** and assuming activities of the metal and oxide as unity and that of the oxygen partial pressure under equilibrium conditions,

$$\Delta G - \Delta G^{\circ} = RT \ln\left(a_{M_xO_y} / a_M^x . a_{O_2}^{\frac{y}{2}} \right) \quad \text{.....(3)}$$

where a is the thermodynamic activity.

Equation 3 may be used to express the oxygen partial pressure at which metal oxides dissociate, as for an ideal gas, the activity a is equal to the partial pressure P, and for a pure condensed phase, the activity a = 1 thus under conditions of equilibrium where ΔG= 0

$$\Delta G^{\circ} = RT \ln\left(p^{\frac{y}{2}} O_2 \right) \quad \text{.....(4)}$$

where pO_2 is the oxygen partial pressure at the dissociation pressure of the oxide.

The determination of the conditions under which a given corrosion product is likely to form are useful, particularly in the design of oxidation/sulphidation resistance alloys and coatings where elemental additions are made, preferentially react with the environment species to form more stable and protective scales. The preferential oxidation/sulphidation, for example, of an alloy component requires that its standard free energy of formation be lower than that of the other alloy components.

When a metal or alloy is exposed to gaseous oxygen or sulphur, the processes of initial oxidation or sulphidation can be envisaged to occur in three main stages [**23**]:

- adsorption of oxygen or sulphur gas on the metal surface,
- formation of individual oxide or sulphide nuclei which grow laterally to form a continuous oxide or sulphide film, and
- further growth of the oxide or sulphide film normal to the metal surface.

Adsorption

Adsorption leads to a decrease in entropy as the gas molecules and atoms normally lose some degrees of freedom. Due to the simultaneous decrease in both the free energy and the entropy, which also imply a decrease of the enthalpy (**equation 5)**, adsorption is normally an exothermic process.

$$\Delta G = \Delta H - T\Delta S \quad \text{……..……..(5)}$$

Adsorption can be termed physisorption and chemisorption. In physical adsorption, gases become bound to the metal surface through relatively weak van der Waals' forces for which the enthalpies are relatively low (< 20 – 50 kJ/mole). Chemisorption is characterised by the formation of a chemical bond, with the enthalphies involved in the range 40 to 600 kJ/mole. Clearly the chemisorbed states are generally more stable than the most stable solid compound of the same system. Chemisorption takes place at specific sites on clean metal surfaces and is dependent on such factors as crystallographic orientation, edges, dislocation links and defects on the surface. Chemisorption continues until a monolayer of the adsorbed species is formed.

When the surface of a metal is placed in contact with an oxidising or sulphidising gas where the chemical activities of the oxygen or sulphur are fixed but are below a specified value, a strong interaction occurs between the metallic atoms of the metal surface and the oxygen or sulphur. Such an interaction leads to the formation of a monatomic layer of oxygen or sulphur chemically adsorbed. In this range of concentrations, the metal surface ceases to react when placed in contact with the ambient gas as soon as the monatomic layer has formed. If, owing to the various fluctuations, nuclei whose thickness corresponds to several atomic layers appear locally, but the latter have a short lifetime. This emphasises the fact that when a metal is placed at a high temperature within a rarefied atmosphere, considered as a reducing agent from the traditional thermodynamic point of view, then

changes in the properties of the external surface and sometimes even in the internal surface (e.g. grain boundaries and sub-grain boundaries) can be caused by the presence of the traces of residual oxygen or sulphur. It was observed [**24**] using radioactive S^{35} that the surface of Cu-S alloys at $pH_2O/pH_2 = 10^{-4}$-10^{-2} at temperatures between 800 and 900°C became covered by a monatomic layer of sulphur. It was believed that under these conditions the grain boundaries were also saturated by a mono-layer of sulphur atoms. Furthermore it was proposed that in cases where pO_2 or pS_2 exceeded the dissociation partial pressure of the oxide or sulphide, the existence of a saturated monolayer preceded the formation of the three-dimensional oxide or sulphide.

Nucleation and growth of three-dimensional compounds

When a metal surface saturated with adsorbed oxygen or sulphur atoms is further exposed to an atmosphere in which the oxygen or sulphur activities are above the dissociation partial pressure of the oxide or sulphide, oxide or sulphide nuclei are formed at some particular points on the metal surface. A model for such a growth process is shown in **Figure 2-2** [**23**]. The nucleation and growth of nuclei are functions of the metal type and its orientation, the temperature and oxygen or sulphur partial pressure. Oxygen or sulphur species in equilibrium with the gas on top of the two-dimensional adsorbed layer lead to the formation of nuclei, which grow laterally by capturing at the perimeter. The growth pattern follows the sequence: nuclei increase → the growth rate increases → growth rate reduced by impingement. This particular manner of growth is ascribed to the inhibition of surface diffusion over the exterior of the metal. The growth process is in competition with perpendicular diffusion, thus modifying the morphologies of the reaction product(s).

Another very important aspect is the location of the nuclei. It might be thought that the nuclei of the oxide or sulphide would most likely start to grow at the existing imperfections. At rather low temperatures when it is difficult for the reaction to start,

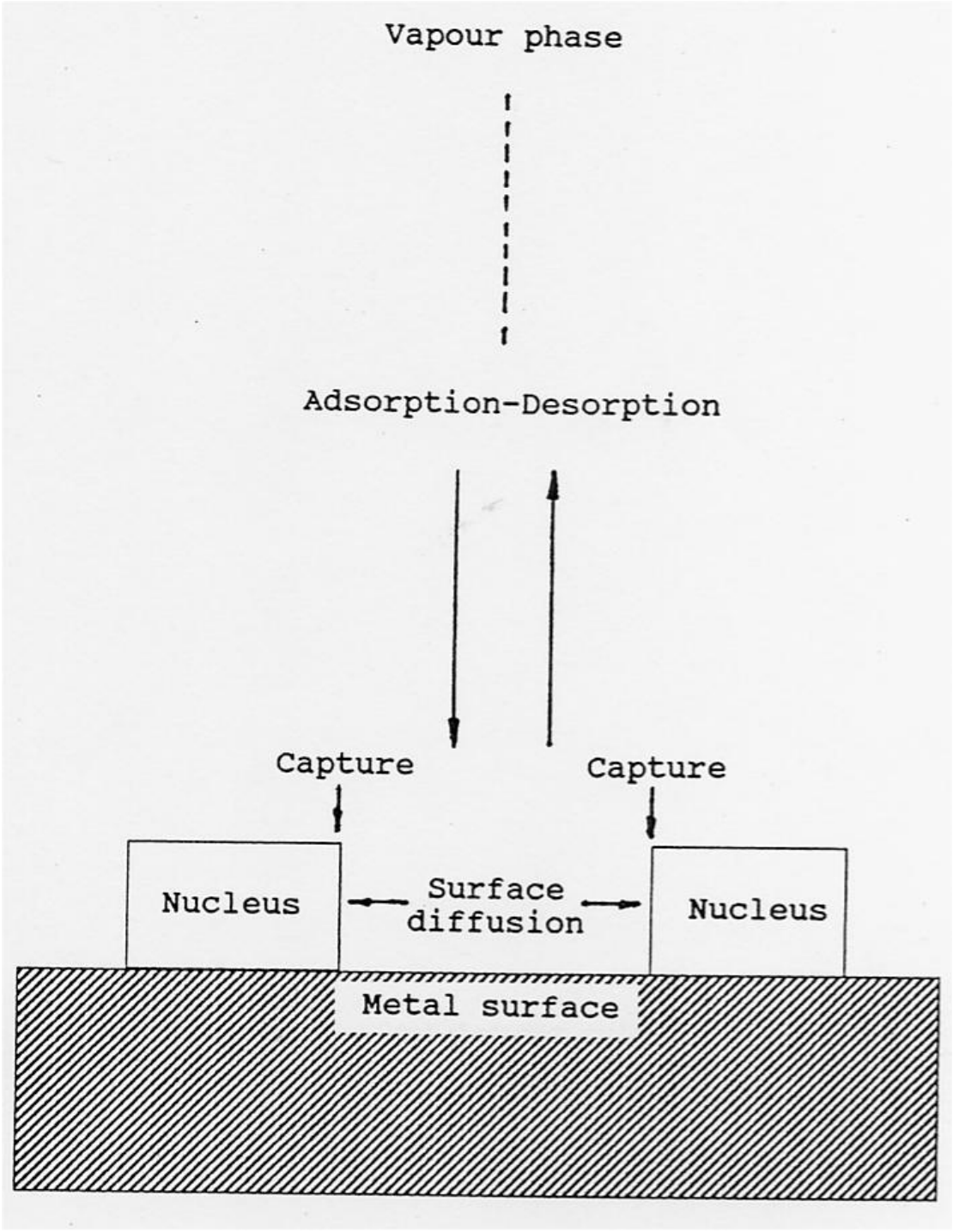

Figure 2-2 Schematic model for the nucleation and growth of oxide or sulphide on a metal surface [**23**]

surface defects are likely to promote heterogeneous nucleation. On the other hand, higher temperature producing higher mobility of species will promote homogeneous nucleation and the influence of defects on the location of nucleation will be minimised. Oxide nucleation at reduced oxygen pressures is characterised by the presence of an incubation period, which in some cases is influenced by the dissolution of oxygen in the metal. Two important observations are that particle density is a function of temperature and oxygen pressure, increasing with increasing pO_2, and decreasing with increasing temperature. At constant particle density, the growth has been assumed to be controlled by Ostwald ripening.

2.2.2 Kinetics and Rates of High Temperature Corrosion

The kinetics of oxidation reaction require for example minimum Al content in the alloy in order to achieve preferential or selective oxidation of Al. The basic stages of the oxidation reaction are shown schematically in **Figure 2-3**. Assuming there is sufficient Al, a protective steady-state Al_2O_3 scale will form. Prior to the steady-state stage is a transient stage, when less noble oxides, such as FeO may form. Typically, this initial layer is undercut by Al_2O_3 to begin the steady-state oxidation. Al_2O_3 grows much more slowly than FeO, so the change to a steady-state also usually implies a substantial reduction in the oxidation rate [**25**]. When the substrate becomes depleted in Al, Fe-rich oxides form rapidly, leading to breakaway oxidation. At this point, protective oxidation is no longer possible, and the reaction proceeds more rapidly to eventual full consumption of the base metal.

There are, of course variations of this simple model. For instance, breakdown may occur in the steady-state period followed by the formation of the healing Al_2O_3 scale. Repeated breakdown/healing cycles may even characterize the steady-state period. The breakaway period implies that the reaction is out of control and no healing will occur. Thus, to produce an oxidation resistant alloy, the goal is to minimize the transient stage and maximize the length of the steady-state oxidation period (**Figure 2-3**). Generally, there are three common

relationships linking scale thickness and the exposure time at a temperature as schematically shown in **Figure 2-4**.

Under certain conditions the oxidation of a metal or alloy proceeds at a constant rate and is said to obey 'linear rate law' as shown in **Figure 2-4**, i.e.

$$x = K_l.t \quad \text{.....(6)}$$

where x is the scale thickness, t is the exposure time and K_l is the linear rate constant.

In some cases, further increase in scale thickness results in a reduction in the metal activity gradient across the scale and, consequently, to a reduction in ionic flux and the reaction rate. At this point the transport of ions across the scale becomes the rate controlling process and the rate falls with time (see **Figure 2-4**) according to a parabolic rate law**,** i.e.

$$x^2 = K_p.t \quad \text{.....(7)}$$

where K_p is the parabolic rate constant.

If metals or alloys oxidised under certain conditions, typically at low temperatures of up to about 400°C, the initial oxide formation, up to the 1000°A range, is characterised by an initial rapid reaction that quickly reduces to a very low rate of reaction. Such behaviour has been found to conform to a rate law described by logarithmic functions (**Figure 2-4**) such as:

$$x = K_{\log} \log (t + t_o) + A \quad \text{.....(8)}$$

where A and t_o are constants at constant temperature. Several interpretations of this type of behaviour have been provided.

2.2.3 Defect Structures, Diffusion and Transport Processes Throughout Scales

The parabolic kinetic law as described before often typified the processes of oxidation and sulphidation. When the scales formed on the metal surface act as an effective barriers, the reactants, i.e. the metals and oxidants, are separated, and the reaction may proceed only

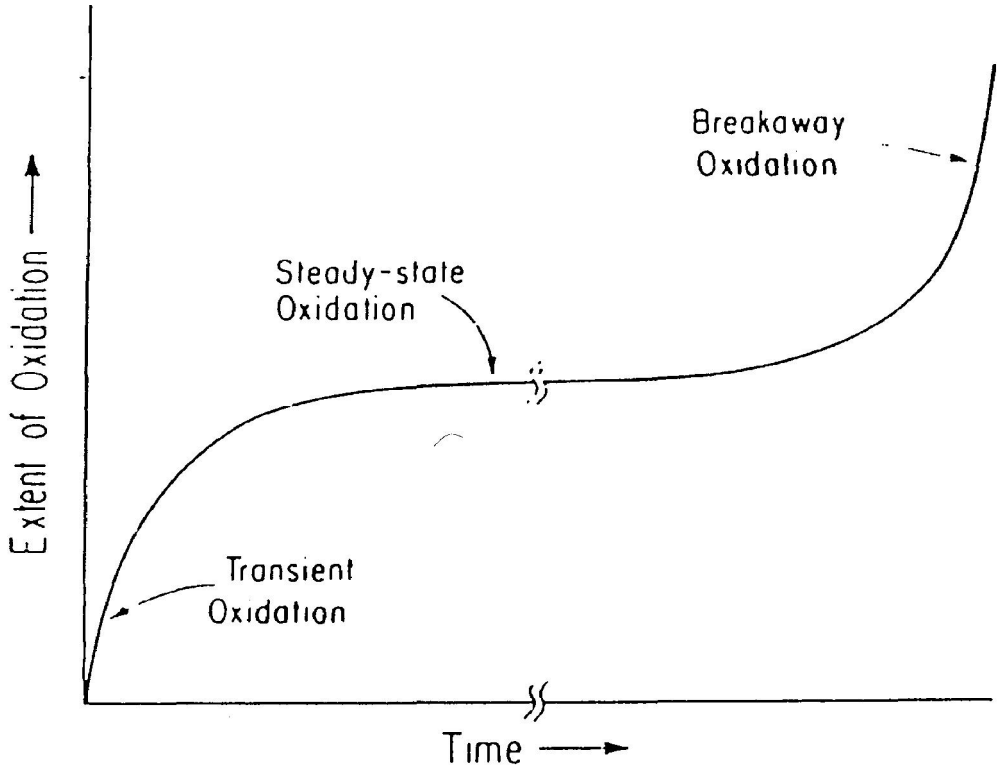

Figure 2-3 Basic stages of oxidation reaction [**26**]

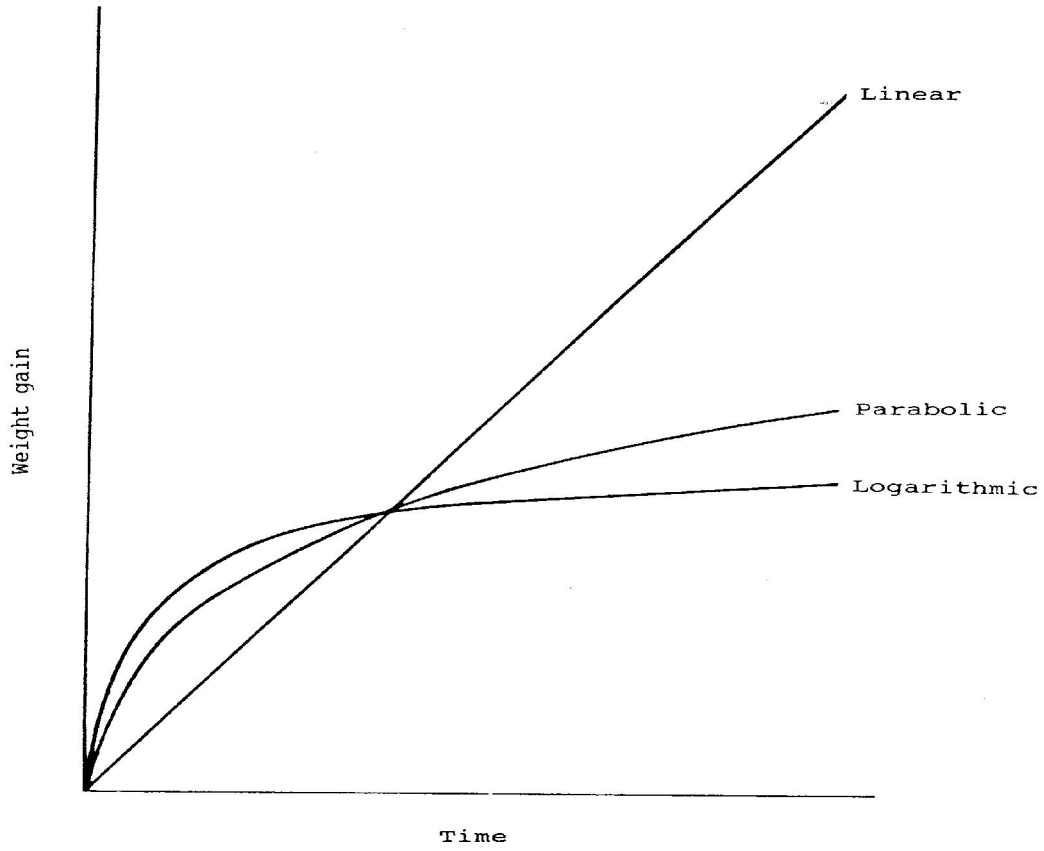

Figure 2-4 Schematic illustration of the variation of weight gains with time for linear, parabolic and logarithmic corrosion kinetics [**23, 27**]

through the scales. The overall reaction will be then governed by the solid-state transport of the reactant molecules, atoms or ions. This underlines the importance of the transport properties of the scales, such as diffusion in the oxides or sulphides, which, are formed as reaction products. The transport properties are largely controlled by the imperfections or defects in solids.

Defects in scales

Since diffusion is dependent upon the defect structure of the oxide through which a species is diffusing, it is necessary to first understand the nature of the defects in oxides and their effect upon the transport of reactants during corrosion of the alloys. Several mechanisms are used to explain the transport of ions through both stoichiometric and non-stoichiometric compounds. In principle, all types of lattice defects may be present to some extent in all compounds, however, it is generally accepted that certain types of defect usually predominate.

At any temperature solids in the form of crystals contain different structural and compositional defects. These are often divided into three groups [**23**]: (1) point defects, (2) line defects and (3) electronic imperfections.

If the imperfection is limited to one structural or lattice site and its immediate vicinity, the imperfection is termed a **point defect**. Simple defects of this type include: (i) empty sites or vacancies where constituent atoms are missing in the structure and (ii) interstitial atoms occupying the interstices of the regular sites. In principle there may also be misplaced atoms, e.g. a cation on an anion site, but this type of defect is probably not important in oxides. The defects formed in pure crystals, e.g. vacancies and interstitial atoms, are commonly termed “native” point defects. Foreign atoms are also usually considered to be point defects.

Line defects or **dislocations** are characterised by displacements in the periodic structure in certain directions. Planar defects comprise stacking faults, internal surfaces (e.g. grain boundaries) and external surfaces.

In addition to structural defects solids also contain **electronic imperfections**, i.e. electrons and holes [**28**], which are relatively free to move in the solid. If the electrons or holes are localised at atoms or regular sites in the structure, the electronic defects may either be formed intrinsically through an excitation of elements from the valence to the conduction band or be formed in association with point defects.

Theoretically, metal oxides or sulphides under equilibrium conditions only have an exact stoichiometric composition under specific conditions of temperature and partial pressure of the components. However, as a general rule, metal oxides and sulphides will exhibit deviations from the exact stoichiometry [**28, 29**]. Non-stoichiometry in oxides and sulphides may arise from a deficit of oxygen or sulphur and metal relative to the stoichiometric composition, namely [**30**]:

(1) Oxides or sulphides with cation defects,

a) metal-deficit, with cation vacancies on the cation sub-lattice (p-type semiconductor), e.g. NiO, CoO, FeO, NiS, CoS, FeS;

b) metal-excess, with interstitial cations (n-type semiconductor), e.g. possibly ZnO, Cr_2S_3.

(2) Oxides or sulphides with anion defects,

a) oxygen (or sulphur)-deficit, with oxygen anion vacancies on the anion sublattice (n-type semiconductor), e.g. Nb_2O_5 or Ta_2O_5;

b) oxygen-excess, with interstitial oxygen (sulphur) anions (p-type semiconductor), e.g. VO_2.

Actually, the defect structures are often more complex, the oxides or sulphides containing several types of defects may be linked to the presence of impurities.

Generally, many metal sulphides are known to be more non-stoichiometric than the corresponding metal oxides [**3**], as shown in **Table 2-1**. Thus the diffusion rates associated with the non-stoichiometry in sulphides are much faster than in the oxides when the scale growth is likely to occur by outward diffusion of metal cations towards the scale/gas interface or by inward migration of sulphur anions via anion defects in the sulphide lattice (**Table 2-2** [**3**]).

$M_{a+y}S_b$	T (°C)	y	$M_{a+y}O_b$	T (°C)	y
$Cu_{1.75}S$	650	- 0.250	$Cu_{1.997}O$	1000	- 0.003
$Ni_{0.92}S$	700	- 0.080	$Ni_{0.9999}O$	1000	- 0.0001
$Co_{0.85}S$	720	- 0.150	$Co_{0.99}O$	1000	- 0.01
$Fe_{0.80}S$	800	- 0.200	$Fe_{0.89}O$	800	- 0.11
$Cr_{2.08}S_3$	700	+ 0.080	$Cr_{1.999}O_3$	600	- 0.001
$Al_{2.01}S_3$	950	+ 0.010	$Al_{2.0001}O_3$	1000	+0.0001

Table 2-1 Comparison of non-stoichiometry of certain metal sulphides with the relative oxides [**3**]

Sulphide	T (°C)	D_M (cm^2/s)	Oxide	T (°C)	D_M (cm^2/s)
$Cu_{1.75}S$	650	5.2×10^{-5}	$Cu_{1.997}O$	1000	1.7×10^{-8}
$Ni_{0.92}S$	800	1.4×10^{-8}	$Ni_{0.9999}O$	1000	1.0×10^{-11}
$Co_{0.85}S$	720	7.0×10^{-7}	$Co_{0.99}O$	1000	1.9×10^{-9}
$Fe_{0.80}S$	800	3.5×10^{-7}	$Fe_{0.89}O$	800	1.3×10^{-8}
Cr_2S_3	1000	1.0×10^{-7}	Cr_2O_3	1000	1.0×10^{-12}
Al_2S_3	600	1.0×10^{-13}	Al_2O_3	1000	1.0×10^{-16}

Table 2-2 Comparison of diffusion coefficient of certain metal sulphides with the relative oxides [**3**]

To summarise the defect properties of metal oxides or sulphides, a comparison of non-stoichiometry of some sulphides and oxides is presented in **Figure 2.5** [**29**]. It is reported that sulphides of important common metals show much higher deviations from stoichiometry, and thereby contain significantly higher defect concentrations than in the corresponding oxides. The only exception is sulphides, which have a lower non-stoichiometry than the oxide. It should be stressed that in the case of high non-stoichiometry, the defect concentration in oxides as well as in the sulphides of iron, nickel and cobalt, decreases with increasing temperature. In the case of sulphides, this behaviour is due to strong repulsive interaction between cation vacancies, and in the case of oxides, it arises from the formation of extended defects. Finally, it should be mentioned that the defect structure in refractory metal sulphides has not been studied extensively probably because of the associated difficulties in measuring deviation from stoichiometry. It has been shown [**29**], for instant, that the non-stoichiometry of molybdenum sulphide at about 1000°C is smaller than $8x10^{-5}$ mole of sulphur per mole of sulphide. The defect concentration in refractory metal sulphides is therefore assumed to be very low.

The presence of foreign ions or "dopants" significantly affects the defect concentration of an oxide/sulphide. There are numerous possible defects, which may occur in different oxides/sulphides. Here the case of an oxide MO doped with small amounts of Mf_2O_3, where Mf denotes a foreign atom, is used to illustrate the theory. Assuming the foreign Mf^{3+} cations occupy normal M^{2+} sites, then Mf ions have a single effective charge. For electroneutrality an equivalent concentration of negative effective charge is required, therefore the electron concentration is increased:

$$Mf_2O_3 = 2Mfm^{\cdot} + 2e^{'} + 2O_o + \frac{1}{2}O_2 \quad \ldots\ldots\ldots\ldots\ldots\ldots\ldots\ldots\ldots\ldots\ldots\ldots\ldots\ldots(9)$$

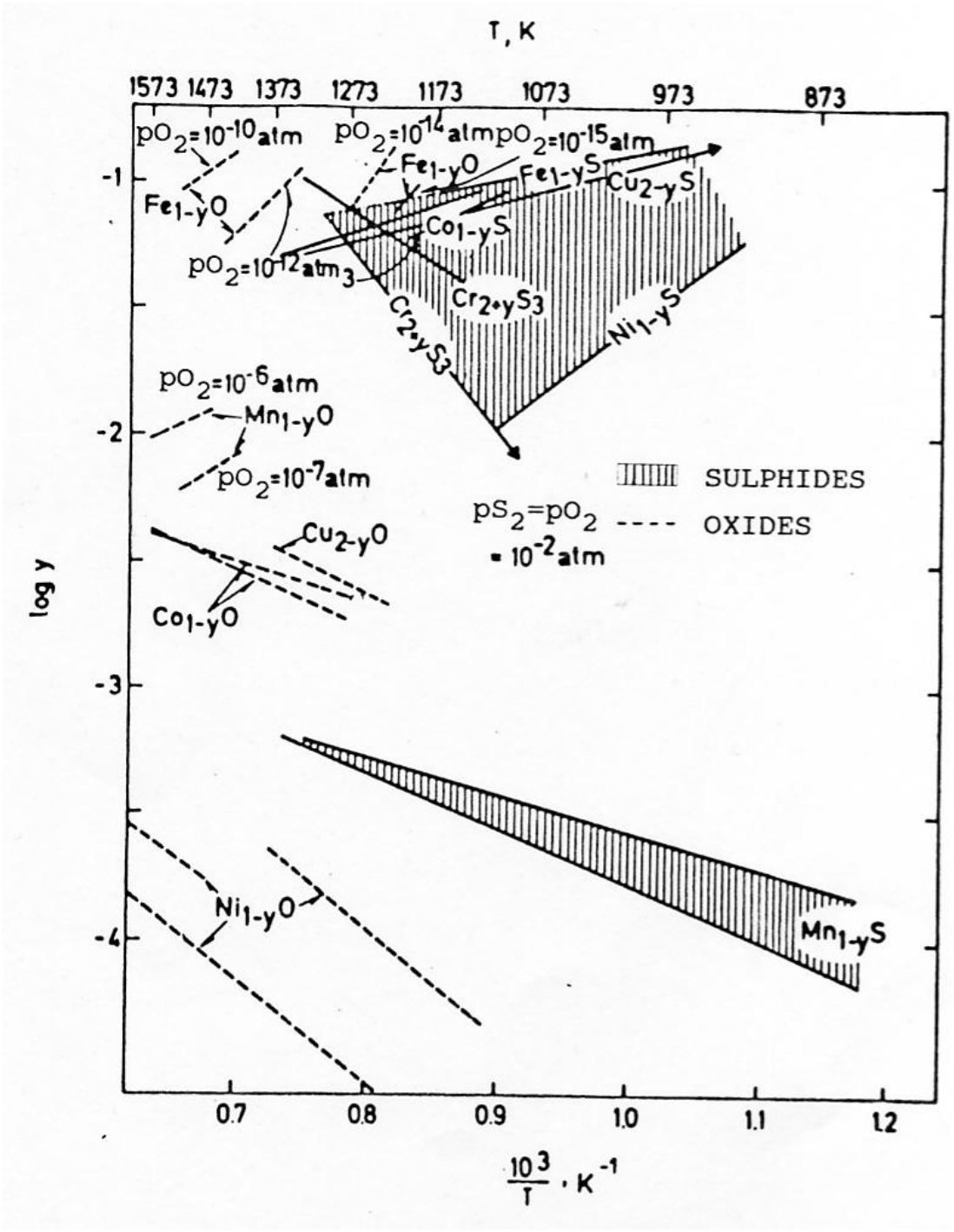

Figure 2-5 Collective plot of the temperature relationship of non-stoichiometry for several metal sulphides and oxides [**29**]

If the MO is oxygen deficient with $VO^{\cdot\cdot}$ the predominant carriers, the increased electron concentration will result in a reduction in the oxygen vacancy (O_o) concentration and O denotes a perfect oxygen crystal.

$$VO^{\cdot\cdot} + Mf_2O_3 = 2Mf_{m^{\cdot}} + 3O_o \quad \text{.....(10)}$$

where VO denotes an anion vacancy so $VO^{\cdot\cdot}$ denotes a double negatively charged anion vacancy. Conversely, a single valent metal oxide as dopant would result in the reduction of electron concentration and an increase in the oxygen vacancy concentration.

The effect of aliovalent cation impurities in p-type semiconductor is opposite to that of the n-type described above and hence addition of Mf_2O_3 to a metal-deficient MO may be written;

$$2h^{\cdot} + Mf_2O_3 = 2Mf_{m^{\cdot}} + 2O_o + \frac{1}{2}O_2 \quad \text{.....(11)}$$

where $2h^{\cdot}$ denotes a single positively charged electron hole.

Dislocations in the crystal lattice may act as paths for fast diffusion, that is they act as a sink for point defects or diffusing ion species. The core field of a dislocation is often a preferred site for vacancies and interstitial atoms as it presents a low resistance path for diffusion and results in its enhanced migration. Grain boundary diffusion is an example of diffusion through planar defects in crystals because of their disordered atomic structure.

The transport of ions across free surfaces is generally considered to be faster than grain boundary diffusion such that $D_{lattice} < D_{gb} < D_{surface}$ and that activation energy varies as $\Delta H_V > \Delta H_{gb} > \Delta H_s$. This however, is not always the case. Diffusion across free surfaces remains the least understood diffusion phenomenon in view of the numerous difficulties associated with its measurement [**31-33**].

Studies of the defect structure in TiO_2 suggest that both oxygen-ion vacancies, $V_o^{\cdot\cdot}$, and interstitial Ti ions, $Ti_i^{\cdot\cdot\cdot}$, or $Ti_i^{\cdot\cdot\cdot\cdot}$ are the predominant point defect [**23**]. Accordingly, the non-

stoichiometry can be written as $Ti_{1+x}O_{2-y}$ [**23**]. The concentration of both kinds of defects is dependent on the oxygen pressure and decreases with increasing pressure. The reaction between $V_o^{\cdot\cdot}$ and gaseous oxygen can be described by

$$V_o^{\cdot\cdot} + \frac{1}{2}O_2 + 2e' = O_o^{\,x} \quad \text{.....(12)}$$

From the law of mass action it follows that

$$K_1 = \frac{1}{C_{V_o^{\cdot\cdot}} C_{e'}^2 (pO_2)^{\frac{1}{2}}} \quad \text{.....(13)}$$

Because

$$C_{V_o^{\cdot\cdot}} = \frac{1}{2} C_{e'} \quad \text{.....(14)}$$

it follows that

$$C_{V_o^{\cdot\cdot}} = \frac{1}{2} C_{e'} = \left(\frac{1}{4K_1}\right)^{\frac{1}{3}} (pO_2)^{\frac{-1}{6}} \quad \text{.....(15)}$$

or

$$pO_2 = \left(\frac{1}{4K_1}\right)^2 C^{-6}{}_{V_o^{\cdot\cdot}} \quad \text{.....(16)}$$

Similar pressure dependence of the defect concentrations can therefore be generalised to:

$$C_{Ti_i^{\cdot\cdot\cdot\cdot}} \propto (pO_2)^{\frac{-3}{16}} \quad \text{.....(17)}$$

and

$$C_{Ti_i^{\cdot\cdot\cdot\cdot}} \propto (pO_2)^{\frac{-1}{5}} \quad \text{.....(18)}$$

The pressure dependence of the defect concentration can therefore be generalised to:

$$C_{defect}(TiO_2) \propto (pO_2)^{\frac{-1}{n}} \quad \text{.....(19)}$$

with n between about 4 to 6.

In general, it is concluded that interstitial Ti ions predominate at low oxygen pressures and high temperatures and oxygen ion vacancies predominate at high oxygen pressures and low temperatures [**34**].

During parabolic oxidation of titanium, most of the scale is formed by inward oxygen diffusion, however, a small portion is also formed by outward cation diffusion; this portion increases with increasing temperature [**8**]. The measurement of Becker *et al.* [**8**] indicated that the disorder in TiO_2 is affected by dissolution of Al_2O_3 in such a way that the concentration of interstitial Ti ions increases and/or that the oxygen-ion vacancies decreases.

If substitutional dissolution is considered and oxygen-ion vacancies predominate, the dissolution reaction can be written as

$$Al_2O_3 = 2\ Al'_{Ti} + V_o^{\cdot\cdot} + 3\ O_o^{x} \quad \text{.....(20)}$$

If interstitial Ti ions predominate by substitutional dissolution, a comparable reaction equation is

$$Ti_{Ti}^{x} + 2\ Al_2O_3 = 4\ Al_{Ti}' + Ti_i^{\cdot\cdot\cdot\cdot} + 6\ O_o^{x} \quad \text{.....(21)}$$

In both cases, the defect concentration increases with an increasing amount of dissolved Al_2O_3. An interstitial dissolution can be described by

$$Al_2O_3 = 2\ Al_i^{\cdot\cdot\cdot} + 6\ e' + \frac{2}{3}O_2 \quad \text{.....(22)}$$

Only in this case does the solubility of Al_2O_3 decrease with increasing oxygen pressure.

In order to understand the formation and re-dissolution of the Al_2O_3 barrier inside the scale it should be noted that the solubility of Al_2O_3 in TiO_2 decreases with increasing oxygen pressure [**35**]. This observation agreed with the measurements of Becker *et al.* [**8**]. Such pressure dependence is to be expected if Al_2O_3 is dissolved predominately as interstitials (**equation 22)**.

Diffusion and transport processes in scales

Diffusion in solids takes place because of the presence of imperfections in the crystal structure. Point or lattice defects, i.e. vacancies or interstitial ions, are responsible for lattice or bulk diffusion. Line and surface defects – which include grain boundaries, dislocation and interfaces – are responsible for short-circuit or fast diffusion [**36**]. In polycrystalline materials the relative contributions of these different types of diffusion are a function of temperature, partial pressure of the atmosphere, grain size and porosity whereby short-circuit diffusion becomes increasingly important at lower temperatures.

A growth process, which is purely governed by volume diffusion should obey a parabolic growth law. In a reaction diffusion experiment, however, it is not always clear if the diffusion couple is at thermal equilibrium throughout the whole diffusion process. Especially at the beginning, when nucleation and growth of newly formed phases take place, deviation from the parabolic growth law can often be observed. Furthermore, in the case where the intermetallic phase formed in the diffusion zone is always polycrystalline and some times small columnar grains are observed, the influence of the grain boundary diffusion on the overall diffusion is unavoidable and often dominant.

Considerations of the transport properties suggested that at high temperatures matter transport in metal sulphides (as in oxides) proceeds mainly through point defects. Thus, these properties can be described by self-diffusion and chemical diffusion coefficients. In contrast to the oxides, however, the transport properties of metal sulphides are less well known. In a few cases only the chemical and self-diffusion coefficients have been determined as a function of temperature and sulphur pressure. **Figure 2-6** [**29**] shows a collective plot of the measured, calculated and estimated values of self-diffusion coefficients in some metal sulphides and oxides. It follows from their plots that the activation energies of diffusion in sulphides are significantly lower than those in oxides. It is

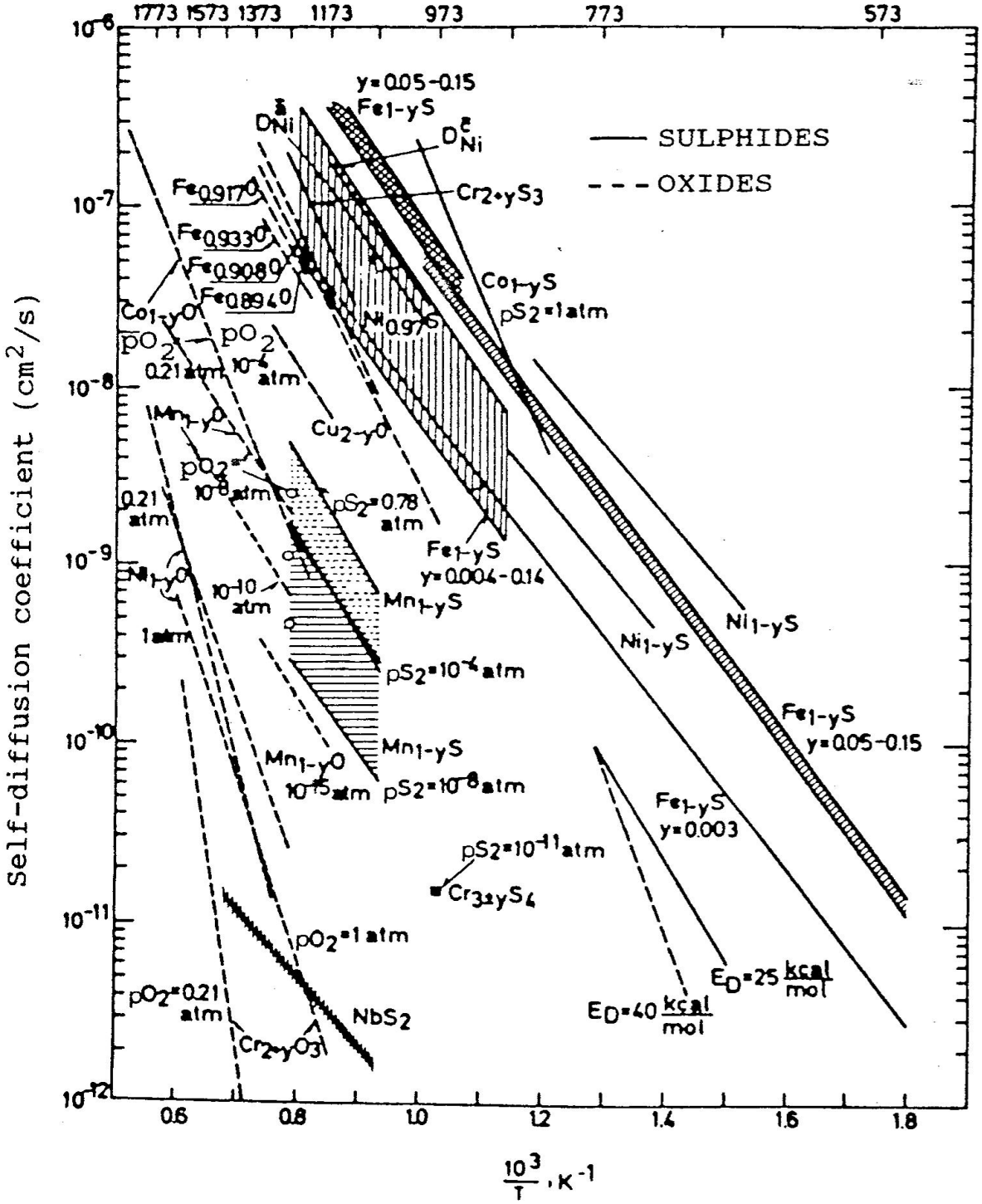

Figure 2-6 Collective plot of self-diffusion coefficients in some metal sulphides and oxides [**29**]

clearly visible that the self-diffusion rate in several sulphides is of the same order of magnitude as in some oxides, e.g. $Mn_{1-y}S$ and $Mn_{1-y}O$, $Fe_{1-y}S$ and $Fe_{1-y}O$, as well as the refractory metal sulphides and oxides. The rates of self-diffusion, on the other hand, in a number of other sulphides are orders of magnitude higher than in oxides. In particular, the rates of self-diffusion in sulphides of such important metals as cobalt, nickel and chromium are several orders of magnitude higher than in their corresponding oxides.

Since the value of self-diffusion is a product of defect mobility and their concentration, deviations from stoichiometry and chemical diffusion coefficients should be compared in both oxides and sulphides of these materials. **Figure 2-7** [**29**] shows a comparison of chemical diffusion coefficients in selected oxides and sulphides. It follows from this plot that the rate of diffusion and consequently the mobility of defects in metal oxides and sulphides do not differ significantly. In fact, the rate of chemical diffusion for metal oxides is generally higher than in metal sulphides, but the differences do not exceed one order of magnitude. This means that in the majority of cases, the significantly higher rate of self-diffusion in metal sulphides results from higher defect concentrations and not from greater defect mobility. It is also interesting to note that the activation energies for chemical diffusion in metal sulphides and oxides are comparable, whereas the activation energies for self-diffusion in metal oxides are much higher than in sulphides.

From the above considerations, it follows that sulphide scales on common metals should possess poor protective properties. One of the most important conclusions is that, as in the case of sulphidation, sulphide scales on all common metals grow primarily by the outward diffusion of cations, and on refractory metals by inward diffusion of sulphur species.

Figure 2-8 [**29**] shows a collective plot of the temperature dependence of sulphidation and oxidation rates for some metals. These plots show clearly that sulphidation rates of such important metals as cobalt, nickel and chromium are significantly higher than those of oxidation. Manganese is in an intermediate position, as its sulphidation rate, is comparable

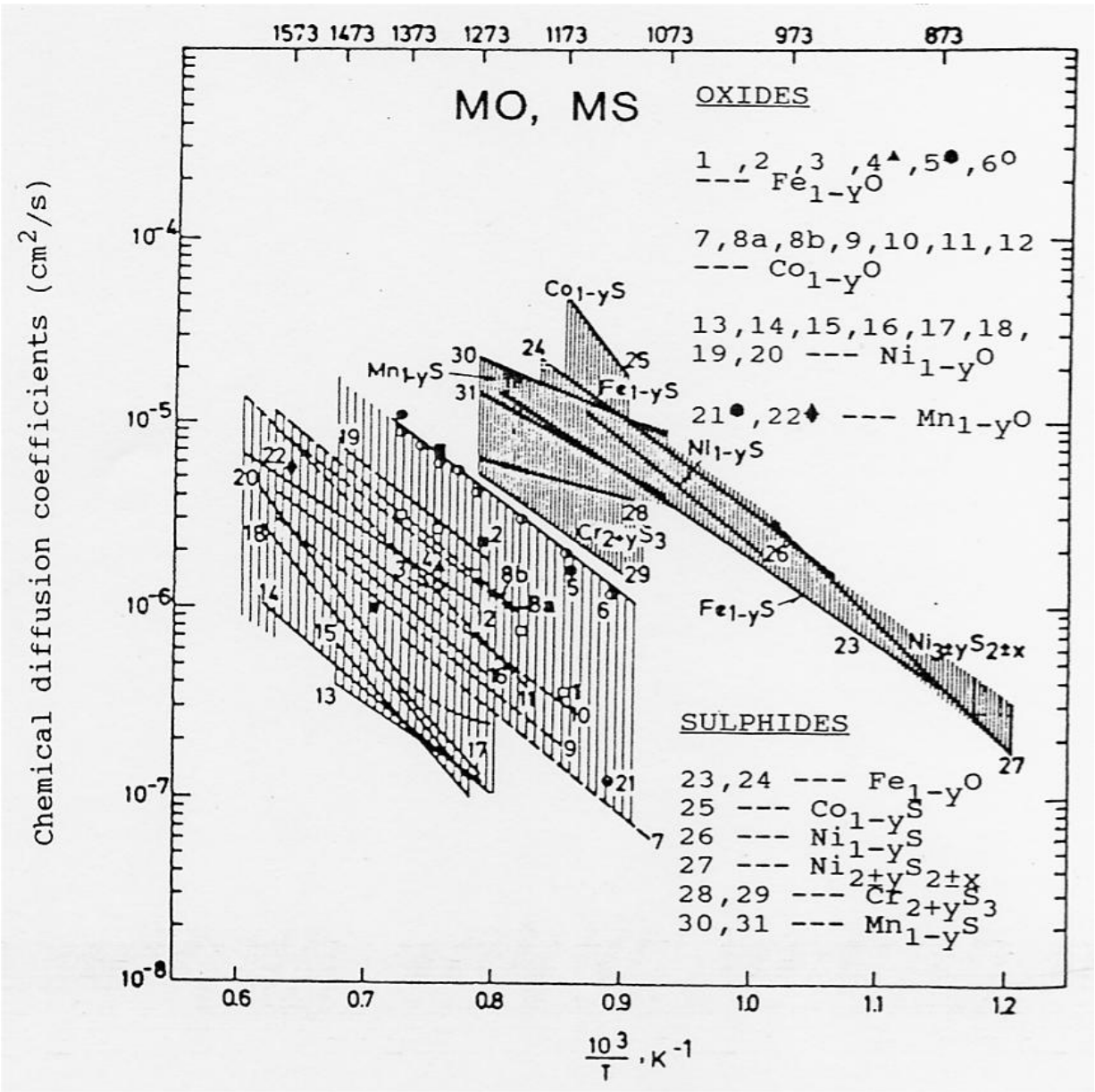

Figure 2-7 Collective plot of chemical diffusion coefficients in some metal sulphides and oxides [**29**]

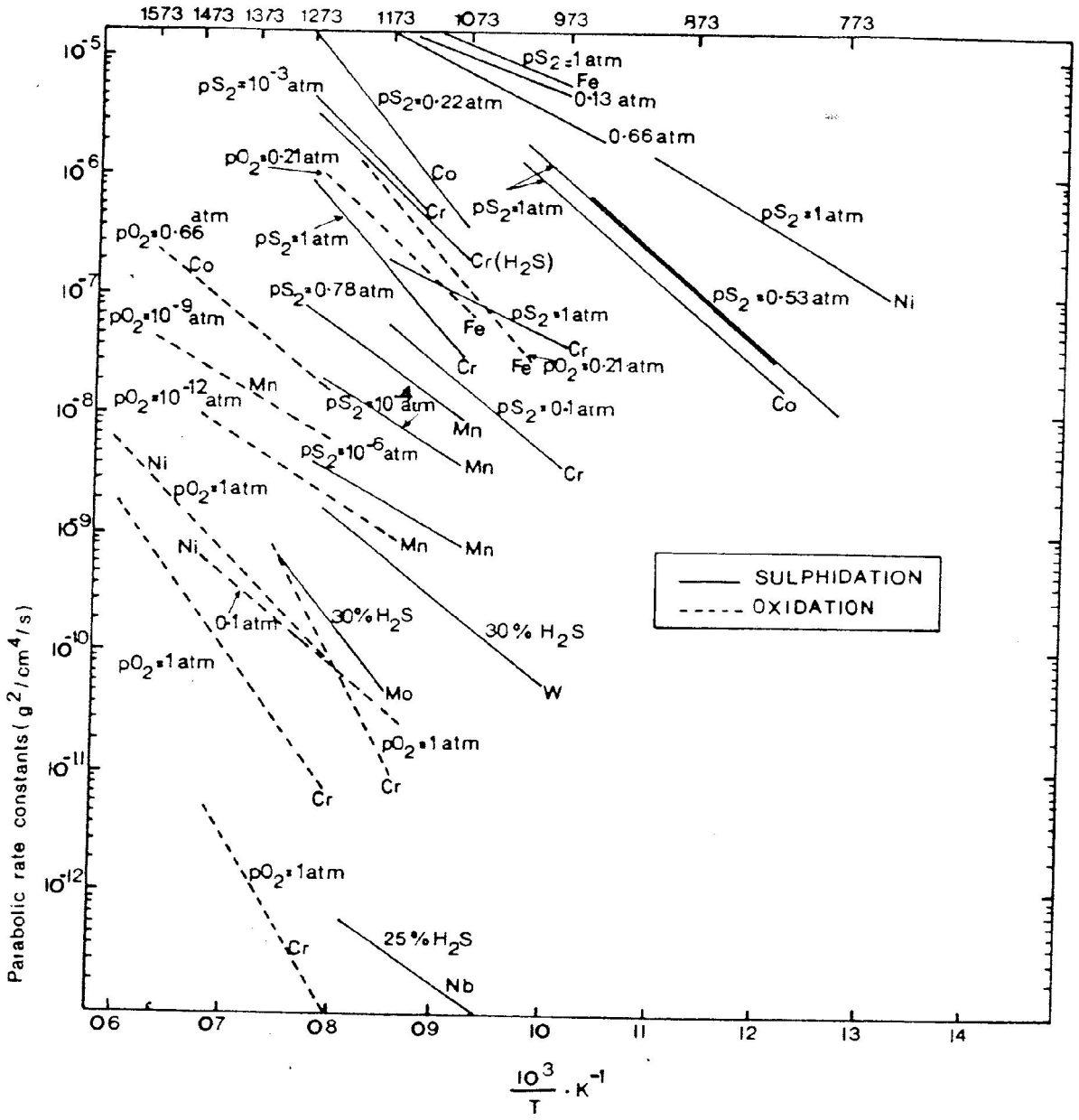

Figure 2-8 Collective plot of the temperature relationship of sulphidation and oxidation rates of pure metals [**29**]

to that of its oxidation. On the other hand, refractory metals are highly resistant to sulphidation, their sulphidation rate being comparable to the oxidation of chromium, which represents one of the most resistant metals to oxidation. It should be emphasised that the sulphidation rate of niobium is about seven orders of magnitude lower than that of iron.

If oxidation of Ti-Al alloys is controlled by diffusion in the scale, it is generally assumed that the concentration gradient of the diffusing species is constant across the scale as shown in (**Figure 2-9** [**8**]. (If the diffusion coefficient D_i is oxygen-pressure dependent, then the product $D_i.\Delta G_i$ is constant.) Then it follows from **equation 16** that the slope of the oxygen pressure across the scale becomes increasingly steeper when approaching the surface (**Figure 2-9**). The variation of the Al_2O_3 solubility (substitutional and interstitial) across the scale depends on the relation between Al_2O_3 solubility and oxygen pressure, which is presently unknown [**8**]. A linear variation across the scale may be assumed for simplification.

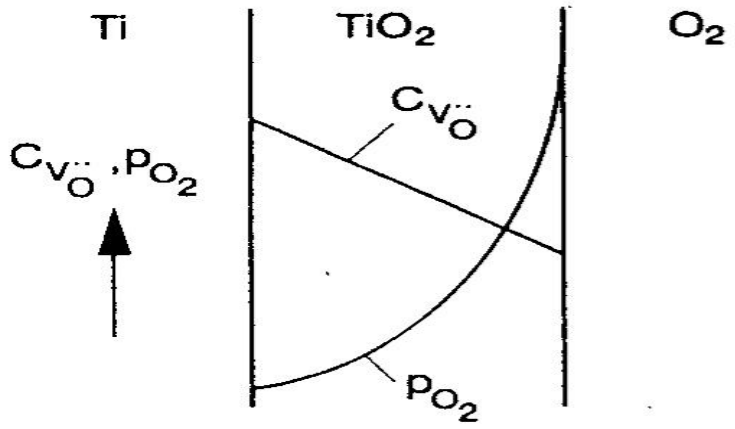

Figure 2-9 Variation of defect concentration and oxygen pressure in a growing TiO_2 scale [**8**]

2.3 Wagner Oxidation Theory

The process of thin film oxidation applies to the very initial stage of high temperature oxidation. As an oxide film thickens to form a compact scale, then the mechanism of continued oxidation is controlled by the diffusion of reactants through the scale under the influence of a concentration gradient. This commonly results in a parabolic rate relationship. Wagner's theory of high temperature oxidation of metals is the best establishing model for the mechanism of thick film formation, although many assumptions in the theory limit its application. It is assumed that scales are compact, adherent and with only small deviation from stoichiometry. Thermodynamic equilibrium is assumed throughout the scale and at its interfaces and that the rate-determining process is the migration of ions and electrons across the scale. Hence interface reactions are assumed to be rapid. Anions, cations and electrons are considered to diffuse independently of each other via lattice defects and under the influence of an electrochemical potential gradient across the scale.

The driving force for the reaction is the reduction in free energy associated with the formation of the oxide and the concentration gradient of the components. The rate of growth is determined by the gradient and rates of diffusion of cations, anions and electrons. The mobility of these defects is not equal and hence a charge separation is created in the scale to the point where a resulting space charge creates an electric field, which opposes further charge separation, and a steady state is achieved.

There is thus a constant concentration difference, Δc across the oxide and the rate of transport across the scale is dependent upon the diffusion coefficient, D and the thickness of the scale, x.

$$dx / dt = D(\Delta c / x) \quad \text{.....(23)}$$

and hence;

$$x^2 = K.t \quad \text{.....(24)}$$

these mechanisms lead to a parabolic rate of oxidation. Models for oxide formation at the metal/oxide interface (via inward anion diffusion) and the oxide/oxygen interface (via outward cation diffusion) have been proposed where the transport of ions and electrons through the scale take into account both diffusion due to chemical and electrical potentials.

The importance of Wagner theory is that it provides a fundamental understanding of the high temperature oxidation of metals and – although it is not always directly applicable to all metal/oxide systems – it offers a theoretical basis for oxidation rate relationships. Numerous investigators have derived the Wagner theory using different models and assumptions [**31, 38**].

2.3.1 Selective oxidation

Selective oxidation is favoured in alloys in which the oxides of the alloy components have large variations in stability, and in which a critical concentration for preferred oxidation is maintained. Wagner derived a model to determine the critical concentration of a component to selectively oxidise and for preferred external oxidation [**38**]. For an alloy AB, the critical concentration of B, N_B for the preferred oxidation of B is:

$$N_B = \frac{V}{Z_B M_o \left(\pi K_p / D\right)^{\frac{1}{2}}} \quad \text{.....(25)}$$

where V is the molar volume of the alloy, Z_B is the valence of B, M_O the atomic weight of oxygen, D the diffusion coefficient of B in the alloy and K_p is the parabolic rate constant.

For an alloy A-B where B is the least noble constituent, then three cases for oxidation may be described: (i) alloy composition rich in the oxide of A until such a time when the concentration of B in the alloy reaches equilibrium, (ii) alloy composition rich in B where only B oxidises until the concentration of A in the alloy similarly achieves equilibrium, (iii) an intermediate composition where both A and B may oxidise.

2.3.2 Internal oxidation

Where oxygen is soluble in the alloy, the less noble alloy constituent may form oxide precipitates within the alloy, beneath the oxide/metal interface. This process requires that the rate of diffusion of oxygen in the alloy must be somewhat faster than that of the oxidising metal thus an oxygen gradient is established in the alloy. The degree of internal oxidation depends on the flux of oxygen into the alloy, which in turn depends on its solubility and the rate of diffusion. An internally oxidised zone extends to the depth at which the concentration of dissolved oxygen becomes too small for the formation of oxide. The result of internal oxidation is not necessarily undesirable, various studies have suggested that improvements in external scale adhesion, increased hardness and improved creep properties result from the presence of oxide particles within the material [**39, 40**].

When the concentration of the less noble metal in the alloy is increased, a critical concentration is achieved and results in the transformation from internal to external, or selective oxidation, with the formation of a protective surface scale of the least noble constituent. This transition may be accompanied by a reduction in the rate of oxidation from the relatively rapid rate of dissociation of oxygen into the alloy to the slower diffusion through the surface scale. **Figure 2-10** [**41**] summarises the most common form of alloy oxidation, showing complete, partial, or largely non-existent oxide miscibility.

An important consideration is whether internal oxidation or surface oxidation of the component likely to yield the protective oxide occurs. For an alloy AB, where only B oxidises, nuclei of BO develop in a matrix of A at the surface. If B can diffuse to the alloy surface fast enough, a complete BO surface layer develops (**Figure 2-10**(**b**), but if not, atomic oxygen diffusing into the alloy precipitates BO internal oxides at preferred sites (**Figure 2-10**(**a**). The formation of BO internally or externally depends then on competition between the outward flux of B (detrimental by the alloy interdiffusion coefficient in AB)

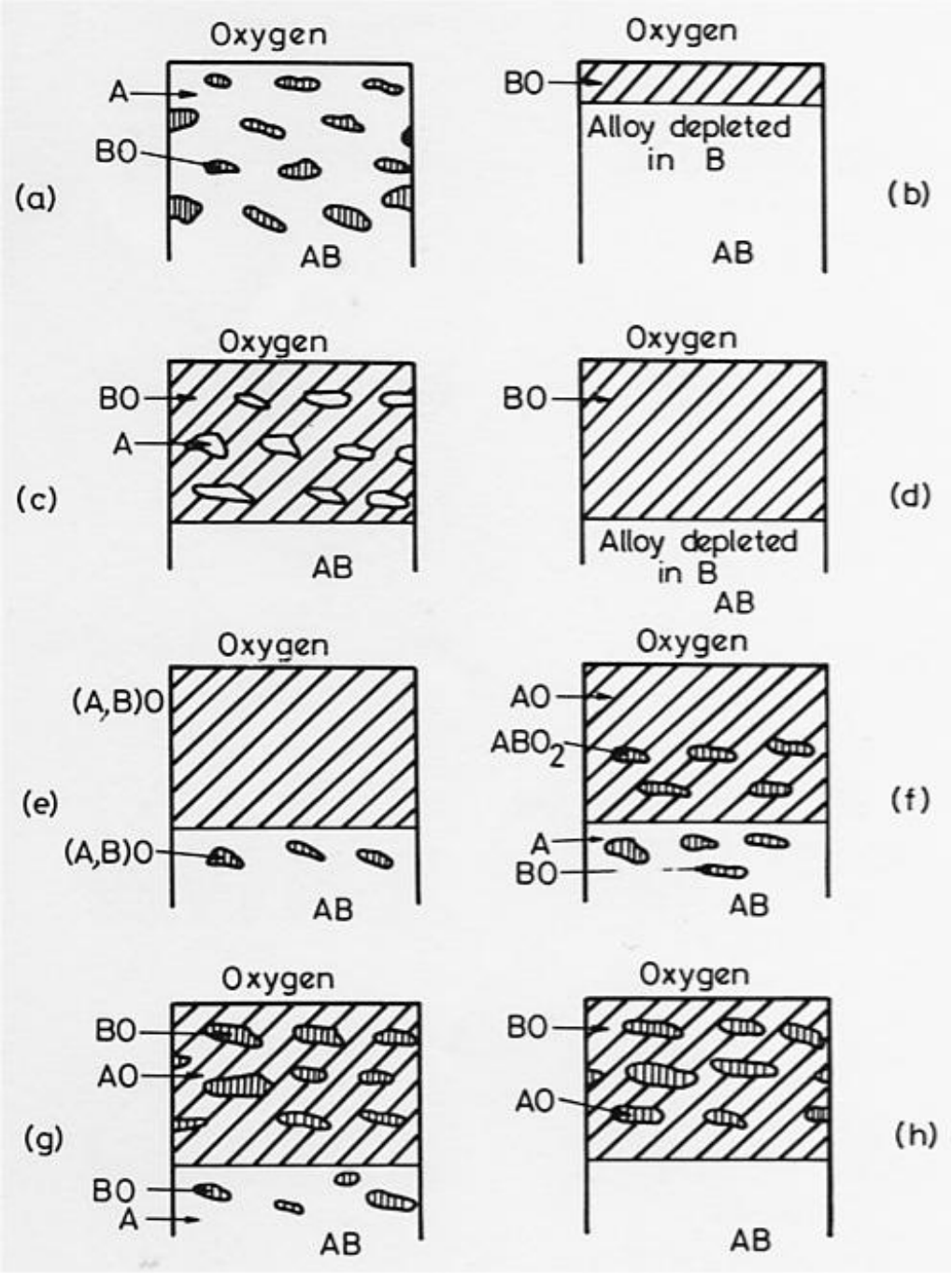

Figure 2-10 Schematic diagram: Classification of alloy oxidation **[41]**

a minor element B oxidises alone, giving internal oxide BO in matrix of A; ***b*** minor element B oxidises alone, giving external oxide BO above alloy depleted in B; ***c*** major element B oxidises alone, giving particles of A in matrix B of BO; ***d*** major element B oxidises alone, giving external oxide BO above alloy depleted in B; ***e*** A and B oxidise to give single solid solution or compound of variable composition (A, B)O; ***f*** A and B oxidise to give compound ABO_2 dispersed in AO matrix; ***g*** A and minor component B oxidises to give insoluble oxidises; ***h*** A and major component B oxidises to give insoluble oxidise with AO in BO matrix.

and the inward flux of oxygen atoms in the alloy (determined by the solubility and diffusivity of oxygen in the alloy). The caption of **Figure 2-10**, explains the meaning of the various diagrams. The concentration of B required to give protective scaling is not an invariant figure but depends on temperature, oxygen potential, surface nucleation sites, alloy substructure, etc.

2.4 Stress Generation in Scales

The previous sections considered how the high temperature corrosion resistance of a metal or alloy is determined by the nature of its protective oxide scale. If these scales crack or spall to expose the base metal directly to the environment, enhanced oxidation can take place. Thus, internal stress development as the oxide scale thickens is of great importance. These include stresses generated by the oxide(s) growth processes and thermal stresses on changing the temperature, which result from differences in thermal expansion between the oxide and the alloy.

2.4.1 Scale growth stresses

If scales are to be protective they must remain intact to the metal substrate. Stress generation in scales may result in the loss of adhesion or cracking and spalling of the film. The two principal sources of stress are growth stresses and thermal stresses. Growth stresses may arise due to a difference in the specific volume of the scales, which is rarely the same as that of the metal. The Pilling-Bedworth ratio (PBR) is used as a measure of sign and magnitude of the stresses caused by volume difference.

$$P.B.R = \frac{Volume\ per\ metal\ ion\ in\ oxide}{Volume\ per\ metal\ atom\ in\ metal}$$

This ratio for the majority of metals is greater than one, which indicates that the scales layer is likely to grow in compression. Typical values of oxides and sulphides are given in **Table 2.3**.

Oxide/Sulphide	Pilling-Bedworth ratio
NiO	1.65
Cr_2O_3	2.07
Nb_2O_5	2.68
V_2O_5	3.19
Al_2O_3	1.28
FeO (on α Fe)	1.68
Fe_3O_4 (on α Fe)	2.10
Fe_2O_3 (on α Fe)	2.14
TiO_2	1.7-1.78
CoO	1.86
Cr_2S_3	2.5
TiS_2	1.11
Al_2S_3	2.6
FeS	2.5
WS_2	3.47

Table 2.3 Pilling and Bedworth ratio for typical oxides and sulphides [**42, 43**]

This also allows the classification of oxides into two different categories:

- if the P.B.R. > 1 (which is the case for most metals), i.e. the specific volume of the oxide phase is higher than that of the metal, then the oxide is protective and the kinetics are generally of a parabolic type,
- if the P.B.R.< 1, then the oxide contains cracks and oxygen penetrates the scale and rapidly consumes the substrate. In this case the kinetics are generally linear.

In the very early stages of oxidation where oxide nuclei have an epitaxial relationship with the substrate, stresses may exist due to the difference in lattice parameter of the metal and the oxide, epitaxial constraints are reduced as the scale thickens. Changes in lattice parameters in alloys where a single component is oxidising and hence becomes depleted in the substrate, may also generate stress. Scales, which exhibit large deviation in

stoichiometry may also generate stresses which arise from a gradient in point defects across the scale with resulting variations in lattice parameters. Where metals oxidise via outward cation diffusion, vacancy injection may result in stress generation within the substrate.

2.4.2 Thermal stresses

Thermal stresses generated during cooling because of the difference in thermal expansion coefficients of metals and their oxide(s). In general the coefficient of thermal expansion of the oxide is less than that of the metal such that compressive stresses are set-up in the oxide. The large thermal stresses result in the cracking and spalling of the oxide from the metal surface [**44**]. The unconstrained mismatch strain $\Delta\varepsilon$ can be written simply as:

$$\Delta\varepsilon = \Delta\alpha_1 . \Delta T \quad \text{...} (26)$$

where ΔT is the change in temperature, $\Delta\alpha_1$ is the difference in thermal expansion coefficients. Typical values of thermal expansion coefficients for a selected systems are presented in **Table 2.4**. The ratio α_m / α_o is also quoted, where α_m is the expansion coefficient of the metal and α_o is the expansion coefficient of the metal oxide. If the ratio is greater than unity, then compressive stresses are generated in the scale on cooling. The greatest stresses occur for ratios significantly greater than one. Hence NiO scale on Ni tend to be adherent, whereas Cr_2O_3 scales on Cr tend to spall at the metal surface.

System	**Metal coefficient (α_m/K^{-1})**	**Oxide coefficient (α_o/K^{-1})**	**Ratio (α_m/α_o)**
Ni/NiO	17.6×10^{-6}	17.1×10^{-6}	1.03
Co/CoO	14.0×10^{-6}	15.0×10^{-6}	0.93
Fe/FeO	15.3×10^{-6}	12.2×10^{-6}	1.25
Cr/Cr_2O_3	9.5×10^{-6}	7.3×10^{-6}	1.30
$Ni\text{-}20Cr/Cr_2O_3$	$12\text{-}16 \times 10^{-6}$	7.3×10^{-6}	1.64-2.19

Table 2.4 Linear expansion coefficients of typical oxides and metals [**43**]

As well as the fracture of the scale and loss of adhesion to the substrate, plastic deformation of the oxide and substrate are further mechanisms of stress relief [**45**] and the adherence of films is strongly dependent upon film plasticity.

Grain boundary sliding and creep are proposed as the most favourable mechanisms of deformation, since slip is unlikely in oxides. The numerous models, which have been proposed for the origin and generation of stresses in oxides have been reviewed by Douglass [**45**] and Stringer [**46**]. Griffin *et al.* [**47**] studied the deformation behaviour of the Al_2O_3 formed on Fe_3Al after cooling from various temperatures. After cooling, the scale spallation from the substrate was found to be temperature dependent. Scale spallation was attributed to the difference of thermal expansion between the substrate and the scale. This finding is in agreement with the results obtained by Wright *et al* [**48**]. The thermal expansion coefficients of Fe_3Al alloy and Al_2O_3 at different temperatures are shown in **Table 2.5**. This demonstrates the need to design alloys and coatings, which can produce scales of better adhesion with their substrate at higher temperatures.

Temperature (K)	**Fe_3Al** ($\times 10^{-6}$ K^{-1})	**Al_2O_3** ($\times 10^{-6}$ K^{-1})
198	15.4	5.4
500	16.1	6.8
700	18.3	7.3
900	20.6	7.7
1100	22.1	8.0
1300	23.4	8.4

Table 2.5 Coefficient of thermal expansion of Fe_3Al and Al_2O_3 [**48**]

CHAPTER THREE

REPORTED HIGH TEMPERATURE CORROSION BEHAVIOUR OF TITANIUM- AND IRON- ALUMINIDES

CHAPTER THREE

3.0 REPORTED HIGH TEMPERATURE CORROSION BEHAVIOUR OF TITANIUM- AND IRON- ALUMINIDES

3.1 Introduction

The present chapter summarises the reported behaviour and the development of high temperature corrosion resistant Ti and Fe aluminides. Emphasis is placed on the high temperature corrosion behaviour of Ti-Al and Fe-Al intermetallics. The aim of the review is to asses the information available in the open literature regarding the corrosion behaviour of γ-TiAl and Fe_3Al alloys in particular.

The available information on the corrosion behaviour of Ti-Al alloys is summarised in **Section 3.2**. The mechanism and rates of the corrosion reaction of titanium aluminides at various experimental conditions reported in the literature are summarised. Previous attempts to study the effects of environmental gas composition (exclusively oxygen, nitrogen and sulphur) on the corrosion behaviour of Ti-Al systems are highlighted and critically assessed. The effects of Ti-Al alloy composition and surface treatments to this class of materials at high temperatures are also concluded in this chapter.

The current understandings of the mechanism of Al_2O_3 scale formation and growth on Fe-aluminides are outlined in **Section 3.3**. Views emphasising the RE effect in relation to Al_2O_3 growth, features and adhesion are briefly discussed. Various aspects of the main methods of RE additions to Al_2O_3-forming materials are summarised. Transport processes and the role of stresses in relation to oxide integrity and adhesion to Fe-aluminides are also discussed

3.2 Reported High Temperature Corrosion Behaviour of Titanium-aluminides

3.2.1 Introduction

Titanium-aluminides based on the intermetallic phase in particular are a new group of intermetallic alloys with a relatively low density (~ 3.76 g/cm^3) and good strength at high temperatures. Gamma titanium aluminide (γ-TiAl) could for example replace nickel-base alloys in certain aircraft engine components. Industrial applications of γ-TiAl above 700°C, however, are still restricted due to the insufficient corrosion resistance of these materials [**49-62**].

The corrosion behaviour of titanium and Ti-Al alloys has been studied by many researchers [**63-82**]. The nature of the oxide scale on titanium aluminides is more complex than that of pure titanium. The scale on Ti-Al is a mixture of fast-growing TiO_2 and potentially protective slow growing Al_2O_3 [**83-98**]. Even though Ti-Al alloys contain about 50 at%Al, this is not sufficient to form a long-lasting protective alumina layer at high temperatures (> 700°C) in air. Poor oxidation resistance of Ti-Al systems in air at high temperatures initially results from the formation of Al_2O_3, TiO_2 (rutile), Ti_2AlN and TiN [**7-10**], with the latter two near the scale/substrate interface. After longer exposure times, the mixed corrosion scale was overgrown by relatively fast growing TiO_2 [**99-106**]. However, since Al_2O_3 does not form a continuous barrier in TiO_2/Al_2O_3 mixtures, generally the scale is non-protective. For long-term oxidation resistance, the formation of an α-AI_2O_3 barrier in the metal/oxide interface zone is necessary.

Corrosion by gaseous environments containing sulphur is a serious problem in various technical high temperature processes, since sulphidation can significantly reduce the service life of metallic components. Whereas in strongly oxidizing conditions adequate corrosion resistance can be achieved, this is more difficult in environments characterized by a low oxygen and high sulphur activity. In these atmospheres the simultaneous nucleation of

sulphides as well as oxides was observed [**64-67, 107-118**]. A great deal of research work has been undertaken to improve the corrosion behaviour of Ti-Al alloys by adding ternary and quaternary elements [**111-117, 119, 120**]. From these studies, both beneficial and detrimental results have been reported and even apparently contradicting conclusions were obtained. This might be partly caused by differences in alloy purity, since several alloying elements have been demonstrated to possess a significant effect on the corrosion properties, even if they are present in small quantities. Also differences in alloy conditions and reactive gas composition can affect the corrosion behaviour of the materials under investigation.

3.2.2 Mechanism and Corrosion Rates of Titanium-aluminides

The oxidation resistance of γ-TiAl-based alloys becomes poor at temperatures near or about 700°C [**121**]. According to Taniguchi [**122**], that is because of the following reasons: (1) the little difference in free energy of the oxidation between aluminium and titanium; (2) the larger oxidation rate of titanium than that of aluminium; (3) the high solution content of oxygen in TiAl; (4) the small diffusion rate of aluminium in TiAl, and (5) the internal oxidation tendency of aluminium in TiAl. Therefore, improving the oxidation resistance of this alloy is key to its practical application. The research activities in this field including surface treatment and alloying addition were extensively carried out, but the achievement of adequate oxidation resistance is still a matter of concern.

It seems likely that the reduction in oxygen diffusion into Ti-Al alloys is a consequence of the improved barrier properties of their oxide scale and the subsequence inhibition of oxygen diffusion through this scale. If aluminium is substituted into the rutile lattice, according to the Wagner-Hauffe theory, the trivalent (Al^{3+}) cations will cause an increase in the number of anion vacancies and consequently enhance their rate of diffusion. Accelerated oxidation is not observed, which might suggest that aluminium takes up interstitial positions

in the rutile. A modification of the flux of oxygen across the scale may arise from a reduction in the rate of ionic charge in the presence of alumina, which has a lower rate of ionic conductivity than rutile. In addition to the electronic effects, which inhibit the diffusion of oxygen through the scale, alumina-containing scales are more protective because they are less porous and have improved adhesion. The multi-layering of oxide scales is less distinct in the mixed scales and the oxide layers are thinner. Hence scales become denser as the aluminium content increases and oxygen has more limited access to the metal/oxide interface.

From the above background self-diffusion data on Ti and Al in Ti-aluminides are necessary to understand the corrosion mechanism of Ti-Al systems and also for the interpretation of the Ti-Al high temperature corrosion phenomena. Unfortunately, experimental studies of diffusion in the Ti-AI system are hampered primarily by the non-availability and expensive radioactive isotopes of Ti and Al. ^{44}Ti is the only suitable radiotracer for Ti [**123**], but it is produced by a nuclear reaction at a cyclotron and is very expensive. The only suitable isotope for Al, ^{26}Al [**123**], which is also a cyclotron product; it is even more expensive than ^{44}Ti and, in addition, has very low specific activity.

Herzig *et al* [**124**] launched a broad programme of extensive experimental investigations of diffusion in the Ti-Al systems. Such investigations included lattice diffusion in different phases of the system and grain boundary diffusion and diffusion along γ/α_2 interfaces. To date, their efforts have resulted in accurate measurements of lattice self-diffusion and Al impurity diffusion in pure α-Ti [**124**], and Ti self-diffusion and single-phase inter-diffusion in bcc Ti-Al alloys [**125**] and in the Ti_3Al aluminide [**126, 127**]. However, Sprengel *et al*. [**128**] could not make any reasonable evaluation of Al diffusivity in TiAl by combining their interdiffusion coefficients with the data of Kroll *et al.* [**129**].

Recently, the work of Herzig *et al.* [**123**] led to accurate measurements of ^{44}Ti self-diffusion coefficients in γ-TiAl over a wide temperature range (**Table 3.1** [**123**]). They also

studied diffusion in three different Ti-Al materials with near-stoichiometric compositions. One of the materials used was the same material as that studied by Kroll *et al*. [**129**].

T (ºC)	Φ	D_{TiAl} (m^2/s)	D_{Ti} (m^2/s)	D_{Al} (m^2/s)
900	3.596	2.07×10^{-17}	1.18×10^{-17}	2.40×10^{-18}
1000	3.088	2.23×10^{-16}	8.87×10^{-17}	3.52×10^{-17}
1100	2.885	6.40×10^{-16}	2.17×10^{-16}	1.69×10^{-16}

Table 3.1 The thermodynamic factors (**Φ**), chemical diffusion coefficients of TiAl ($\mathbf{D}_{TiAl}$), titanium and aluminium self-diffusion coefficients ($\mathbf{D}_{Ti}$ and $\mathbf{D}_{Al}$) at various temperatures [**123**]

They [**123**] evaluated Al self-diffusion coefficients in TiAl by using their new Ti self-diffusion data and the interdiffusion coefficients obtained by Sprengel *et al.* [**128**]. The calculations of Herzig *et al.* [**123**] suggest that, in the compositions studied experimentally, Ti diffusion at low temperatures is dominated by the vacancy mechanism. At higher temperatures the anti-structural bridge mechanism can essentially contribute to the overall diffusivity, which can explain the experimentally observed non-Arrhenius behaviour of Ti diffusivity. Al diffusion occurs predominantly by the vacancy mechanism, but 3-jump cycles and especially anti-structural bridges can also play an important role. These results were in agreement with their experimental data and their calculations predict that Al diffuses with a higher activation energy than Ti. These findings are very useful for the interpretation of our oxidation results of γ-TiAl as presented and discussed in **Chapter 6** and **7** respectively.

3.2.3 Effect of Environmental Gas Composition on the Corrosion Behaviour of Ti-Al Alloys

The reaction of gaseous species (exclusively oxygen) with titanium and titanium-aluminides at different temperatures has been studied in numerous investigations [**130-143**]. A comparison of the different studies however, shows large disagreement and discrepancies in both the mechanism and rates of their corrosion. The reasons for this lie in the complexity of processes involved in the reaction, the different temperatures and pressures of the reacting species. Also the corrosion reaction is influenced by the alloy composition and surface conditions. Several studies by various researchers have dealt with the influence of various alloy composition and surface conditions [**62, 144-152**]. Both improved and decreased environmental resistance of Ti-Al were reported. However, the studies regarding the influence of gaseous species on their corrosion behaviour have been relatively few. The influence of nitrogen in oxidising gases has been discussed in several papers [**6-10**]. These studies imply that the oxygen partial pressure and the presence of nitrogen in air may have some influence on the corrosion behaviour of Ti-Al. Previous attempts to explain the effects of nitrogen, oxygen and sulphur on the corrosion behaviour of Ti-Al are discussed in this section.

Effects of nitrogen on corrosion behaviour of Ti-Al alloys

The majority of the oxidation experiments of Ti-Al intermetallics were performed in air. In general, the oxidation rate was found to be faster in air than in oxygen, and the scatter of the oxidation curves in air is much larger than in oxygen. The oxidation curves relevant to the effect of nitrogen on the oxidation behaviour of Ti-Al systems presented in the literature [**7, 10**] are summarised in **Figures 3-1** to **3-4**, but most – if not all – of these results are contradictory and not satisfactorily understood and need further investigation. Meier *et al.*

[**7**] studied the oxidation of Ti-52 at%Al at 900°C in various atmospheres including air and pure oxygen gas and also in oxygen mixed with different (2, 10, 90, 98 and 100%) nitrogen-containing atmospheres (**Figure 3-1**). Such comparisons of the oxidation behaviour of TiAl without paying attention to the effect(s) of oxygen partial pressure – free of nitrogen – in the reactive gas were detected. Meier *et al.* [**7**] concluded that protective alumina scales in pure O_2 were formed, while in nitrogen-containing atmospheres, continuous alumina scales could not form, but intermixed TiO_2/Al_2O_3 nodules were detected. The density of these nodules was found to be increased as the nitrogen concentration increased in the reactive atmosphere. Also their [**7**] AES results revealed the formation of N_2-rich (not specified) layers. However, the oxidation results of Ti-Al by Zheng *et al.* [**10**] in air and Ar/O_2 atmospheres (**Figure 3-2**) showed contrary – beneficial – effects of nitrogen for Ti48Al-5Nb at 900°C. The beneficial effect of nitrogen was attributed to the internal oxidation of Nb-containing alloy, which occurred during exposure in Ar-20%O_2 [**10**]. However, in the same study of Zheng [**10**] at 900°C, opposite – detrimental – effect of nitrogen were observed for Ti50Al (**Figure 3-3** [**10**]). When comparing oxidation kinetics in air and pure oxygen, two possible effects should be taken into account:

- possible nitridation – especially at high temperatures – in hot air where the pO_2 is equal to ~ 0.2 x 10^5 Pa and
- the oxygen partial pressure, for example pO_2 in pure O_2 is ~1 x 10^5 Pa, i.e. it is five times higher than in air.

The thermogravimetric method was used by Zheng *et al.* [**10**] to study the nitrogen effect on the oxidation behaviour of Ti-Al alloys. The thermogravimetrical analyses were carried out during which the gas atmosphere was changed from air to Ar-20%O_2 and vice versa, without intermediate cooling of the specimen (**Figures 3-4**). The results showed, that

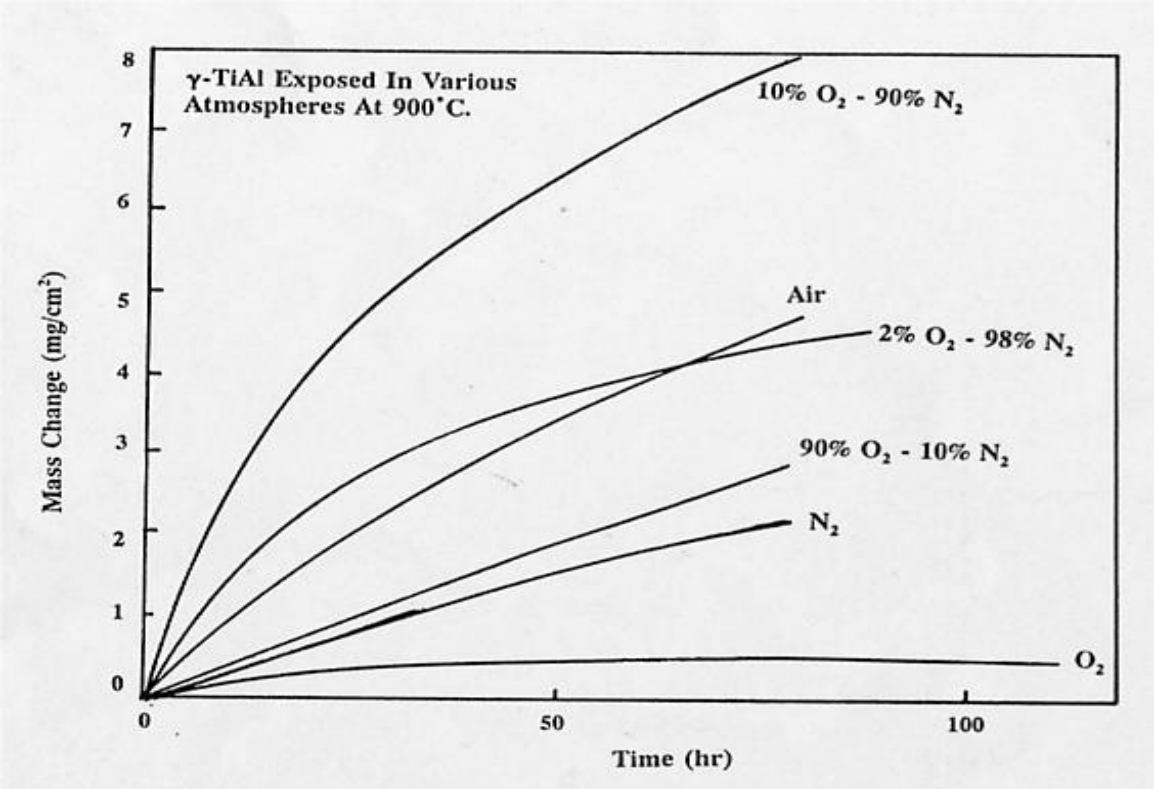

Figure 3-1 Weight change versus temperature for Ti-52 at%Al oxidised at 900ºC in various atmospheres [**7**]

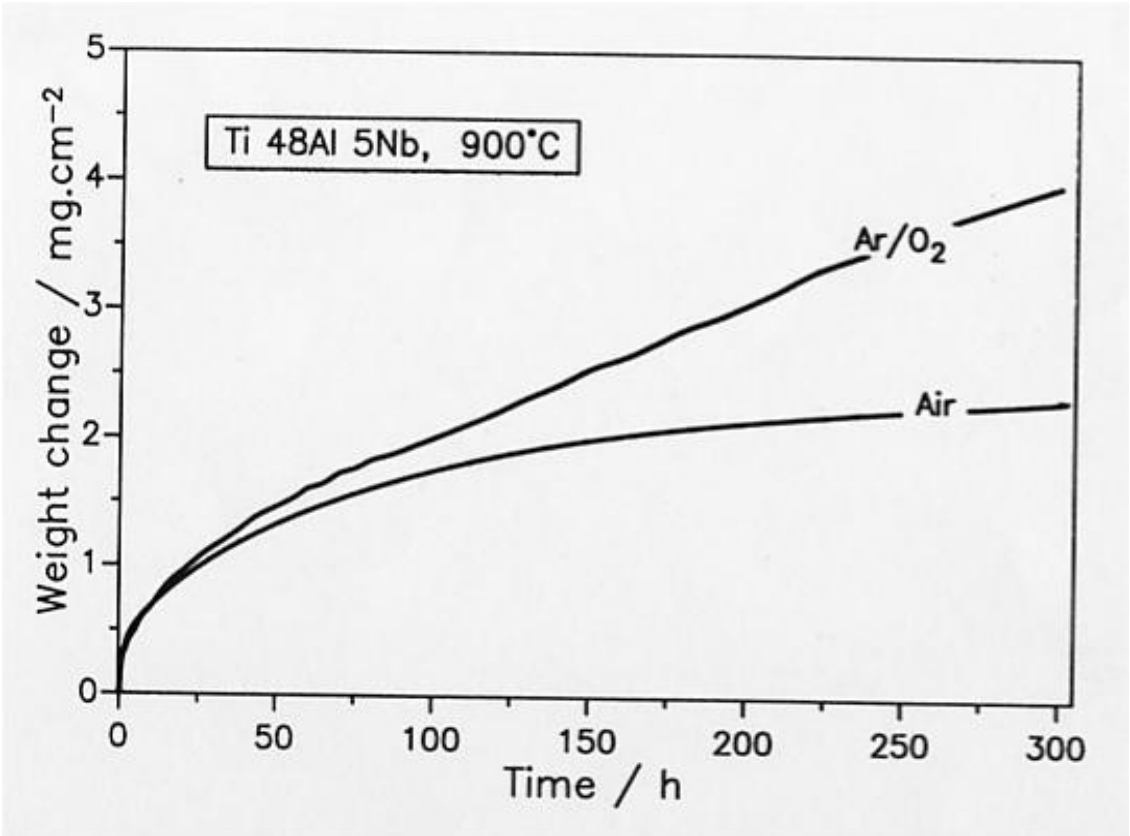

Figure 3-2 Weight change versus temperature for Ti-48 at%Al oxidised at 900ºC in various atmospheres [**10**]

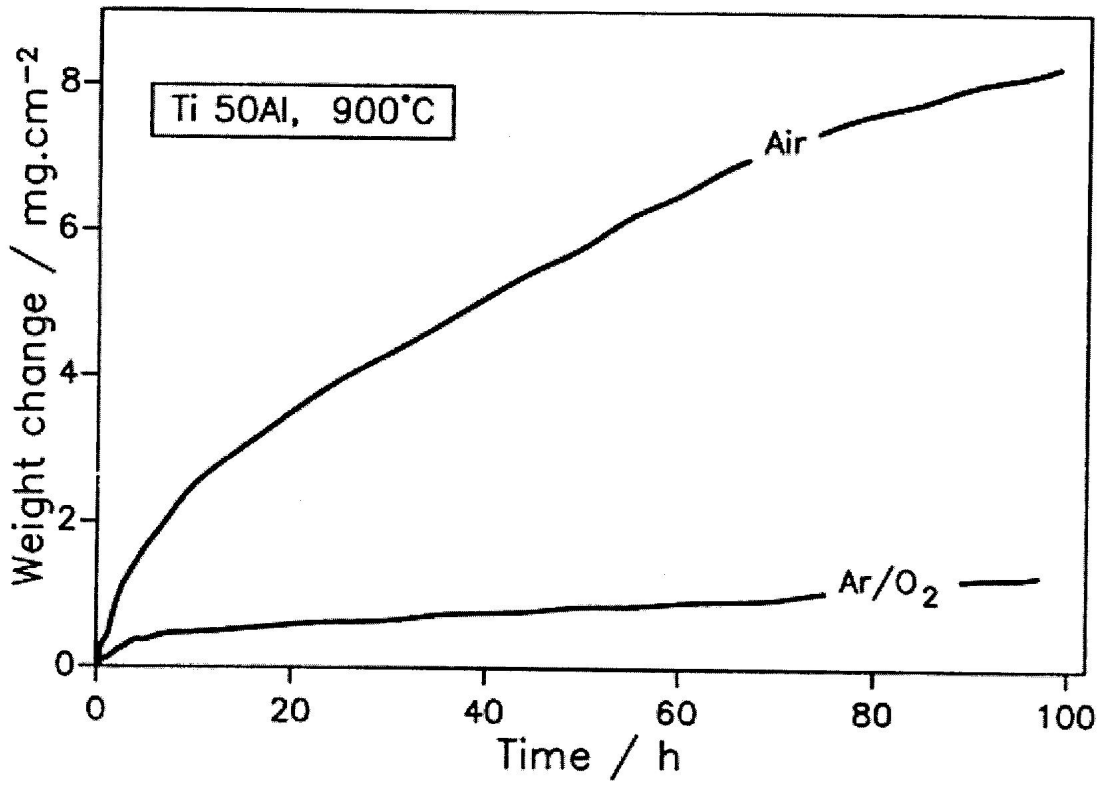

Figure 3-3 Thermogravimetric analysis of Ti-50 at%Al during oxidation at 900ºC in different atmospheres [**10**]

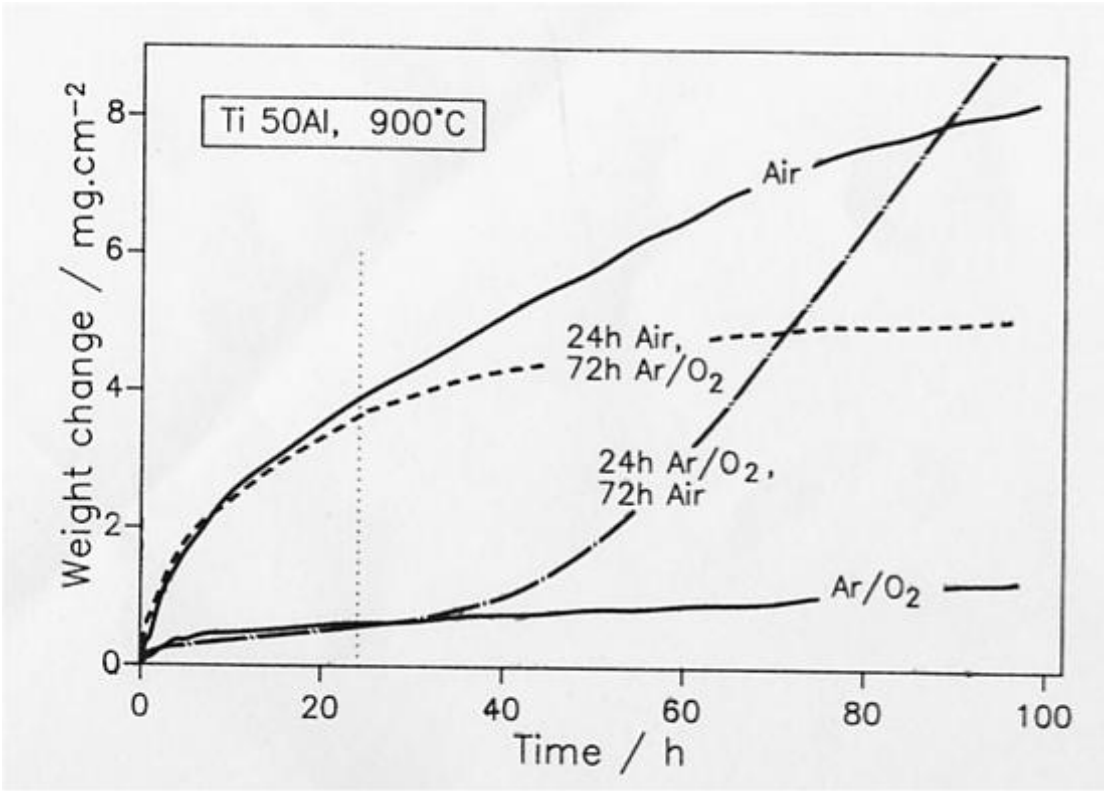

Figure 3-4 Thermogravimetric analysis of Ti-50 at%Al during two stage oxidation at 900ºC in which the gas atmosphere was changed from Ar-O_2 to air and vice versa [**10**]

nitrogen – in air – adversely affected the formation of the initially formed alumina scale and it enhanced the growth rate of the rapidly growing Ti-rich oxide. These effects were observed in the Ti-50Al alloy investigated, but their themogravimetric results indicated an opposite effect of nitrogen for the Ti-48Al-5Nb alloy. However, Choudhury *et al.* [**6**] concluded that the faster oxidation of TiAl in air as compared with that in oxygen was due to nitridation in air. The mechanism by which the nitrogen adversely affects the oxidation behaviour is still not yet satisfactorily understood. It is clear that the authors [**10**] neglected the pre-oxidation effect (before changing over to the second atmosphere – in the first step of oxidation) in each atmosphere on the subsequent oxidation behaviour of the specimen. In order to clarify the contradictory results (regarding the nitrogen effect) on the oxidation behaviour obtained by Zheng [**10**], these results should be referred to other oxidation studies of Ti-Al where the effects of pre-oxidation on the corrosion behaviour were observed [**153, 154**].

Effects of oxygen partial pressure on corrosion behaviour of Ti-Al alloys

Taniguch *et al.* [**155**] used commercial gases (O_2, Ar-21%O_2, Ar-1%O_2, He-1%O_2 and Ar) to explain the effects of the partial pressure of oxygen on the oxidation behaviour of γ-TiAl. These gases contained relatively high levels (1 to 2.6 ppm) of impurities such as CO_2, N_2, H_2O and H_2. All the oxidation curves of their study showed mass gains larger than those expected from parabolic rate laws. The oxidation curve at 1000°C in O_2 was the lowest and it became higher as the oxygen partial pressure decreased in the reactive atmosphere. Surprisingly, the oxidation kinetic results (**Figure 3-5**) in Ar showed the highest mass gain at the same exposure temperature. That was probably because of the other oxidants present in the Ar such as CO_2, H_2, and H_2O. Rapid increase of the mass gain in Ar atmosphere was attributed by Taniguch *et al.* [**155**], as due to the presence of nitrogen (< 2ppm) in the

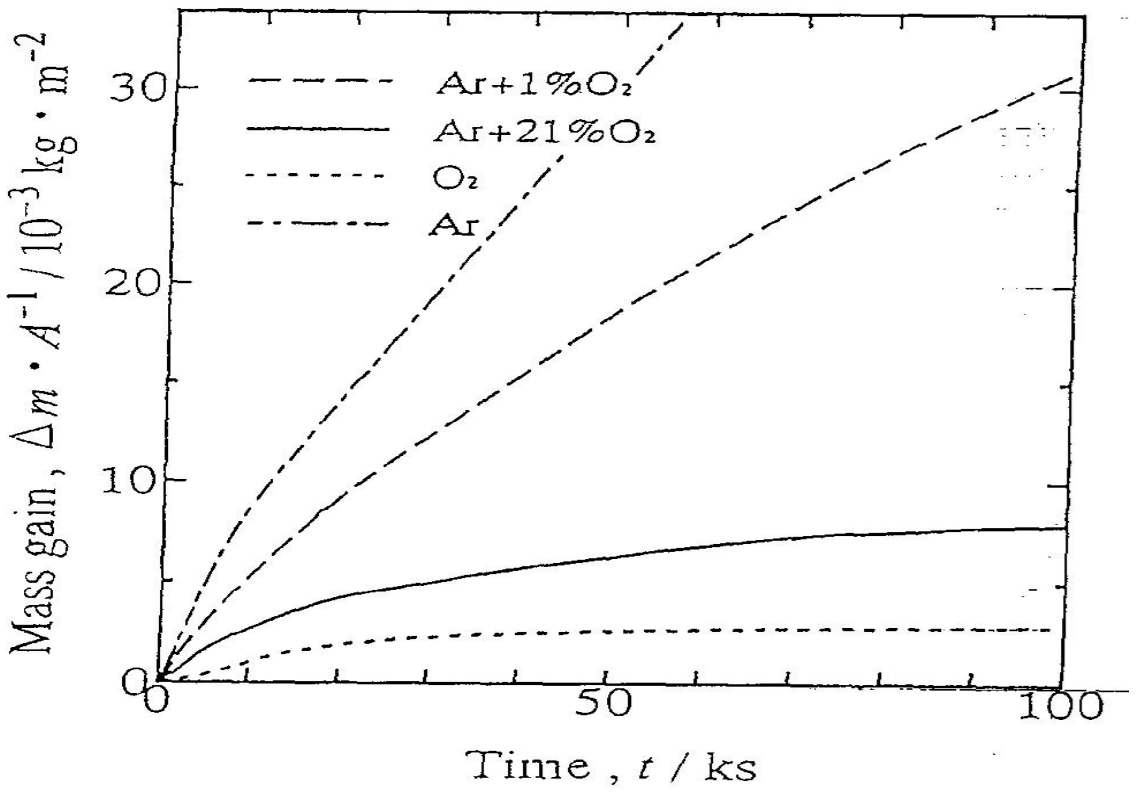

Figure 3-5 Oxidation curves of TiAl at 1027ºC in various gases under atmospheric pressure [**155**]

reactive atmosphere. In fact the rapid increase of the weight gain of the experimental material used by Taniguch *et al.* [**155**] in Ar atmosphere was due to the presence of water vapour (H_2O). The significant effect of water vapour on the γ-TiAl corrosion behaviour was experimentally examined by the present author (see **Figure 3-6**) and also by others (e.g. Kremer – **Figure 3-7** [**156**]). Also, Shigeji *et al.* [**157**] reported that water vapour in the O_2 significantly increased the oxidation rate of TiAl at 727 and 927°C. They [**157**] concluded that the oxidation mass gain significantly increased as the H_2O content increased in the atmosphere and the oxidation rate followed approximately linear kinetics laws at 927°C. The dramatic increase of the weight gain was attributed by Shigeji *et al* [**157**] due to the formation of high intensity of TiO_2 grains in the H_2O-containing atmospheres. Although the outer surface morphology of the scale formed on Ti-Al in the H_2O-containing atmospheres was very different from the normal morphology of such alloys in air and O_2 cited

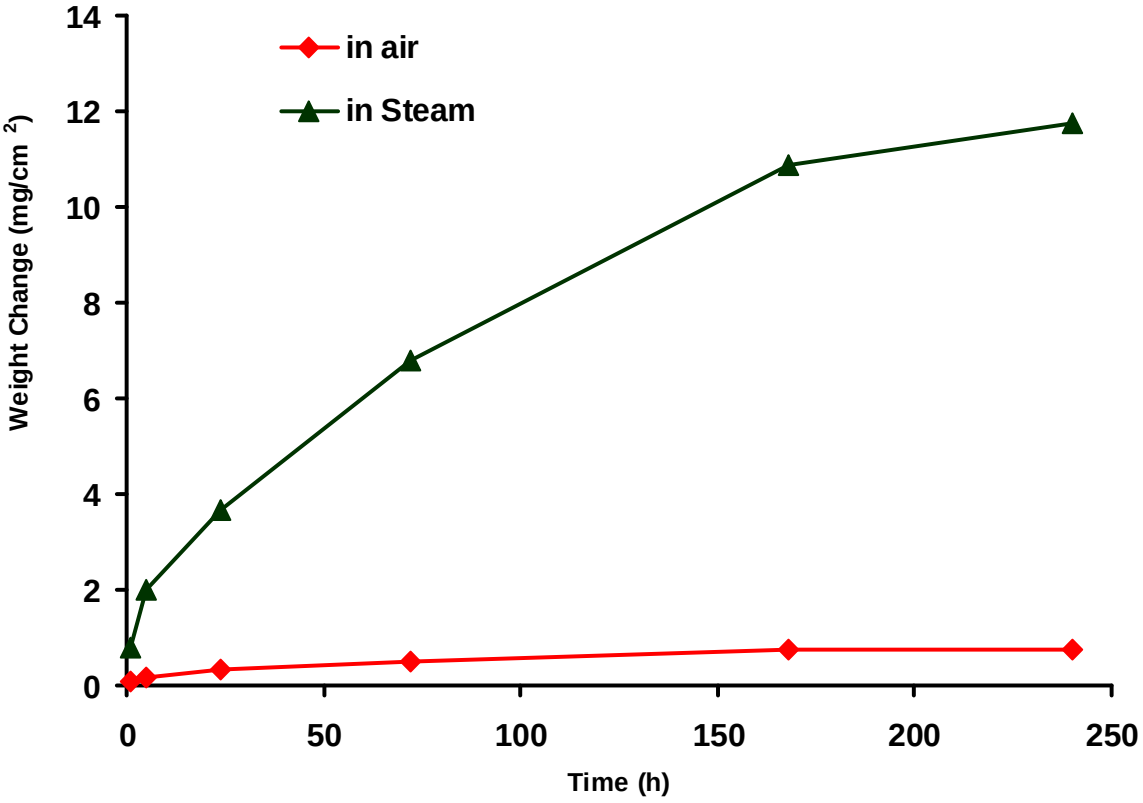

Figure 3-6 Effect of steam on the oxidation of Ti-46.7Al-1.9W-0.5Si alloy at 850ºC

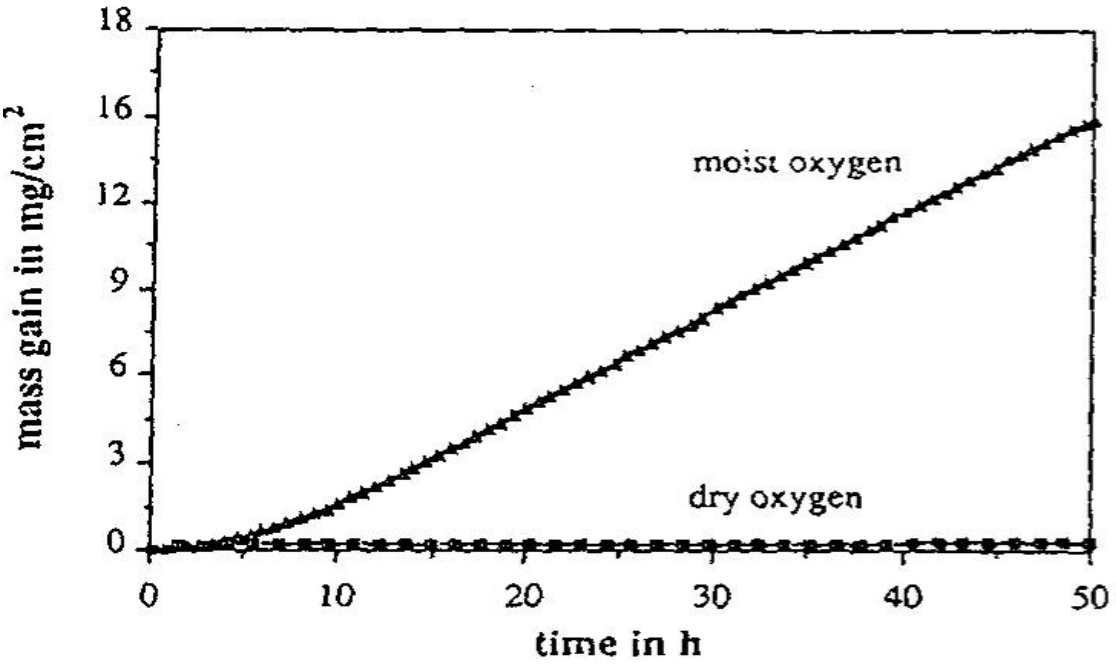

Figure 3-7 Effect of moisture on the oxidation of Ti50 at%Al at 900ºC [**156**]

in the literature, no hydride(s) formation of Ti and/or Al was reported by Shigeji *et al* [**157**]. Another effort to explain the effects of the partial pressure of oxygen in the oxidising environment of Ti-Al systems was undertaken by Becker *et al.* [**8**]. The study showed contrary effects of oxygen partial pressure to the finding of Taniguch *et al* [**155**]. The oxidation rate of TiAl-V reported by Becker (**Figure 3-8** [**8**]) in oxygen was higher than in Ar-1%O_2 at a single temperature (900°C). It should be noted that the purity of the used argon-oxygen gases was not mentioned in the report of Becker [**8**]. In the same study, Becker *et al*. [**8**] extensively investigated the transport processes through Ti-Al scales. The authors concluded, the formation of protective Al_2O_3 increased with the increase of oxygen partial pressure in the reactive atmosphere. This was believed due to; (i) the low solubility of Al_2O_3 in TiO_2 at higher oxygen pressures (the exact relationship is still unclear – refer to **Section 2.2.3**) and (ii) low defect structures in Al_2O_3 if compared to that in TiO_2. The consequences of Al_2O_3 formation (**Figure 3-9**(**a**) at the outer part of the inner layer (at higher oxygen pressures), is that it reduced the oxygen flux through the scale. Once a diffusion 'Al_2O_3' barrier has begun to form, the discontinuity at the border between the inner and outer layers of the scale increased (**Figure 3-9**(**b**) [**8**]).

Corrosion behaviour of Ti-Al in high sulphur and low oxygen potential environments

Ti-Al intermetallics developed for good oxidation resistance may suffer rapid sulphidation attack in several technical processes, such as those involved in the fossil-fuel industry, oil refining and coal gasification, containing appreciable partial pressures of sulphur (~ 1 Pa) and low partial pressures of oxygen (~ 10^{-15} Pa) [**42, 158-166**]. In spite of the extensive research developed on the oxidation of Ti-Al intermetallics, very little work has been done for these alloys under environments containing both sulphur and oxygen. Special interest to understand the mechanism of Ti-Al alloys scale formation especially in

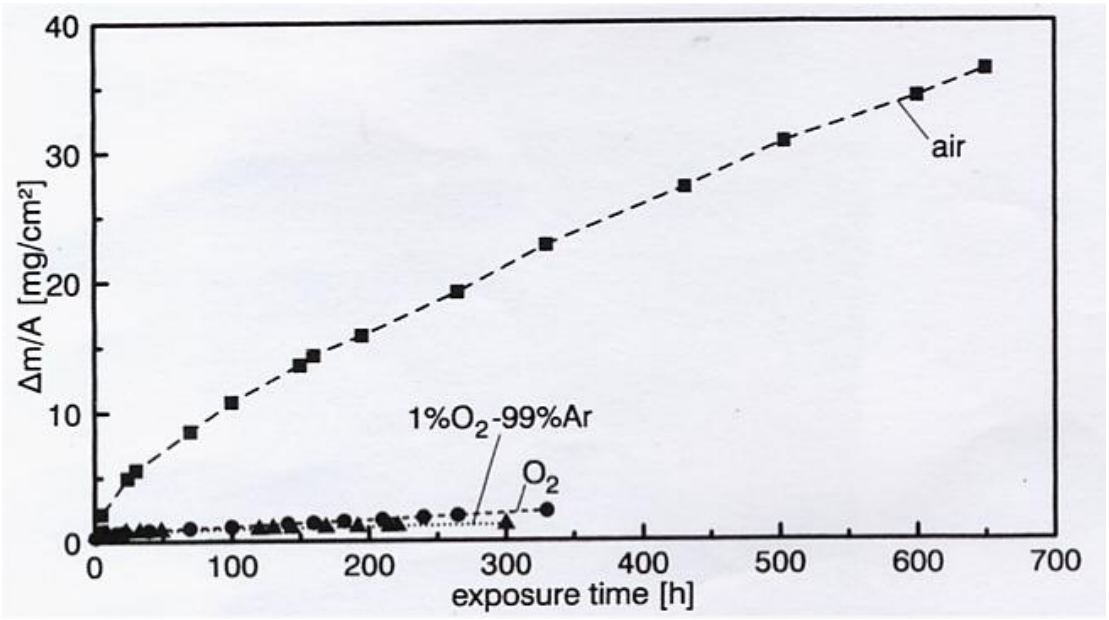

Figure 3-8 Mass gain-time curves of TiAl-V at 900ºC in air, 100%O_2 and 1%O_2-99%Ar [**8**]

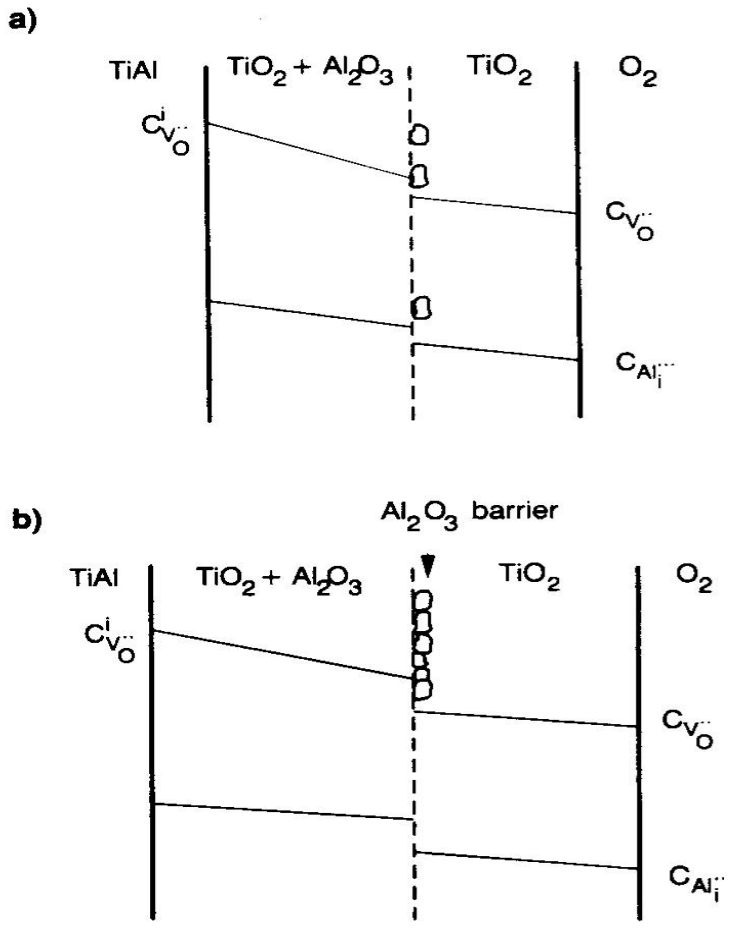

Figure 3-9 Becker [**8**] model for the formation of an Al_2O_3 barrier layer at the border between inward and outward growing parts of the TiAl scale in Ar-O_2 atmosphere

environments of relatively high partial pressure of sulphur and low oxygen activity. Recently, Takayuki *et al.* [**110**] and Kai *et al.* [**167**] extensively investigated the effect of Al content on the Ti-Al alloy scale protectivity in $H_2/H_2S/H_2O$ gas mixture over a wide range of temperatures. General agreement between the authors [**110, 167**] regarding the effect of Al and they concluded that the corrosion behaviour of Ti-Al intermetallics improved with increasing the aluminim content in the alloys. The scale was found to be mainly consisting of rapid growing TiO_2 and Al_2O_3 with a mixture of Ti and Al sulphides.

It is considered that improvement in oxidation/sulphidation resistance may also follow the addition of ternary or even quaternary elements. However, the influence of alloying elements on the mixed gas corrosion and in the presence of deposits is less well understood. Datta *et al.* [**67**] studied the effects of Nb additions on the scaling behaviour of Ti-Al alloys in $H_2/H_2S/H_2O$ gas mixtures of various partial pressures of sulphur at 900°C. Significant reduction in the sulphidation rate of Nb-containing alloy if compared with the binary TiAl was observed. The improvement was attributed to the formation of inert zone of Nb-sulphide [**67**]. However, Datta [**67**] for Ti-48Al-2Nb-2Mn would suggest that even with the addition of Nb this alloy has significant oxidation/sulphidation problems. Prevention of such corrosion by coatings and other surface modifications is a promising route. More recently Takeshi *et al.* [**120**] studied the effect of 2 at% addition of X (X = V, Fe, Co, Cu, Nb, Mo, Ag and W) to TiAl alloy sulphidation behaviour at 900°C. Sulphidation attack of the alloys were almost the same as that of TiAl, while the thickness of the alloy surface layer decreased in the order: V > Co > Fe > Mo > Cr > W and Nb. The sulphide scale was found to be composed of multi-layer structures: an outermost (rich in Ti sulphides), an outer (rich in Al_2S_3), an inner (a mixture of Ti-sulphides and Al_2S_3) and innermost (rich in Ti-sulphides) layer. Comparison study by Du *et al.* [**64**] of the sulphidation behaviour of pure titanium and Ti-Al-V alloy revealed considerable improvement to the sulphidation behaviour of Ti-Al after V addition to the alloy. In another sulphidation/oxidation study by

Du *et al.* [**168**] for two Ti-46.6Al-1.4Mn-2Mo (at%) alloys with duplex and laminar microstructures, the corrosion resistance for the alloy with a laminar microstructure was slightly better than the alloy with duplex structure. Both materials showed superior corrosion resistance at 900°C to that at 750°C. The difference is attributed due to the higher oxygen partial pressure in the environment at 900°C, which altered the defect structure [**168**]. Du *et al.* [**169**] and Takayuki *et al.* [**110**] also studied the effect of sulphur partial pressures on the degradation behaviour of Ti-Al alloys. In the study of Du *et al* [**169**], it was found that the sulphidation amount decreased with increasing the partial pressure of sulphur in the atmosphere, whereas opposite results was obtained by Takayuki *et al.* [**110**]. However, both authors [**110, 169**] concluded that the higher aluminium of Ti-Al alloy exhibited a superior resistance to sulphidation/oxidation resistance.

3.2.4 Effect of Ti-Al Alloy Composition

In spite of their high aluminium content, TiAl-based intermetallics do not generally form long-lasting protective alumina scales [**7, 50, 170**]. After longer exposure times, the scales, which are initially rich in alumina, deteriorate and scales consisting of mixed alumina (Al_2O_3) and titania (TiO_2) predominate, with high growth rates similar to those of pure titania. For this reason the addition of other elements by alloying to improve the corrosion resistance has been studied by several authors [**171 - 184**]. The situation is rather complicated since elements, which might be beneficial for high temperature corrosion, might adversely affect the mechanical properties. Additionally, the published corrosion data show significant scatter and even lead to contradicting conclusions. This is possibly partly caused by differences in alloy purity, because several alloying elements have been demonstrated to possess a significant effect on the corrosion properties even if they are present in small quantities. Hence, there is need for a fast screening procedure of possible

alloying elements with respect to their impact on the corrosion properties of these materials. Another important observation from the previous studies is that for the same alloy composition and very similar environmental conditions, different results were derived. This implies significant effect of other alloy conditions such as surface conditions which must be considered during high temperatures corrosion studies.

Aluminium is a major alloying element in titanium materials, having effective solid solution strengthening and usefully low-density, its presence has a significantly beneficial effect on the oxidation behaviour. The higher the aluminium concentration, the greater the reduction in oxidation rate with respect to that of pure titanium. This applies to all of the oxidation studies [**185 - 187**]. Unfortunately, a high percentage of aluminium in Ti-Al systems is undesirable in terms of their mechanical properties. The critical concentration of aluminium is lowered by the addition of elements, which have the effects of reducing the solubility and diffusivity of oxygen, and increase the diffusivity of aluminium. Diffusivity of aluminium is increased in the (α_2+β) alloys if a larger proportion of β phase is retained. Thus the β stabilising elements are most effective in reducing the critical concentration of aluminium and therefore oxygen diffusivity. The addition of chromium to titanium has a marked influence on the oxidation behaviour, although the effect is complicated and not necessarily beneficial depending on the exact chromium content and temperature [**188 - 190**]. Concentrations up to 11 wt%, chromium have a very unfavourable effect on oxidation during exposure at low temperature, as would be predicted by the Wagner-Hauffe theory. At higher temperatures this situation is reversed and at about 800°C, the rate of oxidation is very much reduced over that of pure titanium [**191, 192**]. The addition of silicon is a significant factor in the alloy development for high temperature applications because of its beneficial effect on creep strength. If silicon is added to titanium, a reduction in oxidation rate will occur due to the formation of SiO_2, which follows a parabolic rate law extending to higher temperatures than for pure titanium. This effect is not directly proportional to silicon

content, although the reduction in oxidation rate is more pronounced at higher silicon levels [**188 - 190**]. Additions of third element to Ti-Al also have been investigated [**171 - 184**] to improve the corrosion resistance of Ti-aluminides at elevated temperatures, and some have shown significant improvements. On the other hand some elements showed detrimental or neutral effects on the corrosion behaviour of Ti-Al. Generally, addition of Nb, Ta, Si, W or Mo reduced the corrosion rate of Ti-Al [**191 - 193**]. Few studies were undertaken to study the combined effects of some elements on the corrosion behaviour of Ti-Al. For example, K. Maki *et al* [**180**] and Li *et al* [**194**] observed the improvement of oxidation behaviour of Ti-Al alloys after the combined addition of Si and Nb. However, the mechanism of the effect of both elements is not yet clearly understood.

Small additions of tantalum, of the order of 1 to 4wt%, were also found to improve Ti-Al oxidation resistance [**191, 192**] and the absence of evidence for the formation of tantalum oxides again suggests that rutile can dissolve large concentrations of Ta_2O_5 or tantalum sub-oxides [**195**]. Vanadium, however, forms volatile oxides and would therefore not have the same ability to improve scale properties as do niobium and tantalum. The addition of phosphorus to titanium aluminides has been found to be very effective in improving their oxidation resistance [**60, 62, 196**]. The reduction in the concentration of oxygen vacancies in the phosphorus-doped rutile seems the obvious explanation for this effect, however one might also be tempted to consider other factors such as ionisation potential and ionic radius, with respect to the mobility of anion vacancies. This effect has the significant implication that the addition of other Group V or VI elements in the periodic table, may also improve oxidation resistance.

3.2.5 Effect of Ti-Al Alloy Surface and Subsurface Conditions

Titanium alloys, in general, readily absorb oxygen leading to oxidation and alpha-case formation when exposed to high temperatures (> 500°C) in air. This is known to severely limit the high temperature capability of alloys in terms of their mechanical properties. In order for titanium alloys to be utilized more effectively at higher temperatures, the ingress of oxygen must be reduced, if not prevented completely. Recent results on bare IMI 834 alloy at different temperatures revealed that the thickness of the oxide scale and the depth of the alpha-case are proportional to the exposed temperature [**197**]. Also alpha-case formation becomes significantly enhanced at and above 800°C. This result stresses the need for application of surface modifications such as pre-oxidation, pre-sulphidation, ion implantation and surface coatings to avoid or to limit oxide scale growth. Surface modification techniques have been examined as a means of limiting ingress of reacting species from the environment by many researchers [**117, 198 - 200**]. However, this subject still needs further investigation.

Effect of Ti-Al alloy surface coatings

One approach of surface modifications is to develop corrosion resistant coating systems based on the usage of high melting point intermetallic layers to act as a diffusion barrier. This approach is not designed to entirely remove the brittle surface layer, but to engineer the intermetallic layer to act as a diffusion barrier, at a thickness considerably smaller than the alpha-case that would form on an unprotected titanium alloy. This will limit the potential reduction in mechanical properties of the alloys after extended exposure within corrosive environments at high temperatures due either to the ingress of reactive gases or secondary intermetallic phase formations.

Protective coatings are required for the successful application and performance of critical airfoil components in gas turbines. The success of a coating in a high temperature application is measured by its ability to remain in place, to resist corrosion, avoid cracking and limit diffusion between the coating and substrate [**201**]. The mechanical behaviour of the coatings is, however, also of importance in high-temperature cyclic oxidation, which is a point not often considered in coating selection or life assessment.

In some studies, For example, Manley *et. al.* [**202**] found that, while surface roughening can occur with coating-affected substrate melting, it is on a much grosser scale and at significantly higher temperature (1200°C) than that of the surface rumpling observed during cyclic oxidation testing. As expected, isothermally exposed specimens did not exhibit rumpling. He then showed that surface rumpling was dependent on the relative changes in strain that occur with thermal cycling. Deb *et al.* [**203**] attributed the amount of rumpling observed to a number of possible effects including coefficient of thermal expansion (CTE) mismatch, the thermal gradient across the coated specimen, the mechanical properties of the coating and the strain and/or thermal cycle experienced by the coating. It was proposed that thermal expansion mismatch could produce either compressive or tensile strains within the coating during cycling, depending upon the state of the CTE mismatch. It was established that for cyclic oxidation, the CTE value for the coating is less than the CTE value for the substrate and therefore the coating experiences compressive strain during cooling. The residual strain state at the start of the cooling cycle (and hence test hold time) is also important, as the low-strength coating can relax to a zero strain state, while the stronger substrate can maintain a significant strain level.

The effect of protective coatings on the oxidation resistance of Ti-AI alloys was widely investigated. Aluminising forms a $TiAl_3$ layer, which could improve the oxidation resistance of TiAl and Ti_3Al [**204, 205**]; MCrAlY overlay coatings could provide good protection for the TiAl alloy with rather low oxidation rate due to the formation of a continuous Al_2O_3

scale [**206, 207**]. However, these two kinds of conventional protective coatings, widely used for the protection of Ni-base super alloys, encounter some problems for the protection of TiAl due to the brittleness of the $TiAI_3$ phase or the severe coating/substrate inter-diffusion, which would be harmful to the long-term oxidation resistance and the mechanical properties of TiAl alloy. Recently, a new class of Ti-AI-Cr coatings has been proposed, providing excellent oxidation protection for TiAl intermetallics [**208 - 210**], e.g. low-pressure plasma spray Ti-51Al-12Cr coating [**209**] and magnetron sputtered Ti-50Al-I0Cr coating [**210**]. Other investigated coatings include nanocrystalline TiAl [**211, 212**], Si_3N_4 [**213**], SiO_2 [**214**], and Al_2O_3 [**214, 215**]. These investigations mainly emphasized their isothermal oxidation behaviours. However, prevention of Ti-Al alloys from both oxygen and sulphur at high temperatures by coatings is of practical importance. Datta, *et al* [**216**] have comprehensively reviewed this area. In this context, Du and Datta *et al*. [**66**] also demonstrated that the coatings of Nb and HfN significantly enhanced the oxidation/sulphidation resistance of Ti and Ti-based alloys. Titanium nitride (TiN) is widely used as a protective coating in multiple applications. TiN hard coatings, despite their excellent mechanical properties, could not be used at elevated temperatures in oxidising/sulphidising atmospheres due to their poor chemical stability. Additives such as Al, Si frequently improve the mechanical and corrosion properties of nitride coatings. An outstanding example is TiAlN coating which are commonly used in dry and high-speed machining operations on aluminium alloys and die steels due to their high temperature (up to 800°C) oxidation [**217 - 220**] and abrasion resistance [**221**]. Increasing the Al/Ti ratio (e.g. in case of AlTiN) in the coatings obviously improves its corrosion resistance at higher temperatures. The present work (see **Section 6.3.1**) showed that AlTiN coatings form stable, protective Al_2O_3 surface layer even at low oxygen activities. Al_2O_3 is also highly insulating oxide, with low ion mobility and acts as effective diffusion barrier to the reacting species such as oxygen and sulphur in the environment. CrN system is also a promising candidate

for high temperature applications and exhibits complementary mechanical and structural properties [**222**] to (TiAI)N coatings.

Although single-layer coatings are finding a range of applications in many sectors of engineering, there are an increasing number of applications where the properties of a single material coating are not sufficient. One way to surmount this problem is to use a multi-layer coating that combines the attractive properties of several materials, each chosen to solve a problem in the application. Simple examples of this include the use of interfacial bonding layers to promote adhesion, or thin inert coatings on top of wear-resistant layers to reduce the corrosion of cutting tools.

Despite the large amount of work present in the open literature on the mechanical and corrosion properties of different coatings on Ti-Al alloys, very few – if non – of the published work was devoted to study the corrosion behaviour for this class of coating (AlTiN, CrN, NbN) materials in sulphur containing environments. As part of the present work is concentrated on isothermal oxidation behaviour of Ti-46.7Al-1.9W-0.5Si alloy, also single (CrN and AlTiN) and multiplayer (AlTiN/CrN, AlTiN/NbN and CrN/NbN) coatings on the Ti-46.7Al-1.9W-0.5Si alloy were developed in order to examine their protectiveness to Ti-46.7Al-1.9W-0.5Si alloy in sulphidising/oxidising environments of relatively high partial pressure of sulphur and low partial pressure of oxygen at 850° C.

Effect of Ti-Al microalloying (ion implantation)

One of the possibilities to improve the corrosion behaviour of Ti-Al alloys is by microalloying (ion implantation). Ion implantation can serve as a research tool and has been used successfully by various researchers [**223 - 227**]. First, the concentration and depth of implantation can be reproduced and controlled with high precision. Secondly, a well-defined profile of the implanted element allows monitoring during oxidation [**228**]. Also, ion

implantation showed unique modification advantages in comparison with others. Because this process does not produce a coating, the dimension and bulk properties of the part remain unchanged, and implanted surfaces have no problems with adhesion and residual stresses. These features are particularly attractive when both oxidation and wear resistance are considered to be issues in a component. Microalloying relates to only a few hundred ppm or even less of the added element. It was found that implantation of Nb gives a good oxidation protection Ti-Al alloys [**225 - 227**] for high implanted doses of $1x10^{17}$ cm^{-2}. It was found recently, that very small amounts of chlorine dramatically improve the oxidation behaviour [**59, 228 - 230**] of Ti-Al alloys. The 'Cl effect' protects TiAl even at very low Cl concentration below 500 ppm.

Recently, ion implantation by the metal vapour vacuum arc (MEVVA) source method was tested to improve oxidation resistance of intermetallic compounds [**231, 232**]. It has been verified that the weight gain of Ti-48Al decreases noticeably with niobium and aluminium implantation, respectively. Also some experimental work of implantation of copper and yttrium in improving the oxidation of Ti-60 alloy has been done and has gained positive results [**233**].

Effect of Ti-Al alloy surface processing

Another effective and simple method of surface processing techniques to improve the corrosion behaviour of Ti-Al systems is the pre-formation – before exposure – of stable oxide or sulphide from the base metal or alloy. Various investigations of Ti-Al alloys oxidation behaviour shown that pre-sulphidation to develop a substantial sulphide scale can improve significantly the subsequent oxidation resistance of such alloys. For example, Yoshioka *et al.* [**113 - 115**], Toshio *el al.* [**117**] and Takeshi *et al.* [**120**] reported the formation of a $TiAl_3$ layer ($TiA1_2$ included) on the alloy surface by preferential sulphidation of Ti in high temperature sulphidation of a TiAl alloy. Oxidation experiments established

that scales of sulphidation processed TiAl alloy could be maintained over long periods of time in air at 800°C, in contrast to the rapid oxidation observed for the conventional TiAl alloy. This has been termed by the authors as the "sulphidation processing" method. In the early stage of oxidation, a sulphidation processed TiAl alloy oxidises like the $TiAl_3$ alloy. After some increase in exposure time, when the phase transformation from $TiAl_3$ to $TiAl_2$ is complete at about 22h, the amount of oxidation increased gradually to 111h and then abruptly after 277h. Compared with the conventional TiAl alloy, the sulphidation processed TiAl alloy demonstrates good high temperature oxidation resistance [**117**]. The process changing $TiAl_2$ to TiAl was not uniform especially where "under cutting" corrosion advances from locally degraded portions and may result in the loss of oxidation resistance. Yoshioka *et al.* [**113 - 115**] found with further oxidation, the thickness of the $TiAl_2$ decreased slowly and disappeared after about 1100h. The cross-section of the sulphidation processed TiAl alloy oxidized at 800°C in air for different times showed different structures. Yoshioka *et al.* [**115**] observed local degradation of a $TiAl_2$ layer, generated at the grain boundary of a TiAl substrate, and this seems to be due to a rapid diffusion of Al along the alloy grain boundary.

There appears to be at least two processes involved in the degradation of the $TiAl_2$ layer a formation of Al_2O_3 and TiO_2 at the airside and a decomposition of $TiAl_2$ to TiAl due to reaction diffusion at the alloy substrate side [**117**]. When a protective Al_2O_3 scale was formed, the oxidation reaction was observed to be very slow, and the rate of the phase transformation from $TiAl_2$ to TiAl may be presumed to play an important role in the rate of degradation. In the phase diagram of the Ti-Al system, the γ-TiAl phase has a composition range between 49 and 54 at% Al at 800° C. Therefore, there would be inward diffusion of aluminium from the $TiAl_2$ to the TiAI substrate and the decomposition rate may be controlled by the diffusion of Al into the TiAl alloy substrate because the diffusion in the $TiAl_2$ phase [**234, 235**] is much faster than in the TiAl phase [**117**]. In this case the grain

boundary of the TiAl substrate could act as a more rapid diffusion path for Al into the alloy substrate.

There are several options when trying to reduce the decomposition rate of $TiAl_2$ to TiAl. Below, the various aims are listed:

- reducing the number of alloy grain boundaries,
- decreasing the diffusivity along the grain boundary,
- increasing AI content in the alloy,
- decreasing in the diffusivity in TiAl,
- controlling microstructures,
- stabilising of an Al_2O_3 scale.

3.3 Reported High Temperature Corrosion Behaviour of Iron-aluminides

3.3.1 Introduction

Iron-aluminides based on Fe_3Al and FeAl are of interest for many land-based applications because of their appropriate mechanical and corrosion properties and low cost. However, until recently their potential use as structural materials was still in doubt due to severe spallation of their alumina scale(s) during cycling [**236 - 242**]. Recent studies indicate small additions of certain ‘’reactive’’ elements have a large beneficial effect on the oxidation behaviour of high temperature alloys [**243 - 252**]. This improvement, known as the reactive element effect (REE), has been used in the manufacture of high temperature, oxidation resistance alloys since their discovery. From an engineering perspective, the primary effect is a marked enhancement in the spallation resistance of protective oxide scales, such as Cr_2O_3 and Al_2O_3, grown on these alloys. However, the reasons for the beneficial effects of reactive elements are still not satisfactorily understood. Using advanced

analytical techniques, a new understanding has emerged of the REE on the Al_2O_3 oxide growth mechanisms, microstructures and adhesion to the Fe-Al substrates will be discussed briefly throughout the following sections of this chapter.

3.3.2 Microstructural Features and Adhesion of Al_2O_3 Scales

There are certain morphologies and microstructures, which are typical of a particular oxide, such as porous or dense scales, columnar or equiaxed grains, even oxide blades and whiskers. The review here concentrates on structures typical of Al_2O_3 scales of Fe-Al systems, especially those which related to the effects of RE. Each of these cases of scale features is briefly reviewed in this section in order to clarify their descriptions as will be used in this study. Scale adhesion testing during isothermal and cyclic conditions of undoped Fe-Al and doped with RE are compared and summarised.

Convoluted Al_2O_3

"Buckling" one of the common structures for undoped α-Al_2O_3 scales formed on FeAl and FeCrAl alloys and it is the case where a scale of uniform thickness is convoluted but the underlying alloy remains relatively flat. For the purpose of this study, a scale exhibiting this type of convolution will be referred to as "buckled". This type of structure is shown schematically in **Figure 3-10**(**a**). The scale in this case has buckled, leaving voids between the alloy and the oxide. In view of the reduced contact between the metal and the oxide, poor adhesion is the inevitable consequence.

Smialek *et al*. [**252**] noted the buckling of Al_2O_3 scales grown on FeAl at 1100°C, this morphology was also noted by Golightly *et al*. [**253**] in Al_2O_3-formers at 1200°C on FeCrAl without RE addition. This structure was attributed to the lateral growth of the scale due to the mixed mode of oxidation, i.e. both Al and O diffusing simultaneously. Poor oxide

adherence was also observed [**253**], whereas in the same study for a Y-containing alloy, no buckling was observed. The doped scale was uniform in thickness and relatively flat, as was the alloy/oxide interface. The elimination of scale buckling was attributed to Y blocking the diffusion of Al through the lattice [**253**]. Thus the doped scale was proposed to grow only by O diffusion and was not buckled.

"Rumpling" is a second type of convolution, characterised by the alloy conforming to the oxide convolutions, making for a more complete oxide/metal interface. This structure is shown schematically in **Figure 3-10**(**b**). From the surface, rumpling and buckling look the same. However, in the case of rumpling, fewer voids are formed within the scale and the scale is in better contact with the substrate. Thus, scale adhesion is not necessarily reduced when rumpling is observed. Bennett *et al.* [**254**] observed this behaviour at 1200 and 1400°C with undoped FeCrAl. The extent to which convolutions of the alloy followed those of the oxide increased with temperature over this range [**254**].

Oxide ridge & whisker structures

"Oxide Ridge Structure" is also identified as another important microstructural feature of alumina scales: the ridge structure of α-Al_2O_3 oxide. In this case, oxide ridges on the gas surface of the scale are formed, which correspond to oxide grain boundaries, **Figure 3-10**(**c**). For the ridges, there is a localized increase in scale thickness. Ridges are observed at the gas/scale interface and less frequently, at the oxide/alloy interface [**255**]. Doychak *et al.* [**256**] proposed that the ridge morphology found after long exposure time at 1000°C was a remnant of the phase transformation of θ-Al_2O_3 to α-Al_2O_3. The ridge spacing was also inversely related to the oxidation temperature. However, at higher temperatures (> 1200°C),

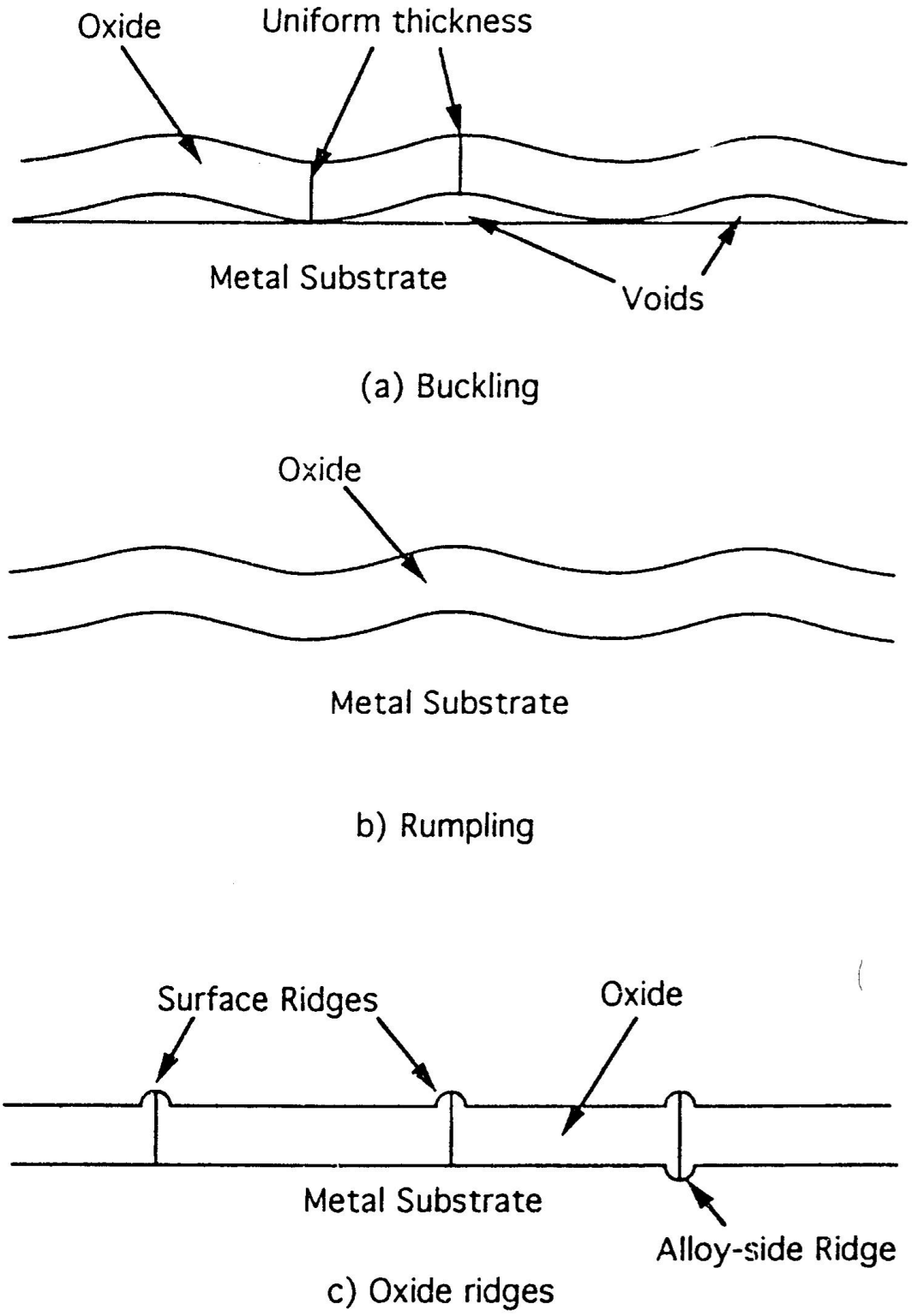

Figure 3-10 Schematic of various Al_2O_3 oxide morphologies [**256**]

meta-stable Al_2O_3 phases were not observed to form. Therefore, it is difficult to relate the finer ridge structure observed at high temperatures to the coarse ridges found at lower temperatures.

"Oxide Blades and Whiskers" is another class of surface morphology typical to alumina-formers. Numerous studies have noted that Al_2O_3 scales grown below 1000°C have a blade-type structure. A number of studies did not characterise the phase of the Al_2O_3 scale [**257 - 260**]. However, more recent studies have conclusively identified this morphology using SIMS and XPS as belonging to the θ-Al_2O_3 [**261 - 264**]. Whiskers have also been observed to form on the surface of undoped α-Al_2O_3 scales from 1000°C to 1200°C [**265**]. Both whiskers and blades are indicators of an outward growth mechanism.

Al_2O_3 scale adhesion testing

One of the most important issues from an engineering standpoint of high temperature materials is oxide adherence. Even if the oxide grows slowly, it spall readily upon cooling (or at a temperature), then the lifetime of the substrate is limited. Eventually the Al (or Cr, Si) content will be depleted to the point where less noble oxides will be formed. If the oxide remains adherent, less spallation occurs and the parabolic nature of the reaction will slow the degradation over long exposure times.

Over the past years, several oxide adherence studies were undertaken, with many concentrating on chromia-formers. Very limited studies were undertaken to investigate the REE on alumina-formers. The RE effects were ignored in order to concentrate on explaining the reasons for oxide spallation. The general conclusions of the comparative studies between undoped and RE-doped (e.g. with Y) showed beneficial effects of RE even if they are in small amounts in the alloys. However, the mechanism of the RE effect is still not clear

satisfactorily. The general conclusion from the previous studies was that the addition of small amounts of RE improves the oxidation resistance of metals and alloys.

While cyclic testing remains the most widely used technique for gauging oxide adhesion, there are other techniques as well. Acoustic emissions have been monitored in order to detect signs of cracking, both isothermally and during cool down [**266**]. Using micro-indentation, Tortorelli and Kaiser [**267**] have attempted to quantify the mechanical properties of scales, including their adhesion. Sigler [**268**] deformed oxidation coupons after oxidation with a punch to examine

oxide adherence. These techniques remain somewhat controversial and difficult to interpret. In general, cyclic testing is favoured because of its simplicity.

3.3.3 Methods of Reactive Element Additions

The benefits of a RE addition have been expounded, the more practical issue of actually adding the RE to a system becomes significant. While most of the first 30 years of RE research examined mainly RE alloy addition, the last two decades have emphasized other types of additions. A RE oxide dispersion is particularly attractive because of the dual purposes of the dispersion. A stable RE oxide (such as Y_2O_3) not only benefits the oxidation behaviour but also improves the creep properties at high temperatures. A second technique, first used in the electronics industry, is ion implantation. This surface treatment essentially allows any element to be added to any solid substrate in the near-surface region. Both oxide dispersion and ion implantation provide a uniform source of the RE and eliminate problems associated with alloying.

Alloying Additions

While alloying of the reactive element would seem to be the simplest and easiest way of adding the element to the system, the success of RE alloy additions is sometimes limited because of their phase separation in the metal. Numerous studies have found a more beneficial effect of a RE when it is more evenly dispersed in the alloy. For example, Hf addition produces better oxidation behaviour than an equal addition of Y in CoCrAl [**269**].

Kuenzly and Douglass [**270**] found general detrimental effects for the addition of 0.5 wt%Y to Ni_3Al at temperatures between 1100°C and 1200°C. However, in the same study the detrimental effect of Y was attributed to Y-enhanced formation of NiO, no internal attack was reported. The authors [**270**] also concluded, Y addition did not affect the weight gain. Similar results were found by Kumar [**271**] in the case of Y addition to NiCrAl alloys.

Ion Implantation

Surface implantation of a RE has been found to yield more uniform effects than alloying, for which RE-rich particles often form in the alloy. Microstructurally, this leads to a more uniform scale, where no oxide pegs or other anomalies are found. For instance, Sprague and Johnston [**272**] found that voids formed beneath oxide films on both CoCrAl and CoCrAl-0.5 wt%Y but they did form when the alloy was implanted with Y. The conclusion was that because Y segregated in the alloy, the voids in CoCrAlY formed in areas denuded of Y.

Jedlinski and Mrowec [**273**] studied the effect of implanted Y on oxidation of Ni-Al (51.9 at%Al) between 1000 and 1300°C. Without Y implants, Al_2O_3 scales exhibited poor adherence. With doses of $2x10^{16}$ Y^+ / cm^2 at 70 keV, adherence was improved and weight gain was reduced [**273**]. Jedinski and Mrowec described the adherence of the scales on Y-implanted NiAl as “perfect”.

There is no experimental evidence to suggest that the implantation process itself affected the oxidation behaviour. For instance, Pivin e*t al.* [**274**] implanted both Y and Ar into Ni-Cr, Fe-Ni-Cr and Fe-Ni-Cr-Al alloys. In each of the alloys, implanted Ar had neutral effect on the oxidation properties. Thus it is a chemical effect of the implanted species and not a result of the radiation damage caused by ion implantation.

Oxide Dispersions

A RE oxide dispersion in an alloy, generally provides the best method for introducing the RE uniformly throughout the material. It has the additional benefit for high temperature structural materials that the oxide dispersion improves the creep resistance of the material by pinning dislocations (oxide dispersion strengthening, ODS). The drawback of the dispersion is in the fabrication. In order to achieve a uniform dispersion, powder metallurgy techniques such as mechanical alloying are necessary [**275**].

There has been general agreement in the literature about the beneficial effects of a RE oxide dispersion. The most significant issue has been the case of a non-RE oxide dispersion (especially Al_2O_3), which reportedly improves the oxide adherence on both Al_2O_3-[**245, 246, 276**] and Cr_2O_3-[**248, 277, 278**] formers. However some of the other results [**279**] are rather strange and frustrating. If they are true, they require a rethinking of some aspects of the REE. For instance the work of Whitte *et al.* [**279**] concludes that 1 wt% addition of Zr, Hf and Ti did not affect the oxidation behaviour of Co-10Cr and Co-15Cr. It should be noted that all of these studies relied on kinetic and some XRD work for their evidence.

3.3.4 Attempts to Explain the Effect of Reactive Element Addition

Small additions of certain “reactive” elements have a large beneficial effect on the oxidation behaviour of alloys. This improvement, known as the reactive element effect

(REE), has been used in the manufacture of high temperature corrosion resistant alloys since its discovery. From an engineering perspective, the primary effect is a marked enhancement in the spallation resistance of protective oxide scales, such as Cr_2O_3 and Al_2O_3, grown on Fe-Al and Fe-Cr alloys. Also reduction in the oxidation rate has been documented, the basic reasons for the beneficial effects of reactive elements have not been fully determined and still a subject of controversy.

Using a number of superior analytical tools, a new understanding has emerged of the effect of REs on the scale growth, adhesion mechanisms, microstructures and growth rates. All of these effects have been observed for the oxidation of alloys that form Cr_2O_3 scales, while only the second effect (better adhesion) has been observed for alloys that form Al_2O_3 scales. These affects have been attributed to the segregation of the RE ions, e.g. Y^{3+}, to scale grain boundaries [**280**]. In both chromia- and alumina-forming materials, the REE is most basically characterized from an engineering or macroscopic view by a reduction in the rate of oxidation and an improvement in oxide adherence. The oxide adherence to the alumina-former substrate is reported to be greater than that to the chromia-former. Both oxides are observed to be more adherent to the substrate when doped with a RE.

Segregation phenomena

The segregation phenomenon in scales was outlined first by Przybylski and Yurek [**281**] for chromia-formers. The major observation by Cotell *et al.* [**280**], was that the growth mechanism for Y-implanted Cr ($2x10^{16}/cm^2$) was changed to primarily oxygen transport inward. The grain boundary flux of outward-diffusing Cr was limited by the segregation of Y to the oxide grain boundaries. Due to this change in mechanism and a solute-drag effect, the segregation also had a profound effect on the oxide microstructure. Without a dopant, new oxide formed at the gas interface, leading to large columnar grains (axis normal to the metal interface) near the gas interface at 900°C. With a dopant, the much thinner scale and a

finer grain size and more equiaxed grains developed. Columnar grains were observed in this case near the metal interface, exactly the opposite situation of the undoped case.

According to the segregation mechanism, the RE addition reduces scale spallation due to a number of factors. The changes in oxidation mechanism and oxidation rate reduce the scale thickness, thus reducing growth stresses. Przybylski and Yurek [**281**] also concluded that while impurities (like sulphur) in the alloy were deleterious to the oxide adhesion, removing them without a RE addition would not improve long-term adherence. Eventually the faster-growing undoped scale would generate sufficient stress to cause failure. Thus sulphur removal could not be substituted for a RE addition in the long-run.

The work of Funkenbush *et al.* [**282**] and Smialek [**283**] determined a relationship between the effect of RE and the segregation of sulphur which may be present in the alloy. Different mechanisms have been proposed for the interaction of a RE and sulphur. The first is that the RE such as Y reacts with the indigenous sulphur to form a stable sulphide, thus preventing the sulphur from degrading oxide adhesion [**284**]. The second premise is that Y segregated to the alloy/oxide interface lowers the driving force for sulphur segregation to this interface, thus eliminating its detrimental role [**285**]. Although all of these ideas remain largely unproven, however, when good adherence is found, the RE and not sulphur is found at the metal/oxide interface, also when adherence is poor (with no RE addition), sulphur is found. Segregation of foreign ions in oxide scales was detected first by Ramanarayanan *et al.* [**286**]. Using TEM of scales grown on a commercial Y_2O_3-dispersed FeCrAl alloy (MA956), Y was found to segregate to the oxide grain boundaries. No mention was made of segregation to the metal/oxide interface. A number of arguments can be made regarding the possible reasons for segregation. The most important point is that there is a variety of driving forces for segregation of foreign ions to oxide grain boundaries including charge and ion size.

Scale/alloy interface

There are several proposed mechanisms to explain the role of the RE in improving scale adherence. These theories are concentrated on the metal/oxide interface, which can be briefly outlined in this section.

(1) **The Graded Seal**. This is the simple idea that a RE-rich layer forms between the substrate and the oxide. According to this hypothesis, the rate-limiting steps modified because of slower diffusion through this layer and adhesion is improved because this layer acts as a strengthening intermediary phase. This theory persisted because early analytical techniques such as EPMA did not have sufficient resolution to detect such a thin layer [**287**]. When more advanced analytical techniques (such as TEM) were used (e.g. by Ramanarayanan *et al* [**288**]) to study the interface between the oxide and the substrate, these indicated that such a layer did not exist.

(2) **Oxide Pegs**. This idea was based on observations of internal oxidation of the RE when the RE was added by alloying. The selective internal oxidation of the RE near the surface would often form oxide protrusions into the substrate which were attached to the external scale. These oxide "finegers" were proposed to grab onto the alloy, thus improving scale adherence [**269, 289, 290**]. Over the past 20 years, as RE additions have moved beyond simple alloying, this theory has become less prominent. Addition of the RE by ion implantation and oxide dispersions improves the oxide adherence without the formation of pegs. Thus, while pegs may play a role, they are not necessary to improve adherence.

(3) **Interface Bonding**. According to this hypothesis, the undoped metal/oxide bond is normally weak. By adding a RE to the alloy, the bond is strengthened. Obviously, this theory is somewhat unspecific regarding exact mechanisms. After the detrimental role of indigenous sulphur was demonstrated (e.g. by Smeggil *et al* [**291**]), sulphur was identified as the reason for the weak undoped interface.

(4) Void Theory. This theory is another hypothesis arising from observations of the alloy/oxide interface. In this case, the undoped interface is observed to have voids at the interface, while the doped interface is adherent and no voids are observed. An idea attributed to Stringer [**292**] is that the RE in the alloy acts as a vacancy sink. Thus, vacancies are captured by the RE rather than coalescing into voids at the alloy/oxide interface. Kumar *et al.* [**271**] proposed that an internally-oxidised RE in the alloy forms dislocation loops which annihilate these vacancies. (No attempt was made to look for these dislocations). Accordingly, when the RE addition becomes saturated with vacancies, voids would form and cause failure.

Tsuzi [**293**] observed, in FeCr with 0.87%Y, that no voids were present at the alloy/oxide interface, but voids were found centred on internally-oxidised Y_2O_3 particles in the alloy. These voids were observed in metallographic cross-sections and no consideration was made of possible polishing effects or the adherence in thermal expansion between Y_2O_3 and FeCr. The void explanation has also been used in numerous other systems including the addition of Y to Ni_3Al [**270**].

Experimental observations have not always been consistent with this hypothesis. A Y_2O_3-dispersed NiCr alloy oxidised at 1000°C [**294**] was investigated for possible void formation near YAl_xO_w particles in the alloy. Before and after oxidation, TEM parallel sections of the alloy near the oxide interface were examined. No voids were found at these interfaces in either case. However, the oxide adherence was excellent. One of the weaknesses of the void theory is that it deals mainly with the issue of improved adherence. It does not address the other RE effects such as the observed changes in the oxidation mechanism or the oxide microstructure.

Scale plasticity

This hypothesis is experimentally based, mainly on the observed reduction in the oxide grain size with the addition of a RE. It is proposed that this reduction in oxide grain size improves the mechanical properties of the scale (e.g. plasticity), thus improving the oxide adherence (e.g. Ramanarayanan *et al* [**286**]). This idea is fully consistent with the segregation theory in that the segregation of the RE to the oxide grain boundaries slows the grain growth, producing a finer grained scale. A reduction in Al_2O_3 scale grain size would alter mechanical properties of the scale, with a likely improvement in ease of creep deformation and thus a greater ability to relieve growth stresses. However, there was no evidence that a finer oxide scale is more adherent than a larger grained scale.

Elimination of growth stresses

This theory is also based on the "rate-limiting step" of oxidation in which for both chromia and alumina scales cation transport is reduced with the addition of a RE. Mrowec *et. al*. [**244**] concluded that the entire REE is due to a change in the oxidation mechanism and not due to any interfacial phenomena, such as sulphur segregation or oxide pegging. Golightly *et al*. [**253**] had earlier proposed a similar explanation for alumina-formers. When cation transport is eliminated, metal vacancies responsible for the outward diffusion are no longer generated, thus eliminating voids at the metal/oxide interface and improving oxide adhesion. Oxide microstructures are also modified by the change in the scale growth mechanism.

Stresses generated in the oxide film – during thermal cycling – are also important factors in scale integrity and adhesion. In chromia-formers, comparing doped and undoped scales is inappropriate, because the faster oxidation rate in the undoped case will cause higher stresses and always leading to a greater failure rate. With a reduction by one to two orders

of magnitude in the scale growth rate for RE-doped substrates, it is more logical to compare scales of equal thickness. However, this type of argument for the case of alumina-formers is not fully covered, because it was believed that the reduction in the oxidation rate of alumina-formers (by the addition of the RE) is not really significant [**1**].

Studies of Al_2O_3 oxidation mechanism and the reactive element effect

Virtually no argument arises in the case of chromia-formers about the oxidation mechanism. Al_2O_3 appears to be a more complicated case with little agreement in the literature. Both of inert markers and ^{18}O tracers are used to explain the mechanism of Al_2O_3 scale formation and growth. The premise on which inert marker experiments are based is quit simple. If anion diffusion is the primary growth mechanism, then the markers should remain at the original metal surface and oxide grow beneath them. In the case of growth by cation diffusion, the oxide should grow over the markers, and the marker should be found beneath the oxide at the metal/oxide interface. In the case of mixed mode growth, the markers should be found within the scale. Pettit's initial work [**295**] on Ni-Al alloys concluded that Al_2O_3 scales grew by inward diffusion of oxygen. However because, of the thin non-adherent scale on these alloys, no marker or other experiments were conducted to confirm this hypothesis. Marker experiments on more adherent Al_2O_3 scales, such as those formed on Ni-Al-3Y alloys at temperatures between 900 and 1100°C, have been performed by Young *et al* [**257**]. They concluded that Al_2O_3 scales grow by inward diffusion of oxygen although the validity of the marker experiment was questioned.

Oxidation models involving grain boundary segregation are based on the ability of foreign ion segregants to effectively block the outward boundary transport of native cations and to inhibit grain growth [**302**]. Small ions, such as Ti, Nb and Ta, may segregate but, owing to their small size, may be unable to effectively inhibit cation diffusion and/or grain growth during oxidation. For example Pint and Alexander [**302**] reported that Nb- and Ti-

doping to FeCrAl reduce the parabolic rate constant at 1200ºC and exhibit scale ridge formation but they do not produce the same fine grain size as does Y to the alloy. Another factor in determining the effectiveness as a segregation regent is the amount of dopant addition. For example, Pint and Alexander [**302**] suggested that 0.025 - 0.05 at% are less effective to change the scale morphology. In the same study [304] it is suggested that the detrimental effect of Hf, Sc and Ce was due to the excessive dopant level (0.2 at%) and can be corrected by lower dopant levels such as the 0.025 at% La addition in which case excellent behaviour was observed.

Strawbridge and Rapp [**303**] also investigated the effect of ion size on dopant effects on the oxidation and interpreted their results to suggest that there was a critical optimum ion size ratio (dopant/native oxide cation) range for the best dopants in Fe, Ni and Co oxides

3.4 SUMMARY

The evidence available from the corrosion studies on titanium alloys and intermetallics, suggests that improvements largely depend on the protective properties of the formed scales, either by the inhibition of the environmental species – such as oxygen and/or sulphur – diffusion through the scale, or by the elimination of fast diffusion paths of the reacting species. It seems probable that some alteration in the characteristics of scale and metal/scale interface also plays an important role. However, this is largely dependent upon the behaviour of individual elemental additions, and there is little information regarding the mechanism involved. Whilst it is generally assumed that the reduction in environmental contamination of the alloyed substrates is the result of improved barrier qualities of the scale, the environmental impact on Ti-Al substrates, have received very little attention and further investigations is needed.

Reactive element(s) additions to Fe-base alloys have significant effects, which could lead to selective oxidation, transient oxidation and oxide adherence. Insufficient characterisation prevents conclusive arguments to be made about these effects. Yet most of the studies relied mainly on kinetics work for their effectiveness. A review of the various studies about the REE reveals significant effect of small addition of RE for chromia-formers, whereas very limited amount of work on the REE on alumina-formers exists. Several hypotheses have been proposed based on various theories and models, without sufficient accompanying experimental observations.

Despite the vast body of technical information on Ti-Al and Fe-Al intermetallics, the literature appears to be deficient in the corrosion behaviour of these materials at high temperatures. The relative contributions and properties of the corrosion products of the intermetallic materials – in different environment gas composition – would provide the necessary information for both alloy development and coatings technology.

Part of the present work is undertaken with the aim of elucidating the effect of environmental oxidising gas composition on the scale morphology and formation mechanisms on Ti-46.7Al-1.9W-0.5Si alloy. Also the research programme is undertaken to examine the 'protectiveness' of a selected single and double layer(s) coatings on γ-TiAl in a sulphidising/oxidising atmosphere. A considerable part of the current research programe also concentrates on determining the REE (Y and/or Hf) on the scale formation and scale adhesion to Fe_3Al intermetallics. The adhesion testing procedure was carried out by the comparison of the isothermal and cycling conditions over a wide range of temperatures.

CHAPTER FOUR

INTRODUCTION TO THE PRESENT EXPERIMENTAL WORK

CHAPTER FOUR

4.0 INTRODUCTION TO THE PRESENT EXPERIMENTAL WORK

It is evident from the information set out in **Chapters 2** and **3** of this thesis that the corrosion behaviour of engineering alloys exposed at high temperatures (HT) in corrosive environments, especially those containing oxygen and sulphur, is a subject of theoretical interest, and also of technological significance. The environmental conditions experienced by materials, for example in combustion atmospheres of boilers and gas turbines give rise to complex corrosion products, consisting of external scales and varying degrees of degradation, accounted for by both oxide and sulphide formation; the formation of sulphide(s) as an inner layer underneath the oxide scale may also occur even though the thermodynamic considerations suggest exclusive external oxide formation.

It is clear that the nature of the external scales formed in these atmospheres of oxygen- and sulphur-containing environment is important. The degree of ‘‘protectiveness’’ offered by the scales in terms of minimising the extent of further scaling and especially in preventing, or reducing the degree of sulphur penetration is critical. Environments of relatively high oxygen activity may be expected to reduce the amount of internal degradation. The “protective” scales formed on most HT alloys during oxidation consist of either Cr_2O_3 or Al_2O_3. The formation of the latter as an external oxide scale is considered desirable principally because of its lower growth rate compared with chromia; and also because unlike Cr, Al does not form volatile oxide species at high temperatures (> 1200°C). The poor adherence of alumina scales, it has been seen, may be considerably improved by small additions of reactive elements such as Y, Zr or Hf.

The aim of this chapter is not to summarise the previous work reported in the literature on the HT behaviour of Fe_3Al and γ-TiAl, but the intention here is to examine the importance of the present experimental work in order to explain various aspects of the high temperature degradation processes of the selected experimental materials.

A survey of the relevant open literature reported in **Chapter 3** revealed that significant progress in recent years has been achieved on Ti- and Fe-aluminides. In particular, considerable research efforts have been paid on studying the mechanical properties of these intermetallic alloys. The main problem to the use of the intermetallic Ti-Al compounds for aerospace and automobile engine components is its oxidation resistance at high temperatures is considerably inferior to that of conventional super-alloys. Improvement of oxidation resistance and understanding of Ti-Al corrosion mechanisms are important before their practical applications can be realised. The poor oxidation resistance of Ti-AI has been attributed to the difficulty in forming protective external alumina scales and undesired rapid growth of rutile.

Iron-base intermetallics are generally considered to be corrosion resistant (especially in sulphur-containing environments) because of their ability to form slow-growing Al_2O_3 scale(s). However, their applications at HT are hampered by easy spallation of the external scale and also due to their susceptibility to intergranular degradation. The primary advantages of iron intermetallic compounds are high strength of ~ 500 MPa up to 500°C. However, these materials should possess the minimum amount of aluminium to form protective alumina scale. High aluminium content in the alloy detrimentally affects its mechanical properties. Additions of RE is believed to maintain and facilitate the formation of alumina scales, even if they are present in very small quantities in the alloy.

Several efforts have been reported (refer to **Chapter 3**) to improve the corrosion resistance of Ti-Al and Fe-Al including alloying additions and surface treatments. However, very limited research has been conducted to study the corrosion behaviour of Fe_3Al and γ-

TiAl intermetallics as candidate structural and coating materials for HT applications. Although some investigations have been carried out on HT corrosion behaviour of both types of intermetallics, most of the results derived from these studies are controversial and still unclear. Further investigations – using clear and more reliable experimental procedures – are needed in order to resolve these conflicts and to clarify their degradation behaviour. Several aspects governing the corrosion mechanism(s) of Fe_3Al and γ-TiAl form the basis of the current investigation.

As noted in **Section 3.2**, it therefore appeared that the previous work mentioned above and similar studies were not sufficient enough to reach an unequivocal conclusion regarding the effects of nitrogen and oxygen partial pressure on the oxidation behaviour of Ti-Al. To investigate the nitrogen effect, it was considered necessary to compare air oxidation results at a given temperature with those in atmospheres free of nitrogen and other impurities of the same partial pressure of oxygen, whereas, the effect of oxygen partial pressure must be performed in environments free of nitrogen (and other impurities), with different oxygen contents in the reactive atmosphere. Also for better conclusion and more reliable outcomes, these investigations must be done in a wide range of temperatures and exposure times as explained in some detail in **Chapter 5**.

With the above background, a considerable part of the present research programme deals with the influence of nitrogen and oxygen partial pressure (separately) on the oxidation behaviour of Ti-46.7Al-1.9W-0.5Si alloy as follows:

- The results of the air oxidation of Ti-46.7Al-1.9W-0.5Si alloy at 750 - 950°C for up to 240h are compared with its oxidation results in Ar-20%O_2 (free of impurities such as hydrocarbons and water vapour). The reactive gases – air and Ar-20%O_2 – are of the same pO_2 (~ 0.2 x 10^5 Pa) also, the two oxidation experimental conditions such as the ranges of temperature and exposure time are standardised.

- The influence of the oxygen partial pressure on the oxidation behaviour of Ti-46.7Al-1.9W-0.5Si alloy has been also studied in high purity – specially prepared for this purpose – Ar-5%O_2, Ar-20%O_2 and Ar-80%O_2 gases.

For the accuracy of the results, the heating and cooling rates of the specimens in the atmospheres are kept very similar (furnace heating and cooling) as reported in **Chapter 5**.

As stated in **Section 3.2.5**, AlTiN coatings form stable, protective Al_2O_3 surface layer at high temperatures even at low oxygen activities in the environment. This is due to their high Al/Ti ratio compared to other types of coatings including TiAlN. Al_2O_3 is also highly insulating oxide, with low ion mobility and acts as an effective diffusion barrier to the reacting species. CrN coating, are also thermally stable system in oxidising environments due to their Cr_2O_3 (chromia) formation and promise excellent HT corrosion resistance for many applications. Further more they also exhibits complementary mechanical and structural properties to (TiAI)N coatings. In some technological and industrial applications, interlayer coatings are found to be necessary to provide further advantages to the coating systems such as; diffusion barrier and/or for better adhesion between the substrate and the external coatings. NbN coatings are an example for the high inert barrier (chemically stable) coatings especially in sulphur containing atmospheres. For this reason, part of the undertaken research programme is to examine the sulphidation/oxidation protection of a selected nitride coatings to Ti-46.7Al-1.9W-0.5Si alloy.

Although there was very limited research reported in the open literature on the corrosion behaviour of Fe-Al, several different mechanisms have been proposed to explain the REE on the corrosion behaviour of Fe-aluminides at high temperatures (see **Section 3.3**). These effects are still unclear and need further investigations. Iron-aluminides based on Fe_3Al have been less widely studied than other alumina-formers, but recently they have received special attention due to their low densities and also their ability to form external alumina scales. As more detailed experimental work has been performed on Fe-aluminides some conflicts

between researchers have been noted in oxide morphology, scale thickness and mass gains depending on test parameters and alloy conditions. Large scatters have been reported in mass change data and scale adhesion after cooling of Fe-Al (with and without RE) from high temperatures. More detailed studies on the REE on the high temperature oxidation kinetics of Fe-Al systems are essential. Adhesion testing techniques are also required to examine critically the REE on the Al_2O_3 adhesion of Fe-aluminides scales during cycling at high temperatures. For this purpose, single and combined effects of selected RE on the isothermal oxidation behaviour of Fe_3Al have been investigated in this thesis. Isothermal air oxidation studies of iron-aluminides at high temperatures were conducted in order to explain the REE. Most of the reported studies (refer to **Section 3.3**), believed that REs such as Y, Hf, Ce and Zr dramatically change the oxidation behaviour of iron-aluminides even if they only exist in small quantities in the alloy. However, the effects of the RE are still subject of controversy and are still far from satisfactory and so further investigations are needed.

The majority of the previous workers confirmed that spallation occurs as a result of cooling and they concluded that thermal stresses are more important than growth stresses. Thermal cycling (heating and cooling) was thought to reflect more realistically what is happening in practice where components are subjected to variations in temperature. Very little has been published about the Fe_3Al (with and without RE) oxidation under thermal cycling conditions. In the present thesis the REE has been examined on Fe_3Al using a newly developed – by the researcher – thermal cycling technique built within the Advanced Materials Institute (AMRI)'s laboratory, the technique enabled us to control – to a wide range of time – precisely the number of cycles as well as the heating and cooling periods at a set of temperatures.

The oxidation behaviour of undoped Fe_3Al and Fe_3Al doped with Y and/or Hf under isothermal and cyclic conditions was studied within the temperature range 900 - 1100°C for up to 240h. Considerable part of the research programme has been undertaken to examine

critically the effects of nitrogen and oxygen partial pressure on the oxidation behaviour of Ti-46.7Al-1.9W-0.5Si alloy in the temperature range between 750° and 950°C for up to 240h. Also in this study, single and double nitride layer coatings were developed on Ti-46.7Al-1.9W-0.5Si alloy in order to examine thermodynamically stable nitrides – CrN and AlTiN – as a single coatings to improve HT corrosion behaviour of Ti-46.7Al-1.9W-0.5Si (at%) intermetallic alloy in an environment of $H_2/H_2S/H_2O$ yielding high sulphur ($pS_2 \sim 6.8 \times 10^{-1}$ Pa) and low oxygen ($pO_2 \sim 1.2 \times 10^{-15}$ Pa) potentials at 850°C. Due to the possibility of achieving further improved corrosion resistance, NbN and CrN – as diffusion barriers – together with external CrN and AlTiN coatings have been examined in the same sulphidising/oxidising environment.

An integrated experimental approach has been adopted in the determination of reaction kinetics and characterisation of the morphology and composition of the corrosion products using the available XRD, SEM and EDX techniques. Such programme of study it was believed would provide information, which was expected to be of considerable interest and of commercial/technological significance in the field of HT corrosion.

CHAPTER FIVE

METHODOLOGY OF THE CURRENT RESEARCH PROGRAME

CHAPTER FIVE

5.0 METHODOLOGY OF THE CURRENT RESEARCH PROGRAME

5.1 Introduction

This investigation into the high temperature corrosion behaviour of γ-TiAl and Fe_3Al and some selected types of experimental coatings has included the study of their corrosion kinetics and scale characteristics. The experimental procedures and techniques, which have been employed, are described in **Section 5.2** of this chapter. The oxidation and sulphidation experiments were carried out using available and recently developed rigs in AMRI. Corrosion products have been assessed using SEM, XRD and EDX.

5.2 Experimental

This section is a summary of the methodology of the current research programme. In **Section 5.2.1**, description of the materials used in this study, as well as the preparation procedure of the experimental coupons before exposure are described. **Section 5.2.2** summarises the oxidation/sulphidation procedures as well as the gas compositions used in this study. **Section 5.2.3** specifies the characterization techniques used to assess the nature and composition of the corrosion product(s) of the experimental materials.

5.2.1 Materials Composition and Preparation

Materials

All of the experimental materials used in this study were procured from outside sources. Fe_3Al (un-doped and doped with small amounts of RE) ingot alloys were made at the IRC-

Birmingham University. The chemical composition of Fe_3Al intermetallics is given in **Table 5.1**.

Alloy	Element (wt%)			
	Fe	**Al**	**Y**	**Hf**
Fe_3Al	Bal	21.29		-
Fe_3Al - Y	Bal	21.29	0.15	-
Fe_3Al - Hf	Bal	21.29	-	0.25
Fe_3Al - (Y+Hf)	Bal	21.29	0.15	0.25

Table 5.1 Chemical composition of Fe_3Al intermetallic alloys

Conventionally cast Ti-46.7Al-1.9W-0.5Si (at%) alloy rods of 22mm diameter were provided by ABB-Switzerland. The γ-TiAl intermetallics chemical compositions are given in **Table 5.2**.

Element (wt%)	**Ti**	**Fe**	**Al**	**W**	**Si**	**C**	**O**	**Cu**
γ-TiAl	Bal	0.052	31.05	8.56	0.34	0.01	0.0698	0.01

Table 5.2 Chemical composition of Ti-46.7Al-1.9W-0.5Si intermetallic alloy

While most of the work in the study concentrated on the oxidation behaviour of the two Fe_3Al and Ti-46.7Al-1.9W-0.5Si intermetallic alloys, single (CrN and AlTiN) and multiplayer (AlTiN/CrN, AlTiN/NbN and CrN/NbN) coatings on Ti-46.7Al-1.9W-0.5Si alloy were also developed in order to examine their protectiveness to Ti-46.7Al-1.9W-0.5Si alloy in sulphidising/oxidising environments of relatively high partial pressure of sulphur and low partial pressure of oxygen. All CrN (single or diffusion barriers) and NbN coatings of about 1.5μm thickness were deposited on all sides of Ti-46.7Al-1.9W-0.5Si alloy coupons using Ionbond PVD coating unit. The Ionbond procedure is summarised in **Appendix A**.

In cases where combination (double-layered) of coatings were required (e.g. AlTiN/NbN), improved adhesion between the AlTiN and NbN coatings was achieved by

depositing an inter-layer of about 1μm thickness of pure titanium film. Following the deposition of the inter-layer, AlTiN coating of about 2.5μm was made in TecVac Ltd, using similar coating procedure (described in **Appendix A**) made by Ionbond Ltd.

Specimen preparation and surface area calculations

Square 10x10mm coupons of 2.5mm thickness were cut from Fe_3Al ingots by means of wire cutting machine (spark erosion cutting). The 3mm outer layer of the casted γ-TiAl rods was removed using lathe machine. The removal of the outer layer is to ensure that the whole surfaces of the test samples could be free from any possible scale or voids resulting after the casting processes. Half disks of 19mm diameter coupons from γ-TiAl billets and 2.5mm thickness were cut by means of a Buehler Isomet 2000 precision saw. A hole of 1mm diameter, to facilitate suspension by platinum wire in the specimen boat, was bored in each sample of Fe_3Al and γ-TiAl (coated and uncoated) using WC drills. The surfaces of the specimens were prepared by grinding on metallographic SiC papers up to 1200 grit. As a matter of record, the specimen dimensions prior to exposure were accurately measured in three locations using a digital micrometer, followed by degreasing in (IMS) and cleaning by acetone. The samples were then weighed before and after exposure on a Mettler HLS balance capable of reading to a resolution of ±0.02mg. The total mass gain of the sample was determined by the mass change of the sample plus the alumina crucible in order to include any spalled scale. However, one possible source of error is that, without a lid, any violently spalled scale may not have been captured in the crucible. In most cases this loss was minimal. The weight changes of the material (with the spalled scale) were necessary to determine the kinetic data for each material at a temperature. To reflect the realistic weight change data, the weight change of the sample after exposure was calculated by the

difference in weight of the sample after exposure (with the spalled scale) and the weight of the sample before exposure.

The geometry of the experimental materials and the samples surface area calculations are described in **Appendix B**. Microsoft Excel was utilised to facilitate the method of surface area calculation.

5.2.2 Oxidation and Sulphidation Experiments: Rigs, Procedures and Gases

Isothermal air oxidation

The principal features of the apparatus used for isothermal air oxidation monitoring are shown in **Figure 5.1**. The rig consisted essentially of an horizontal vitreous silica tube, the mid-section of which was heated by an electric resistance type furnace (Carbolite). The heating rate of the used furnaces was 50°C/min.

A Eurotherm proportional regulator, coupled with thyristor units, controlled the furnace operating temperature, was capable of maintaining a minimum "hot zone" (defined by an N-type thermocouple) of the working tube length in the reaction tube of 8cm with a maximum temperature fluctuation of ± 5°C. The temperature measurement and control were achieved using two separate thermocouples. The control thermocouple was located between the furnace wall and the silica reaction tube, whilst the measuring thermocouple connected with a temperature probe was used to check the hot zone temperature.

The prepared specimens were suspended – in a silica crucible – above a small alumina boat (see **Figure 5-2**) – for scale collection – using 0.1mm diameter platinum wire. At the end of the Ti-46.7Al-1.9W-0.5Si alloy isothermal air oxidation tests, the specimens were furnace cooled, whereas, the specimens of Fe_3Al alloys were rapidly cooled to room temperature after each exposure time at the test temperature. The mass change of the

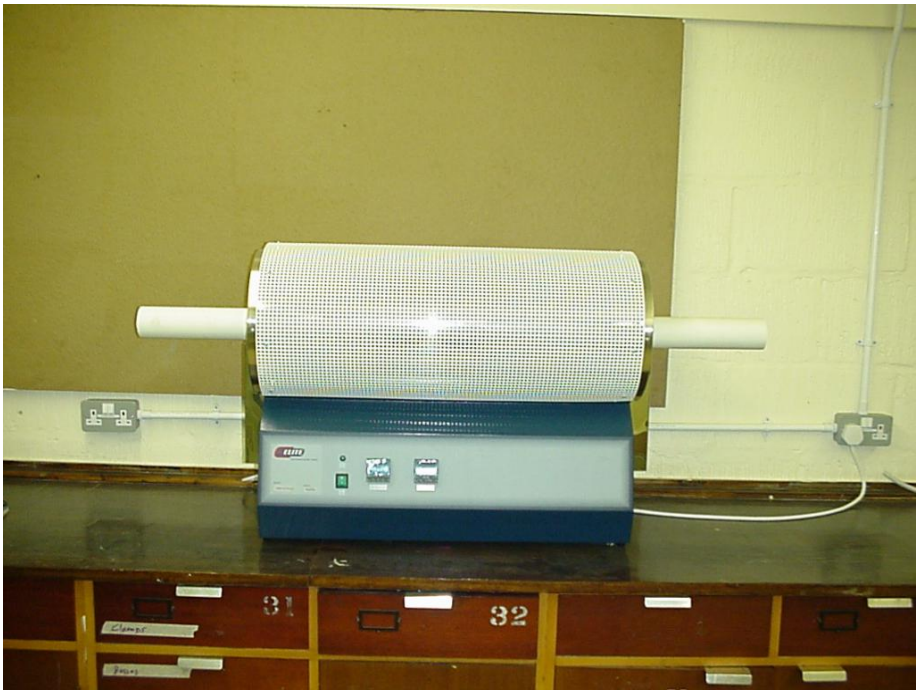

Figure 5-1 Horizontal electrical tube furnace

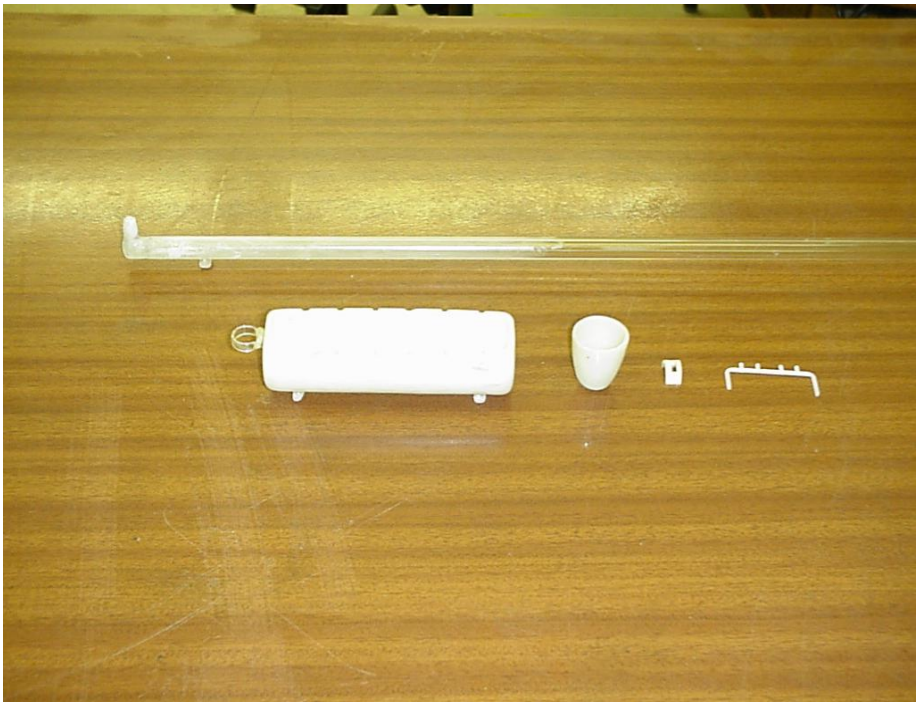

Figure 5-2 Silica push rod, cruciable, boat and cross member

specimens of both intermetallics was measured including spalled oxide scales (individual boats were used for scale collection, **Figure 5.2**) after each run.

Cyclic air oxidation

Cyclic air oxidation experiments (for Fe_3Al alloys) were carried out using the same type of furnace used for isothermal air oxidation experiments (**Figure 5.1**). An automatic device to insert and withdraw of the silica crucible carrying four specimens (with their individual alumina boats and seats) of Fe_3Al alloys was newly built as shown in **Figure 5.3**. Readily available computer – Pneu Alpha Visual Logic – software was used to control precisely the frequency of cycling such as; exposure time in the furnace (holding in the furnace hot zone), cooling period (at the end of the furnace tube) and the number of cycles at the test temperature.

The samples were loaded in a silica crucible in a similar way to the isothermal oxidation experiments. The loaded silica crucible with the experimental Fe_3Al samples were linked to a ceramic push rod (**Figure 5.2**) from one end and the other end of the push rod was joined to a sliding cylinder by means of a two-piece metallic adapter (**Figure 5.3**). The length of the push rod was enough to bring the silica crucible (with the samples) to the furnace hot zone. The movement of the adapter (with the push rod) was automatically controlled through a controller card, which is linked to the computer. Compressed air was used to move the adaptor and the push rod according to the pre-stored cycling data – such as the number of cycles, exposure time of the samples and the cooling time – through a controller card. A continuous supply of compressed air to the system was essential to ensure regular cycling of the samples as specified by the computer programme. The cyclic oxidation experiments were performed in static laboratory air. Each cycle consisted of a period of one

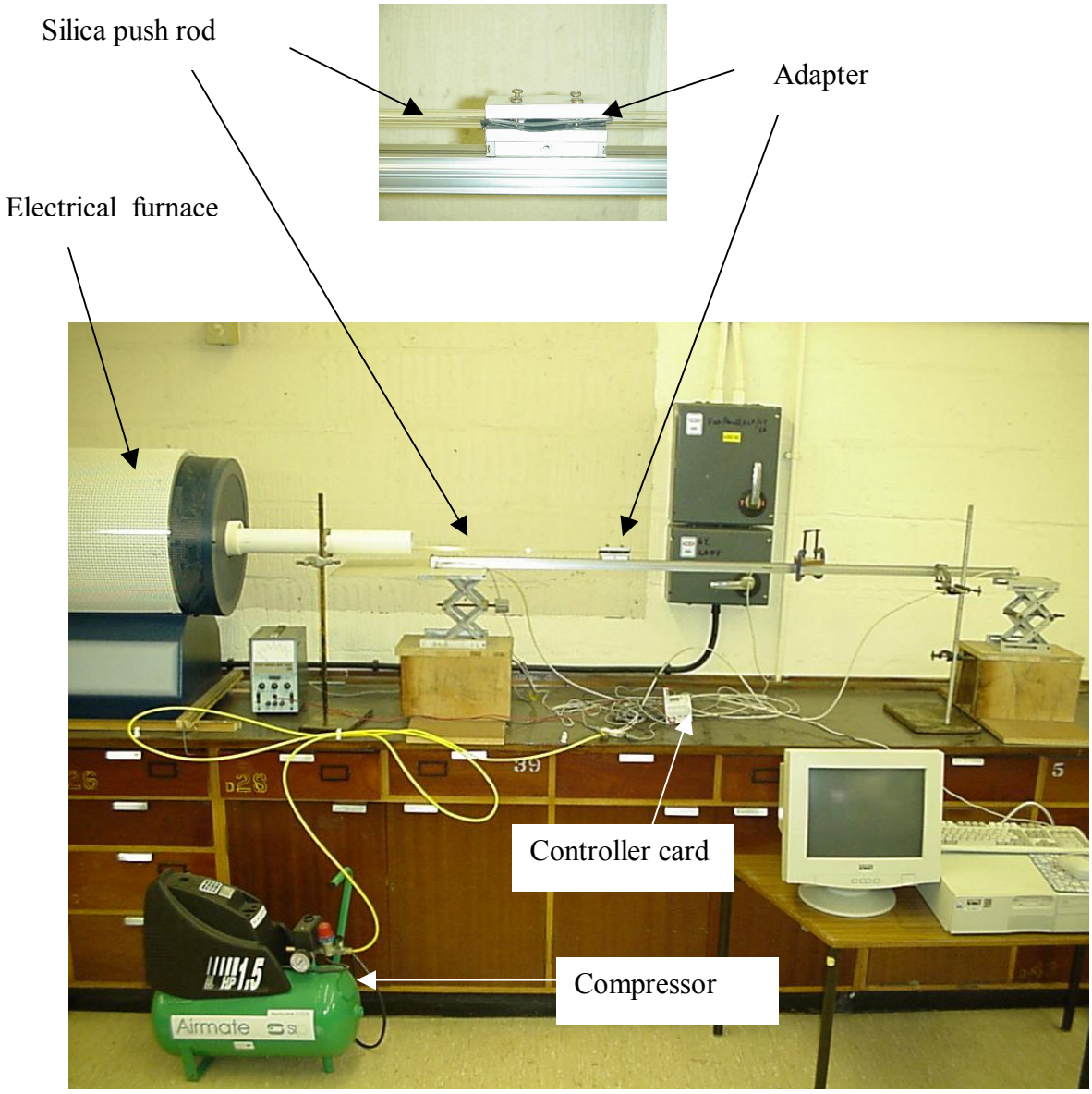

Figure 5-3 Cyclic air oxidation rig

hour at the test temperature and 12 minutes at the ambient temperature, the latter was sufficient to cool the specimens below 50°C. The specimens were inserted into and removed from the hot zone of the preheated furnace – at the test temperature – within a few seconds to guarantee rapid heating and cooling of the samples.

Gases

All of the gas cylinders used in this study were supplied by B.O.C. special gases (UK). The specially prepared gases used in this study had negligible levels of impurities as listed in **Table 5.3**. For the sulphidation/oxidation experiment, the ratio of H_2/H_2S was chosen so as to yield a pS_2 value of (~ 6.8 x 10^{-1} Pa) at the reaction temperature (850°C). In A-O_2 oxidation experiments, Ar-5%O_2, Ar-20%O_2 and Ar-80%O_2 was chosen. Ar-20%O_2 was used to adjust the oxygen partial pressure to that of ordinary air to study the effect of nitrogen on the oxidation of Ti-46.7Al-1.9W-0.5Si alloy, whereas the Ar+5%O_2, Ar-20%O_2 and Ar+80%O_2 gases were used to study the effect of oxygen partial pressure on the oxidation behaviour of Ti-46.7Al-1.9W-0.5Si alloy.

Gas	**Impurities (ppm)**					
	CO	**CO_2**	**H_2**	**H_2O**	**N_2**	**O_2**
Ar	< 1	< 1	< 1	< 20	-	< 15
H_2			-	< 8	< 80	< 5
H_2/H_2S			-	< 2	< 30	< 2
Ar-O_2	< 0.01	< 0.01	< 0.01	< 0.01	< 0.01	-

Table 5.3 Impurity levels of various gases supplied by B.O.C. special gases (UK)

Controlled isothermal oxidation rig

The controlled isothermal oxidation rig used the same type of furnace as shown in **Figure 5.1**. Provision was made for the controlled oxidation – using special (Ar-O_2) gases mentioned in the previous paragraph – in order to admit and exit the reactive gases at the tube ends via fabricated glass end-pieces, which incorporated appropriate taps as in **Figure 5.4**.

The oxidation tests were performed in a flow of highly purified Ar-5%O_2, Ar-20%O_2 or Ar-80%O_2 under atmospheric pressure. In all Ar-O_2 oxidation experiments, the reactive gas was passed through dryer and a gas flowmeter, then entering the reaction chamber. The flow of the gas is also monitored using a water bubbler at the gas outlet. The furnace-heating rate was 50°C/min. At the end of the oxidation test, the Ti-46.7Al-1.9W-0.5Si alloy specimens were furnace cooled in the reactive gas. To avoid any possible contaminating impurities such as H_2O or hydrocarbons which might be present in the argon, so the reactive gas (Ar-O_2) was used as a purging gas as well.

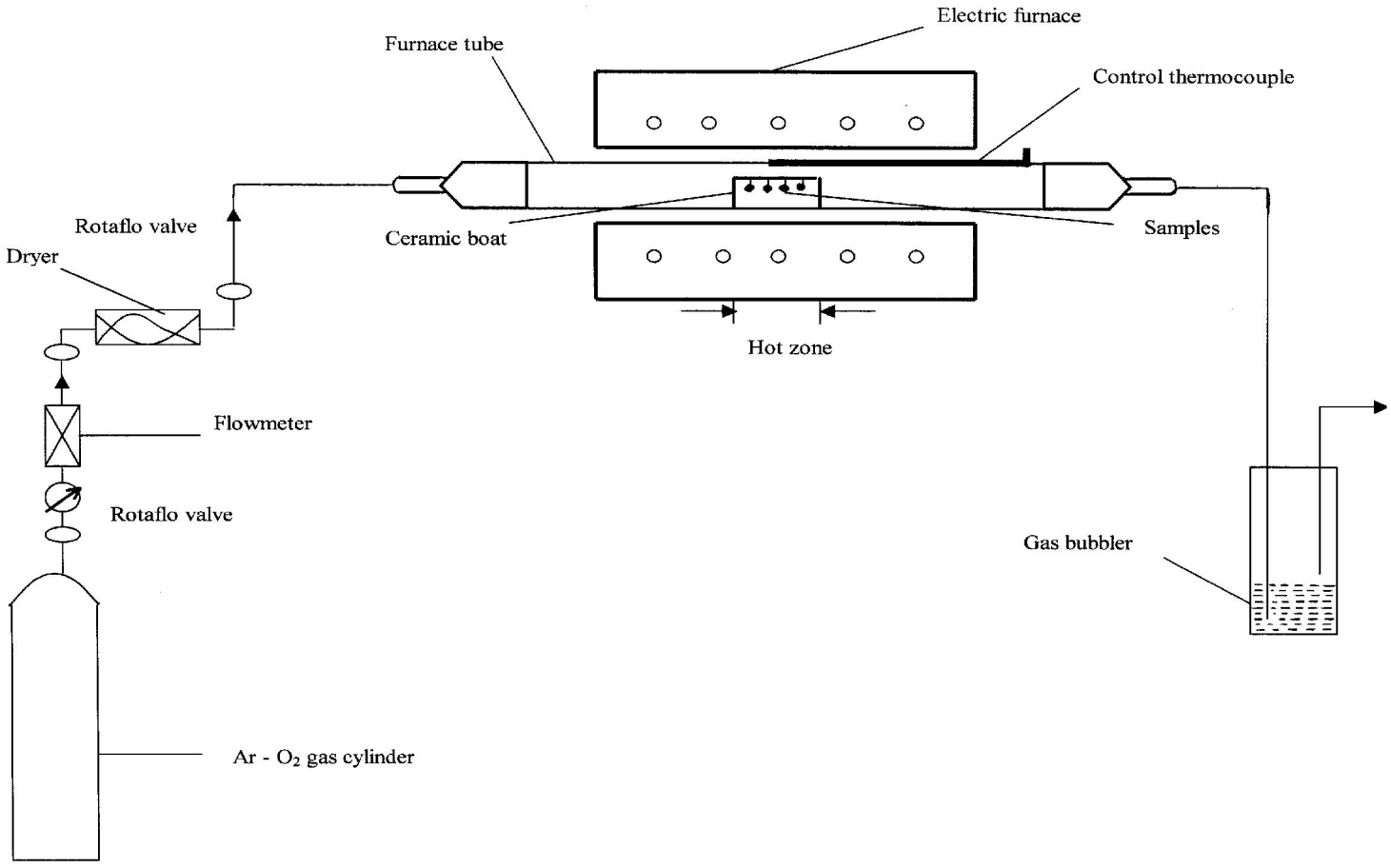

Figure 5-4 Schematic of the experimental rig for Ar-O_2 isothermal oxidation

Sulphidation/Oxidation rigs

The pathways of the reactive and the purging (Ar and H_2) are schematically represented in **Figure 5-5**. For sulphidation/oxidation experiments the system was flushed for three hours with Ar and two hours with H_2 at a flow rate of 12 l/h to remove the residual air from the reaction chamber. the premixed H_2/H_2S (10% H_2S and 90% H_2) gas mixture was introduced at a rate of 2 l/h through two Dreschel bottles containing de-ionised water held at a temperature of 23°C to yield $pO_2 \sim 1.2 \times 10^{-15}$ Pa; this flow rate was maintained for the duration of the experiment. The sulphidation/oxidation experiments were performed in an H_2/H_2S gas mixture yielding a pS_2 of ~ 6.8×10^{-1} Pa at 850ºC (The method used to calculate the pS_2 and pO_2 values is set out in **appendix C**). The pre-mixed H_2/H_2S gas mixture was passed through a gas flow rate gauge. One gas bubbler partially filled with inert silicones oil for flow-monitoring purposes was located just downstream from the furnace gas-outlet. After complete flushing of the reaction chamber with the reactive gas, the furnace was switched on (adjusted already to the desired temperature). The samples were exposed for various periods up to 240h. At the end of each experiment, the specimens were furnace cooled in Ar at a flow rate of 8 l/h over a period of 12h. At the ambient temperature, the experimental rig system was opened and the corroded specimens were withdrawn for examination.

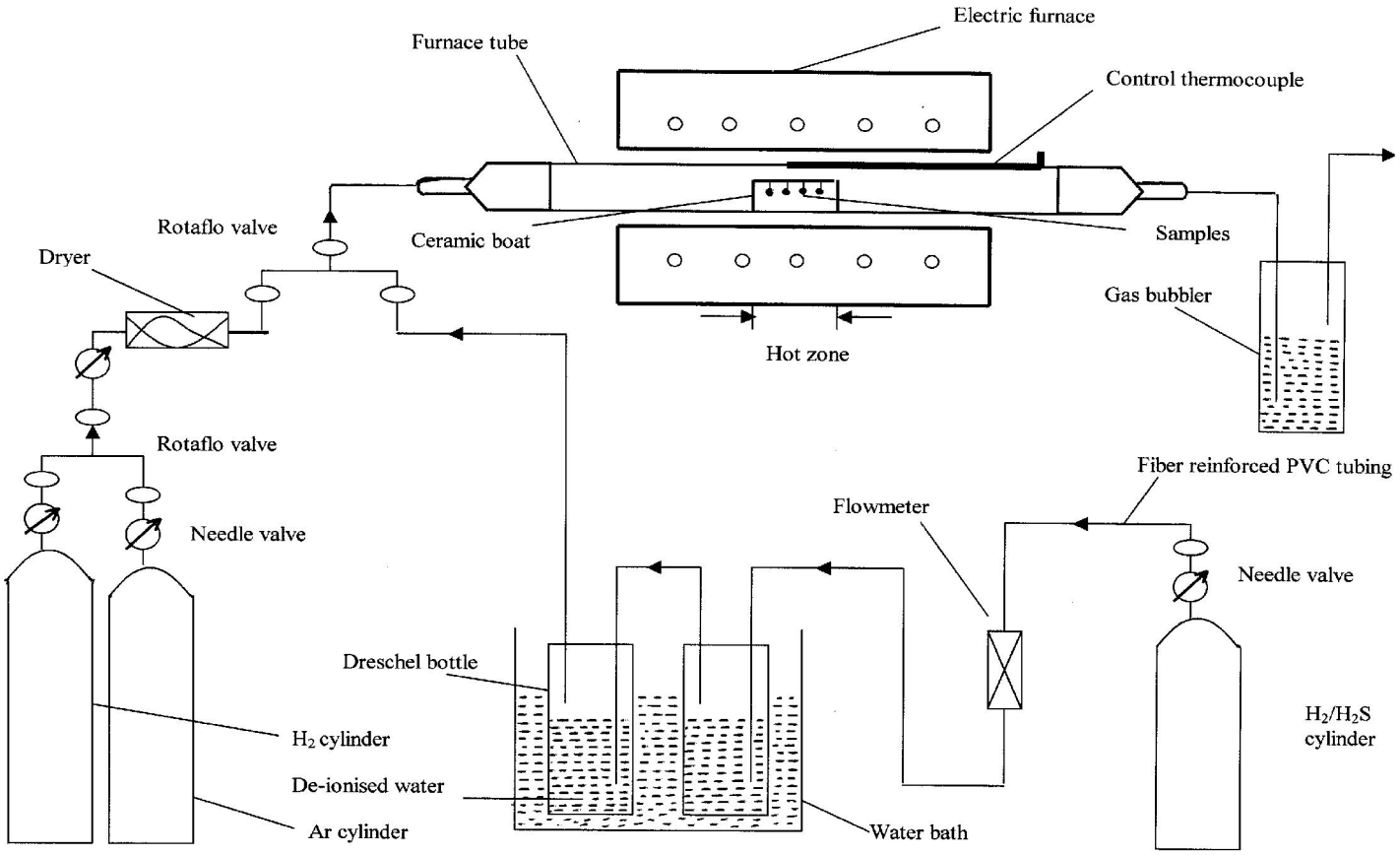

Figure 5-5 Schematic of the experimental rig for isothermal sulphidation monitoring

5.2.3 Characterisation Procedures

SEM

After an initial visual examination, the corroded samples were examined by scanning electron microscope (SEM), which was Cambridge MK2. Representative samples of corroded alloys were examined in order to evaluate the scale surface morphology. Scales were also examined in cross-section using SEM for an accurate measurement of each scale thickness and to observe the extent of stratification or layering of the scales and the conditions of the metal/oxide interface. The corroded Fe_3Al samples were coated with Au in order to avoid any possible charging effect.

EDX

An Energy Dispersive analysis by X-ray (EDX) system of Jeol JSM 352 and Link AN 10000, attached to the SEM, enabled the distribution of elements in the as received materials and in the scales of the corroded samples to be qualitatively and semi-quantitavely determined. Qualitative (not quantitative), X-ray distribution maps (Digimaps) of the elements present in the samples were recorded photographically.

XRD

X-ray Diffraction (XRD) analysis was also used in this investigation to identify the phases of the various corrosion products. The samples were fixed in SEIMENS Diffract 5000 while being bombarded with Cu-K_α radiation. This technique has the advantage of enabling the convenient use of bulk specimens rather than powder specimens. Only the major phases present were identified by X-ray diffraction techniques because of the complex nature of various scales produced. For some of the thick-scaled samples, subsequent polishing – using 1200 SiC grit – was performed and examined separately by XRD in order to determine the phases at each layer in the scale.

5.2.4 Difficulties of the Present Characterisation Work

Quantitative estimates of the nitrogen and nitrogen compound were found to be very difficult to detect and characterise using the available techniques. The nitride compounds (e.g. TiN) which was present in the corrosion product of Ti-46.7Al-1.9W-0.5Si alloy (after air oxidation) was found to be complicated by the fact that the nitrogen – as a very light element – was much below the resolution ability of the detector of the used EDX. Also the peaks from Si and W in Ti-46.7Al-1.9W-0.5Si alloy overlapped due to their similar emission wavelengths. Qualitative analysis of the corroded Ti-46.7Al-1.9W-0.5Si alloy by conventional XRD revealed clear peaks of TiN, SiO_2 and WS_2. The peaks vary in their orientations as the experimental condition changed, which reflects the reliability of the results obtained from the XRD. SEM was conducted on cross-sectioned samples of Ti-46.7Al-1.9W-0.5Si alloy, in order to determine the thickness, nature and location of the nitride layer. Useful information was derived from the X-ray maps regarding the formation of TiO_2, Al_2O_3 and the enrichment or depletion of Ti and Al at the subsurface of Ti-46.7Al-1.9W-0.5Si alloy. By correlating these obtained data from various characterising techniques in this study, it was possible to understand the corrosion mechanism(s) of Ti-46.7Al-1.9W-0.5Si alloy. Based on this understanding, the corrosion models were derived and clear interpretations regarding the effects of the nitrogen, oxygen and sulphur became possible.

One of the difficulties in characterising the scale properties of Fe_3Al alloys (with and without reactive element) such as growth mechanism and adherence is not being able to observe – using the available techniques – the substrate/scale interface on these alloys. It should be pointed out that examining oxide adherence of similar alloys in the literature was not possible in many studies. Conclusions about non-adherent scales thus can be based on SEM morphologies. While the morphology gives an indication of where the failure originated, it does not indicate why failure occurred. Thus while the RE addition is observed

in each case of the previous studies and this investigation to at least temporarily improve oxide adherence, no definite and clear experimental evidence to date, suggests a reason(s) for this improvement(s). In order to examine the REE – as in the present case – on the scale adhesion after oxidation of Fe_3Al with and without RE, a set of characterisation work was undertaken using SEM. The surface and the cross-sections of the oxidised (isothermal and cyclic oxidation) samples were critically examined. However, results based on the SEM were not satisfactory to explain the REE. So it was suggested that EDX should be used to identify the locations of the reactive element(s) in the oxidised samples, but due to the small amounts of the RE present in the experimental alloys, it was difficult in many instances to reach definite conclusions from the EDX results. For the same reason, the peaks from the conventional XRD of the oxidised alloys showed that Al_2O_3 is the main constituent of the external scale.

CHAPTER SIX

RESULTS

CHAPTER SIX

6.0 RESULTS

6.1 Introduction

In this chapter high temperatures (HT) corrosion results of Ti-46.7Al-1.9W-0.5Si and Fe_3Al (with and without REs) alloys are presented. **Section 6.2**, reports the isothermal oxidation of Ti-46.7Al-1.9W-0.5Si alloy in air and in Ar-O_2 atmospheres of various oxygen contents within a temperature range 750 to 950°C for up to 240h exposure time. The aim of the Ti-46.7Al-1.9W-0.5Si alloy oxidation studies is to investigate the effects of nitrogen – present in air – and the oxygen partial pressures of (0.05, 0.2 and 0.8) x 10^5 Pa on the oxidation behaviour of Ti-46.7Al-1.9W-0.5Si intermetallic alloy. The oxidation was performed in Ar-20%O_2 atmospheres (free of nitrogen) in order to avoid any possible nitridation (or any other nitrogen effects) with the same partial pressure of oxygen (0.2 x 10^5 Pa) in air. The difference between 0.05 x 10^5 Pa and 0.8 x 10^5 Pa (free from other impurities) of oxygen pressure in the reactive atmosphere was aimed to clarify the effect of oxygen partial pressure on the oxidation behaviour of Ti-46.7Al-1.9W-0.5Si alloy. After comparison of the oxidation results of Ti-46.7Al-1.9W-0.5Si alloy in different oxidising atmospheres, several interesting findings were obtained – these will be presented in **Section 6.2**. Summary of the sulphidation/oxidation behaviour of the coated and uncoated Ti-46.7Al-1.9W-0.5Si alloy is reported in **Section 6.3**. The obtained sulphidation/oxidation (in pS_2 ~ 6.8 x 10^{-1} Pa and pO_2 ~ 1.2 x 10^{-15} Pa at 850°C) results revealed sever attack of the uncoated Ti-46.7Al-1.9W-0.5Si alloy and a thick scale was formed, therefore, single (AlTiN and CrN) and double (AlTiN/CrN, AlTiN/NbN and CrN/NbN) layered coatings have been designed to protect Ti-46.7Al-1.9W-0.5Si alloy from such aggressive environment. The

developed coatings have proven their high protection capability to Ti-46.7Al-1.9W-0.5Si alloy for prolonged exposure time (240h) at 850°C as summarised in **Section 6.3**.

Isothermal and cyclic air oxidation results of the undoped and doped Fe_3Al intermetallics with the selected REs (Y and/or Hf) are presented in **Section 6.4**. The oxidation experiments for Fe_3Al alloys were carried out in the temperature range 900 and 1100°C for up to 240h (or cycles). Comparison of the oxidation behaviour of undoped and doped Fe_3Al intermetallic materials in isothermal and cyclic conditions is made. The aim of the comparison is to investigate the effects of thermal cycling and the REE on the kinetics and scale properties of the Fe_3Al alloys. During thermal cycling, the materials were subjected to a number of cycles. Each cycle period was one hour in the hot zone of the preheated furnace – to the desired temperature – and rapid cooling to approximately room temperature in air for 12 minutes. However, the materials under isothermal conditions were continuously heated in the furnace chamber – without interruption – for each exposure time. The exposure time – in cyclic condition – can also be considered as the number of cycles. The kinetic data of Fe_3Al alloys presented are based on the gross (with the spalled scale) weight gain, which is the difference in the weight of the oxidised materials (with the spalled scale) and its weight before exposure at a temperature. In general, the microscopic examination for the oxidised samples reflects the REE of scale adhesion to Fe_3Al intermetallics. However, the kinetic data are important in understanding the mechanism of the scale formation and growth process. In the present study and in most of the cases, and for better understanding of the REE, the microscopic investigation should be correlated to the kinetic data as will be explained throughout this section.

6.2 Isothermal Oxidation of Ti-46.7Al-1.9W-0.5Si Intermetallic Alloy

The microstructure of the as-cast Ti-46.7Al-1.9W-0.5Si alloy was investigated using optical microscope as illustrated in **Figure 6-1**. The microstructure consisted of predominately γ/α_2 lamellar structure. EDX results also shows the existence of WSi_2 as shown in **Figure 6-2**. Analysis of the spectra from conventional XRD confirm that the principal phases existing in the alloy are composed of γ-TiAl, α_2-Ti_3Al and small amounts of WSi_2.

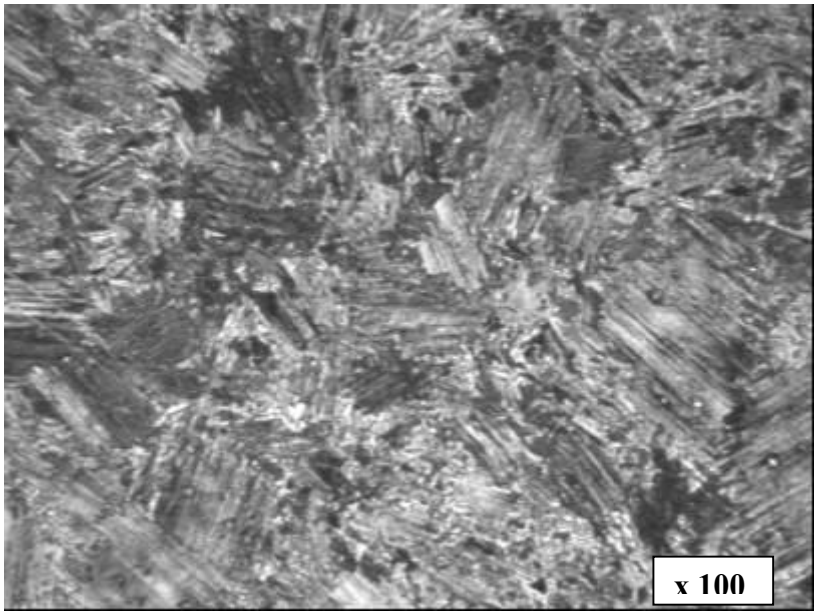

Figure 6-1 Optical micrograph of the as-cast Ti-46.7Al-1.9W-0.5Si intermetallic alloy

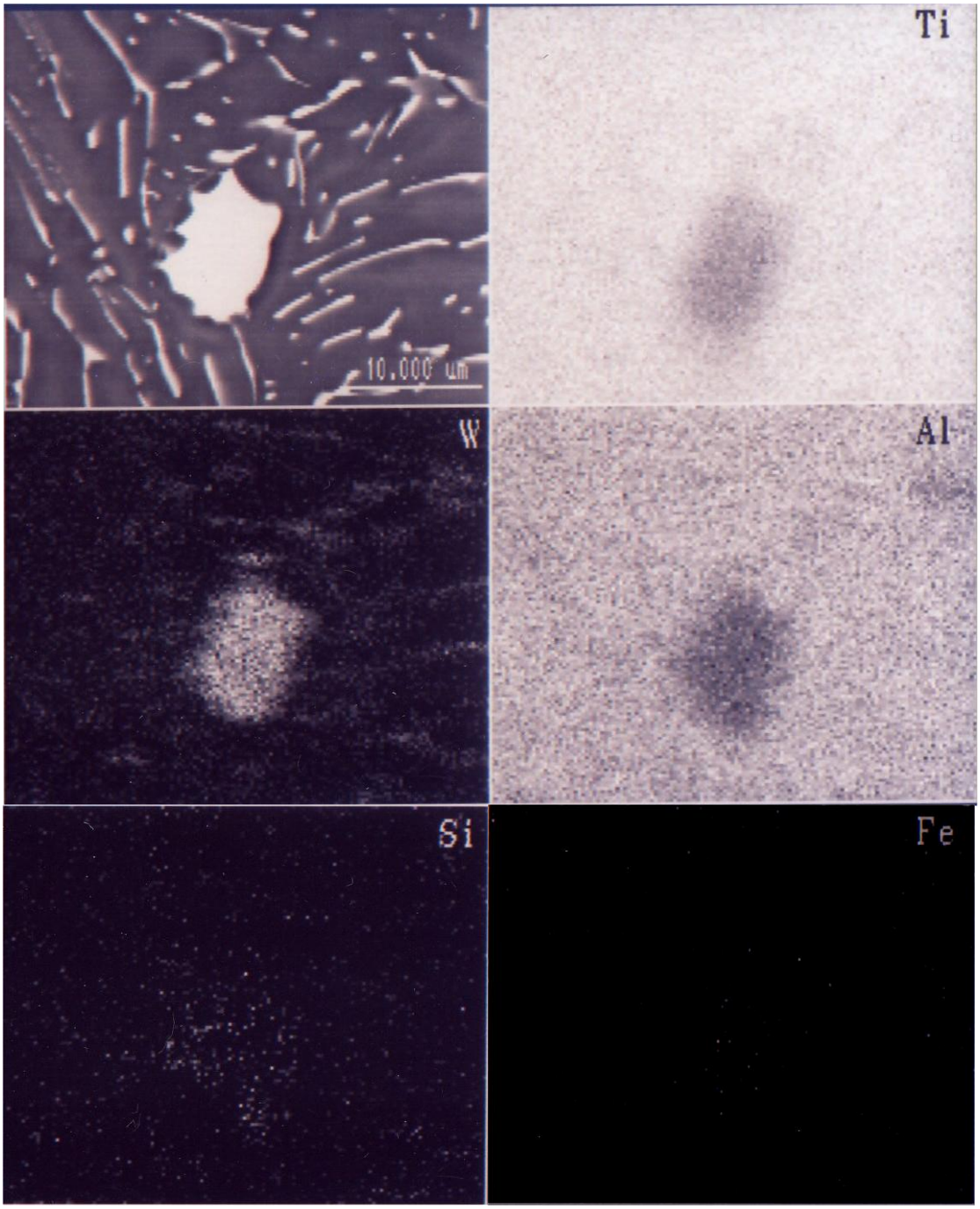

Figure 6-2 Back scattered electron image and Digimaps of the as-cast Ti-46.7Al-1.9W-0.5Si intermetallic alloy

6.2.1 Isothermal Oxidation of Ti-46.7Al-1.9W-0.5Si Alloy in Air and Ar-20%O_2

Mass change of Ti-46.7Al-1.9W-0.5Si alloy after isothermal oxidation in air and Ar-20%O_2

Figures 6-3 to **6-5** illustrates the oxidation kinetic results for the Ti-46.7Al-1.9W-0.5Si alloy in environments of air and Ar-20%O_2 at 750, 850 and 950^{o}C respectively. In general, oxidation rates in air are higher than those in Ar-20%O_2 at all three temperatures. The oxidation rate in both atmospheres increases with the increase of exposure temperature. However the effect of air on the oxidation behaviour of the alloy is more remarkable with increasing oxidation temperature. Marginal difference in weight gains of the alloy after oxidation in air and Ar-20%O_2 is observed at 750^{o}C (**Figure 6-3**) and the oxidation rate was doubled at 850^{o}C after 240h exposure. The corrosion rate in air was three times faster than that in Ar-20%O_2 at 950^{o}C for 240h oxidation. The oxidation of the alloy follows a parabolic rate law in both air and Ar-20%O_2 at 750^{o}C. At 850^{o}C, the alloy oxidised parabolically in air, whereas, the alloy oxidised parabolically at early stage of exposure (up to 24h) in Ar-20%O_2 then its oxidation rate was significantly reduced (**Figure 6-4**). The alloy also oxidised parabolically in air at 950^{o}C prior to 72h exposure but the corrosion rate was reduced after prolonged exposure. A quasi-parabolic rate was observed for the oxidation of the alloy in Ar-20%O_2 at 950^{o}C (**Figure 6-5**). **Table 6-1** gives the oxidation parabolic rate constants of Ti-46.7Al-1.9W-0.5Si alloy in both air and Ar-20%O_2 between 750 and 950^{o}C. The parabolic rate constants in both atmospheres are comparable at lower temperature (750^{o}C) whilst the parabolic rate constant in air at 950^{o}C is one order of magnitude higher than that in Ar-20%O_2.

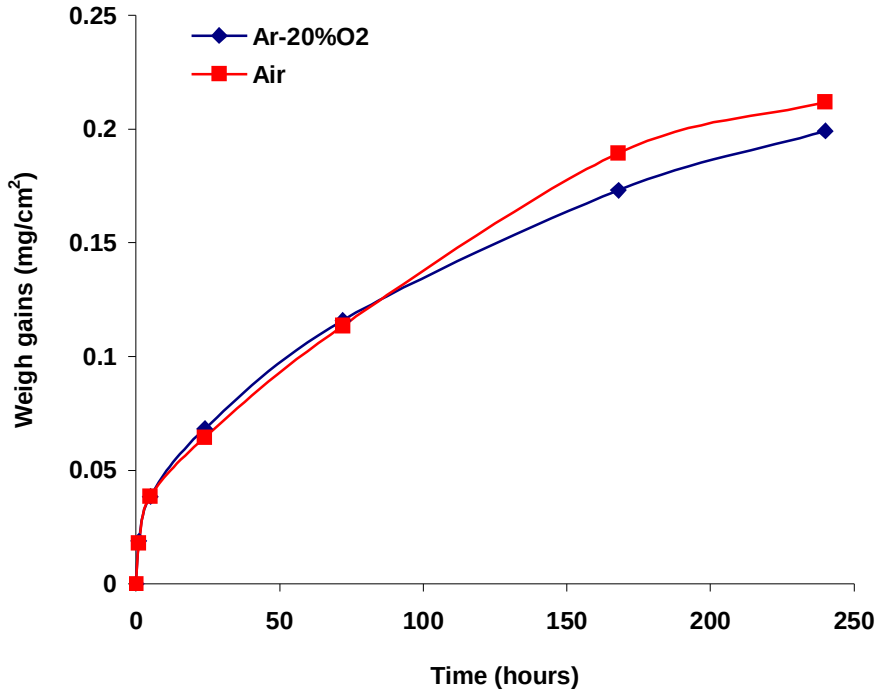

Figure 6-3 Weight gains versus exposure time for the Ti-46.7Al-1.9W-0.5Si intermetallic alloy after oxidation in air and Ar-20%O_2 at 750ºC for up to 240h

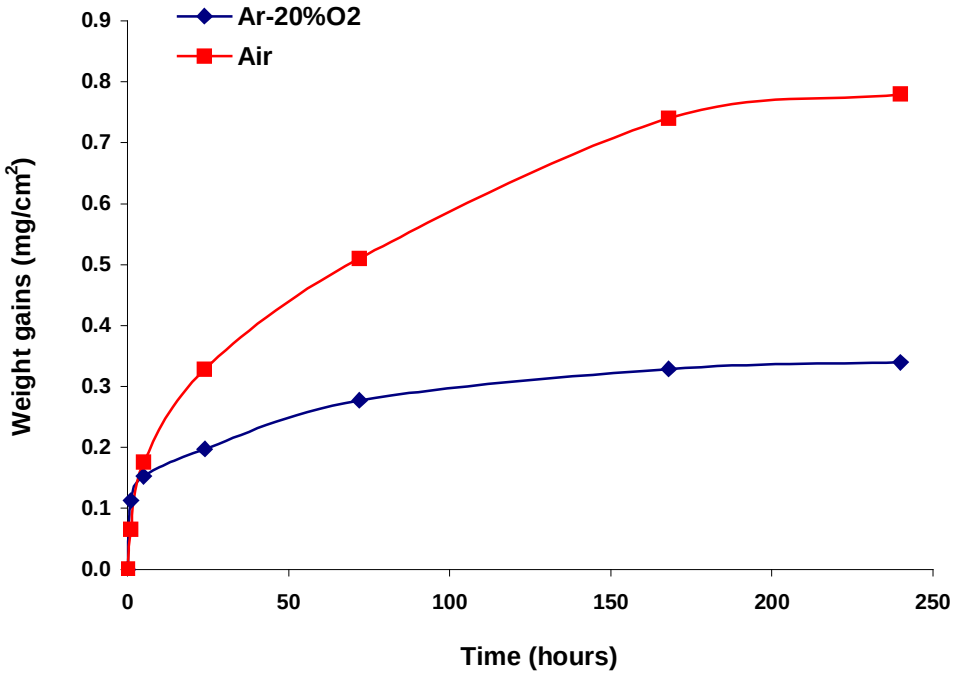

Figure 6-4 Weight gains versus exposure time for the Ti-46.7Al-1.9W-0.5Si intermetallic alloy after oxidation in air and Ar-20%O_2 at 850ºC for up to 240h

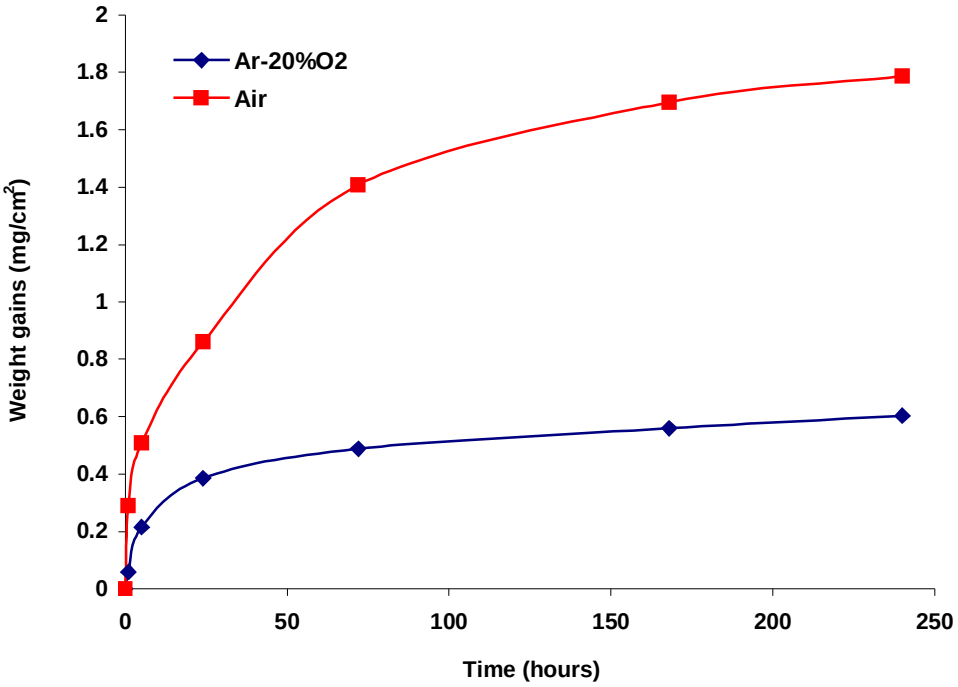

Figure 6-5 Weight gains versus exposure time for the Ti-46.7Al-1.9W-0.5Si intermetallic alloy after oxidation in air and Ar-20%O_2 at 950ºC for up to 240h

	750°C	**850°C**	**950°C**
Ar-20%O_2	$4.6x10^{-14}$	$1.2x10^{-13}$	$3.8x10^{-13}$
Air	$5.4x10^{-14}$	$7.3x10^{-13}$	$3.7x10^{-12}$

Table 6-1 Oxidation parabolic rate constants ($g^2/cm^4/s$) of Ti-46.7Al-1.9W-0.5Si intermetallic alloy after exposure in air and Ar-20%O_2 at 750, 850 and 950ºC for up to 240h

The oxidation parabolic rate constants versus reciprocal of temperature are plotted in **Figure 6-6**. The activation energies for oxidation of the alloy in both air and Ar-20%O_2 atmospheres are calculated from the slopes. The values of activation energy are 508,365 J/mole in air and 251,516 J/mole in Ar-20%O_2. The activation energy for oxidation of the Ti-46.7Al-1.9W-0.5Si alloy in air is more than double in Ar-20%O_2, which implies that the temperature dependence of the parabolic oxidation rate in Ar-20%O_2 was significantly lower than in air. This is due to the nitridation of the alloy after oxidation in air.

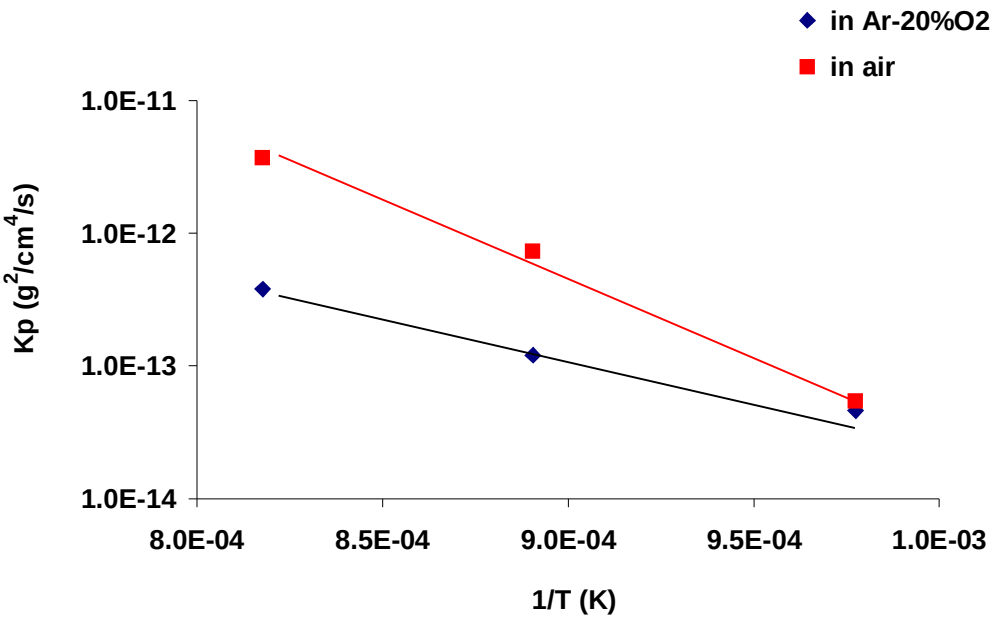

Figure 6-6 Parabolic rate constants of Ti-46.7Al-1.9W-0.5Si intermetallic alloy after oxidation in air and Ar-20%O_2 versus reciprocal of exposure temperatures

Scale morphology and composition of Ti-46.7Al-1.9W-0.5Si alloy after isothermal oxidation in air and Ar-20%O_2

Initially, when the Ti-46.7Al-1.9W-0.5Si alloy specimens were exposed to both air and Ar-20%O_2 atmospheres, isolated islands of TiO_2 formed on the alloy surface. A continuous alumina layer, which was identified by XRD as Al_2O_3 appeared to develop. With increasing exposure time, the alumina scale grew. However TiO_2 grew very slowly and did not form a continuous layer at low temperature (e.g. 750^oC) in both atmospheres even after long-term exposure (240h), as shown in **Figures 6-7**(**a**) and (**b**). At higher experimental temperature (e.g. 850^oC), the oxide scales were developed much more rapidly than at lower temperature. For example, a continuous Al_2O_3 layer was fully generated after just one hour exposure, as illustrated in **Figures 6-7**(**c**) and (**d**). Raising experimental temperature also promoted the outward diffusion of titanium, particularly in air atmosphere. **Figures 6-7**(**e**) and (**f**) show typical surface morphologies of Ti-46.7Al-1.9W-0.5Si specimens after 240h exposure in air and Ar-20%O_2 at 950^oC respectively. The TiO_2 layer had fully cover the sample surface in air (**Figure 6-7**(**e**)) whilst it did not fully cover the sample surface in Ar-20%O_2 (**Figures 6-7**(**f**)). Thickening of TiO_2 layer in air atmosphere caused a great deal of thermal stresses during the cooling period and gave rise to partial spallation of the oxide scale (**Figure 6-7**(**e**)).

The cross-sectioned morphologies and EDX analysis together with XRD results give more detailed information for the oxidised Ti-46.7Al-1.9W-0.5Si alloy in both air and Ar-20%O_2 environments. At 750^oC, any corrosion products were undetectable at early stages (e.g. 5h) of oxidation in air. However, increasing exposure time both TiO_2 and Al_2O_3 became detectable. For example, TiO_2, Al_2O_3 and TiN phases were found on the oxidised

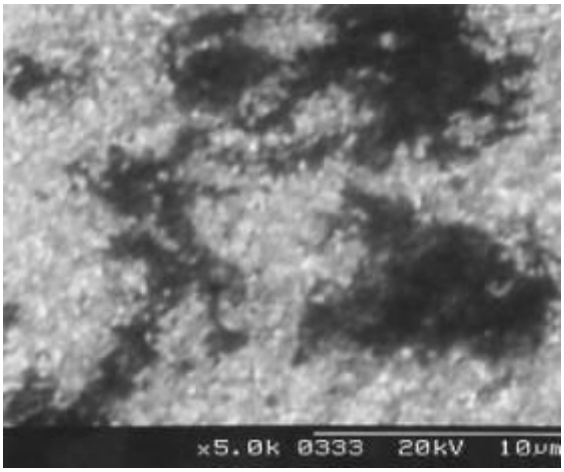

(**a**) In air, 750°C, 240 hours

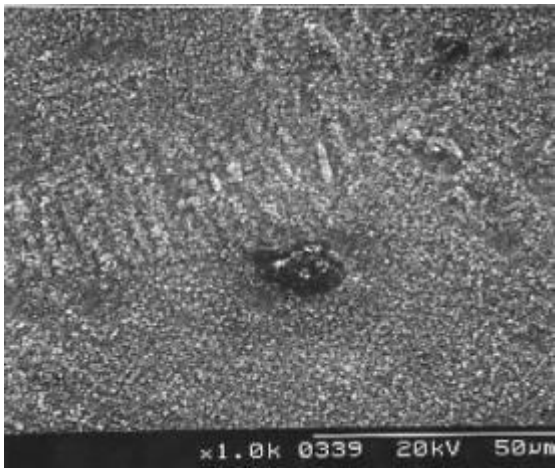

(**b**) In Ar-20%O_2, 750°C, 240 hours

(**c**) In air, 850°C, 1 hour

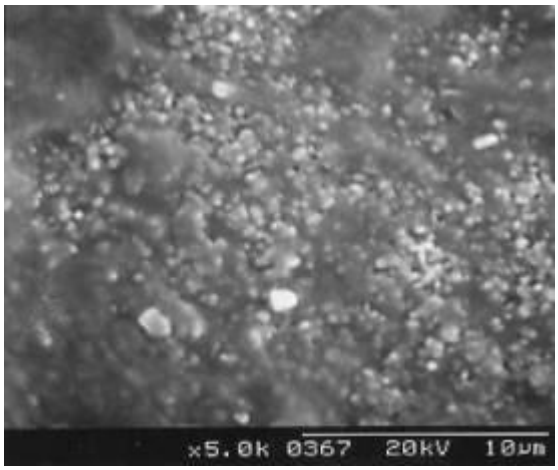

(**d**) In Ar-20%O_2, 850°C, 1 hour

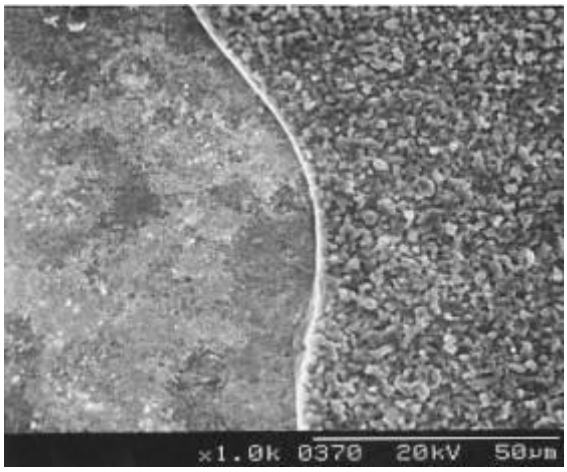

(**e**) In air, 950°C, 240 hours

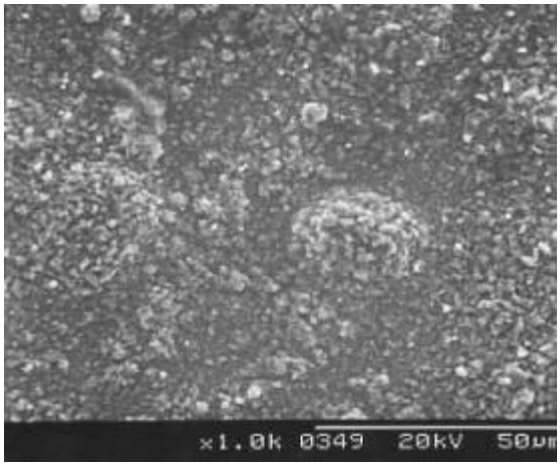

(**f**) Ar-20%O_2, 950°C, 240 hours

Figure 6-7 SEM morphologies of Ti-46.7Al-1.9W-0.5Si intermetallic alloy after oxidation in air and Ar-20%O_2 at 750, 850 and 950ºC for 240h

sample in air at 750°C after 240h exposure, as shown in **Figure 6-8**.

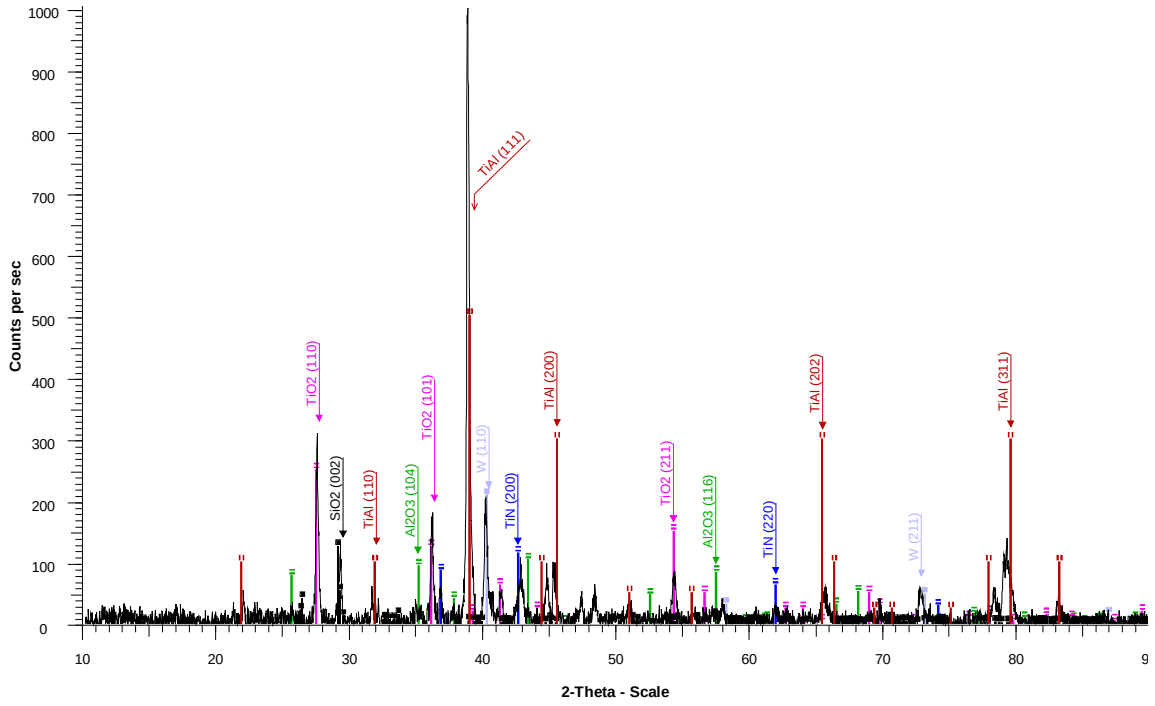

Figure 6-8 XRD pattern of Ti-46.7Al-1.9W-0.5Si intermetallic alloy after oxidation in air at 750ºC for 240h

X-Ray maps of the oxidised Ti-46.7Al-1.9W-0.5Si alloy sample in air at 750ºC for 240h are shown in **Figures 6-9.** It is clear that the scale of the sample oxidised in air is consisting of multi-layers of TiO_2 and Al_2O_3 with very thin layer of aluminium depletion. Increasing exposure temperature led to acceleration of the growth rate of the scales. **Figures 6-10** depicts the back-scattered (BS) micrographs and Digimaps for air oxidised Ti-46.7Al-1.9W-0.5Si alloy at 850°C after 240h exposure. The scale is multi-layered and thicker than that formed at 750°C and consisted of a continuous Al_2O_3 layer above which a discontinuous TiO_2 layer also formed. Beneath the Al_2O_3 layer, a thick TiO_2 layer developed with large

voids existed underneath this layer, then a thin TiN layer can be observed. The formation of the TiN layer in air at 850ºC gave rise to the development of a dark Al-enriched band that was identified by XRD (**Figures 6-11**) as $TiAl_2$. When the experimental temperature was further increased to 950°C, the outward diffusion of Ti was remarkably accelerated, hence, a continuous TiO_2 developed much earlier than at 750 and 850°C. **Figures 6-12** to **6-14** show the cross-sectioned BS micrographs and X-ray maps of oxidised Ti-46.7Al-1.9W-0.5Si alloy at 950°C in air for 5h, 72h and 240h respectively. Clearly a continuous TiO_2 had formed after 5h exposure (**Figure 6-12**). The overall microstructure of the scales is similar to that formed at 850°C. However, it is interesting to note that the scale and the dark $TiAl_2$ band became thicker with the increase of exposure time at 950°C. It is also obvious that the Al_2O_3 precipitated within the TiO_2 layer between the Al_2O_3 layer and TiN layer. A great deal of W (white spots in **Figure 6-14**) segregated at the interface of substrate and $TiAl_2$ band.

In the Ar-20%O_2 environment, a multi-layered scale of $TiO_2/Al_2O_3/TiO_2/Al_2O_3$ formed on the Ti-46.7Al-1.9W-0.5Si alloy at all three exposure temperatures. However the outer TiO_2 and the Al_2O_3 layer near the substrate were discontinuous at lower temperature (750°C) even after 240h exposure time, as illustrated in **Figure 6-15**.

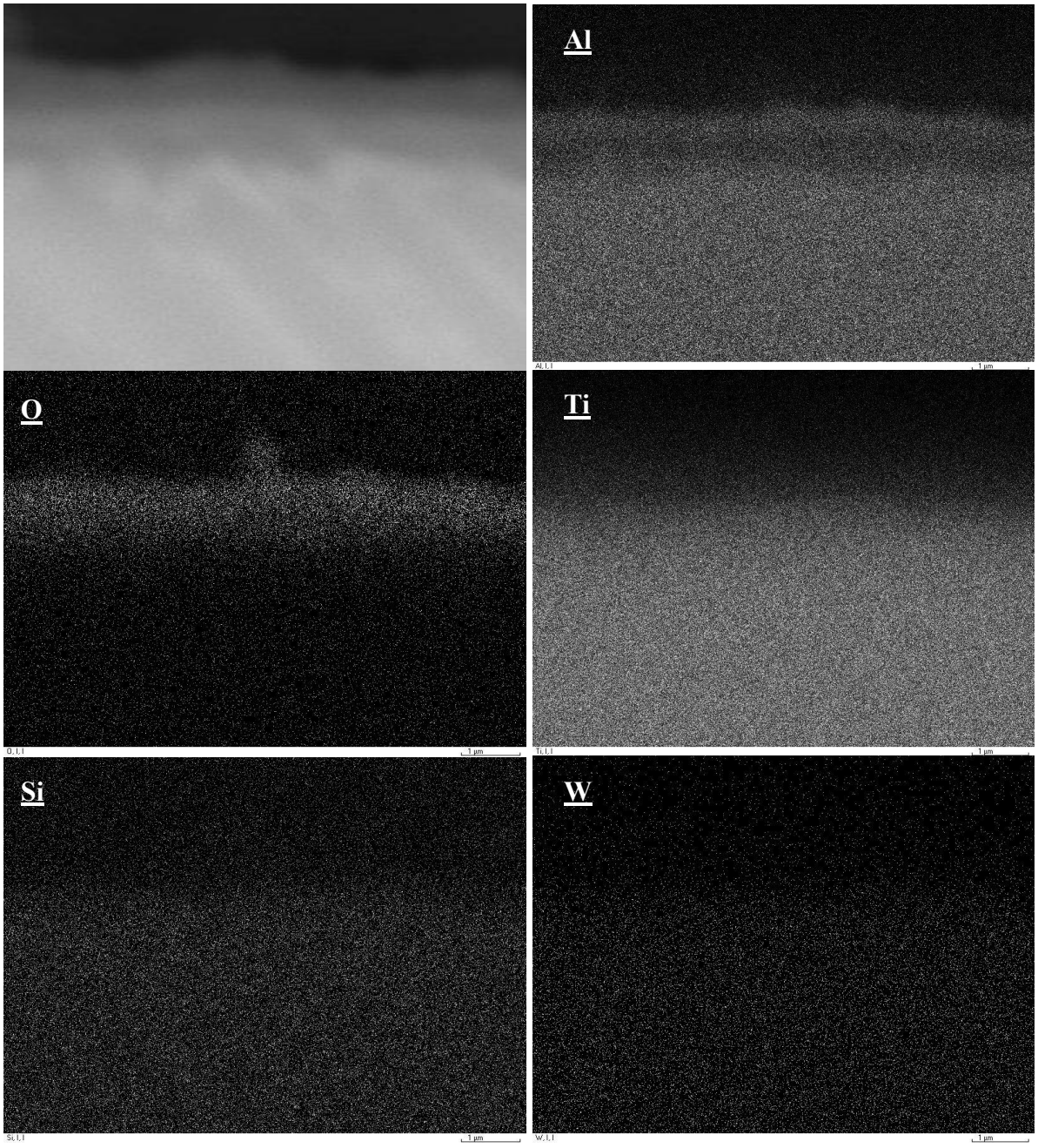

Figure 6-9 Back scattered electron image and Digimaps of Ti-46.7Al-1.9W-0.5Si intermetallic alloy oxidised in air at 750ºC for 240h

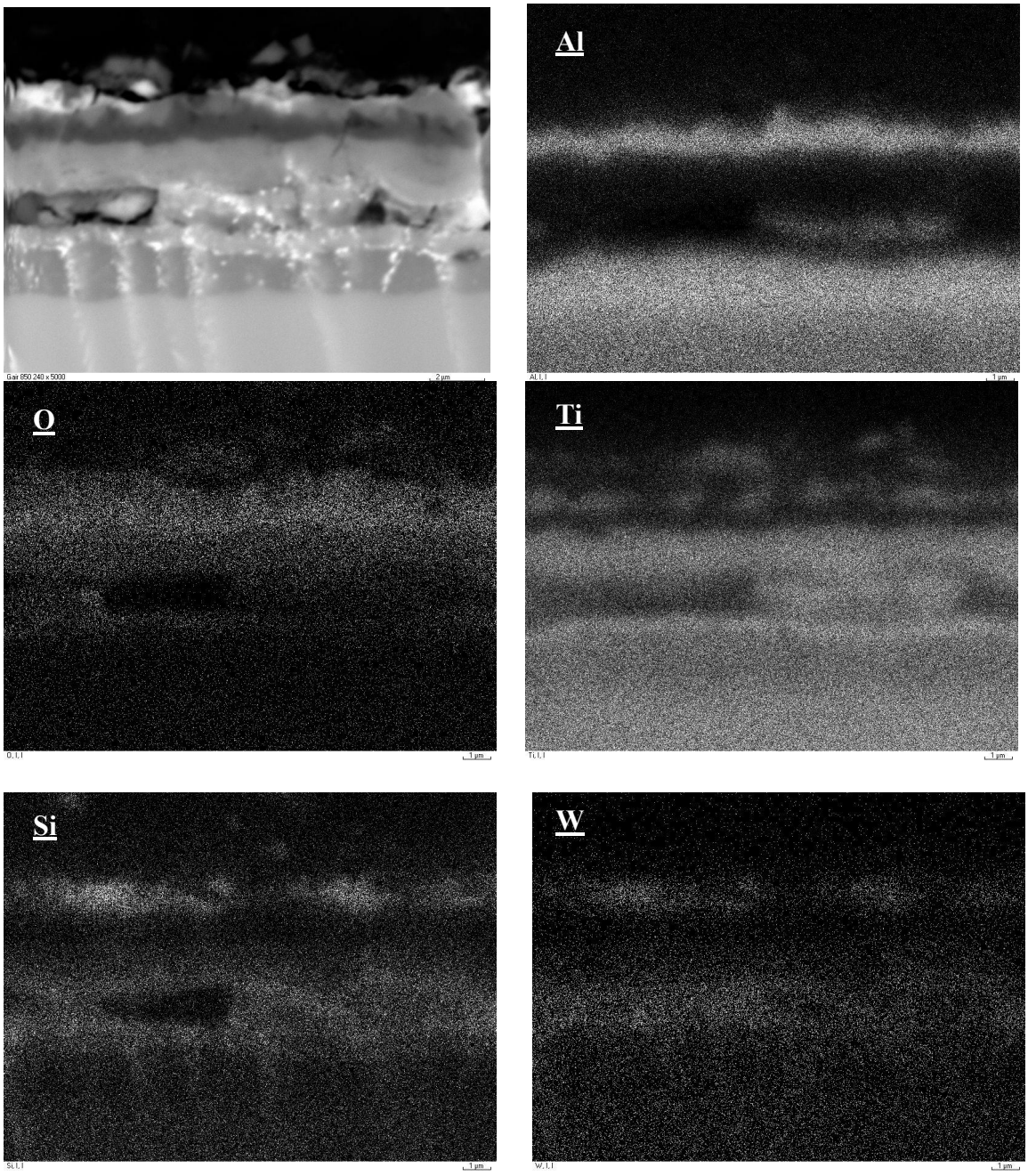

Figure 6-10 Back scattered electron image Digimaps of Ti-46.7Al-1.9W-0.5Si intermetallic alloy oxidised in air at 850ºC for 240h

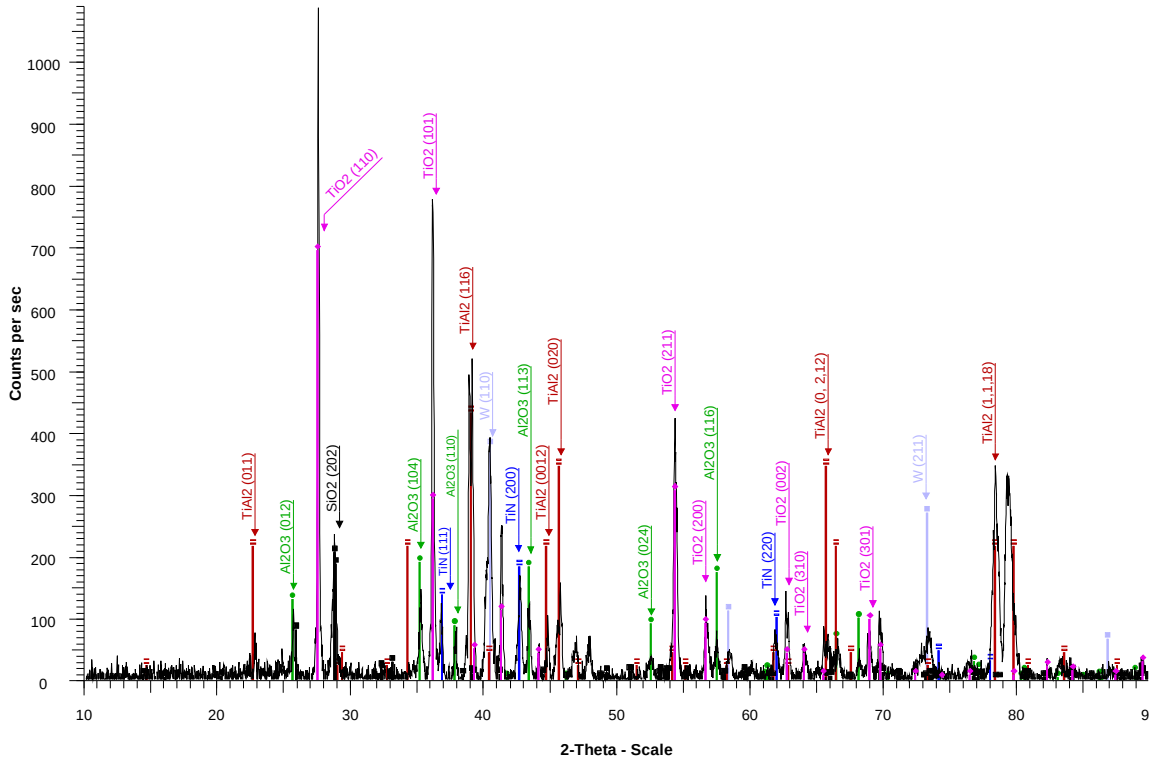

Figure 6-11 XRD pattern of Ti-46.7Al-1.9W-0.5Si intermetallic alloy after oxidation in air at 850ºC for 240h

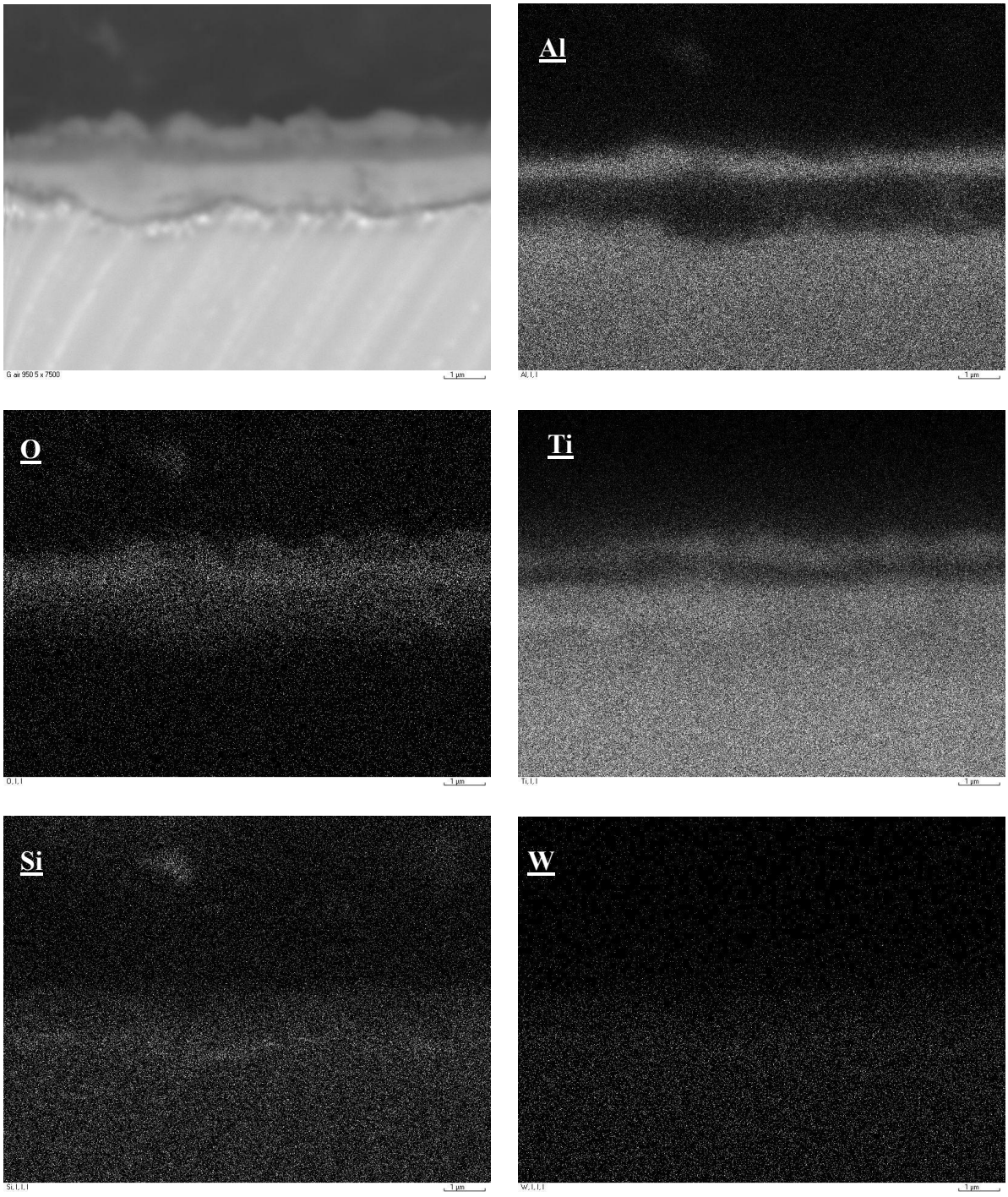

Figure 6-12 Back scattered electron image and Digimaps of Ti-46.7Al-1.9W-0.5Si intermetallic alloy oxidised in air at 950ºC for 5h

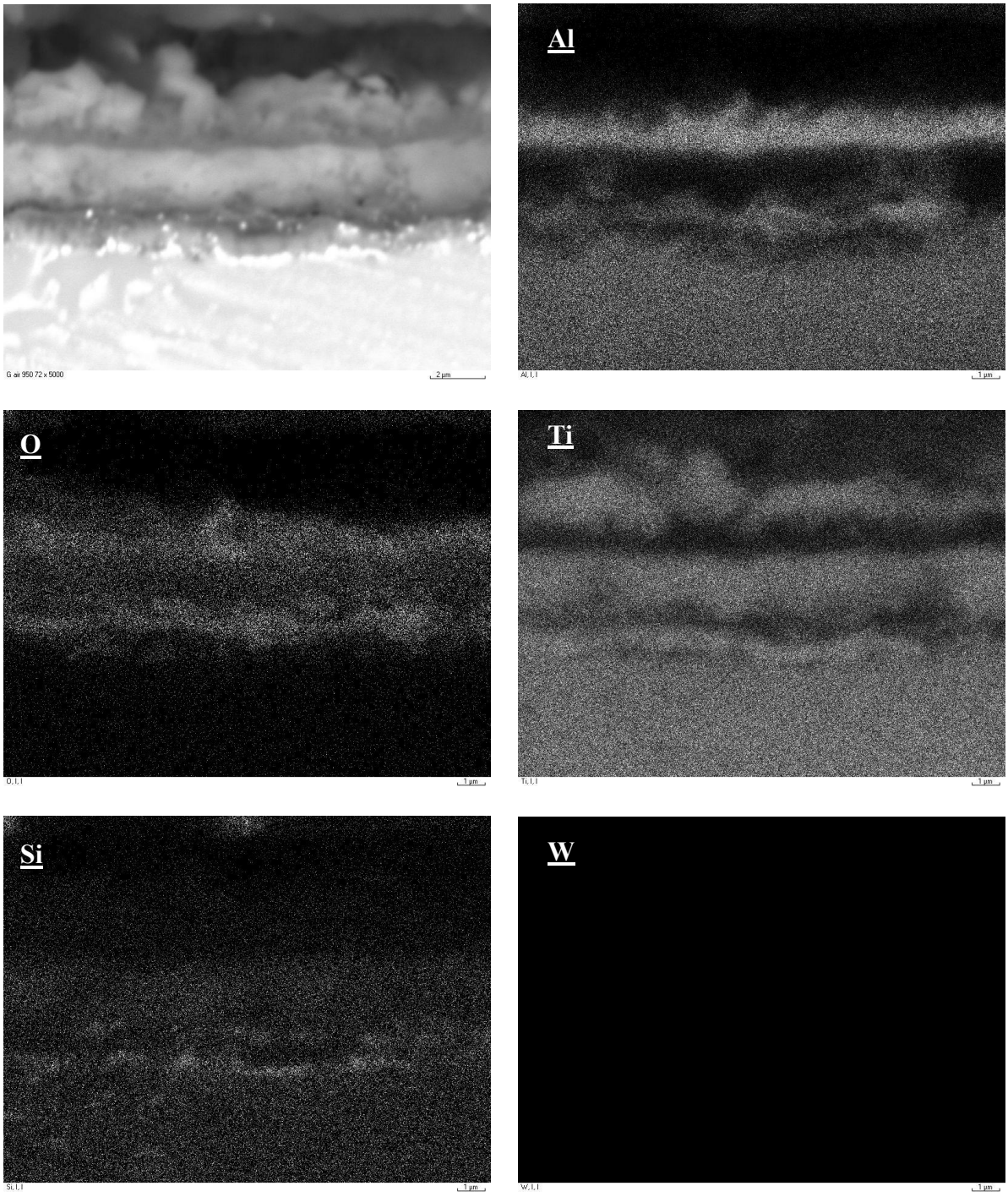

Figure 6-13 Back scattered electron image and Digimaps of Ti-46.7Al-1.9W-0.5Si intermetallic alloy oxidised in air at 950ºC for 72h

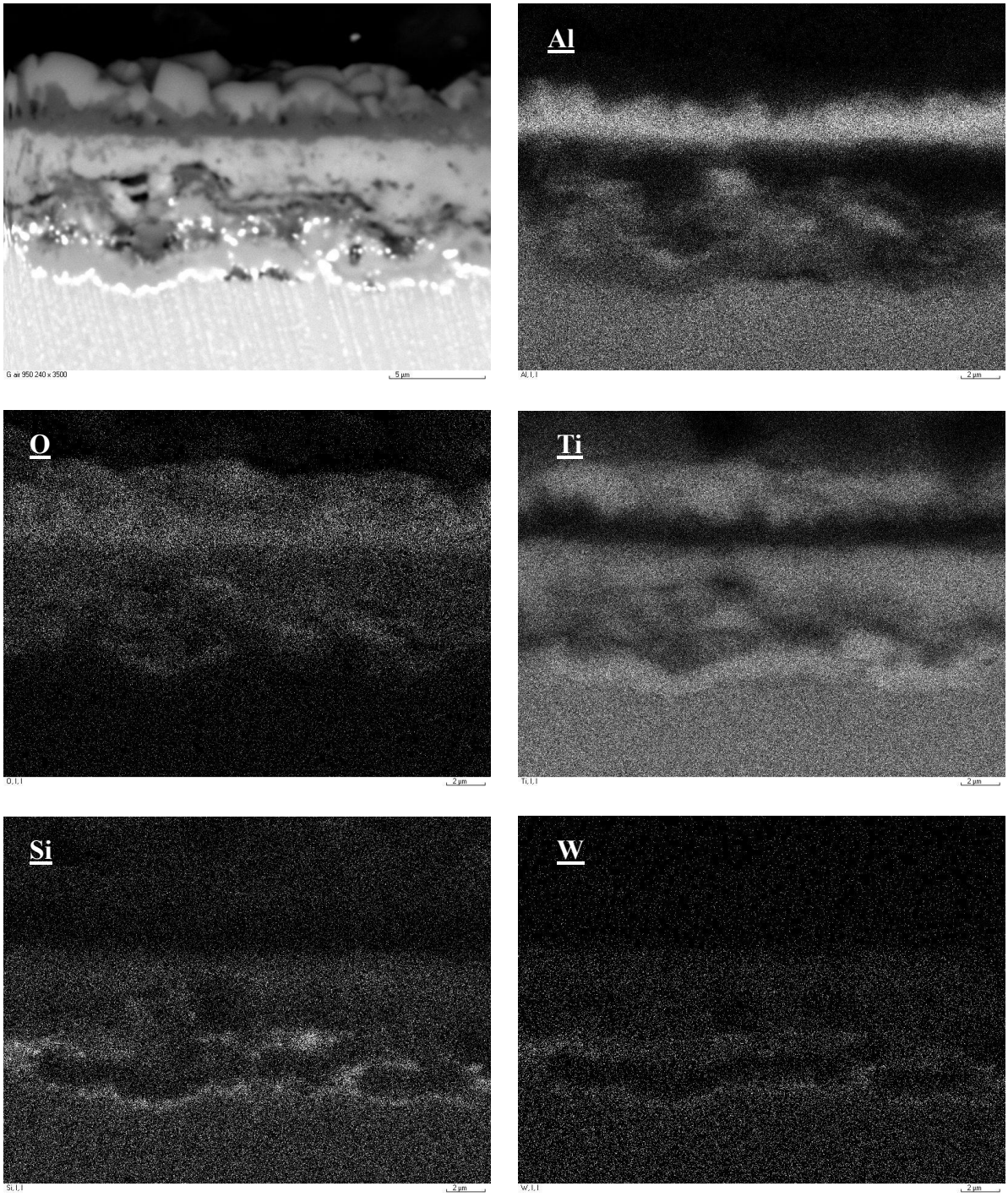

Figure 6-14 Back scattered electron image and Digimaps of Ti-46.7Al-1.9W-0.5Si intermetallic alloy oxidised in air at 950ºC for 240h

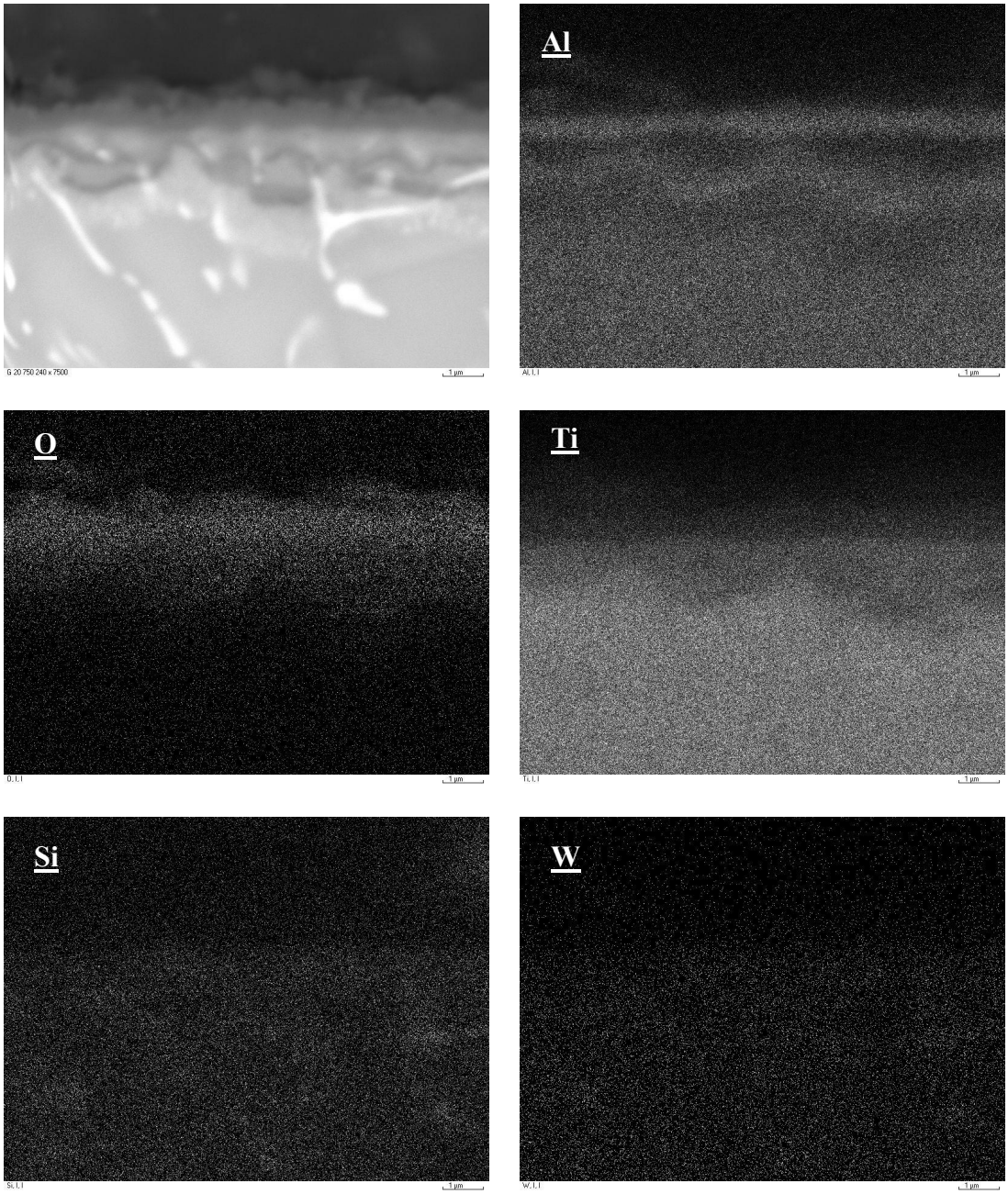

Figure 6-15 Back scattered electron image and Digimaps of Ti-46.7Al-1.9W-0.5Si intermetallic alloy oxidised in Ar-20%O_2 at 750ºC for 240h

When the temperature increased to 850°C in Ar-20% O_2, both layers of TiO_2 and Al_2O_3 became clear and continuous, as revealed in **Figure 6-16**. **Figure 6-17** contains the micrograph and Digimaps of the Ti-46.7Al-1.9W-0.5Si alloy after 240h oxidation at 950°C in Ar-20%O_2. It is noted that a substantial amount of Al_2O_3 precipitated in the second TiO_2 layer. Also considerable amount of pure W segregated through the aluminium depleted layer – identified by XRD as Ti_3Al – **Figure 6-18**. Spallation of the scale formed on Ti-46.7Al-1.9W-0.5Si alloy after air oxidation by a wedging process was observed as illustrated in **Figure 19**(**a**). The cross-sectioned morphologies of the cooled samples after oxidation in air – especially after longer exposure time at higher temperature (850 and 950ºC) – showed evidence of transverse cracks normal to the scale/TiN layer interface and also cracks formed along the interface just above the TiN layer. On the other hand, the multi-layered scale formed in Ar-20%O_2 environment were adherent but the scale grew non-uniformly (**Figure 19**(**b**)).

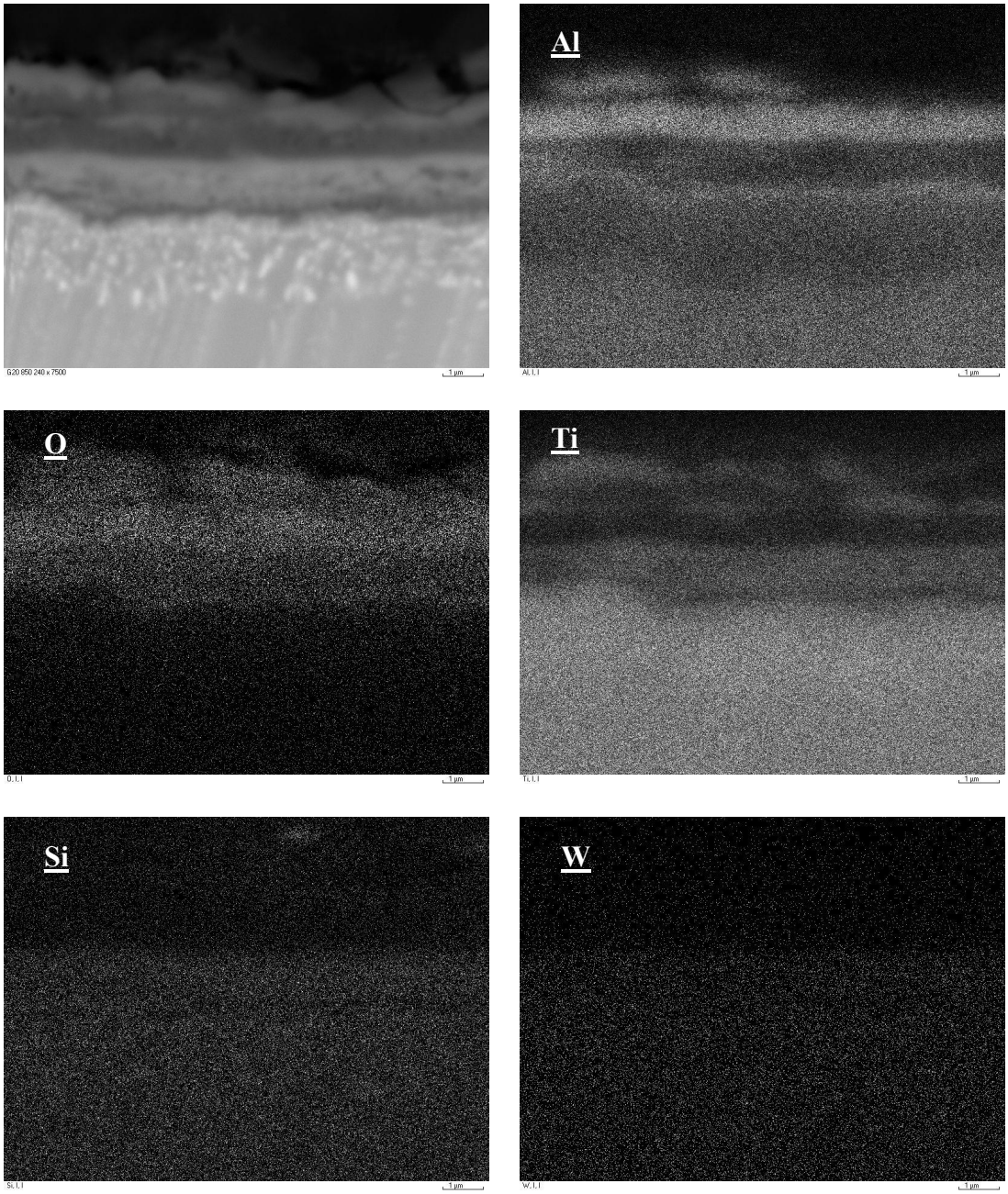

Figure 6-16 Back scattered electron image and Digimaps of Ti-46.7Al-1.9W-0.5Si intermetallic alloy oxidised in Ar-20%O_2 at 850ºC for 240h

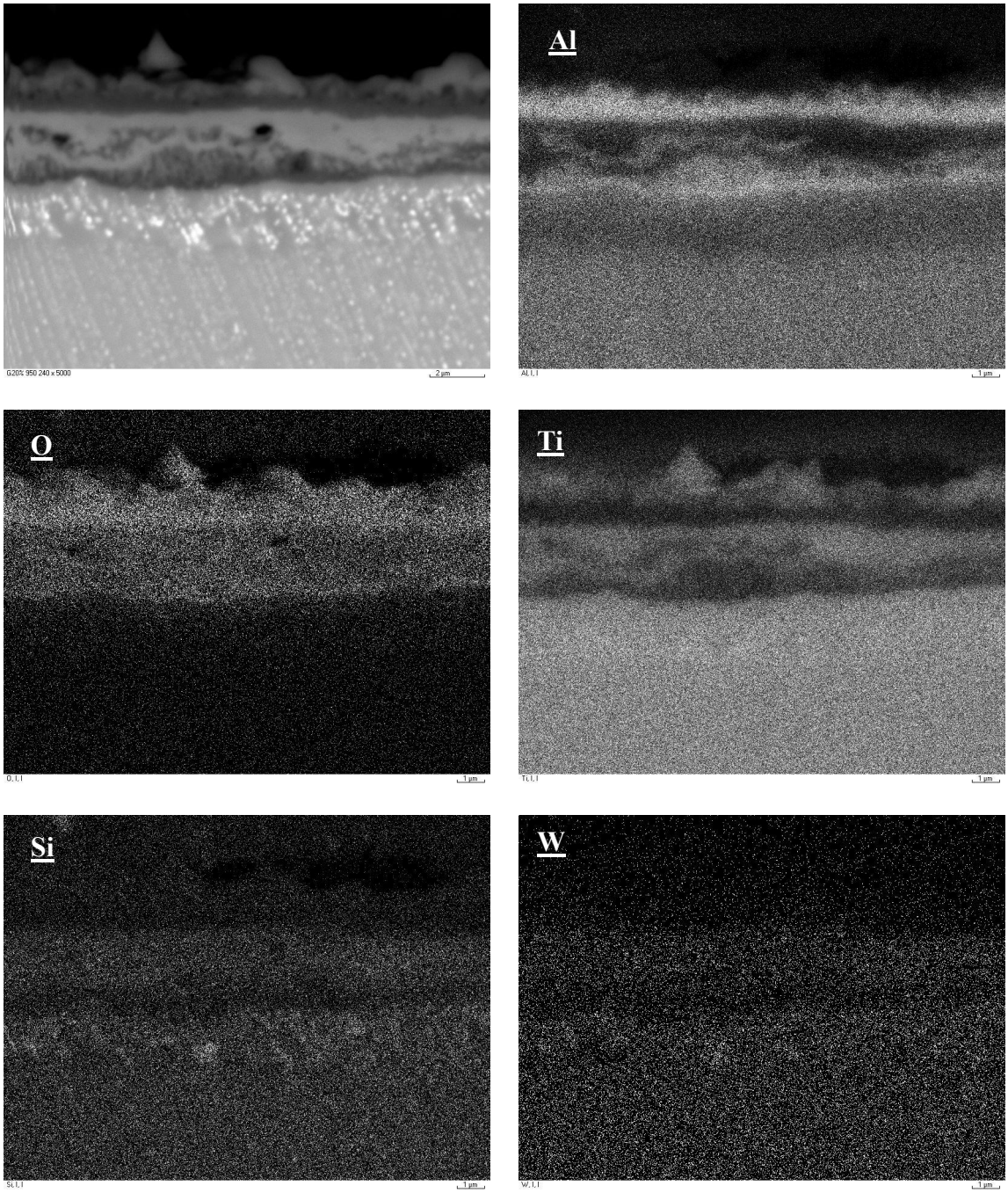

Figure 6-17 Back scattered electron image and Digimaps of Ti-46.7Al-1.9W-0.5Si intermetallic alloy oxidised in Ar-20%O_2 at 950ºC for 240h

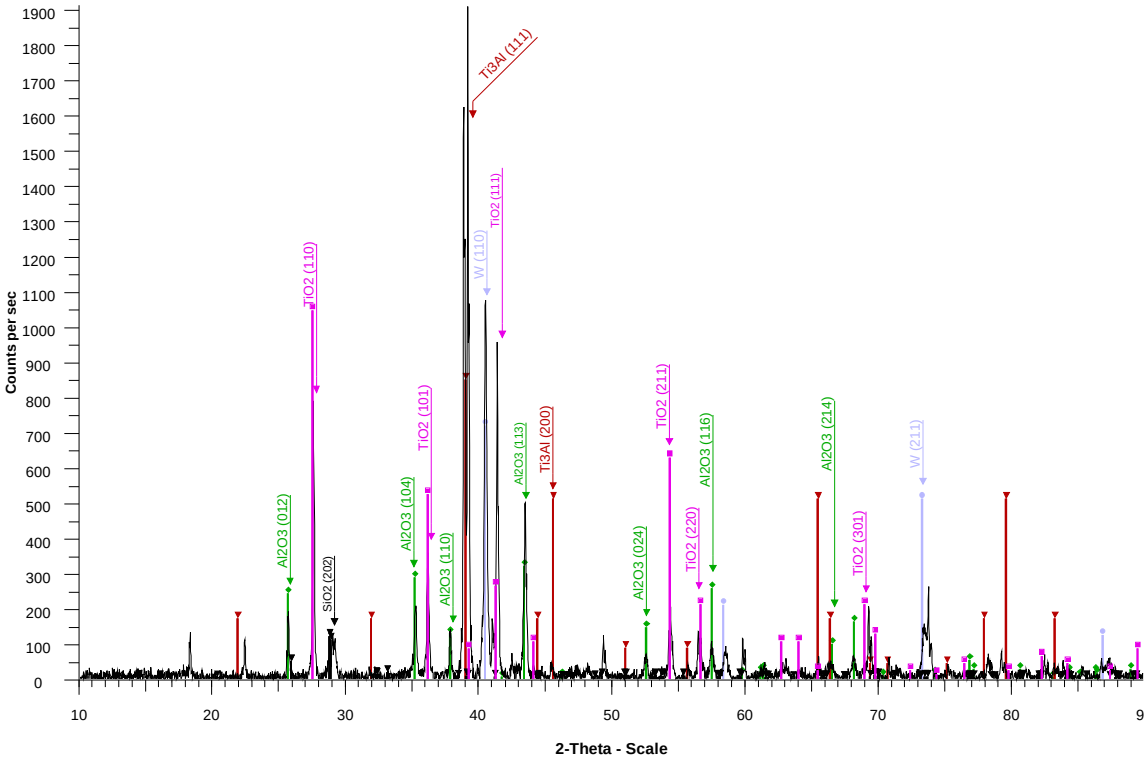

Figure 6-18 XRD pattern of Ti-46.7Al-1.9W-0.5Si intermetallic alloy after oxidation in Ar-20%O_2 at 950ºC for 240h

(**a**)

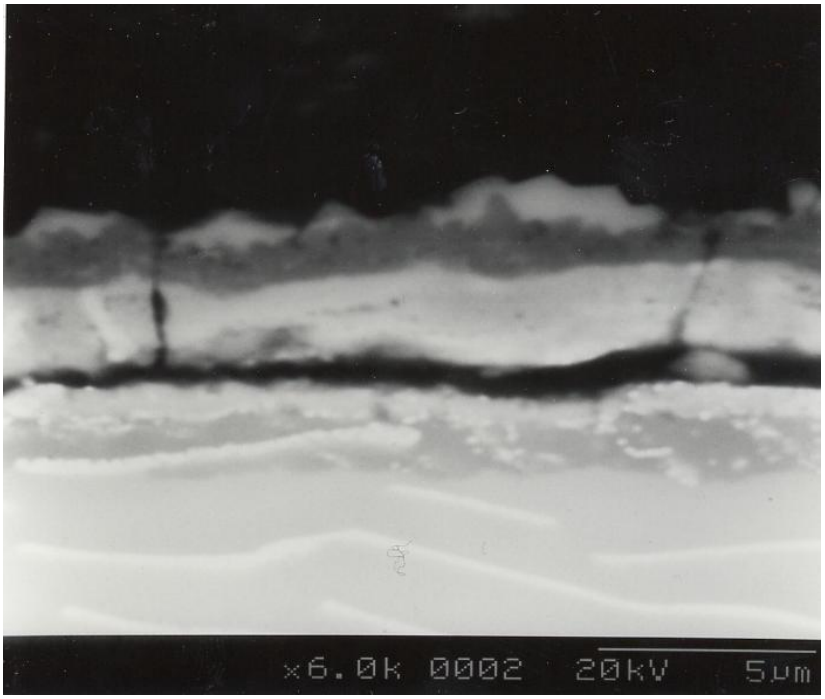

(**b**)

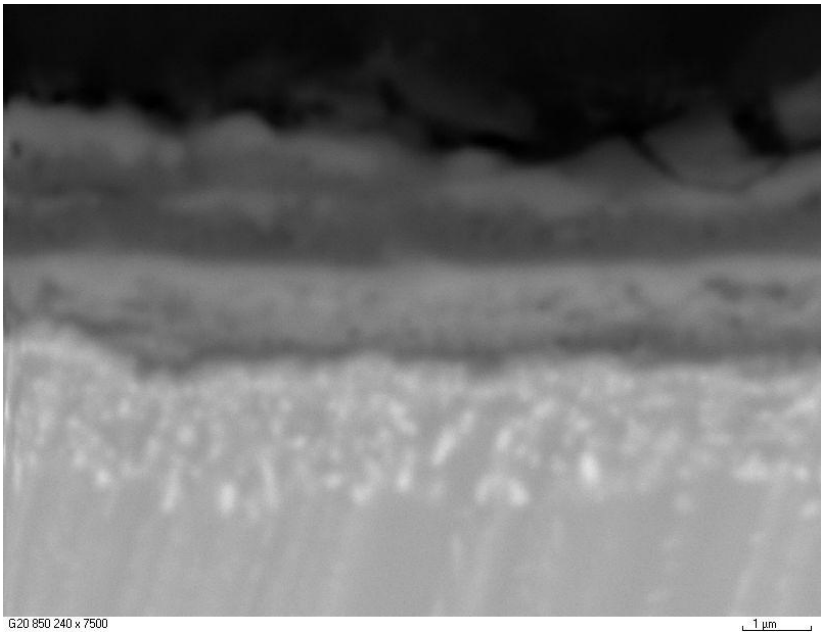

Figure 6-19 Back scattered SEM micrographs of Ti-46.7Al-1.9W-0.5Si intermetallic alloy after oxidation at 850ºC (**a**) in air for 168h and (**b**) in Ar-20%O_2 for 240h

6.2.2 Isothermal Oxidation of Ti-46.7Al-1.9W-0.5Si Alloy in Ar-5%O_2, Ar-20%O_2 and Ar-80%O_2 Atmospheres

Mass changes of Ti-46.7Al-1.9W-0.5Si alloy after isothermal oxidation in Ar-5%O_2, Ar-20%O_2 and Ar-80%O_2 atmospheres

Figures 6-20 to **6-22** show the isothermal kinetic weight changes of Ti-46.7Al-1.9W-0.5Si alloy in Ar-5%O_2, Ar-20%O_2 and Ar-80%O_2 at 750, 850 and 950°C respectively for up to 240h exposure time. Generally, the isothermal oxidation curves and the kinetic data analysis (**Table 6-2**) obtained at the three temperatures indicated some effects of oxygen partial pressure on the oxidation behaviour of Ti-46.7Al-1.9W-0.5Si alloy especially at higher temperatures. It is apparent that the oxidation rate of the material is higher in Ar-5%O_2 than in Ar-20%O_2 and Ar-80%O_2 within the entire range of exposure time and temperatures. At 750°C, the isothermal oxidation behaviour of the alloy for up to 72h exposure time in the three Ar-O_2 atmospheres was similar (**Figure 6-20**). As the exposure time increased, more increase of weight gain of the alloy in Ar-5%O_2 was observed, whereas the alloy showed parabolic behaviour in Ar-20%O_2 and Ar-80%O_2 for up to 240h. Although the parabolic oxidation rate constants of the alloy at 750°C and 850°C in Ar-5%O_2, Ar-20%O_2, Ar-20%O_2 and Ar-80%O_2 were of the same order of magnitude (**Table 6-2**), the reaction rate constant of the alloy in Ar-5%O_2 is approximately two times than in Ar-80%O_2. The divergence of mass gain data of the alloy in the three Ar-O_2 atmospheres at 850°C is very similar for up to 240h (**Figure 6-21**). At 950°C, the effect of oxygen partial pressure became more noticeable and the oxidation parabolic rate constant in Ar-5%O_2 is one order of magnitude higher than in Ar-80%O_2 (**Table 6-2**). In Ar-5%O_2 and Ar-20%O_2 at 950°C, the alloy showed parabolic oxidation behaviour, whereas in Ar-80%O_2 atmosphere quasi-parabolic 'protective' oxidation kinetic behaviour was observed (**Figure 6-22**).

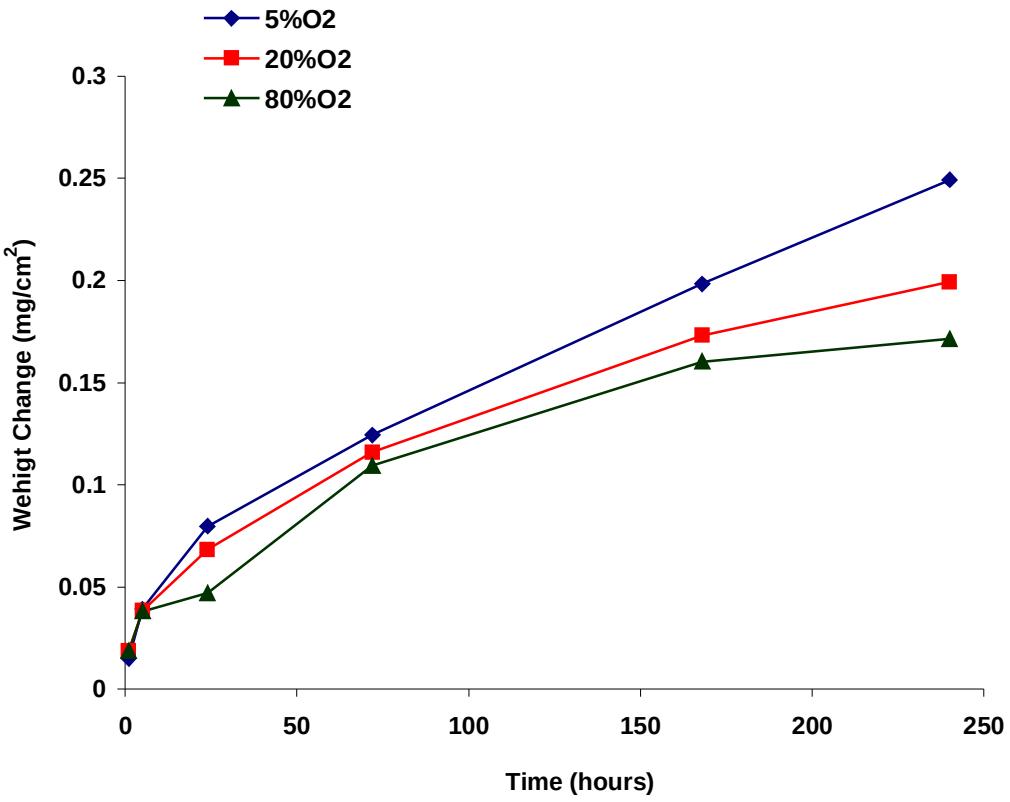

Figure 6-20 Weight gains versus exposure time for the Ti-46.7Al-1.9W-0.5Si intermetallic alloy after oxidation in Ar-5%O_2, Ar-20%O_2 and Ar-80%O_2 at 750ºC for up to 240h

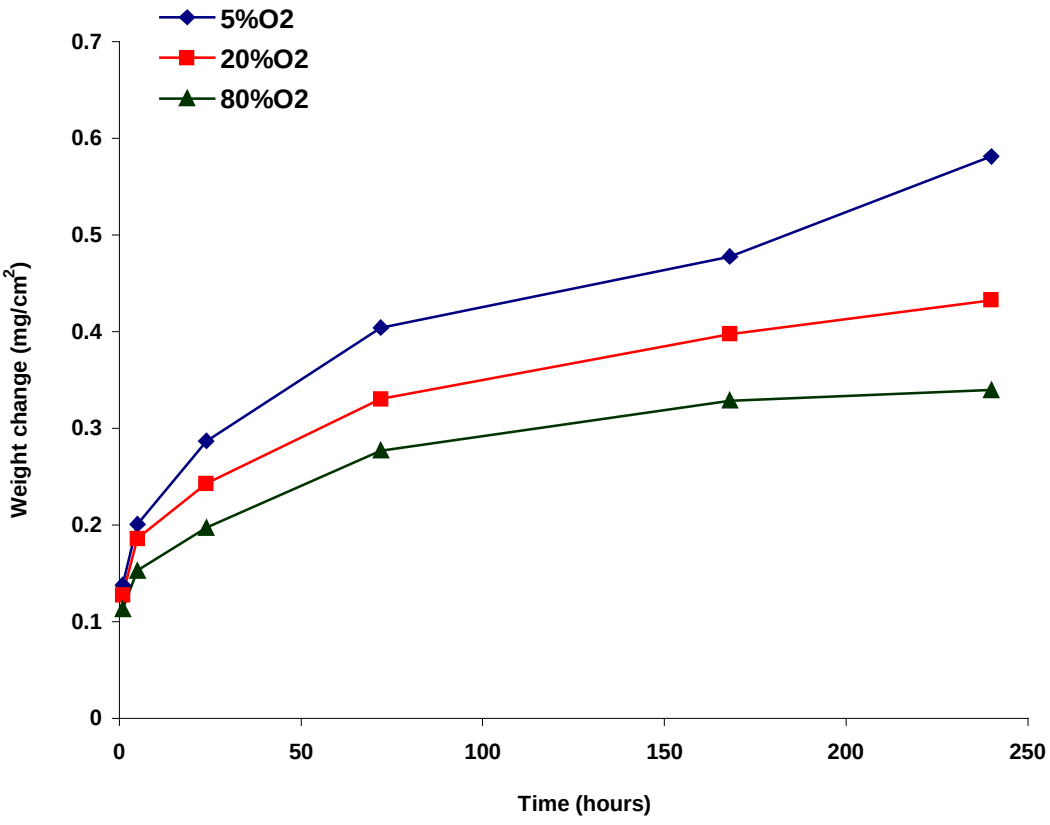

Figure 6-21 Weight gains versus exposure time for the Ti-46.7Al-1.9W-0.5Si intermetallic alloy after oxidation in Ar-5%O_2, Ar-20%O_2 and Ar-80%O_2 at 850ºC for up to 240h

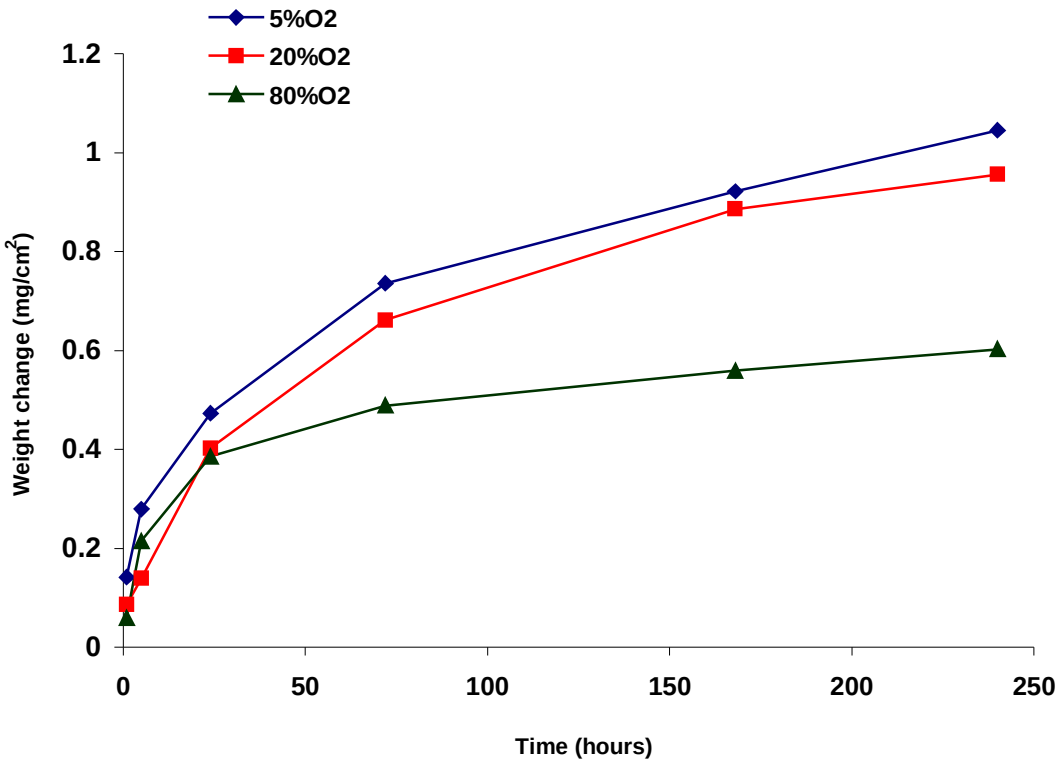

Figure 6-22 Weight gains versus exposure time for the Ti-46.7Al-1.9W-0.5Si intermetallic alloy after oxidation in Ar-5%O_2, Ar-20%O_2 and Ar-80%O_2 at 950ºC for up to 240h

	750°C	**850°C**	**950°C**
Ar-5%O_2	6.8 x 10^{-14}	3.41 x 10^{-13}	1.21 x 10^{-12}
Ar-20%O_2	4.26 x 10^{-14}	1.89 x 10^{-13}	1.08 x 10^{-12}
Ar-80%O_2	3.59 x 10^{-14}	1.18 x 10^{-13}	3.80 x 10^{-13}

Table 6-2 Oxidation rate constants ($g^2/cm^4/s$) of Ti-46.7Al-1.9W-0.5Si intermetallic alloy after exposure in Ar-5%O_2, Ar-20%O_2 and Ar-80%O_2 at 750, 850 and 950ºC for up to 240h

Scale morphology and composition of Ti-46.7Al-1.9W-0.5Si alloy after isothermal oxidation in Ar-5%O_2, Ar-20%O_2 and Ar-80%O_2 atmospheres

Generally, the scale formed in Ar-5%O_2 at 750°C was similar to that in Ar-20%O_2 but slightly different in Ar-80%O_2. During the initial periods of oxidation at 750ºC (up to 5h), no corrosion product was detected in the three Ar-O_2 atmospheres. After 72h exposure at 750°C, very low intensity peaks of TiO_2 and Al_2O_3 in the XRD pattern was identified. With the increase of exposure time to 240h, the scale became visible at high magnification (**Figure 6-23**). The proportion of TiO_2 and Al_2O_3 islands in the scale in the three Ar-O_2 atmospheres was very hard to distinguish at 750°C for up to 240h exposure. However, the intensities of TiO_2 peaks in Ar-5%O_2 was higher than those in Ar-80%O_2 – **Figures 6-24(a)** and **(b)** respectively. Although the XRD patterns – **Figures 6-24(a)** and **(b)** – of the oxidised samples.indicated the presence of both TiO_2 and Al_2O_3, the EDX results (**Figures 6-25** and **6-26**) of the corresponding samples revealed a mixed scale of TiO_2 and Al_2O_3 was formed in both Ar-5%O_2 and Ar-80%O_2 atmospheres. However, it is more obvious in Ar-5%O_2, the scale showed transverse micro-cracks perpendicular to the scale/alloy interface – **Figures 6-25**. Also a very thin depleted layer of aluminium at 750°C after 240h oxidation in Ar-5%O_2 and Ar-80%O_2 atmospheres was detected by EDX analysis (**Figures 6-25** and **6-26**). However, it was not possible to identify this thin layer by the available XRD.

Figure 6-27 show the surface morphologies of the scale formed on Ti-46.7Al-1.9W-0.5Si alloy after oxidation in Ar-5%O_2 and Ar-80%O_2 at 850°C for 5h exposure. The rutile in Ar-5%O_2 started to overgrow (**Figure 6-27**(**a**)) resulting in a scale predominant of TiO_2

(**a**)

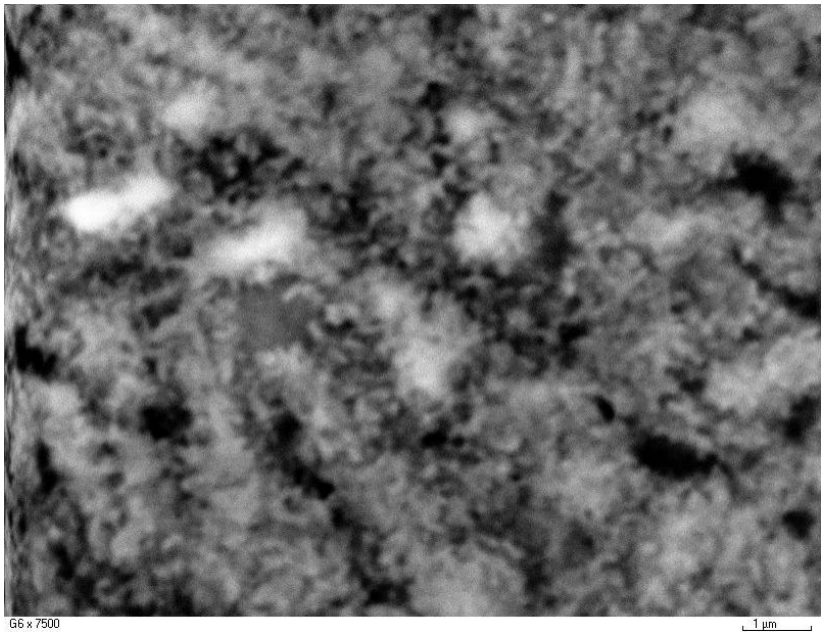

(**b**)

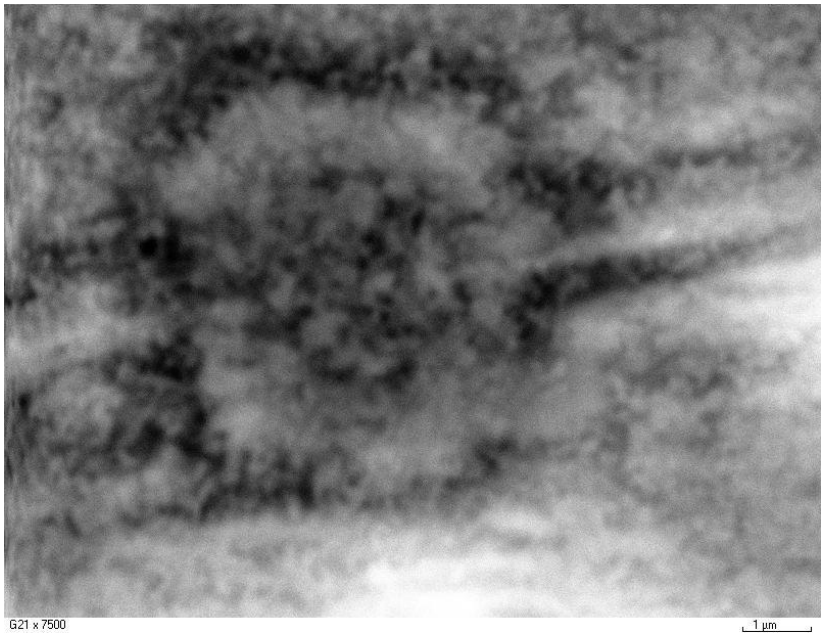

Figure 6-23 SEM micrographs of Ti-46.7Al-1.9W-0.5Si intermetallic alloy after oxidation at 750ºC for 240h (**a**) in Ar-5%O_2 and (**b**) in Ar-80%O_2

(**a**)

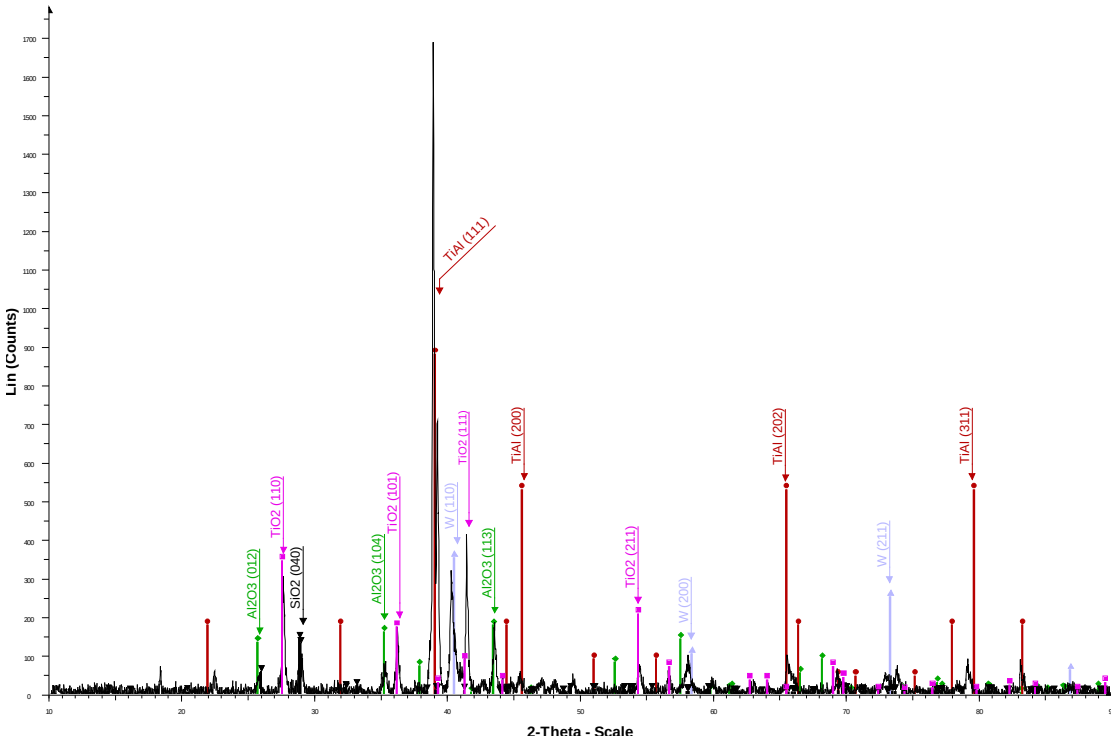

(**b**)

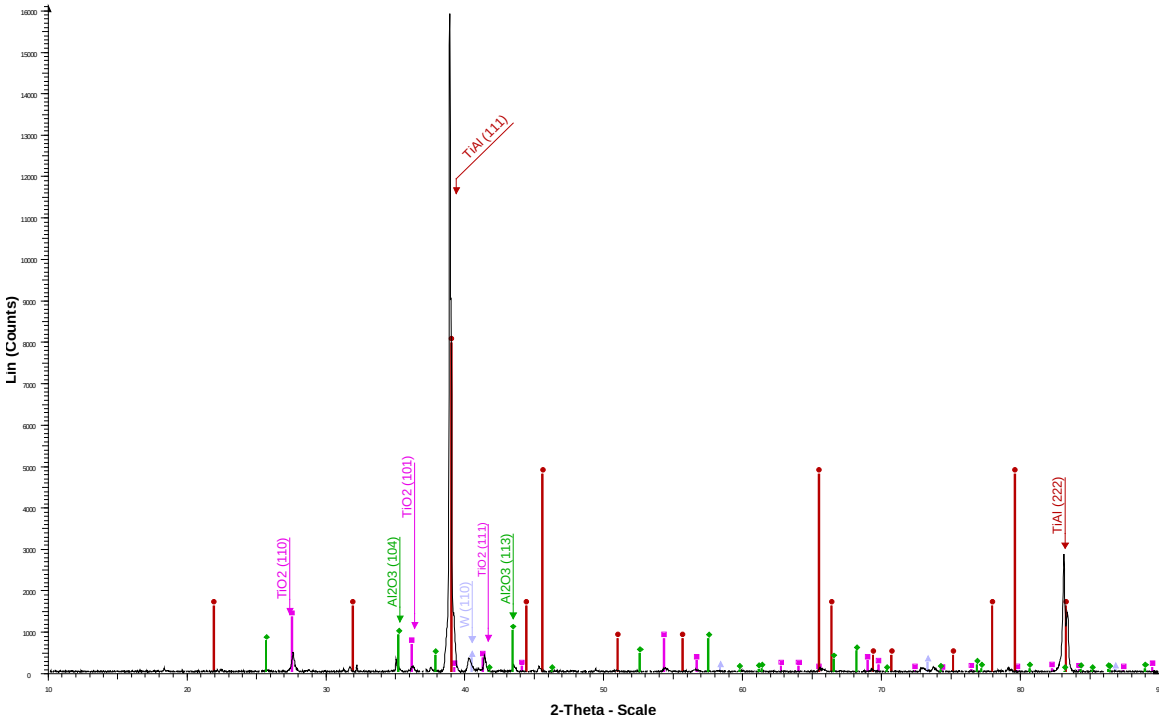

Figure 6-24 XRD patterns of Ti-46.7Al-1.9W-0.5Si intermetallic alloy after oxidation at 750ºC for 240h (**a**) in Ar-5%O_2 and (**b**) in Ar-80%O_2

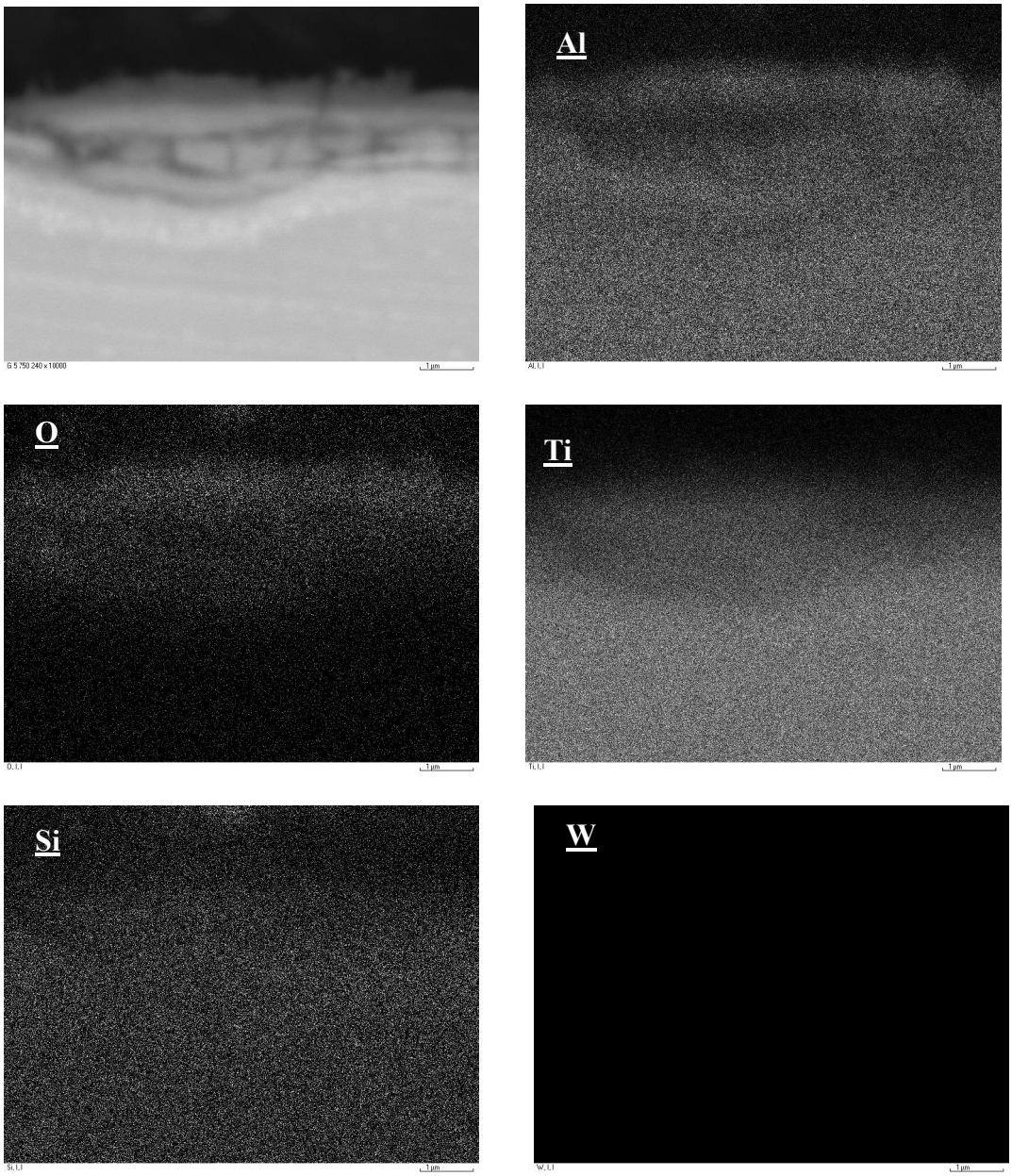

Figure 6-25 Back scattered electron Digimaps of Ti-46.7Al-1.9W-0.5Si intermetallic alloy oxidised in Ar-5%O_2 at 750ºC for 240h

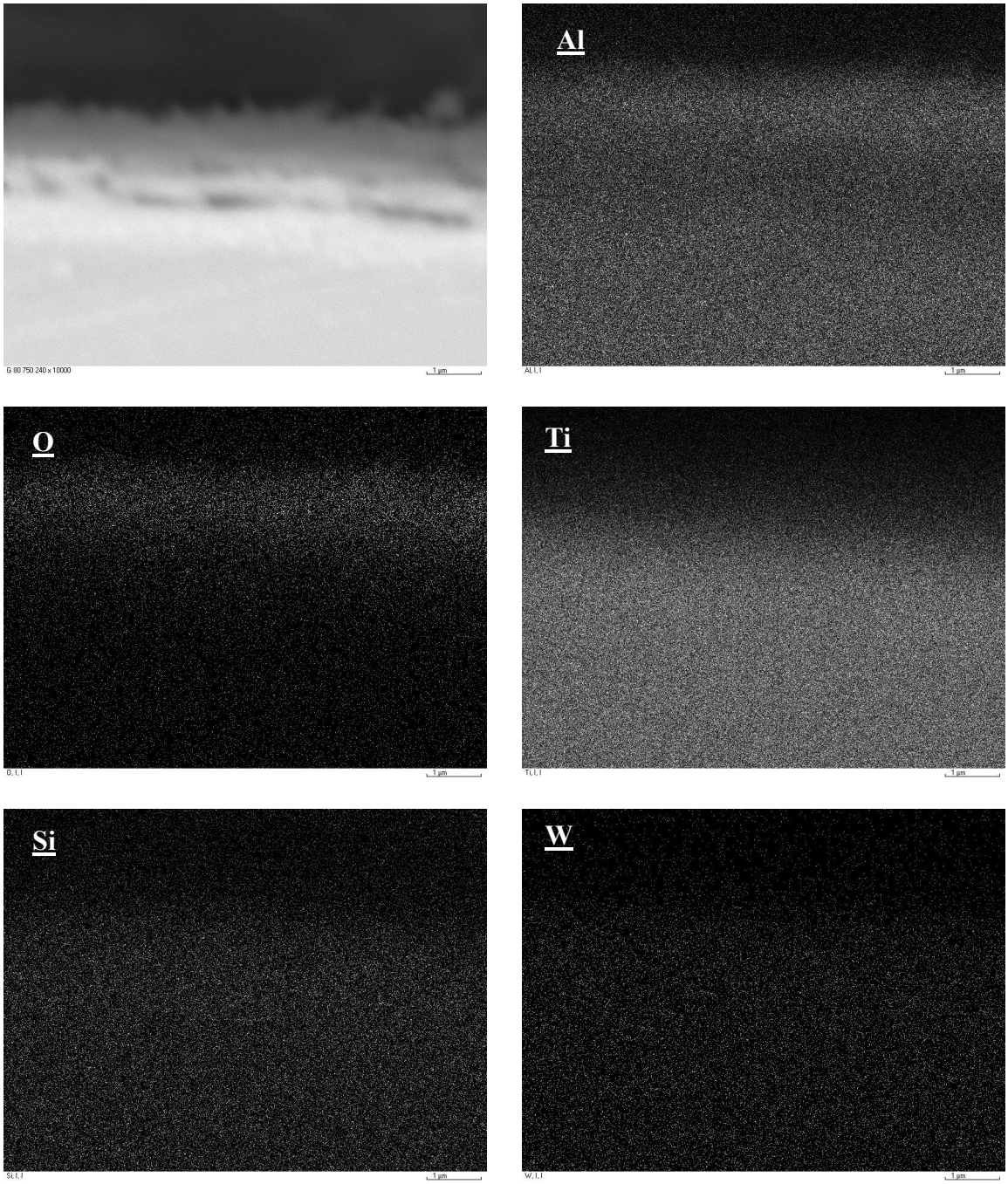

Figure 6-26 Back scattered electron image and Digimaps of Ti-46.7Al-1.9W-0.5Si intermetallic alloy oxidised in Ar-80%O_2 at 750ºC for 240h

(**a**)

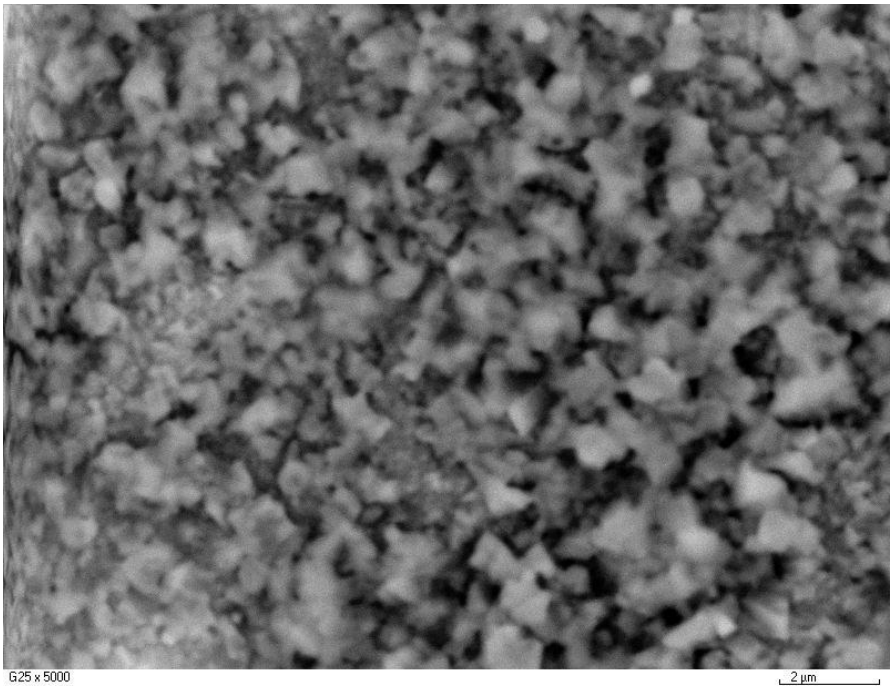

(**b**)

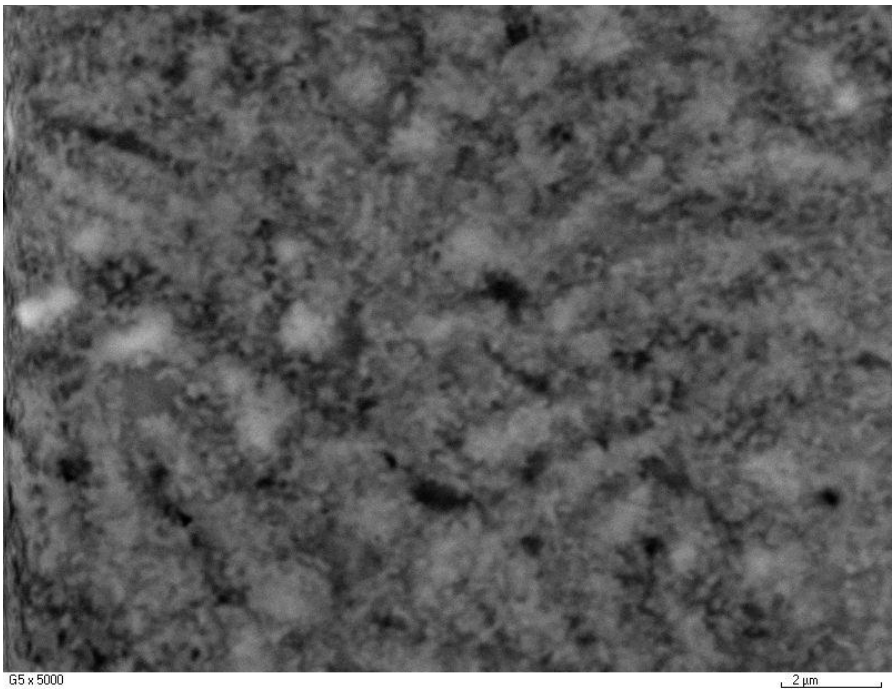

Figure 6-27 SEM micrographs of Ti-46.7Al-1.9W-0.5Si intermetallic alloy after oxidation at 850ºC for 5h (**a**) in Ar-5%O_2 and (**b**) in Ar-80%O_2

with some islands of Al_2O_3 (TiO_2/Al_2O_3) scale, as revealed by EDX analysis – **Figures 6-28**. Whilst for the scale in Ar-80%O_2, the concentration of TiO_2 and Al_2O_3 has changed over, i.e. more Al_2O_3 can be observed (**Figure 6-27**(**b**)) and the scale becomes predominant in Al_2O_3 (Al_2O_3/TiO_2), **Figure 6-29**. A very thin layer rich in titanium in Ar-5%O_2 and Ar-80%O_2 was detected by EDX (see **Figures 6-28** and **6-29**). However, this layer was not possible to be identified by XRD (see **Figures 6-30**(**a**) and **6-30**(**b**)) in both atmospheres. The intensity of the SiO_2 peak is higher in Ar-5%O_2 than that in Ar-80%O_2 (e.g. **Figures 6-31**(**a**) and **6-31**(**b**)). By increasing the exposure time at 850ºC to 72h, more islands of TiO_2 were observed in Ar-5%O_2 than that at Ar-80%O_2. After 240h of oxidation in Ar-5%O_2 and Ar-80%O_2 atmospheres the top surface of Ti-46.7Al-1.9W-0.5Si alloy is almost covered with TiO_2 in both atmospheres, **Figures 6-32**(**a**) and (**b**). However, still Al_2O_3 islands could be seen after oxidation in Ar-80%O_2 for 240h at 850ºC, **Figure 6-32**(**b**). Also localised oxidation was observed in Ar-5%O_2 atmosphere especially in places where W was observed, **Figure 6-33**(**a**) whilst, the scale in Ar-80%O_2 was protective and almost flat to the substrate (**Figure 6-33**(**b**)). The thickness of the aluminium-depleted layer identified by XRD as Ti_3Al (see **Figure 6-31**) increased with the increase in exposure time in both Ar-5%O_2 and Ar-80%O_2 atmospheres.

At 950°C, the surface morphologies of the oxidised samples in Ar-5%O_2, Ar-20%O_2 and Ar-80%O_2 were covered with rutile. However, the cross-sectioned scales of the samples oxidised in Ar-5%O_2 showed substantially thicker TiO_2 layer (**Figure 6-34**), whereas, the scale in Ar-80%O_2 is consisting almost of "protective" Al_2O_3 containing very thin of discontinuous layers of rutile, **Figure 6-35**. More interesting features of the cross-sectioned scales were observed at 950°C in both Ar-5%O_2 and Ar-80%O_2 atmospheres: The thickness

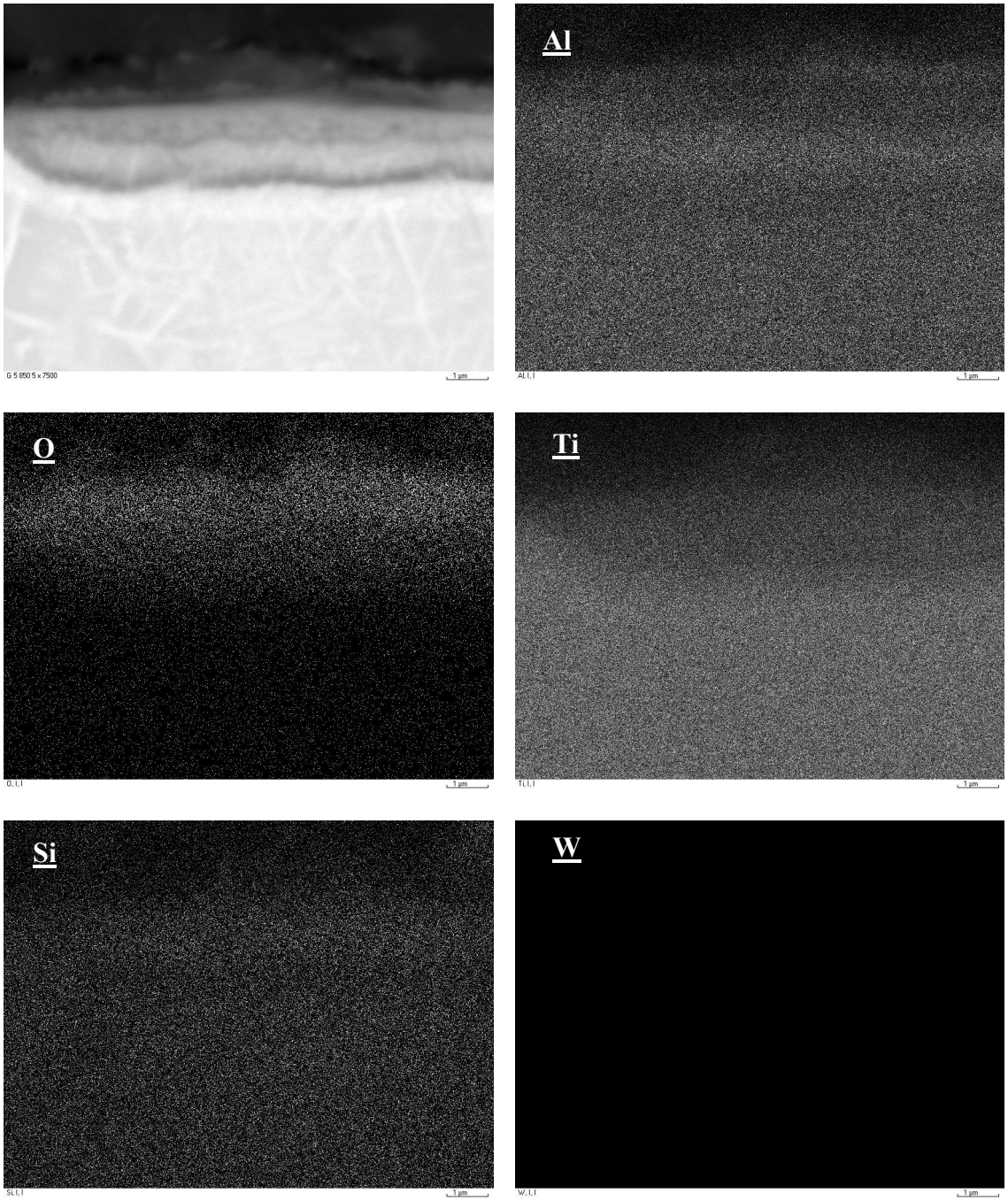

Figure 6-28 Back scattered electron image and Digimaps of Ti-46.7Al-1.9W-0.5Si intermetallic alloy oxidised in Ar-5%O_2 at 850ºC for 240h

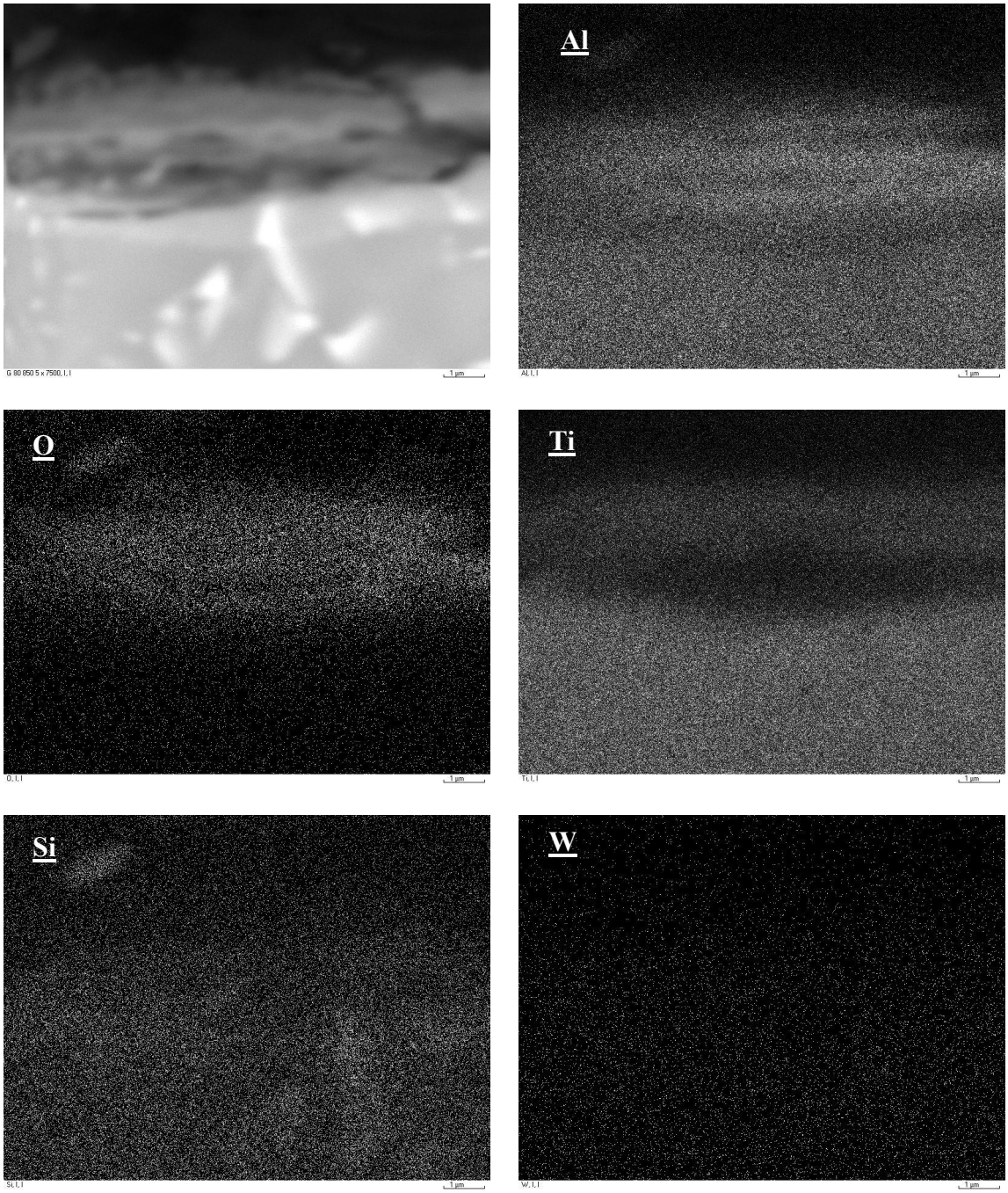

Figure 6-29 Back scattered electron image and Digimaps of Ti-46.7Al-1.9W-0.5Si intermetallic alloy oxidised in Ar-80%O_2 at 850ºC for 240h

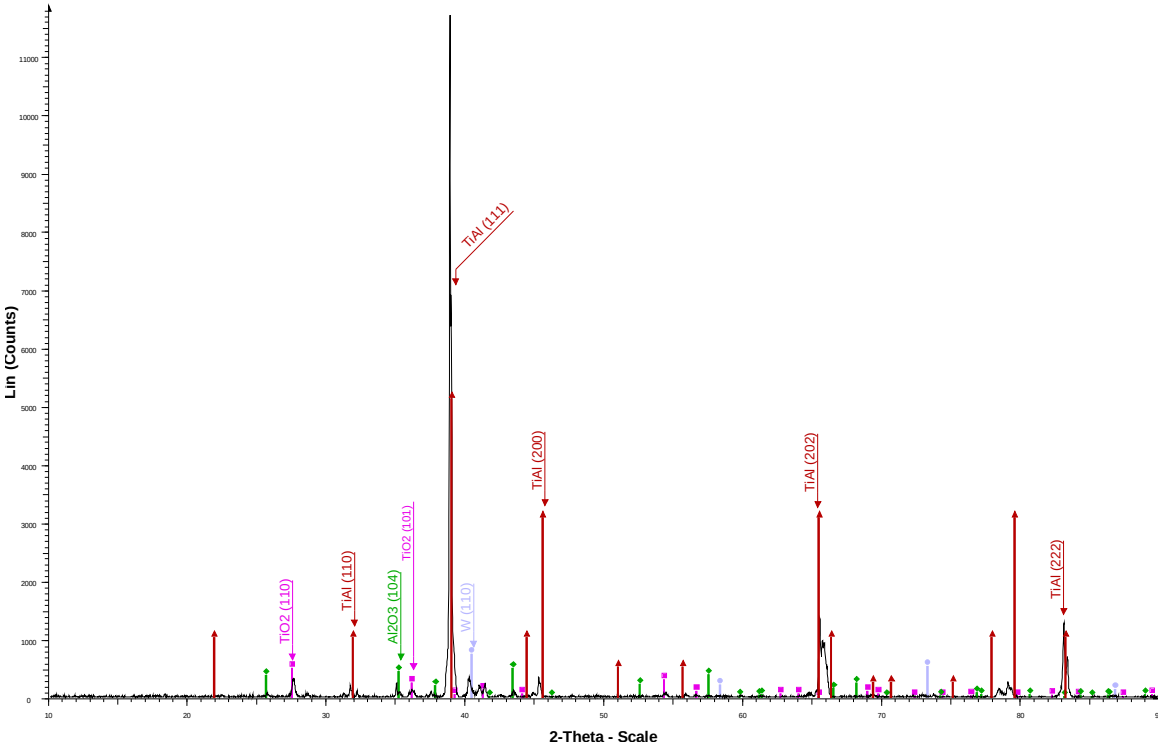

(**a**)

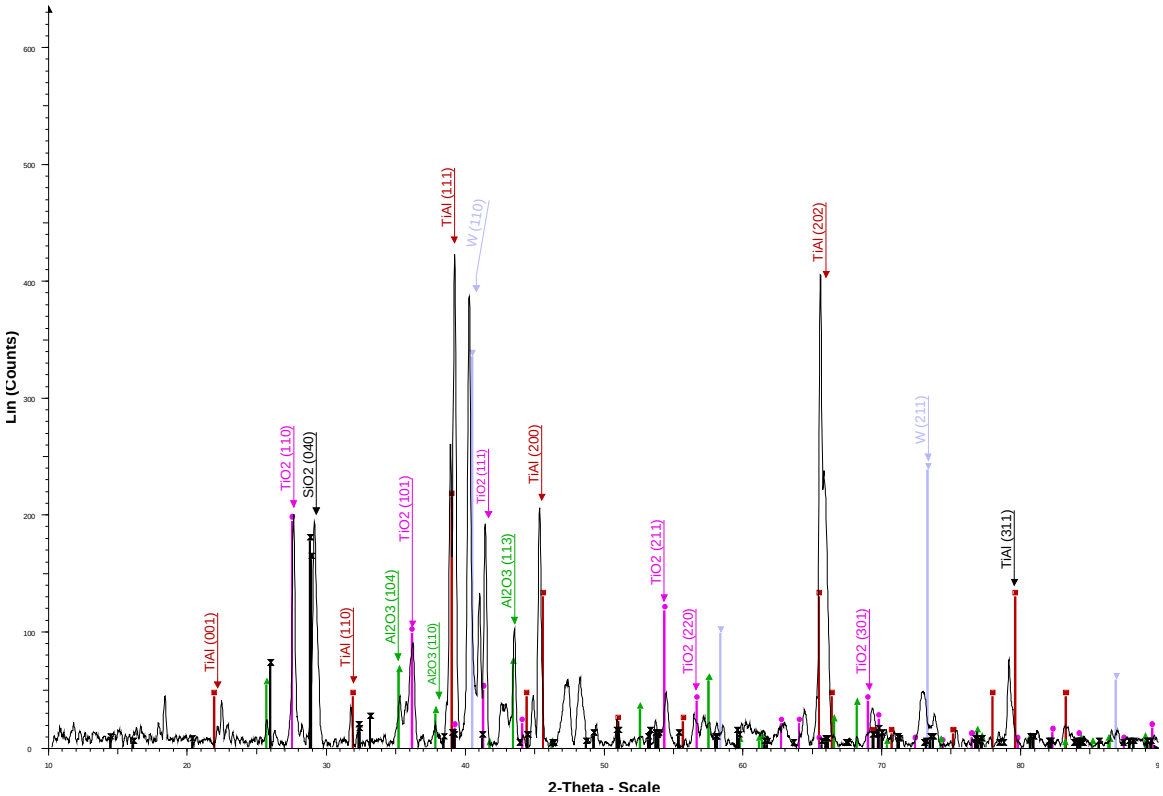

(**b**)

Figure 6-30 XRD patterns of Ti-46.7Al-1.9W-0.5Si intermetallic alloy after oxidation at 850ºC for 5h (**a**) in Ar-5%O_2 and (**b**) in Ar-80%O_2

(**a**)

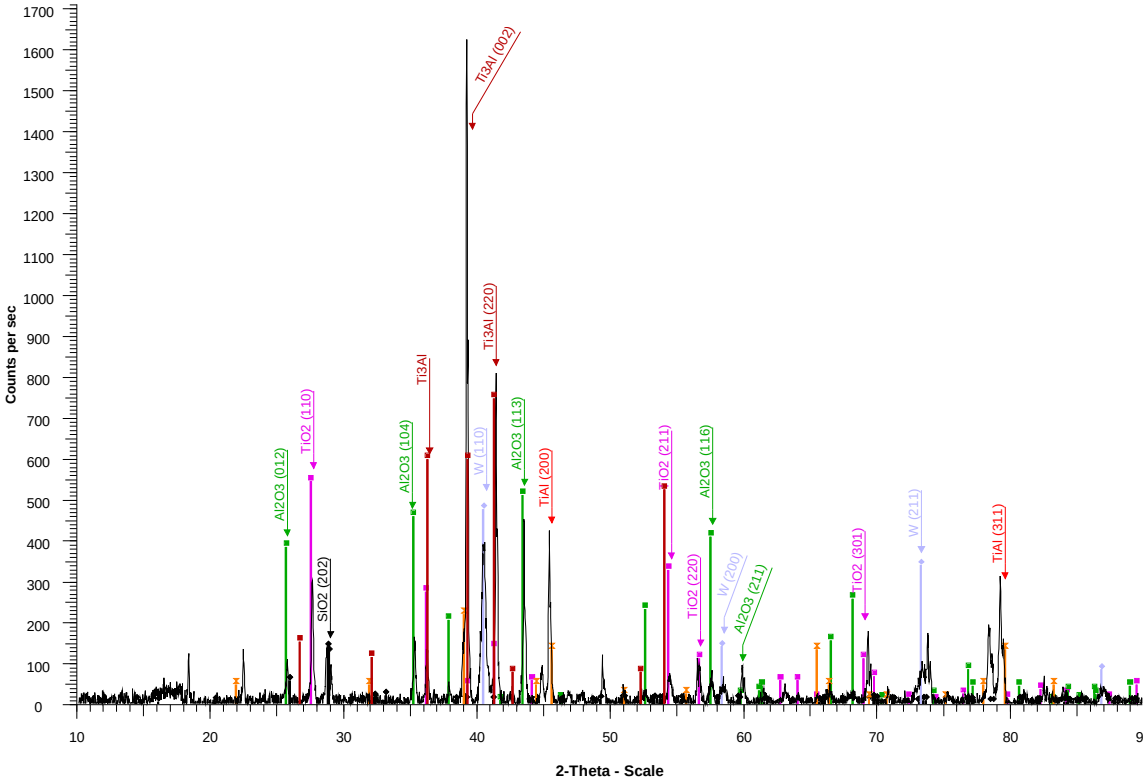

(**b**)

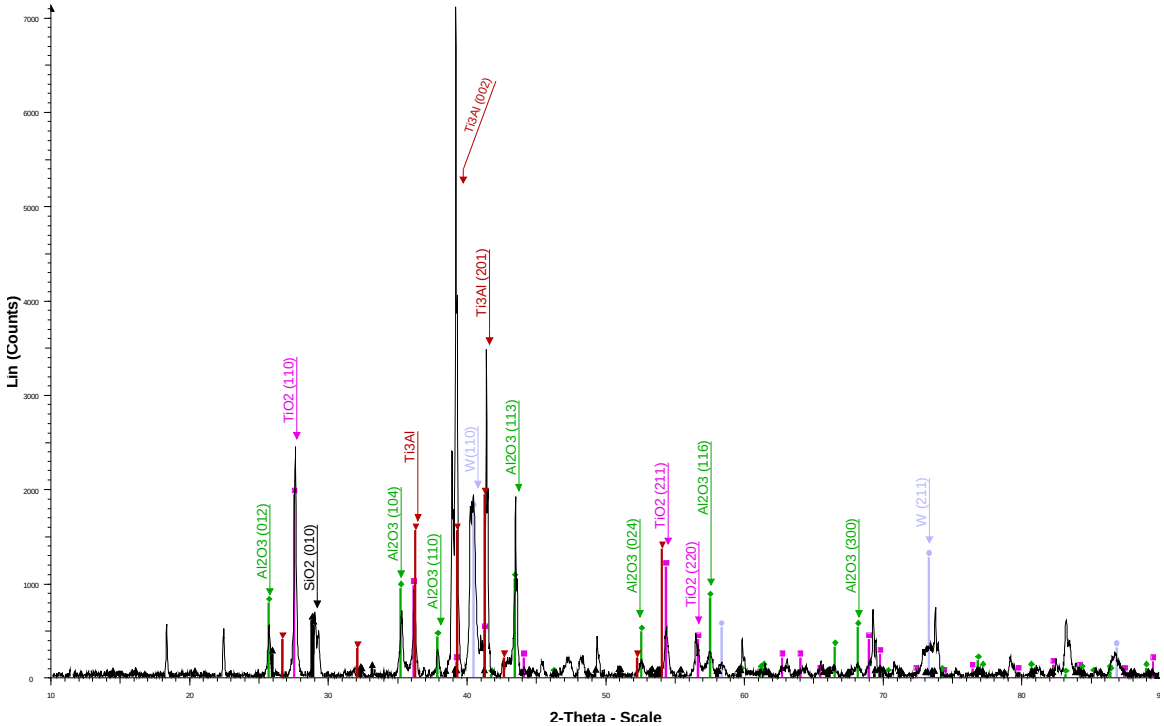

Figure 6-31 XRD patterns of Ti-46.7Al-1.9W-0.5Si intermetallic alloy after oxidation at 850ºC for 240h (**a**) in Ar-5%O_2 and (**b**) in Ar-80%O_2

(**a**)

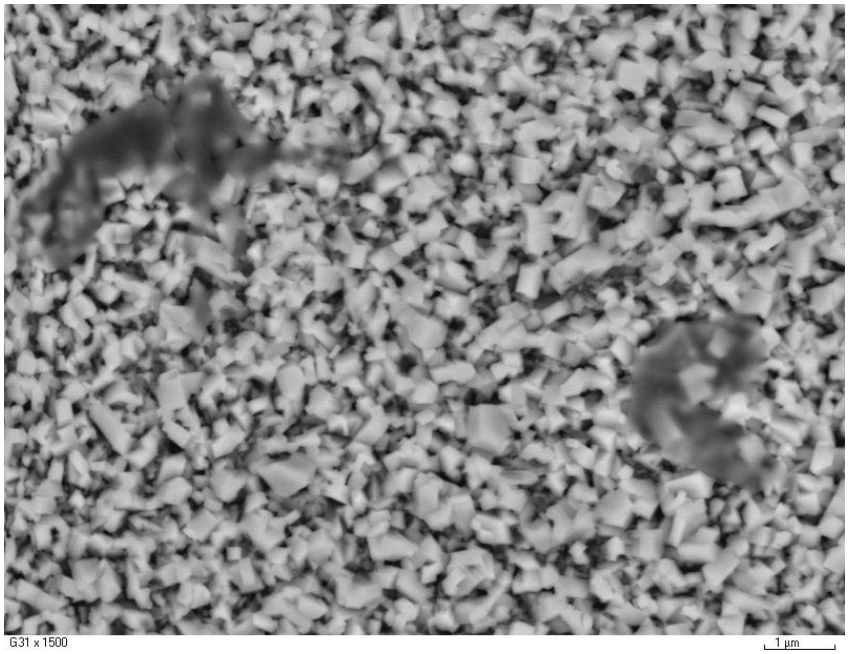

(**b**)

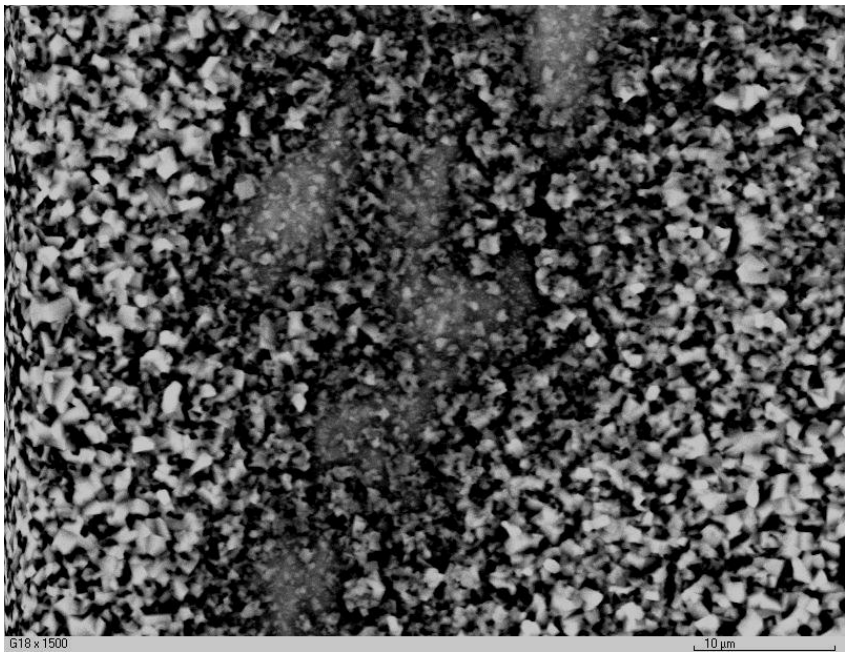

Figure 6-32 Back scattered SEM micrographs of Ti-46.7Al-1.9W-0.5Si intermetallic alloy after oxidation at 850ºC for 240h (**a**) in Ar-5%O_2 and (**b**) in Ar-80%O_2

(**a**)

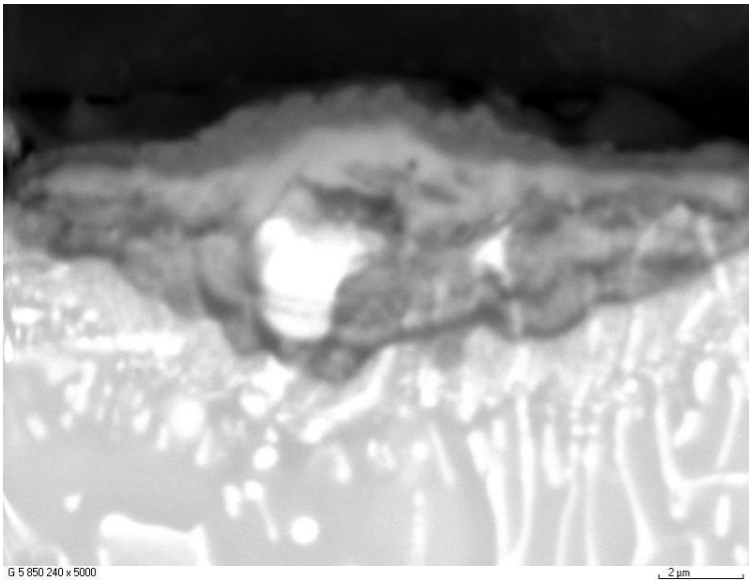

(**b**)

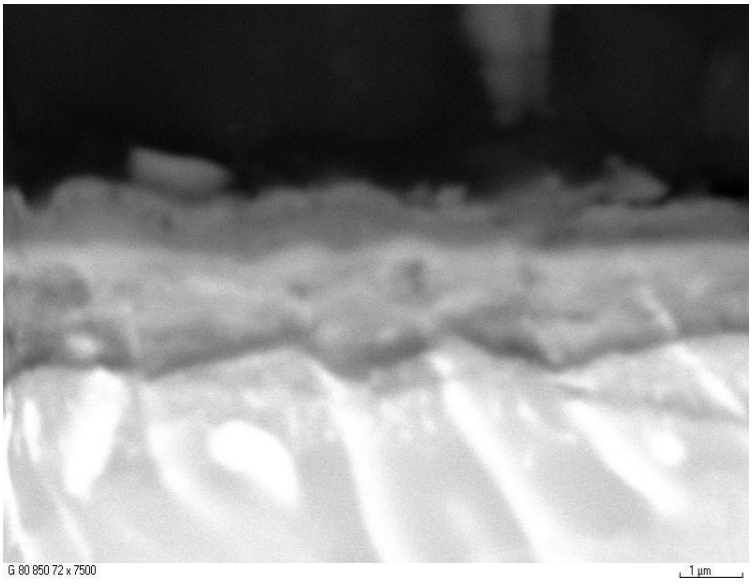

Figure 6-33 Back scattered SEM cross-sectional micrographs of Ti-46.7Al-1.9W-0.5Si intermetallic alloy after oxidation at 850ºC for 240h (**a**) in Ar-5%O_2 and (**b**) in Ar-80%O_2

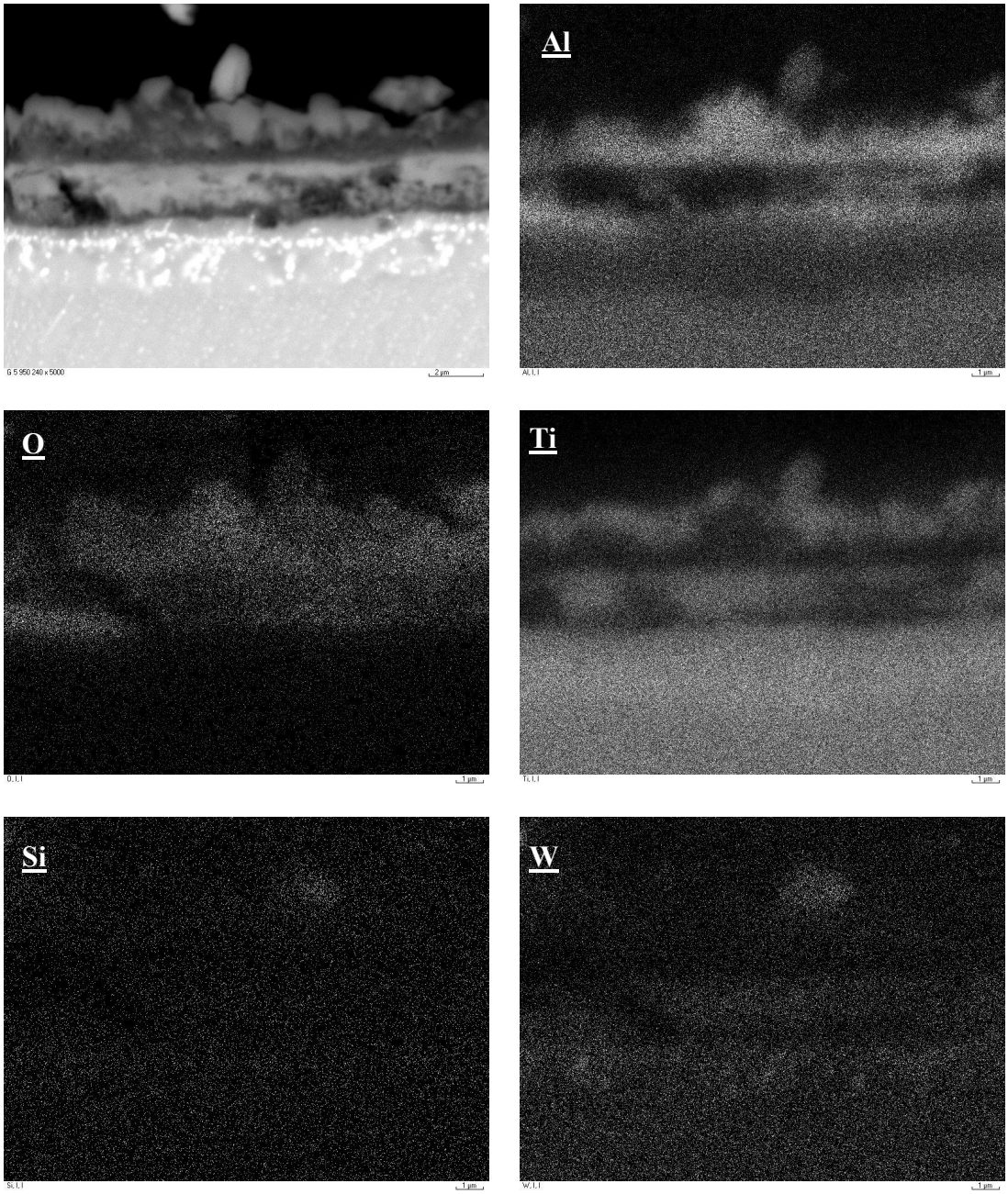

Figure 6-34 Back scattered electron image and Digimaps of Ti-46.7Al-1.9W-0.5Si intermetallic alloy oxidised in Ar-5%O_2 at 950ºC for 240h

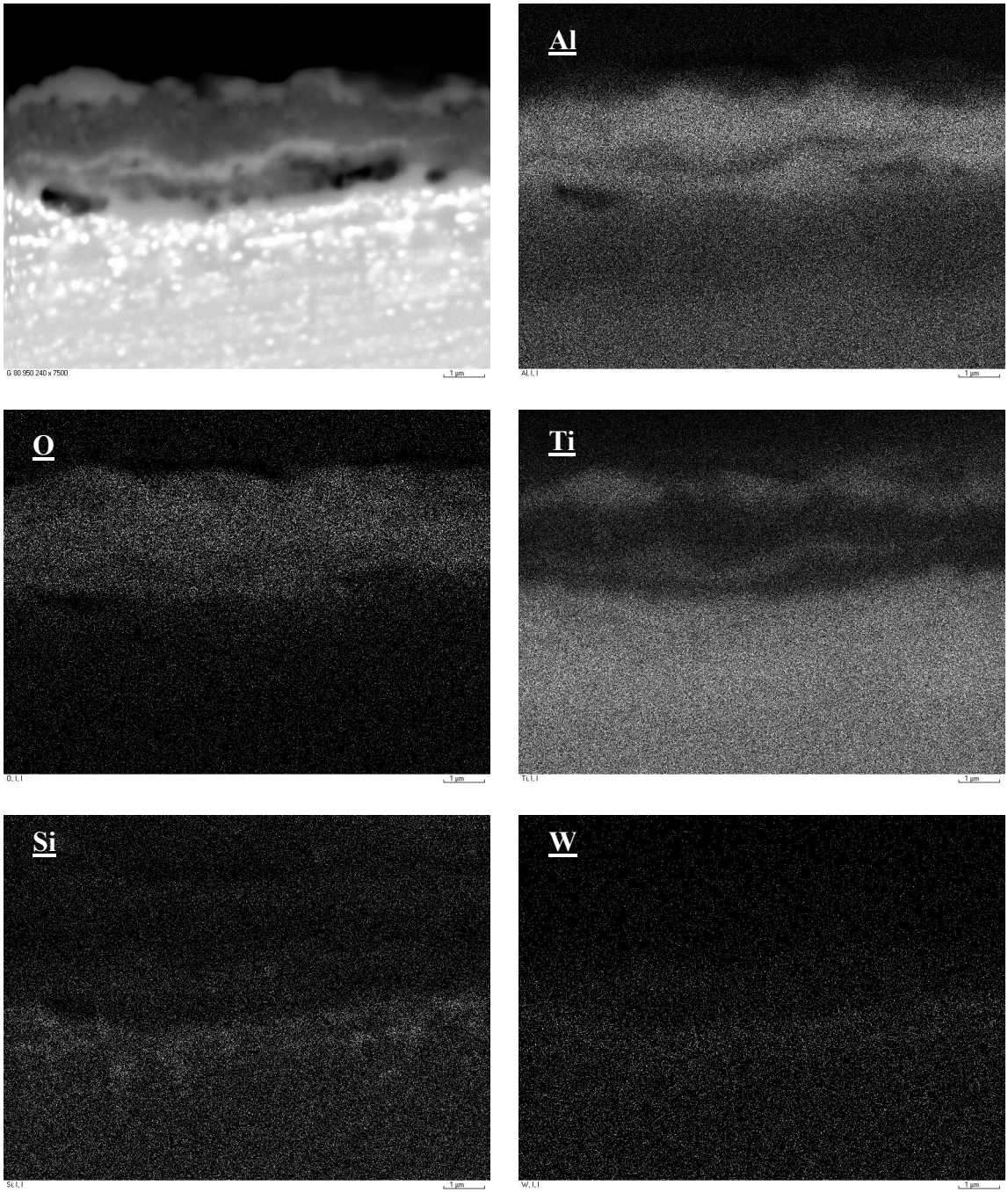

Figure 6-35 Back scattered electron image and Digimaps of Ti-46.7Al-1.9W-0.5Si intermetallic alloy oxidised in Ar-80%O_2 at 950ºC for 240h

of the depleted layer increases as the exposure time increased in both atmospheres. However, the depletion band of aluminium increased as the oxygen partial pressure increased at a temperature. For example, the thickness of the depleted layer at 950°C after 240h oxidation in Ar-80%O_2 (**Figure 6-35**) is about two times than in Ar-5%O_2, **Figure 6-34**. Another important feature of the scale formed in Ar-5%O_2 and Ar-80%O_2 at 950°C is that, after 240h the existence of porosities within the inner layer of the scale in Ar-5%O_2 and voids at the scale/alloy interface in Ar-80%O_2 can be observed. Generally, the XRD results of the oxidised samples in Ar-O_2 atmospheres revealed no sign of nitridation of the Ti-46.7Al-1.9W-0.5Si substrate were detected. Also the oxidation results obtained in Ar-20%O_2 reported in **Section 6.2.1** is consistent with the findings in Ar-5%O_2 and Ar-80%O_2 atmospheres (refer to **Figure 6-15, 16 and 17**). As mentioned in **Section 5.2.4**, it was difficult to quantify the SiO_2 in the scale using EDX analysis due to the similarity in the emission-wave lengths of Si and W. However, the XRD patterns of the oxidised samples in all oxidising atmospheres at all exposures (except at 750°C) showed clear peaks of SiO_2 characteristic. Also, pure W was identified by the XRD analysis in most of the oxidised samples.

6.3 Sulphidation/Oxidation of Coated and Uncoated Ti-46.7Al-1.9W-0.5Si Intermetallic Alloy

While most of the work in the study concentrated on the oxidation behaviour of Ti-46.7Al-1.9W-0.5Si intermetallic alloy, single (CrN and AlTiN) and multiplayer (AlTiN/CrN, AlTiN/NbN and CrN/NbN) coatings on Ti-46.7Al-1.9W-0.5Si alloy were also developed in order to examine their protectiveness to Ti-46.7Al-1.9W-0.5Si alloy in sulphidising/oxidising environments. **Figure 6-36** show the SEM micrographs of the as received single and double layer coatings.

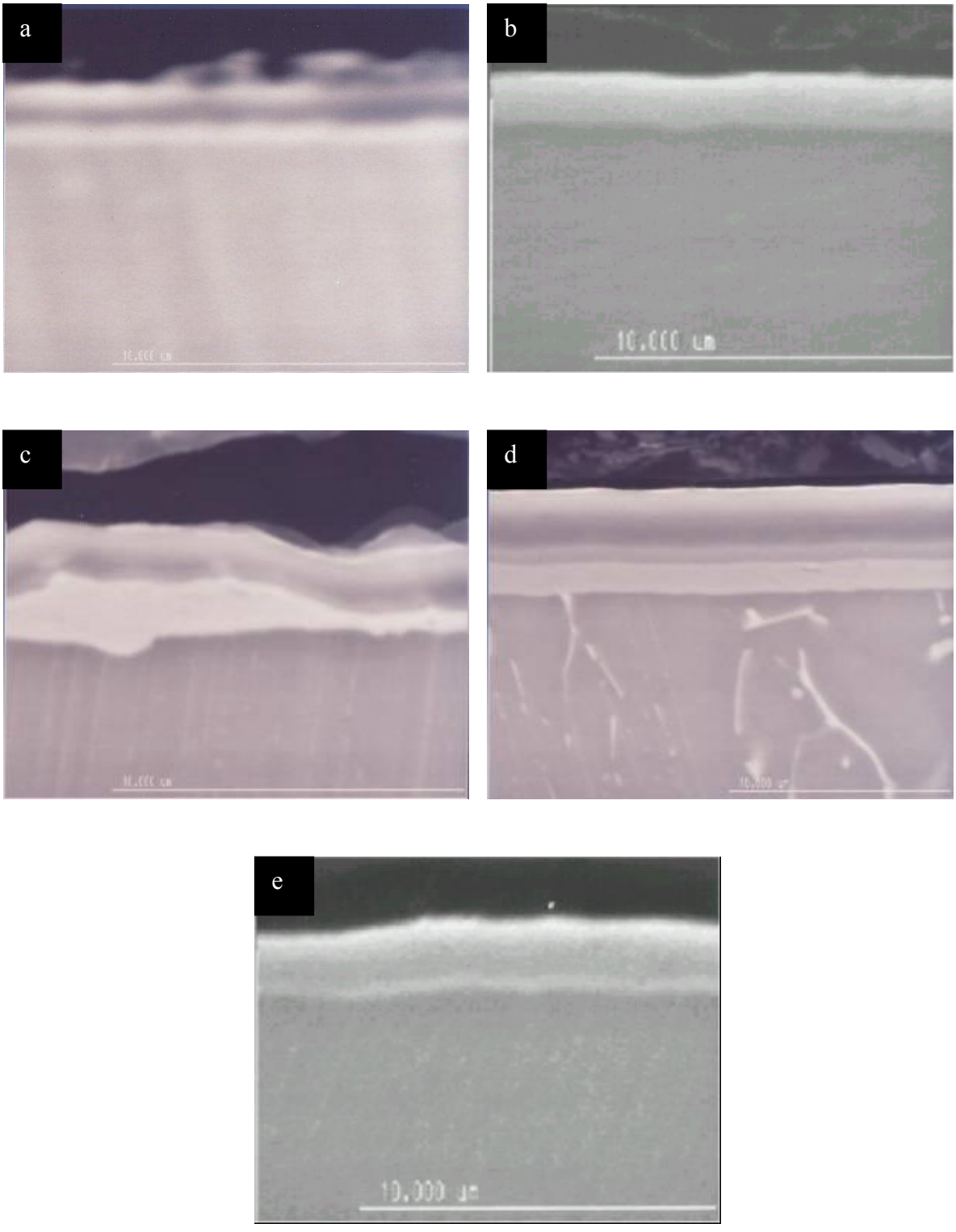

Figure 6-36 SEM micrographs of (**a**) AlTiN, (**b**) CrN, (**c**) AlTiN/NbN, (**d**) AlTiN/CrN and (**e**) CrN/NbN coatings

6.3.1 Mass Changes and Kinetics of Coated and Uncoated Ti-46.7Al-1.9W-0.5Si Intermetallic Alloy in $H_2/H_2S/H_2O$ Atmosphere

Figure 6-37 depicts the kinetics of sulphidation/oxidation for the coated and uncoated Ti-46.7Al-1.9W-0.5Si alloy at 850°C in the environment of $H_2/H_2S/H_2O$ ($pS_2 \sim 6.8x10^{-1}$ Pa and $pO_2 \sim 1.2x10^{-15}$ Pa) for up to 240h. The sulphidation/oxidation of uncoated 46.7Al-1.9W-0.5Si alloy follows a parabolic reaction law with a parabolic rate constant of 6×10^{-11} $g^2/cm^4/s$. The kinetic data analysis demonstrate that all the coatings significantly enhanced the corrosion resistance of Ti-46.7Al-1.9W-0.5Si alloy over the range of exposure time at 850°C, **Table 6-3**.

From **Figure 6-37**, at the early stages of exposure (e.g. 5h), the degree of protection among all the coatings was hardly distinguishable. However it was observed that the AlTiN combined with diffusion barriers (CrN or NbN) provided better protection for prolonged exposure, in particular the AlTiN with NbN showed the best sulphidation/oxidation resistance. Slightly inferior corrosion resistance were offered by AlTiN/CrN and CrN/NbN coatings over prolonged exposure (up to 240h) at 850°C. The single layer coatings of AlTiN and CrN behaved differently; AlTiN coating enhanced significantly the corrosion resistance of Ti-46.7Al-1.9W-0.5Si alloy at 850°C in the environment of $H_2/H_2S/H_2O$ for up to 100h, beyond which the AlTiN coating became no longer protective. However, the alloy coated with CrN showed continuous and rapid weight gains with the increase of exposure time. Weight gain data for the CrN coating after sulphidation/oxidation at 850°C showed the highest parabolic constant relationship with the exposure time compared to other coatings.

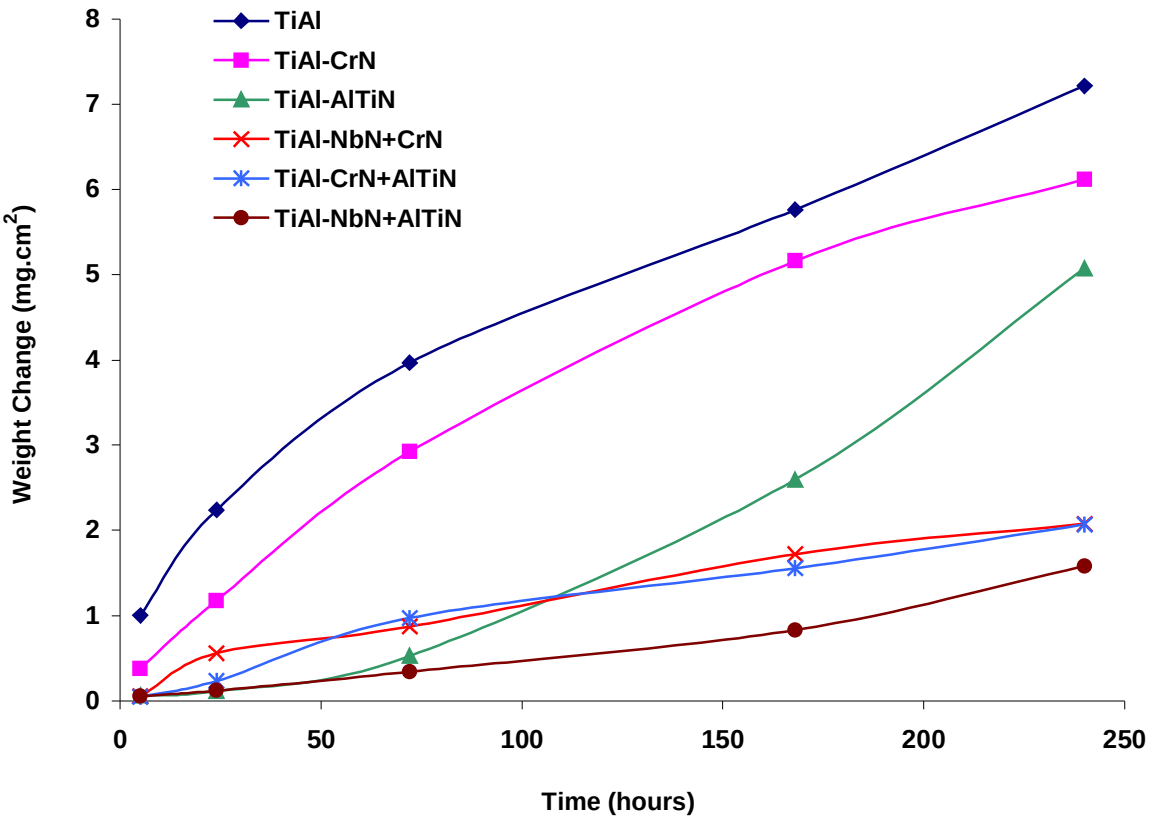

Figure 6-37 Weight gains versus exposure time for the coated and uncoated Ti-46.7Al-1.9W-0.5Si intermetallic alloy after sulphidation/oxidation in environment of $pS_2 \sim 6.8 \times 10^{-1}$ Pa and $pO_2 \sim 1.2 \times 10^{-15}$ Pa, at 850ºC for up to 240h

	Uncoated alloy	**Coated alloy with**				
		CrN	AlTiN	CrN/NbN	AlTiN/CrN	AlTiN/NbN
Kp ($g/cm^4/s$)	6×10^{-11}	4.4×10^{-11}	2.6×10^{-11}	5×10^{-12}	4.8×10^{-12}	2.5×10^{-12}

Table 6-3 Sulphidation/Oxidation rate constants ($g^2/cm^4/s$) of coated and uncoated Ti-47Al-1.9W- 0.5Si intermetallic alloy after exposure in environment of $pS_2 \sim 6.8 \times 10^{-1}$ Pa and $pO_2 \sim 1.2 \times 10^{-15}$ Pa, at 850ºC for up to 240h

6.3.2 Scale Morphology and Composition of Uncoated Ti-46.7Al-1.9W-0.5Si Alloy in $H_2/H_2S/H_2O$ Atmosphere

Figure 6-38 illustrates the cross-sectioned SEM morphology of uncoated Ti-46.7Al-1.9W-0.5Si alloy after 240h exposure. The top layer of the scale consisted of rutile (TiO_2). Beneath the rutile layer, a continuous layer of Al_2O_3 formed. Then a thick and relatively porous layer of TiS containing scattered pure W was observed. Beneath this scale, a $TiAl_3$ layer was identified whilst a thin $TiAl_2$ layer developed between the substrate and the $TiAl_3$ layer. In order to clarify the observed results, XRD analyses was carried out by careful and sequential polishing of the exposed sample for 168h. On the surface (before polishing), only rutile phase was detected as indicated in **Figure 6-39**(**a**). After removing the top part of this layer, the Al_2O_3 phase was revealed (**Figure 6-39**(**b**)) which also demonstrates the existence of pure W. Further removal of the scale surface by polishing revealed the presence of TiS – see **Figure 6-39**(**c**). After subsequent polishing, XRD was able to identify two phases of aluminium-rich $TiAl_3$ and $TiAl_2$ – **Figure 6-39**(**d**). The semi-quantitative analysis shows that there was a gradient of Al concentration, which decreased toward the substrate.

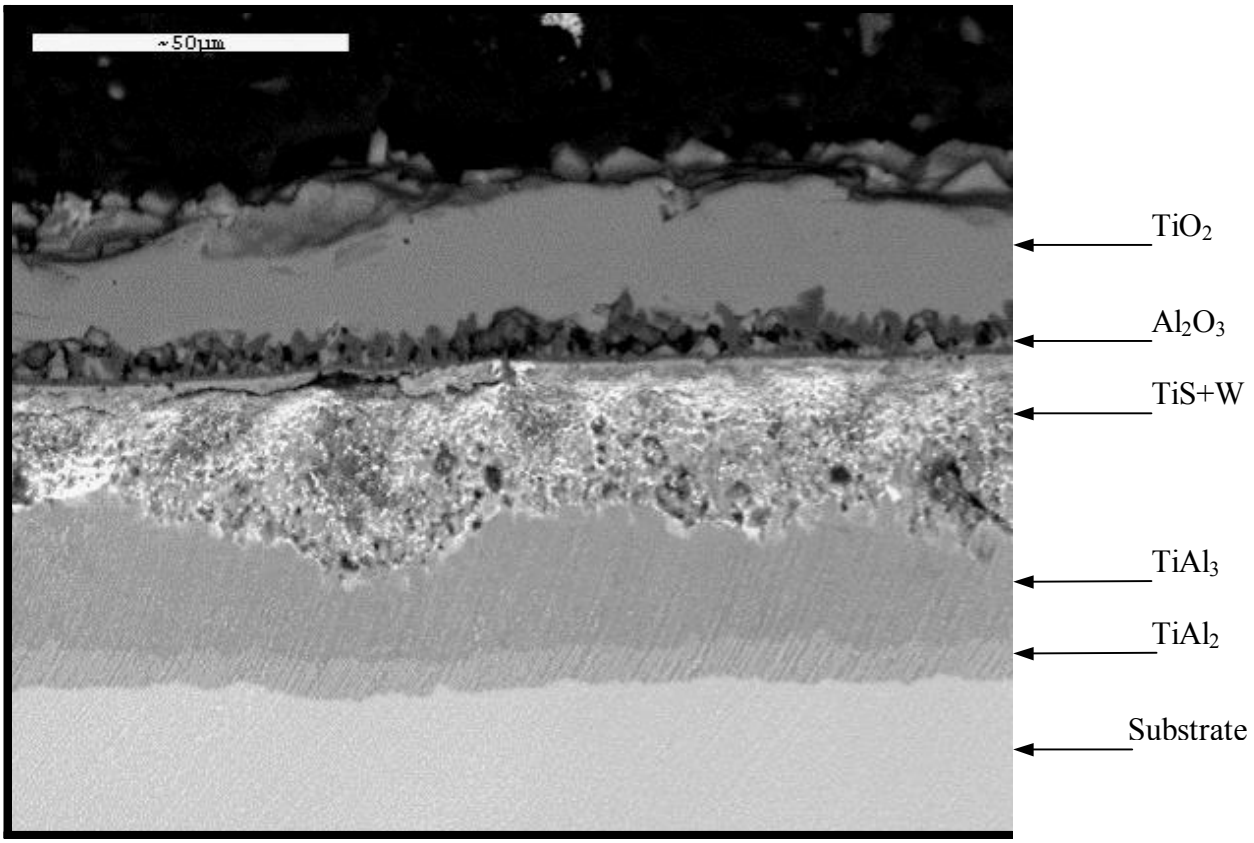

Figure 6-38 Back scattered SEM micrograph of uncoated Ti-46.7Al-1.9W-0.5Si intermetallic alloy after exposure in environment of $pS_2 = 6.8 \times 10^{-1}$ Pa and $pO_2 = 1.2 \times 10^{-15}$ Pa at 850ºC for 240h

(a)

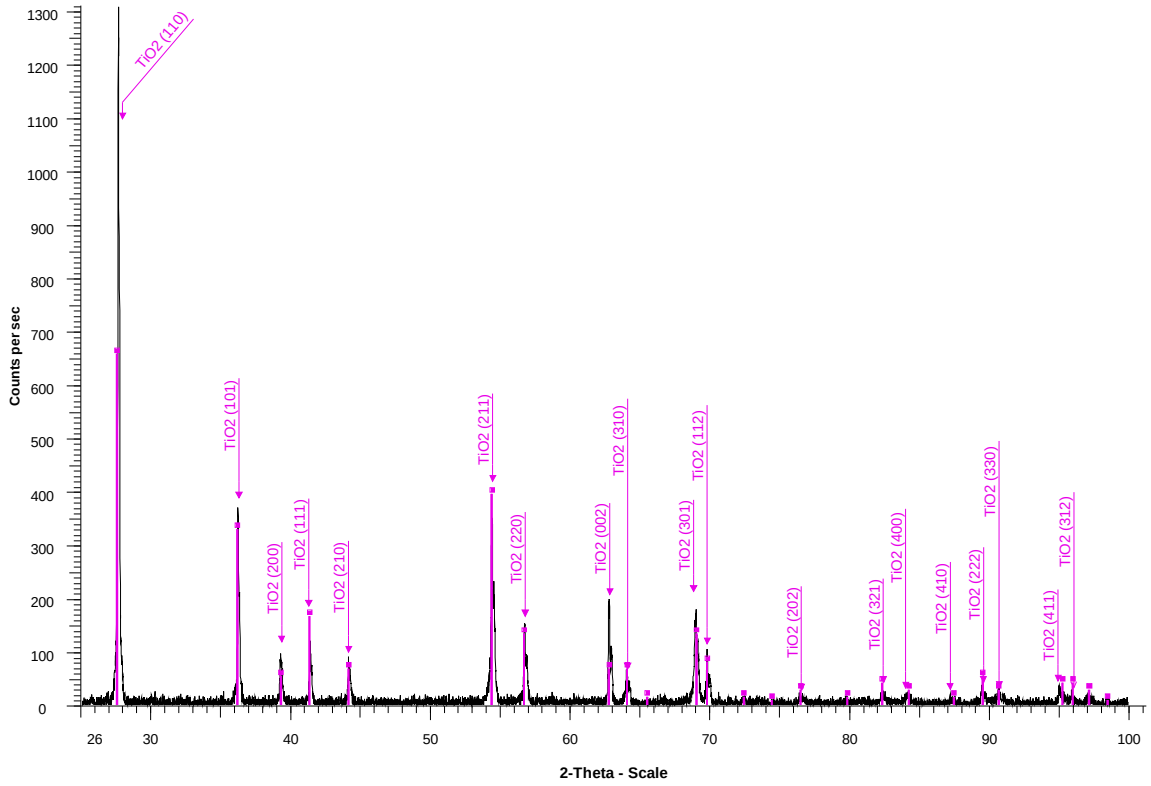

(b)

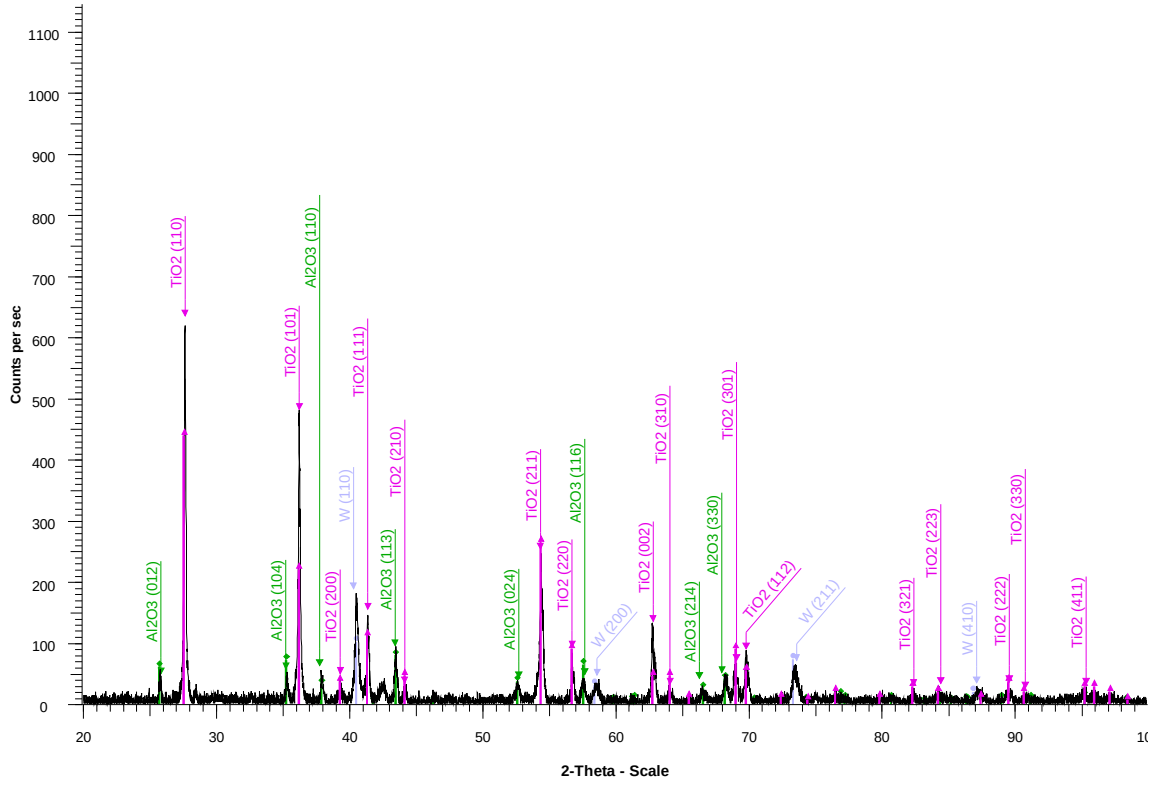

Figure 6-39 XRD patterns of Ti-46.7Al-1.9W-0.5Si intermetallic alloy after exposure in environment of pS_2 ~ 6.8 x 10^{-1} Pa and pO_2 ~ 1.2 x 10^{-15} Pa at 850ºC for 168h

(c)

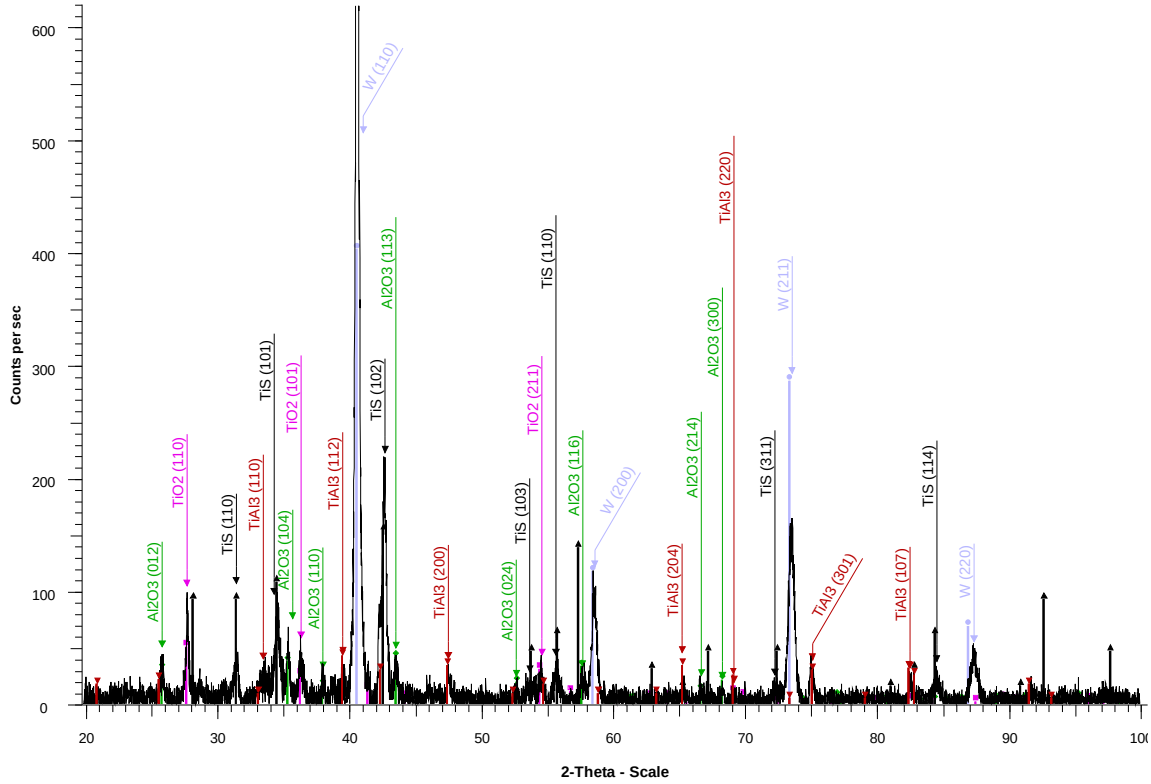

(d)

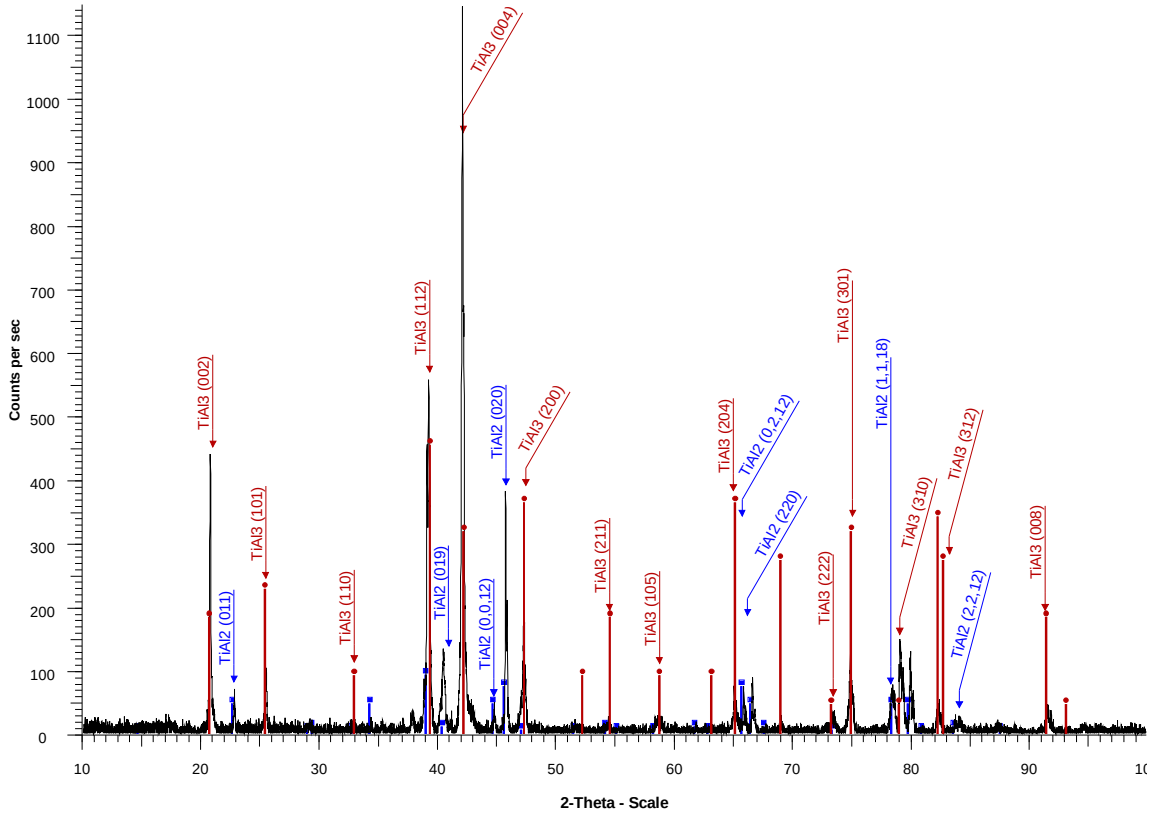

Cont. **Figure 6-39** XRD patterns of Ti-46.7Al-1.9W-0.5Si intermetallic alloy after exposure in environment of pS_2 ~ 6.8 x 10^{-1} Pa and pO_2 ~ 1.2 x 10^{-15} Pa at 850ºC for 168h

6.3.3 Scale Morphology and Composition of Coated Ti-46.7Al-1.9W-0.5Si Alloy in $H_2/H_2S/H_2O$ Atmosphere

The lack of corrosion of the Ti-46.7Al-1.9W-0.5Si alloy coated with AlTiN after short exposure (e.g. 5h), demonstrated by the kinetic data, is also confirmed by the morphological state of the scale, which remained compact and adherent during this exposure period. The XRD results indicate that all the phases existing on the non-exposed sample were present on the exposed samples with a minor amount of titanium oxide as confirmed by the EDX results. However sulphur diffused through the AlTiN coating and locally formed TiS after prolonged exposure. **Figure 6-40** shows the cross-sectioned morphology and Digimaps for the AlTiN coated Ti-46.7Al-1.9W-0.5Si alloy after 240h corrosion. It demonstrates that the coating was almost consumed within the corrosion product nodule. Although it remained attached to the substrate, the Al_2O_3 became arch-shaped which was caused by the outward push of TiS which formed beneath the Al_2O_3 scale as the formation of TiS led to a positive volume expansion. In front of the TiS a band of Al-enriched adjacent to the substrate is observed. The morphologies and compositions of the nodule were similar to those of the uncoated Ti-46.7Al-1.9W-0.5Si sample.

The CrN in both single and double-layered coatings specimens after short exposure time was completely converted to Cr_2S_3 layer. For the CrN single-coated layer after 5h exposure time (**Figure 6-41**), a discontinuous TiO_2 layer is formed. The outward diffusion of titanium led to the development of aluminium-rich zone beneath the pre-formed Cr_2S_3 layer. In the case of the double layer coating of CrN and NbN, there was no evidence for the formation of TiO_2, which indicates the significant barrier effect on the outward migration of Ti. With increasing exposure time to 240h, the amount of titanium increasingly migrated outwards to form TiO_2. At the same time, species of oxygen and sulphur diffused inwards and a layer of Al_2O_3 formed beneath the TiO_2/Cr_2S_3 mixed layer and a TiS zone also developed beneath

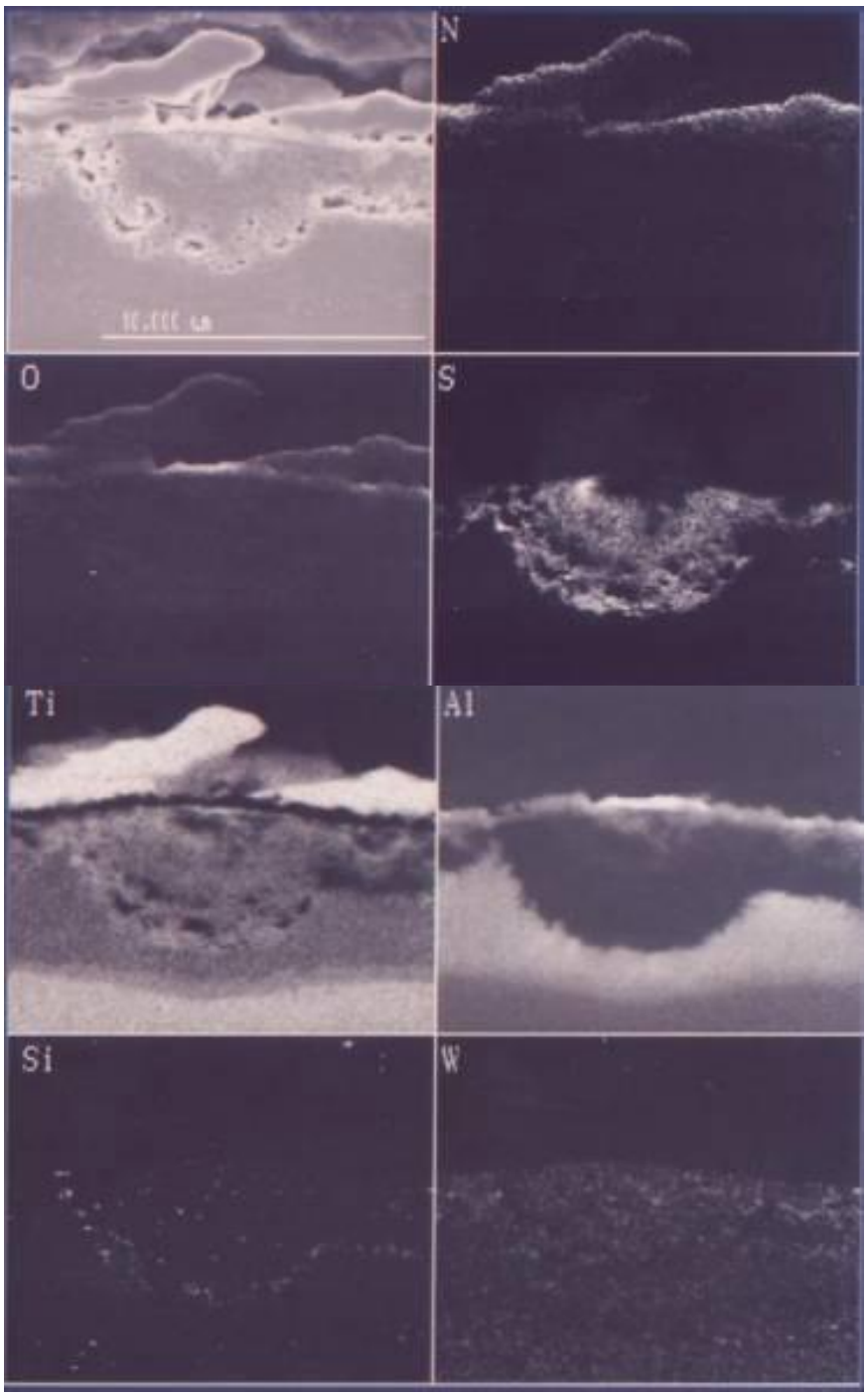

Figure 6-40 Electron image and Digimaps of Ti-46.7Al-1.9W-0.5Si alloy coated with AlTiN in environment of $pS_2 = 6.8 \times 10^{-1}$ Pa and $pO_2 = 1.2 \times 10^{-15}$ Pa at 850ºC for 240h

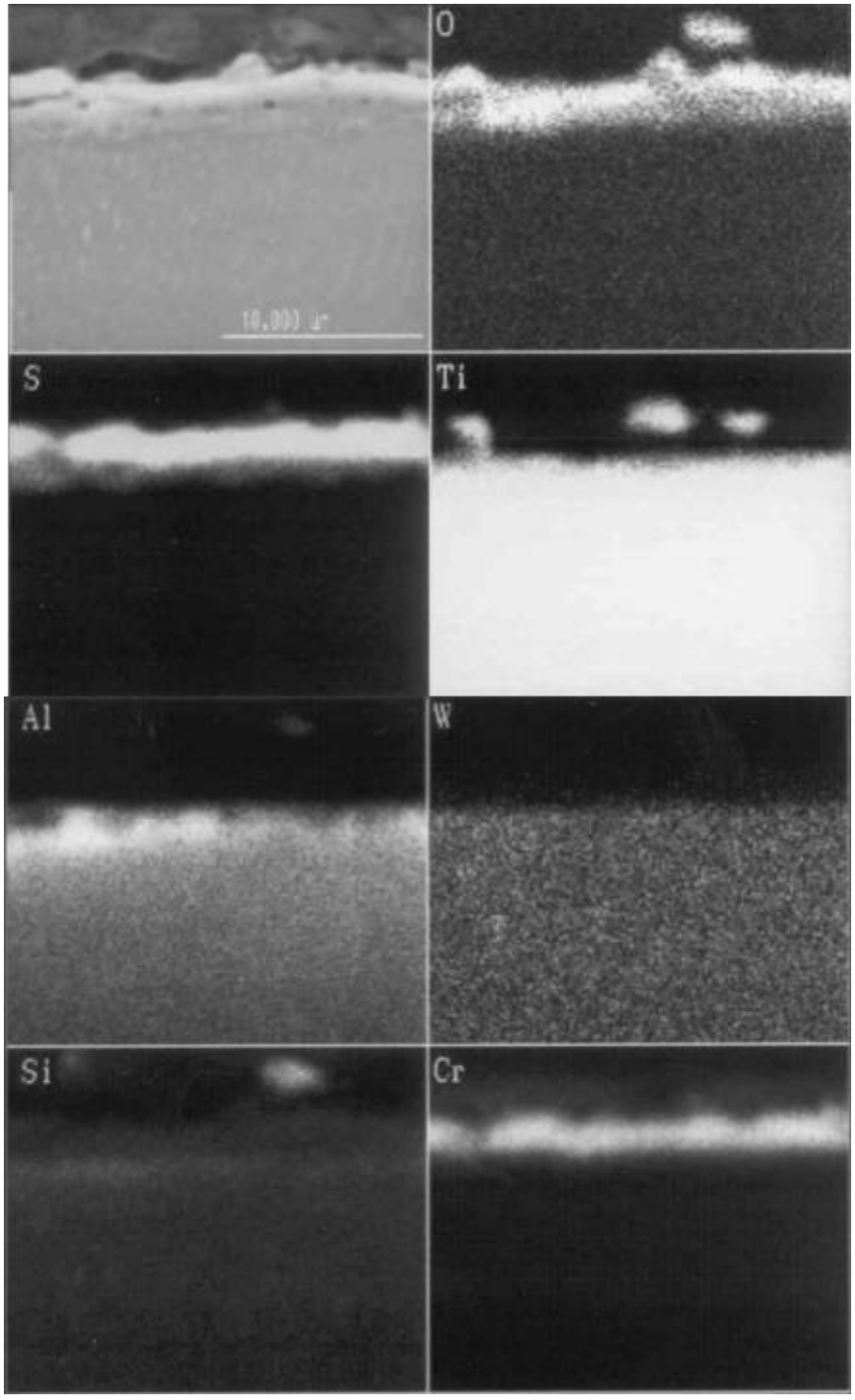

Figure 6-41 Electron image and Digimaps of Ti-46.7Al-1.9W-0.5Si alloy coated with CrN in environment of $pS_2 = 6.8 \times 10^{-1}$ Pa and $pO_2 = 1.2 \times 10^{-15}$ Pa at 850ºC after 5h exposure

the Al_2O_3 layer. The formation of TiO_2 and TiS depleted the alloy of titanium, consequently a aluminium-rich bright zone was also observed.

The kinetic results demonstrate superior corrosion resistance for the double layer coatings compared to the single layer coating. Similar to the case of the single layers (AlTiN or CrN), the double layer coatings of AlTiN/CrN and AlTiN/NbN were firmly attached to the substrate after short periods of exposure (e.g. 5h). However the XRD results showed some degree of transformation of NbN and CrN into Nb_2N and Cr_2N indicating the dissociation of NbN and CrN and the release of nitrogen. Prolonged exposure (240h at 850ºC) led to the development of detectable TiO_2 and Al_2O_3. For the double layer coatings AlTiN/NbN) and (AlTiN/CrN – **Figures 6-42** and **6-43** respectively, NbS_2 and Cr_2S_3 were detected. It is apparent that the formation of NbS_2 and Cr_2S_3 acted as a diffusion barrier to the outward diffusion of substrate elements and ingress of sulphur and oxygen. However, some localised attack occurred leading to the development of nodular corrosion products beneath the coatings, growing toward the substrate as shown in **Figures 6-42** and **6-43**. It should be pointed out that such localised attack did not affect the overall integrity of the coatings. The coatings remained compact and adherent and provided effective protection even after 240h exposure.

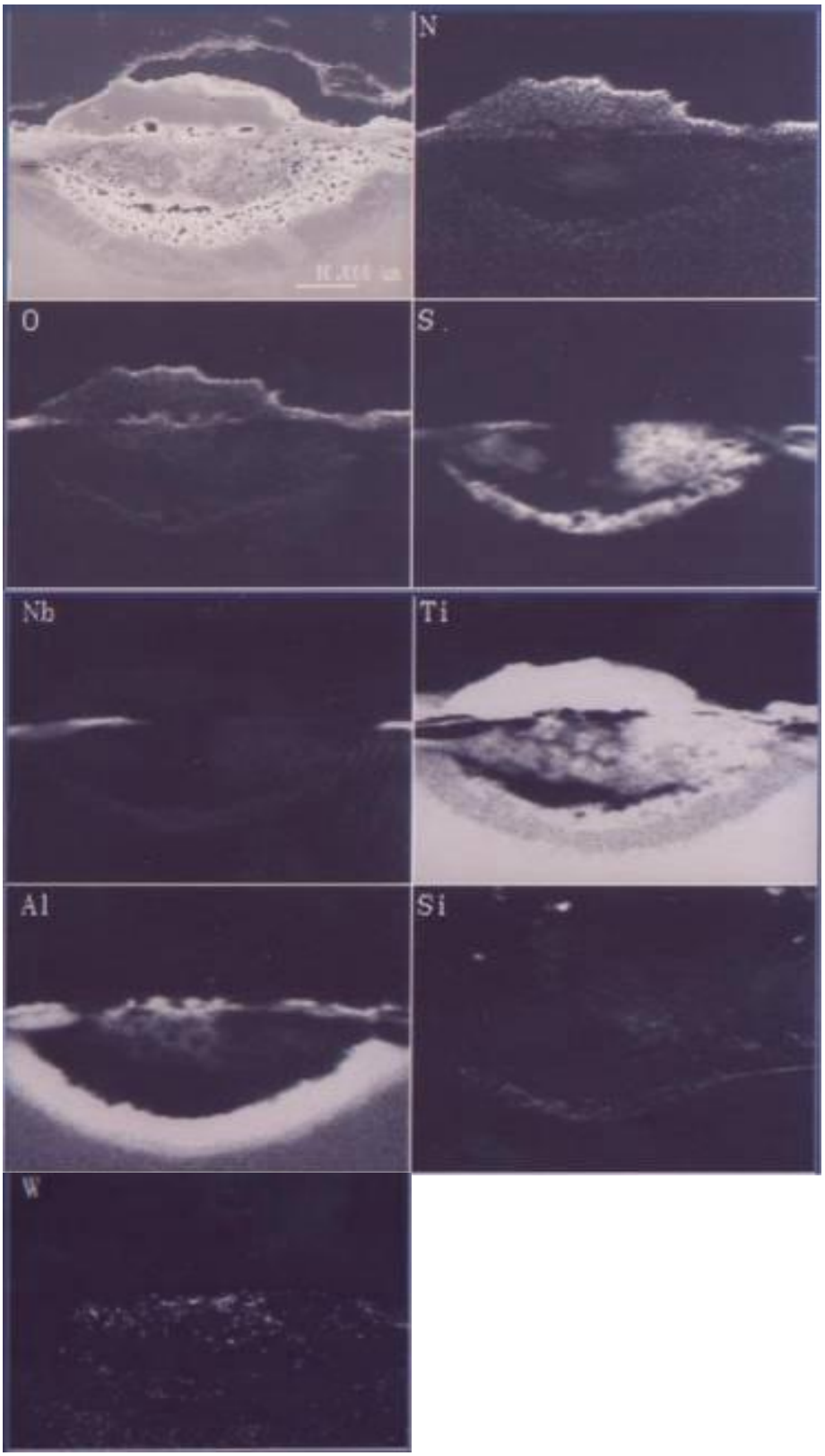

Figure 6-42 Electron image and Digimaps of Ti-46.7Al-1.9W-0.5Si alloy coated with AlTiN/NbN in environment of $pS_2 = 6.8 \times 10^{-1}$ Pa and $pO_2 = 1.2 \times 10^{-15}$ Pa at 850ºC after 240h exposure

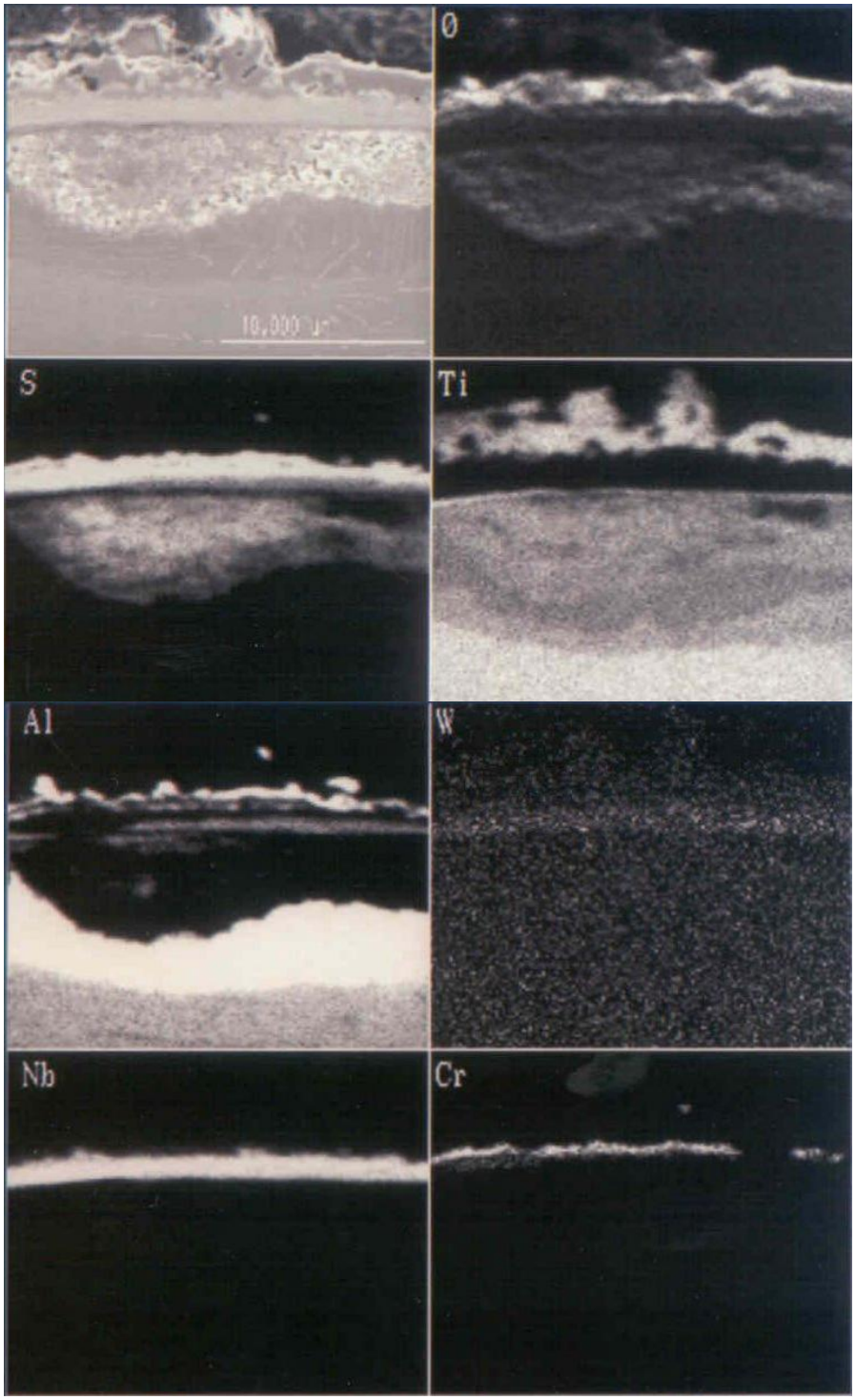

Figure 6-43 Electron image and Digimaps of Ti-46.7Al-1.9W-0.5Si alloy coated with CrN/NbN in environment of $pS_2 = 6.8 \times 10^{-1}$ Pa and $pO_2 = 1.2 \times 10^{-15}$ Pa at 850ºC after 240h exposure

6.4 Oxidation Behaviour of Fe_3Al Intermetallic Alloys

6.4.1 Introduction

Four Fe-based intermetallic alloys, Fe_3Al, Fe_3Al-Y, Fe_3Al-Hf and Fe_3Al-(Y+Hf) were used among the experimental materials in the present oxidation studies. In the as-recieved conditions, the Fe_3Al alloys presented a microstructure of longitudinal grains with a non-uniform size. The average grain size (as determined by optical microscop) of the four Fe_3Al intermetallics were very similar and it was about 83μm (**Figure 6-44**). The isothermal and cyclic air oxidation behaviour of the four Fe_3Al intermetallics will be dealt separately throughout this section. For better understanding of the isothermal and cyclic oxidation behaviour of the experimental materials, it was found necessary to describe and compare them at single temperature. As would be expected for the REE, the Fe_3Al with RE(s) have a lower oxidation rate than the undoped materials. However, from the results obtained, the situation seems to be more complicated and needs rethinking. Also it was reported in the literature that more severe weight losses of similar undoped materials after a number of cycling than RE doped materials. However, these cases may not be true in the present study.

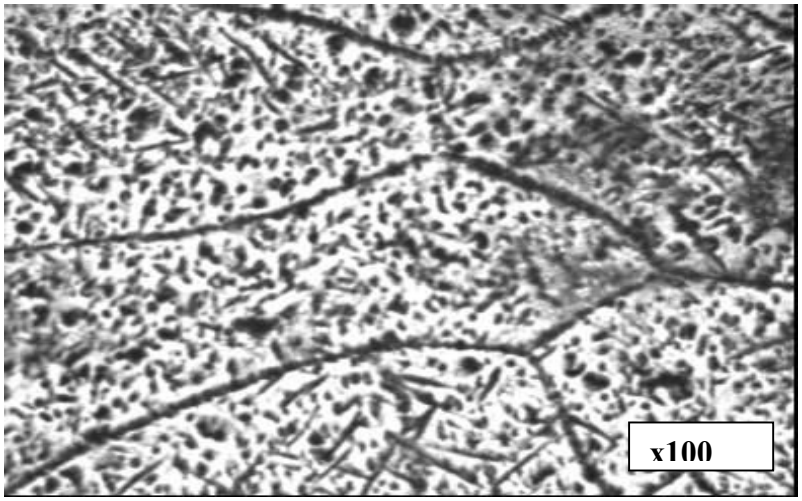

Figure 6-44 Optical micrograph of Fe_3Al intermetallic alloy

6.4.2 Isothermal Air Oxidation Behaviour of Fe_3Al Intermetallic Alloys

Mass changes after isothermal oxidation of Fe_3Al intermetallic alloys

The recorded mass changes for the undoped Fe_3Al and doped with Y and/or Hf under isothermal air oxidation conditions at 900, 1000 and 1100°C are shown in **Figures 6-45**, **6-46**, and **6-47** respectively. Generally, the mass gains of the alloys increased as the exposure time and temperature increased. As a matter of simplicity, the explanation of isothermal oxidation kinetic data at the three temperatures will be dealt separately.

At 900°C, the oxidation curves indicated that all alloys exhibited parabolic oxidation behaviour (refer to **Figure 6-45**). The oxidation kinetic data show variations of the mass gain and oxidation rate constants of the experimental materials. Surprisingly at 900°C, the weight gain of the Fe_3Al alloy doped with Y is higher than that of the undoped material under the same isothermal conditions. On the other hand the material doped with both Y and Hf [Fe_3Al-(Y+Hf)] showed the lowest weight gain among all Fe_3Al experimental materials. Initially and up to 24h, the weight gain of Fe_3Al-Y alloy at 900°C is significantly higher than the other materials. After the initial incubation of oxidation at 900°C, a steady state condition of the alloys oxidation is reached with a parabolic mass gain – with the spalled scale. However, the scatter of the mass gain of alloys in isothermal oxidation conditions at 900°C was very similar throughout the whole exposure time (up to 240h).

At 1000°C, the scatter of the kinetic data is similar to that at 900°C, but with higher weight gain. Again the Y-doped intermetallic showed the highest weight gain among the Fe_3Al experimental materials (**Figure 6-46**). However, the diverging of the mass gain of the four materials looks very similar throughout the whole exposure time at 1000°C. At 1100°C, the kinetics of isothermal oxidation behaviour of Fe_3Al based intermetallics is far

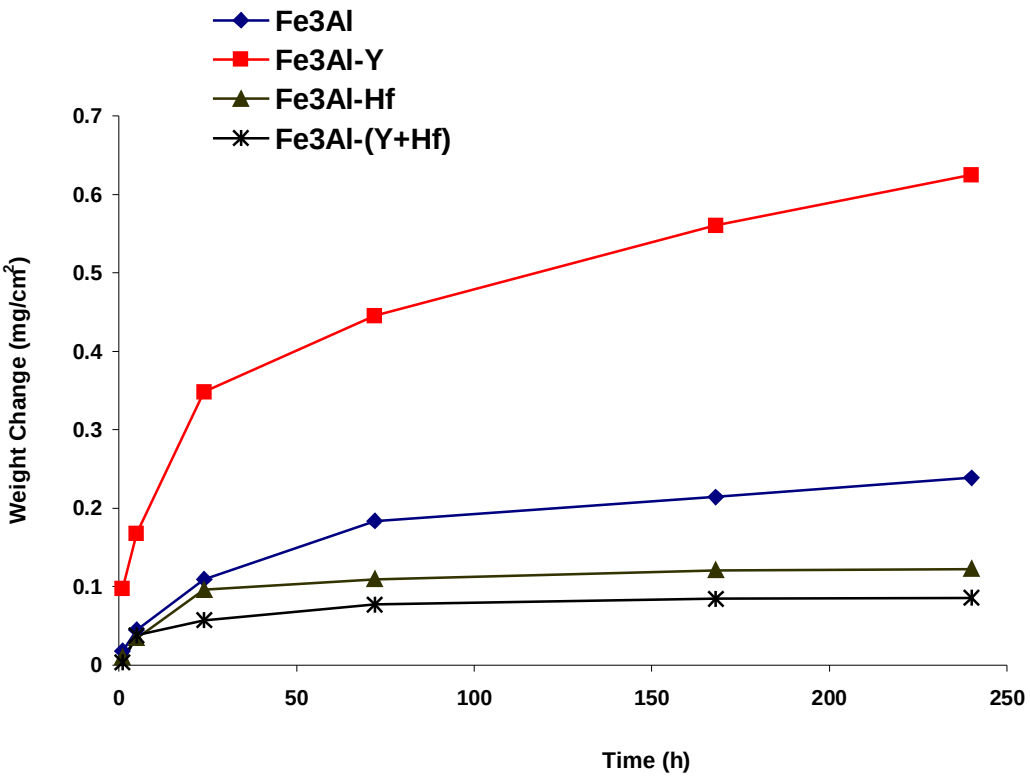

Figure 6-45 Weight gains versus exposure time for the Fe_3Al intermetallic alloys after isothermal air oxidation at 900ºC for up to 240h

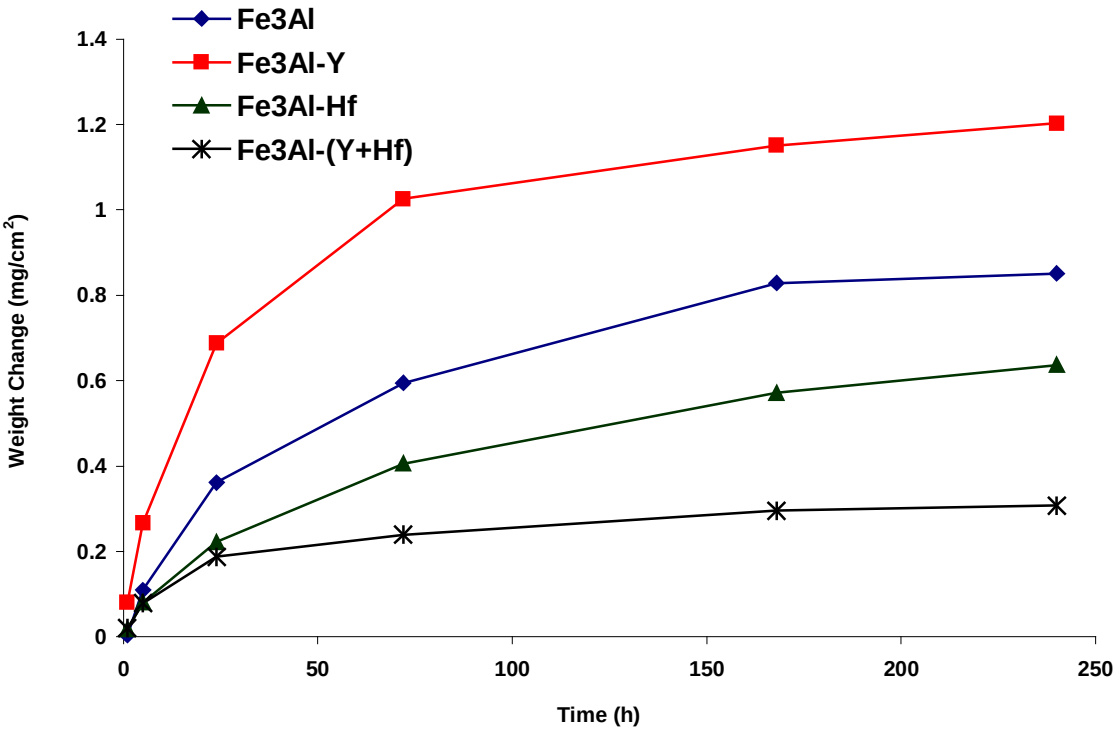

Figure 6-46 Weight gains versus exposure time for the Fe_3Al intermetallic alloys after isothermal air oxidation at 1000ºC for up to 240h

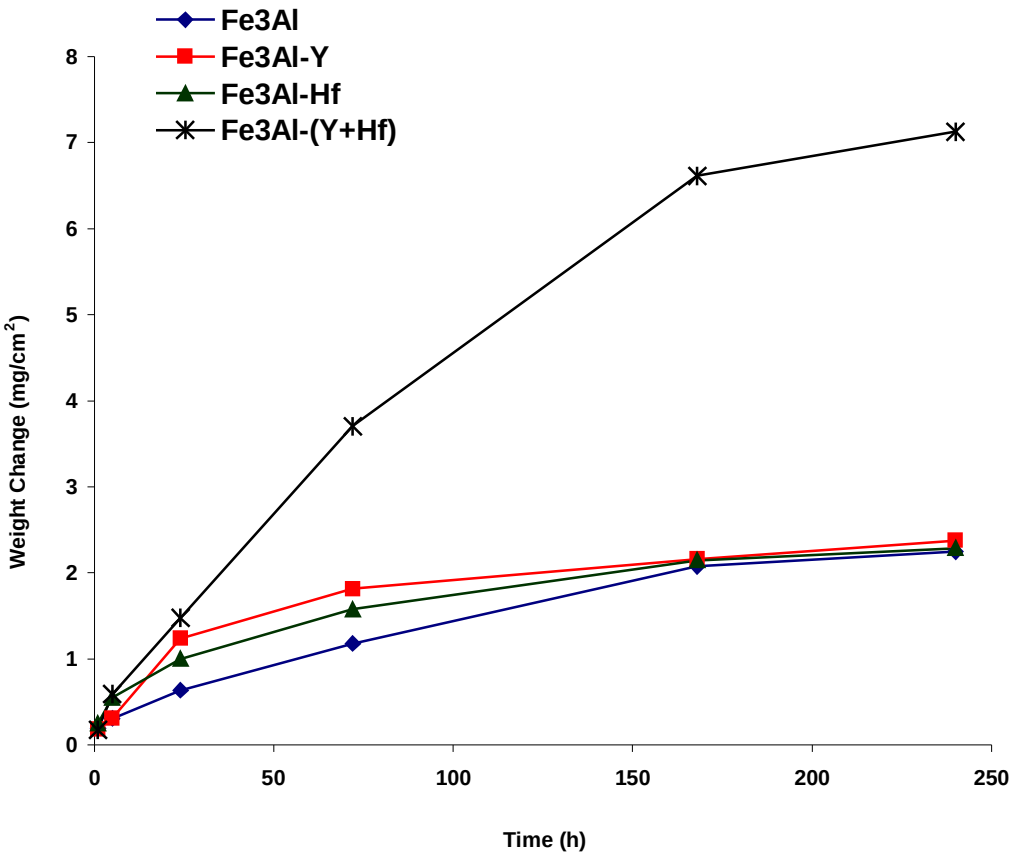

Figure 6-47 Weight gains versus exposure time for the Fe_3Al intermetallic alloys after isothermal air oxidation at 1100ºC for up to 240h

more complex than that at 900 and 1000°C. Although the weight gain of the experimental materials [except Fe_3Al-(Y+Hf)] at 1100°C, beyond 150h looks very similar (**Figure 6-47**), however, their scale properties are found to be very different.

The isothermal oxidation data from this study show significant changes in the oxidation rate of Fe_3Al especially with the addition of yittrium. In certain cases (depending on the exposure temperature), the RE adversely affected the kinetic oxidation behaviour of Fe_3Al intermetallics. This is because of various reasons as will be discussed in **Chapter 7**. For comparison between the isothermal oxidation behaviour of the Fe_3Al alloys, the calculated kinetic oxidation data of the materials between 900 and 1100°C are presented in **Table 6-4**. It is clear that the reaction rate constants for each material increased with increasing

Material	**Kp** ($g^2/cm^4/s^{-1}$)		
	at **900ºC**	at **1000ºC**	at **1100ºC**
Fe_3Al	6.9×10^{-14}	8.9×10^{-13}	6.2×10^{-12}
Fe_3Al-Y	4.2×10^{-13}	1.6×10^{-12}	6.4×10^{-12}
Fe_3Al-Hf	1.5×10^{-14}	4.8×10^{-13}	6.1×10^{-12}
Fe_3Al-(Y+Hf)	7.6×10^{-15}	1.06×10^{-13}	8.8×10^{-11}

Table 6-4 Isothermal air oxidation rate constants ($g^2/cm^4/s$) of Fe_3Al intermetallic alloys at 900, 1000 and 1100ºC for up to 240h

the exposure temperature. From **Table 6-4**, it is obvious that Y adversely affected the oxidation rate of Fe_3Al alloy by one order of magnitude. However, the Y-doped material is less sensitive among Fe_3Al alloys to the temperature increase under isothermal conditions. For example, the oxidation rate constant of Fe_3Al-Y at 1100°C is just one order of magnitude higher than that at 900°C, whilst the difference in the oxidation rate constant of other materials at these two temperatures is at least two orders of magnitude. More interestingly, it is clear from **Table 6-4** that the combined additions of Y and Hf adversely affected the oxidation rate of Fe_3Al alloys especially at higher temperatures. For example, the reaction rate constant of the Fe_3Al doped with both Y and Hf at 1100°C is one order of magnitude higher than that of the undoped Fe_3Al alloy at a given temperature. The beneficial addition of both Y and Hf to the oxidation rate of Fe_3Al alloy was observed up to 1000°C, beyond which the alloy with both Y and Hf showed the highest isothermal oxidation rate constant among the Fe_3Al alloys. Surprisingly, addition of Hf alone to the alloy did not alter significantly the isothermal oxidation rate of Fe_3Al alloy in the whole range of exposure temperatures. This finding confirms that Y addition is detrimental to the oxidation kinetics of Fe_3Al alloys under the present experimental conditions.

While some authors have insisted (in some case in spite of their data) that a RE addition, especially Y, beneficially affected the oxidation rate of alloys similar to our experimental materials. In other studies, authors have concluded that RE addition does not change the oxidation rate (refer to **Section 3.3**). However, the present investigation revealed complex and dramatic change in the oxidation rates of Fe_3Al alloys when temperature increased from 900 to 1100°C. This makes it difficult to explain the REE base only on the oxidation kinetic data and further investigations on the scale morphology and composition of the experimental materials were made in order to clarify the REE on Fe_3Al alloys.

Scale morphology and composition after isothermal air oxidation of Fe_3Al intermetallic alloys

Although the scale thickness of the experimental materials at a given temperature was comparable especially at low temperatures, the scale morphologies and protectiveness to the substrate are significantly different. At the early stages of oxidation (e.g. 5h) at 900°C, no corrosion product was detected. With increasing the exposure time to 240h, fast growing (probably θ-Al_2O_3 of a blade-like nodules – **Figure 6-48**(**a**)) formed. The scale formed on undoped Fe_3Al alloys after 240h under isothermal conditions at 900°C was not continuous and showed some porosity (**Figure 6-48**(**b**)). Also the scale was neither compact nor adherent to the substrate – severely cracked and spalled easily during cooling (**Figure 6-48**(**c**)). XRD analysis (e.g. **Figure 6-49**) of the oxidised Fe_3Al alloys at 900ºC revealed trace peaks of Fe_2O_3 together with Al_2O_3. The scales formed on Y-containing Fe_3Al intermetallics [Fe_3Al-(Y) and Fe_3Al-(Y+Hf)] under the same isothermal conditions were slow growing, coherent and adherent 'protective' to the substrate. The scales formed on Fe_3Al-Y alloy were found more adherent than those formed on Fe_3Al-(Y+Hf) as depicted from **Figure 6-50**(**a**) if compared to **Figure 6-50**(**b**). However, in both alloys, no significant detachment of large oxide particles was observed at the flat surfaces of the specimens. Careful examination

to the scale formed on Fe_3Al-Y substrate under isothermal oxidation at 900° C revealed continuous and integrated 'coherent' oxide scale, even in places where large cavities between the substrate and the scale were found (refer to **Figure 6-50(c)**). On large areas at the corners of oxidised materials (except Fe_3Al-Y alloy) at 900°C, the scale completely delaminated (lifted) from the substrate during cooling after 240h exposure. Although the external oxide layer of the Y-containing materials were thin and adherent to the substrate, the phenomenon of intergranular – at the alloy grain boundaries – oxidation starts to appear at low temperature as 900°C in the Y-doped alloys (e.g. **Figure 6-50(d)**). The phenomenon, directly changes the overall oxidation kinetics of Y-doped alloys (refer to **Figure 6-45**) by increasing the weight gain of the oxidised materials doped with yittrium. Although, the scale of Hf-doped alloy was not protective (**Figure 6-50(e)**) – where the surfaces of the scale and the substrate were corrugated and porous – the intergranular oxidation was not observed in Hf doped alloy at 900°C. Under the same exposure conditions, Hf in Fe_3Al-(Y+Hf), reduced the weight gain of Fe_3Al probably by limiting or preventing the intergranular oxidation of the alloy (**Figure 6-50(f)**. This leads to the conclusion that Y is the main cause of the intergranular attack of Fe_3Al alloys even at low temperatures as 900°C. The effects of the RE become clearer as the temperature of the oxidation increased.

(**a**)

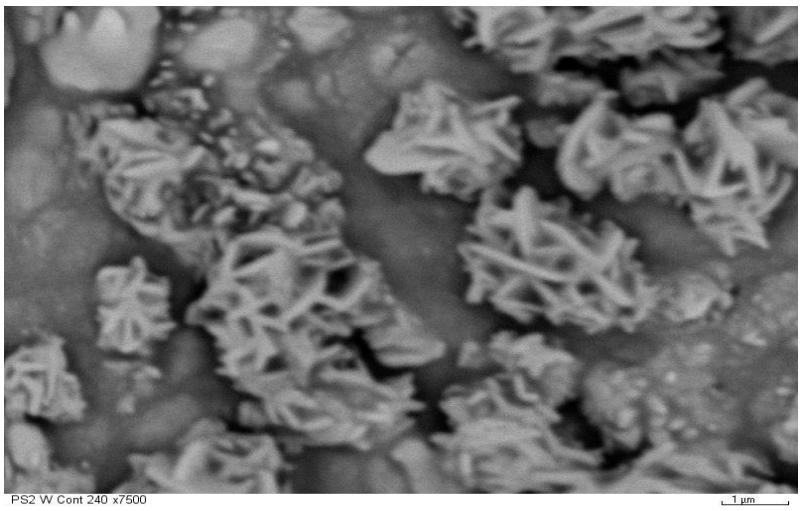

(**b**)

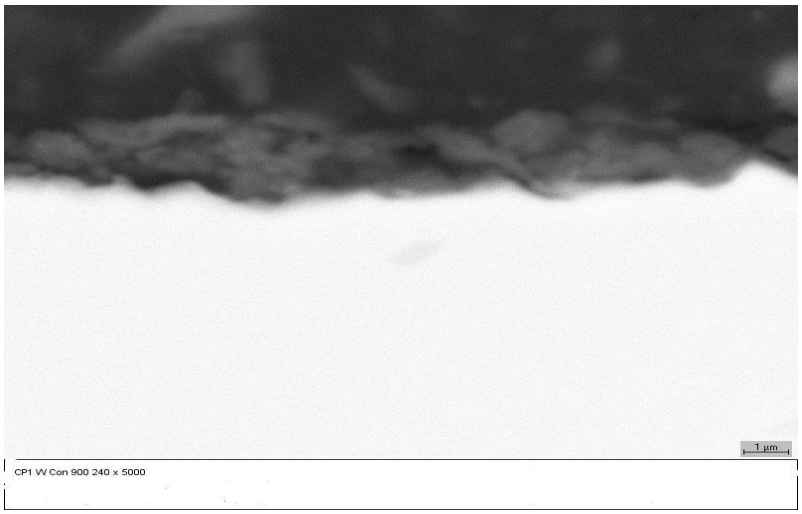

(**c**)

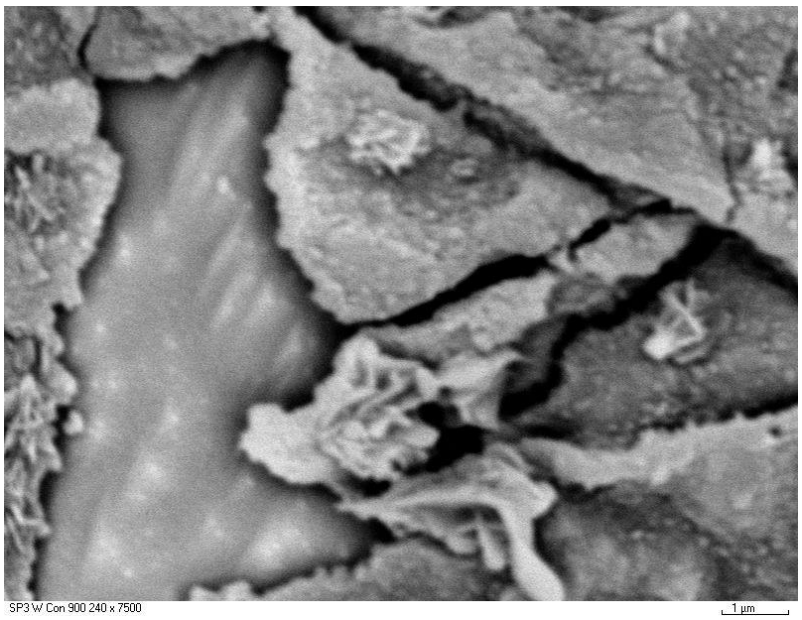

Figure 6-48 SEM micrograph of Fe_3Al intermetallic alloy after isothermal air oxidation at 900ºC for 240h

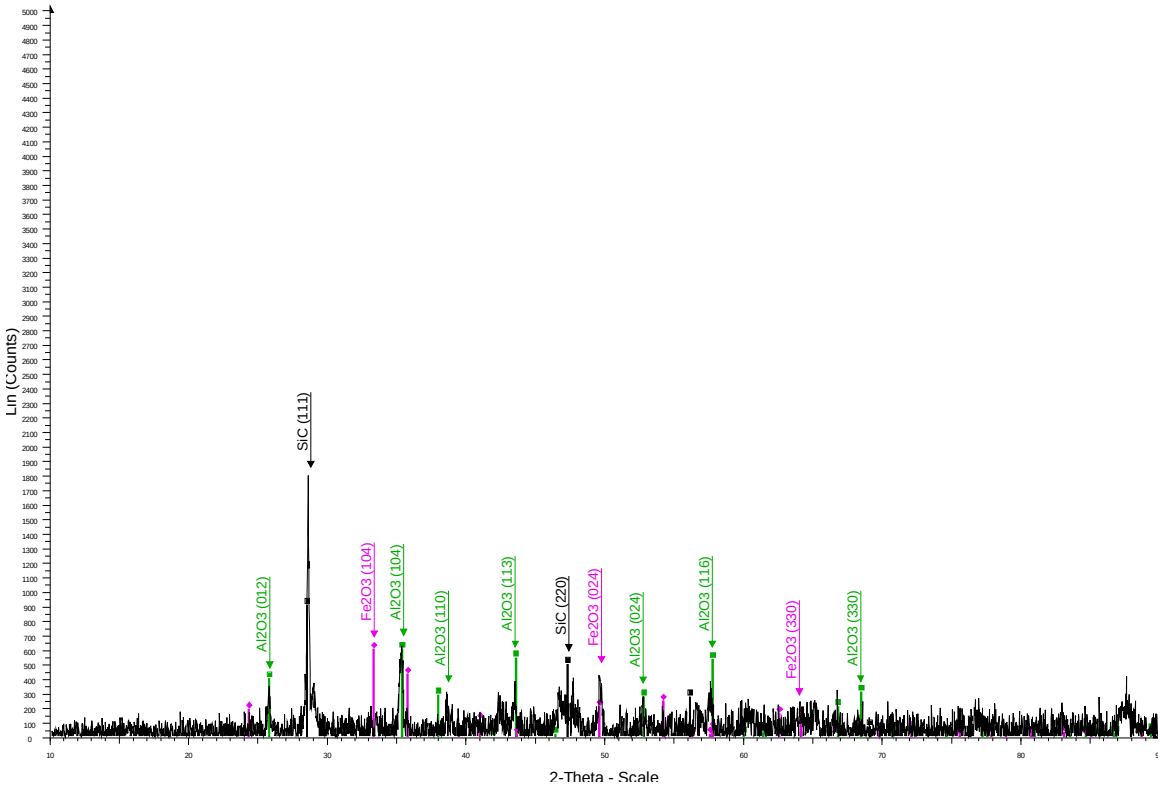

Figure 6-49 XRD pattern of Fe_3Al intermetallic alloy after isothermal air oxidation at 900ºC for 240h

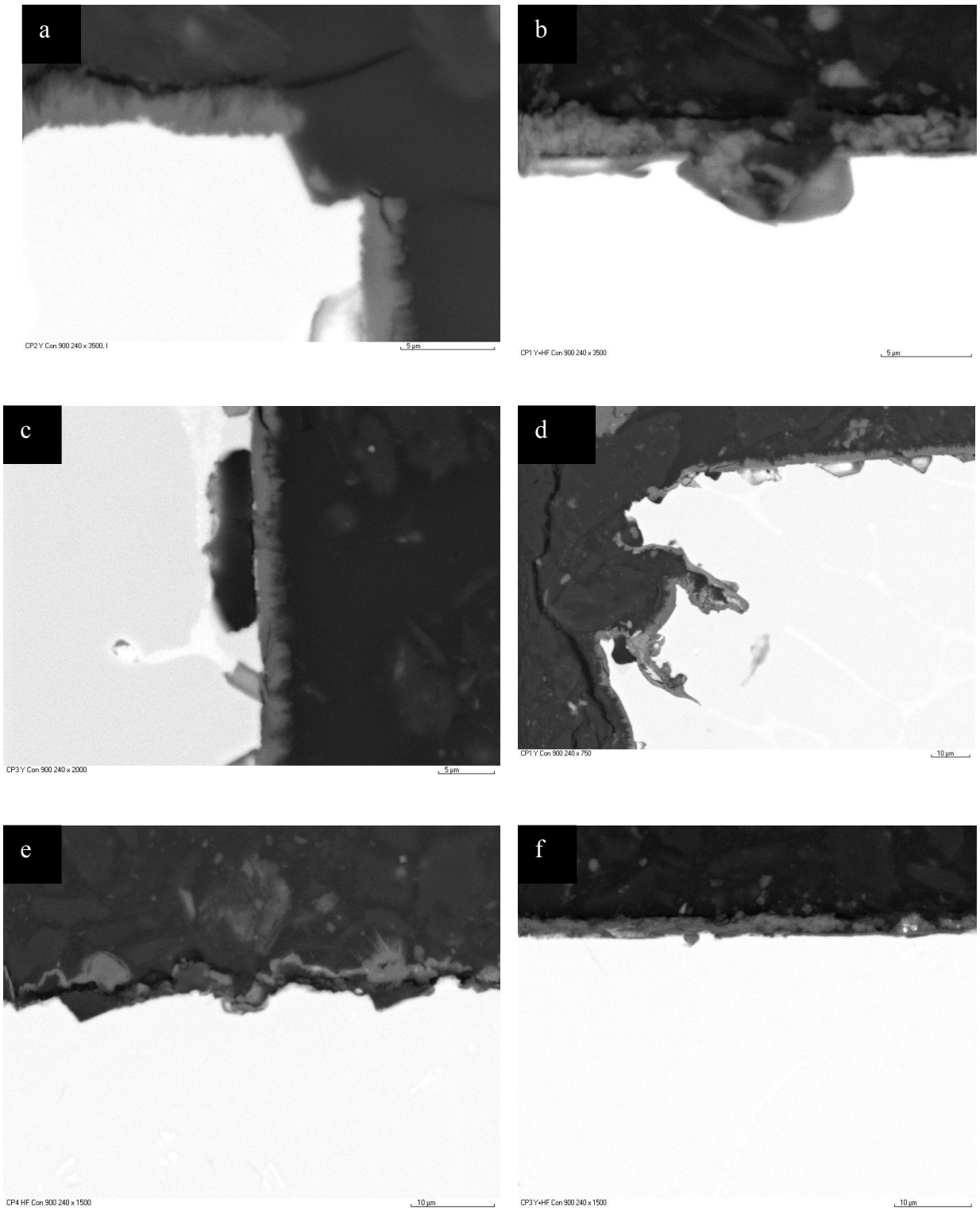

Figure 6-50 Back scattered SEM micrographs of (**a**, **d** and **c**) Fe_3Al-Y, (**b** and **f**) Fe_3Al-(Y+Hf) and (**e**) Fe_3Al-Hf intermetallic alloys after isothermal air oxidation at 900ºC for 240h

At 1000°C, and under isothermal oxidation conditions, the scale thickness of undoped Fe_3Al and Fe_3Al doped with Hf increased dramatically with increase of exposure time (**Figure 6-51**(**a**) and **Figure 6-51**(**b**)) respectively. For the undoped Fe_3Al at 1000°C after 5h exposure in air, the scale consists mainly of Al_2O_3, with trace peaks of spinel of iron and aluminium oxides as indicated by XRD pattern (**Figure 6-52** (**a**). With increasing exposure time to 72h the spinel were no longer detected and the scale became only Al_2O_3 (**Figure 6-52**(**b**). The oxides tend to spall easily from the undoped Fe_3Al after 240h during cooling as shown in **Figure 6-53**. However, at 1000°C, the scale of the Hf-doped material remain in contact with the substrate even at the sample corners (**Figure 6-54**(**a**) and (**b**). With the infinite supply of Al from the substrate, relatively thick scales from the undoped Fe_3Al and doped with Hf were formed. Furthermore, no sign of aluminium depletion from both materials even after prolonged exposure time (168h) at 1000ºC as shown in **Figures 6-55** and **6-56** respectively. Again and for the same reason (intergranular oxidation – **Figure 6-57**(**a**)), the Y-doped alloy recorded the highest weight gain at 1000ºC (refer to **Figure 6-46**). However, the external scale is very thin and remain adherent even at sample corners (**Figure 6-57**(**b**)). The depth of the internal attack of Fe_3Al-Y increased as the exposure time increased. The internally attacked areas (oxide pegs) for the material doped with Hf was relatively thick, whereas the intergranular oxidation of the Fe_3Al-Y material was narrow and deeper than the oxide pegs of Hf-doped material. Furthermore, the surface morphology of the oxide formed on the Y-doped materials at the same experimental conditions are also different. The alloy grain boundaries of the Y-doped material are clearly marked – convoluted scale – by the formation of oxide ridges at the alloy grain boundaries (**Figure 6-57**(**c**)). Generally, the scale formed on Y-containing alloys has rough surface of cigar-like shop (**Figure 6-57**(**d**)), whereas the scale formed on Hf-doped materials has relatively smooth surfaces – rumpling shape (refer to **Figures 6-51**(**b**) and **6-54**(**a**)). Both

(**a**)

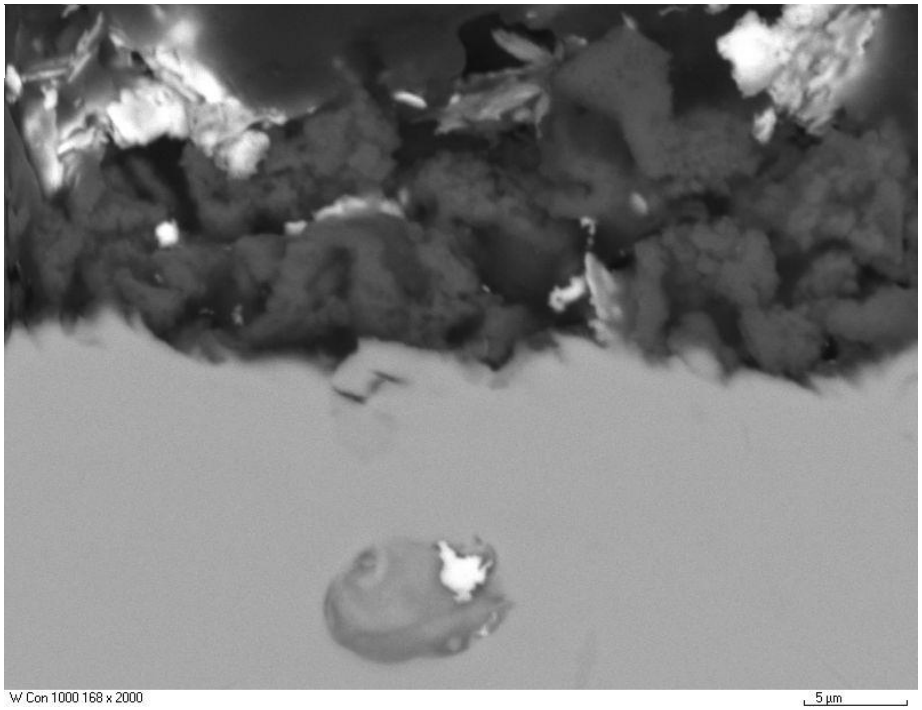

(**b**)

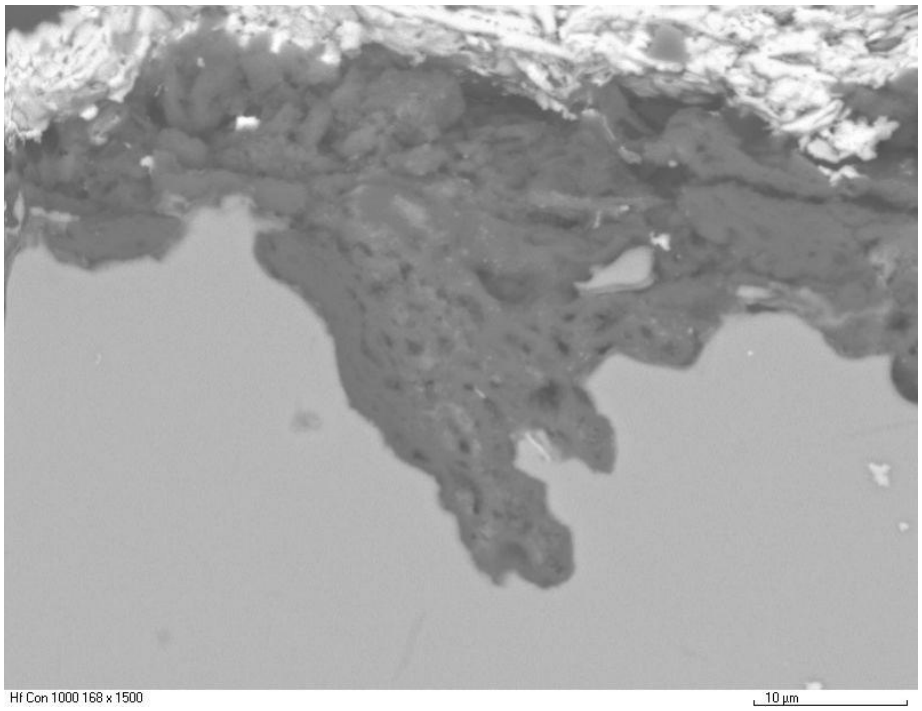

Figure 6-51 Back scattered SEM micrographs of (**a**) Fe_3Al and (**b**) Fe_3Al-Hf intermetallic alloys after isothermal air oxidation at 1000ºC for 168h

(**a**)

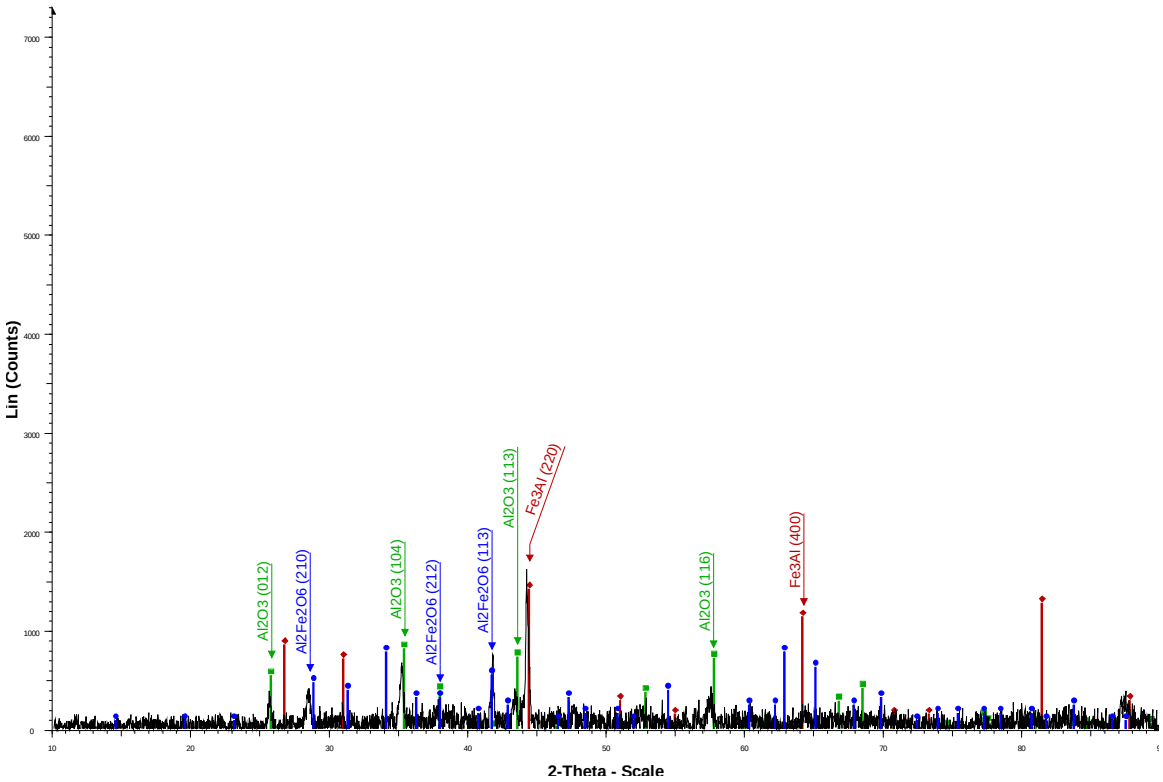

(**b**)

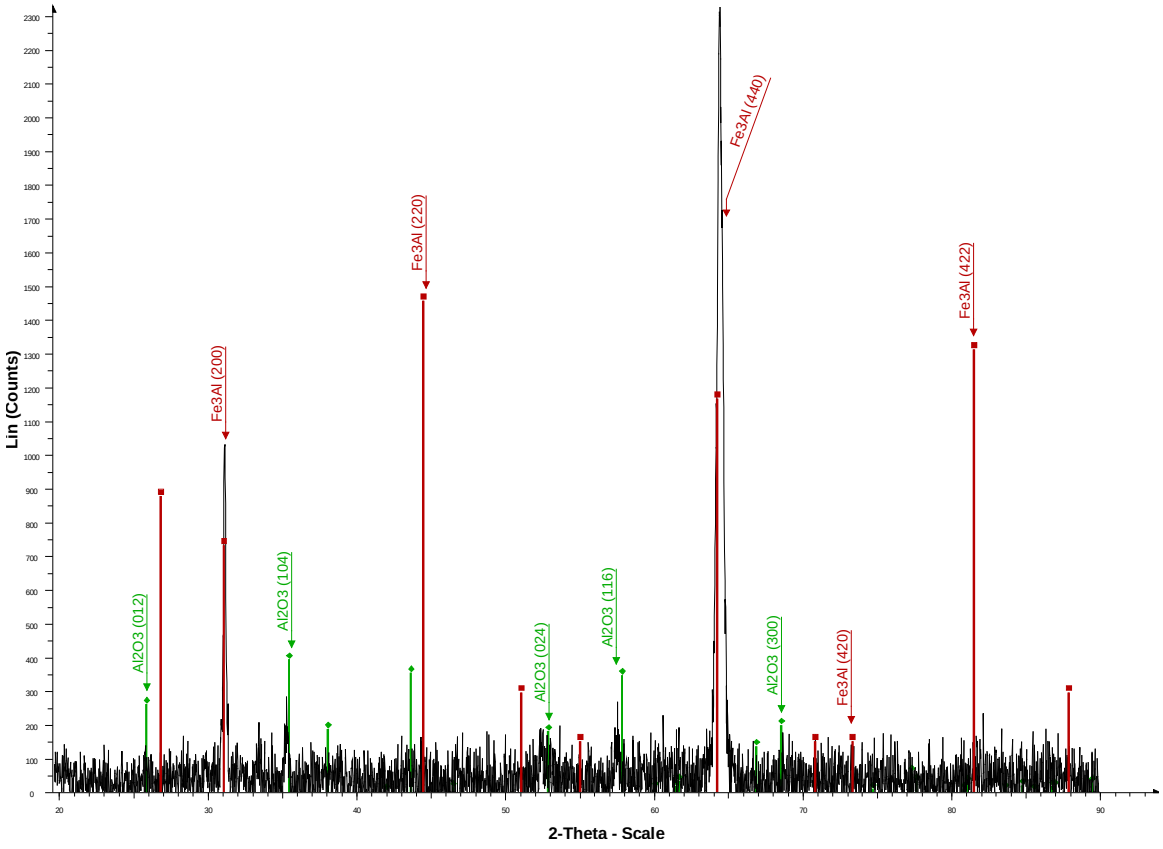

Figure 6-52 XRD patterns of Fe_3Al intermetallic alloy after isothermal air oxidation at 1000ºC (**a**) for 5h and (**b**) for 72h

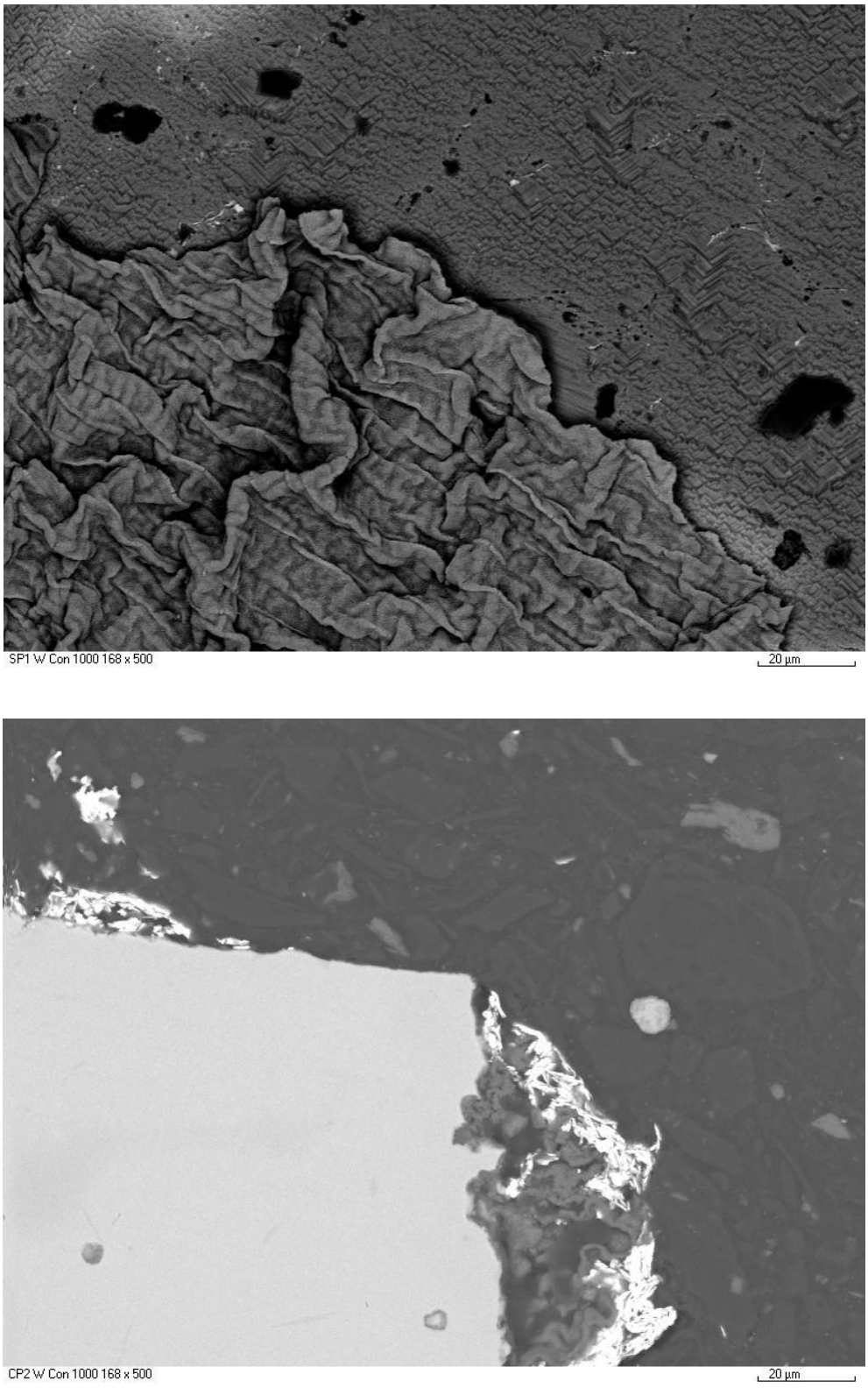

Figure 6-53 Back scattered SEM micrographs of Fe_3Al intermetallic alloy after isothermal air oxidation at 1000ºC for 240h

(**a**)

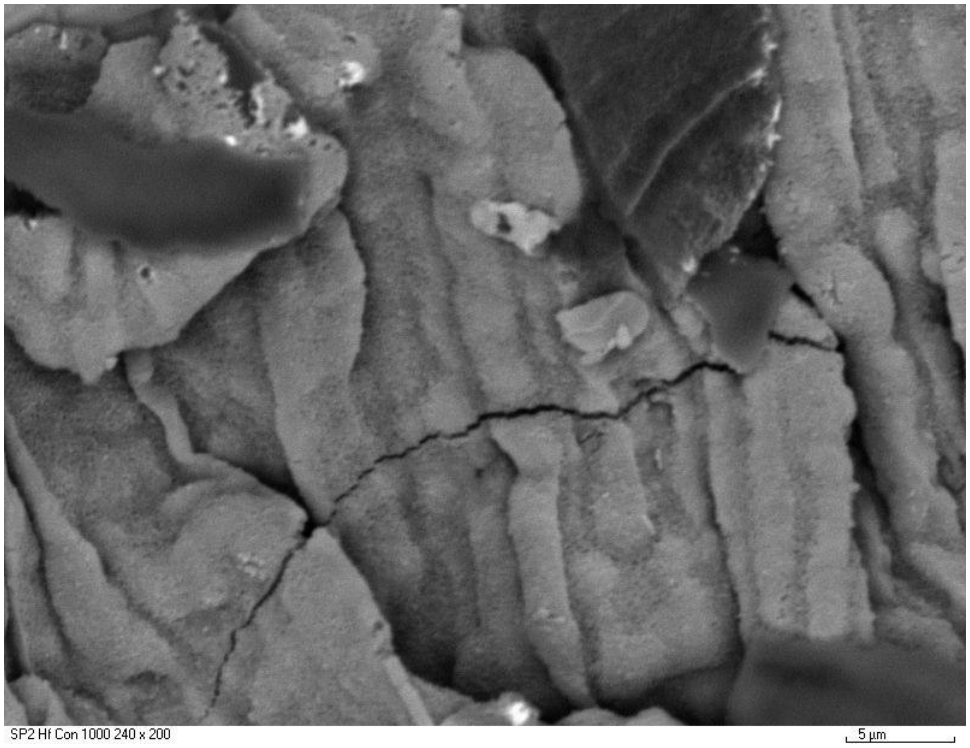

(**b**)

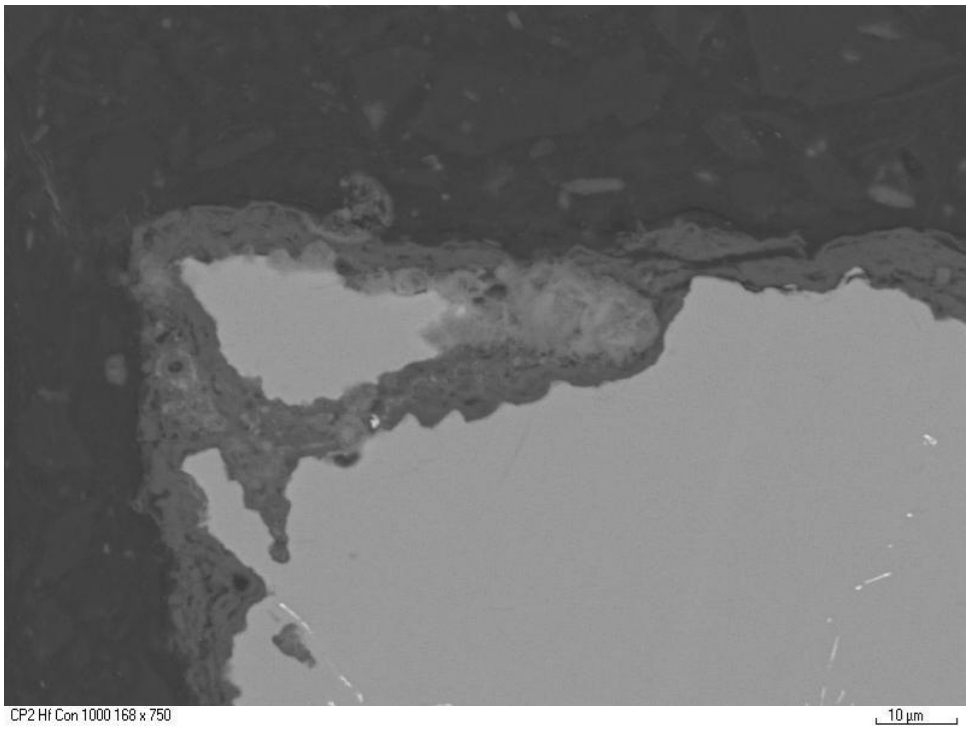

Figure 6-54 Back scattered SEM micrographs of Fe_3Al-Hf intermetallic alloy after Isothermal air oxidation at 1000ºC for 240h

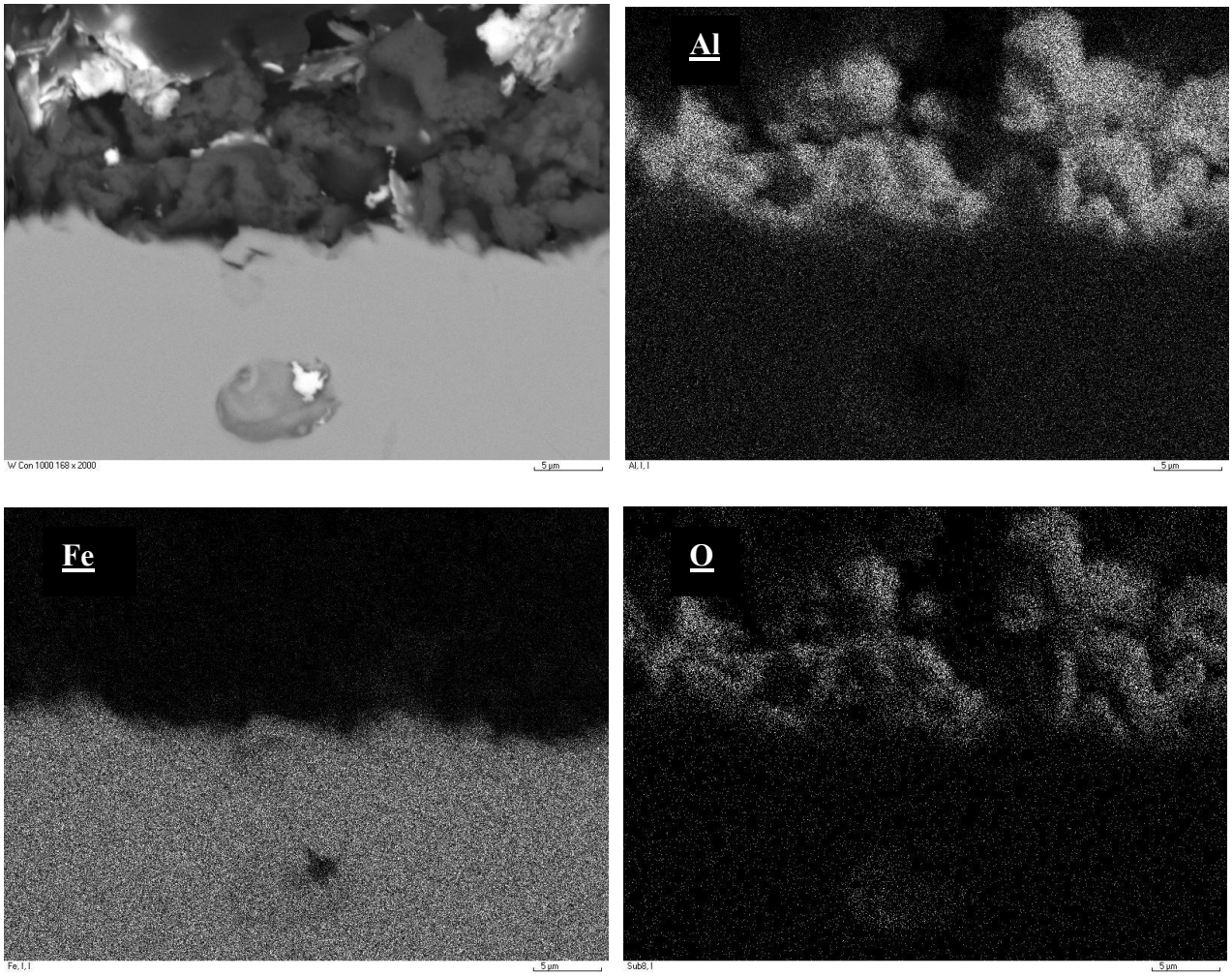

Figure 6-55 Back scattered SEM micrographs and Digimaps of Fe_3Al intermetallics alloy after isothermal air oxidation at 1000ºC for 168h

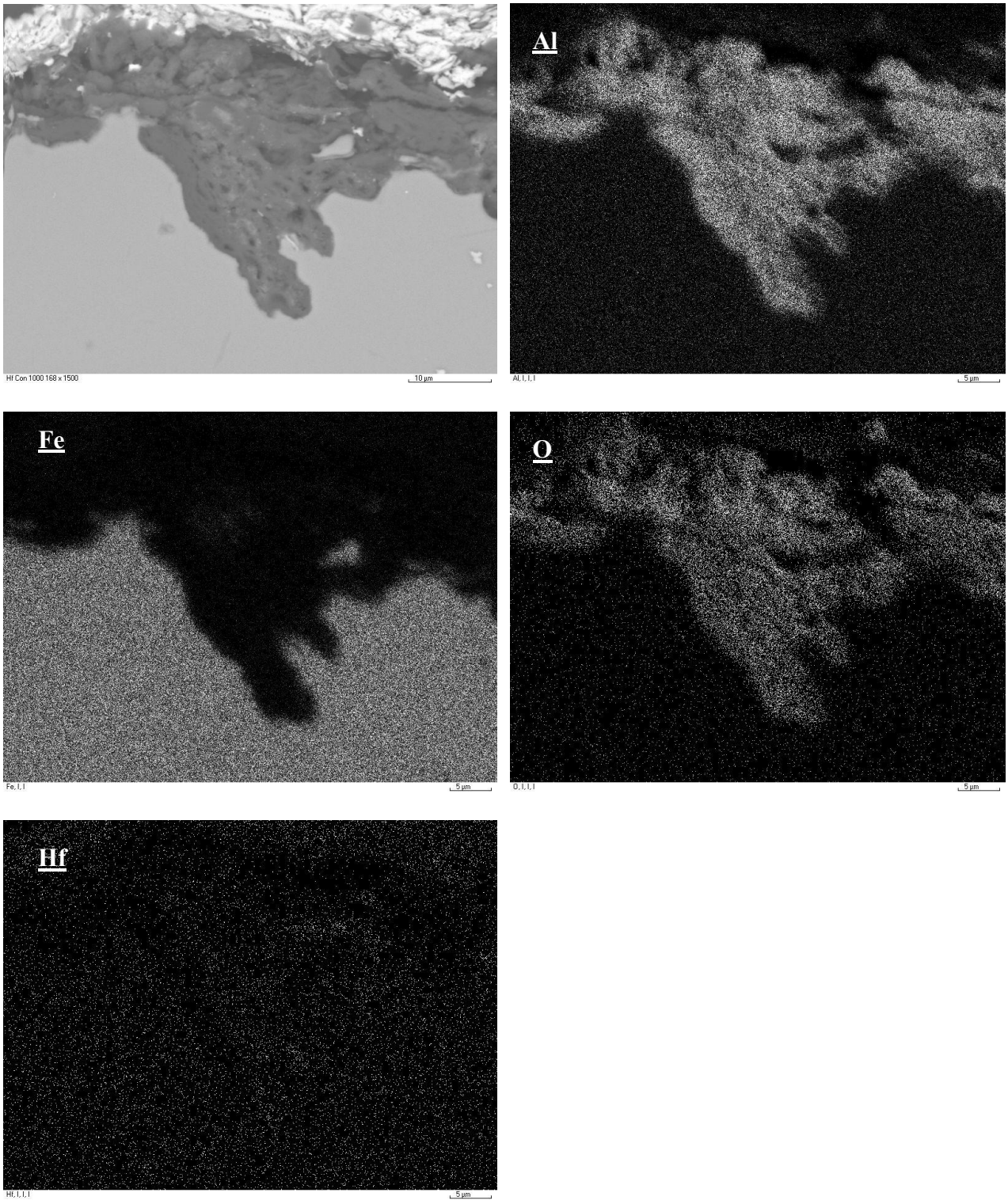

Figure 6-56 Back scattered SEM micrographs and Digimaps of Fe_3Al-Hf intermetallic alloy after isothermal air oxidation at 1000ºC for 168h

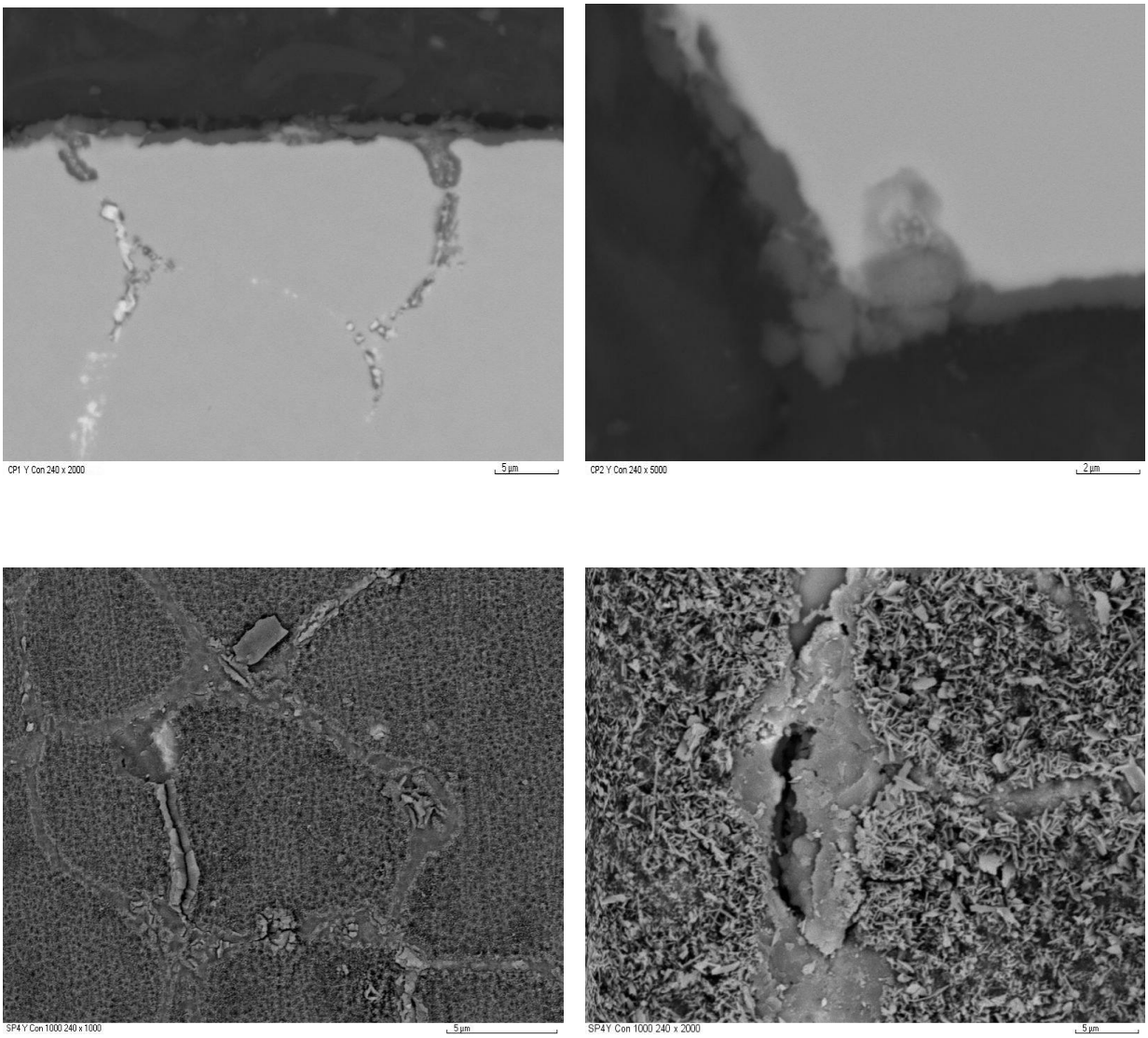

Figure 6-57 Back scattered SEM micrographs of Fe_3Al-Y intermetallics alloy after isothermal air oxidation at 1000ºC for 240h

morphologies of the Al_2O_3 scales are briefly described in **Section 3.3.2**. The external scale of Fe_3Al doped with both Y and Hf showed double layered scale, the inner layer remained in contact and almost flat with the surface of the alloy (**Figure 6-58**(**a**)), whereas the outer layer is convoluted and tends to spall easily especially at the sample corners (**Figure 6-58**(**b**)). The micrograph and the digimaps of the Y and (Y+Hf) doped Fe_3Al alloys after 240h isothermal air oxidation at 1000ºC are shown in **Figures 6-59** and **6-60** respectively. Although the REs (Y and/or Hf) are present in the Fe_3Al alloys in small quantities (refer to **Table 5.2**) EDX analysis of the oxidised alloys (at 1000ºC for 168h) doped with only Y indicated presence of Y at the alloy grain boundaries (**Figure 6-59**). However, Y after oxidation of Fe_3Al-(Y+Hf) was not visible at the alloy grain boundaries, **Figure 6-60**. Again, it is clear that Y is the main cause of the scale adhesion – beneficial effect – as well as it is the primary reason for the Fe_3Al alloy internal attack – detrimental effect.

Although the single and combined addition of Y and/or Hf adversely affected the isothermal oxidation kinetics of Fe_3Al at 1100°C (refer to **Figure 6-47**), the scale thickness of undoped Fe_3Al after 72h exposure at 1100°C is more than three times than that of Fe_3Al-Y and Fe_3Al-(Y+Hf) alloys as depicted from **Figure 6-61**. The scale of the undoped Fe_3Al alloy is thick, convoluted and spall easily from the substrate (**Figure 6-61**(**a**) and (**b**)). However, under similar isothermal oxidation conditions, the scale of the Y-containing materials remained relatively thin and adherent to the alloys (**Figure 6-61**(**c**)). Again, the oxide on Fe_3Al-(Y+Hf) consists of two layers of which the outer layer is normally convoluted, while the inner layer which is in contact with the substrate is almost flat and adherent to the substrate (**Figure 6-61**(**d**)). After 168h, cooling the Fe_3Al alloys from 1100ºC, serious breakdown of their external layer took place. For example, severe internal attack to Fe_3Al-(Y+Hf) was observed (**Figure 6-62**(**a**)). Also, beneath the oxide scale and at the internally oxidised areas of Fe_3Al-(Y+Hf) at 1100°C after 168h exposure, large numbers

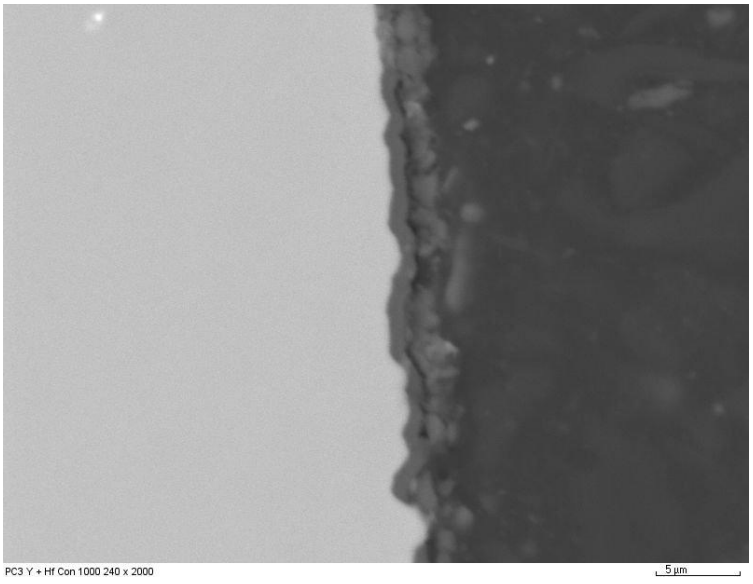

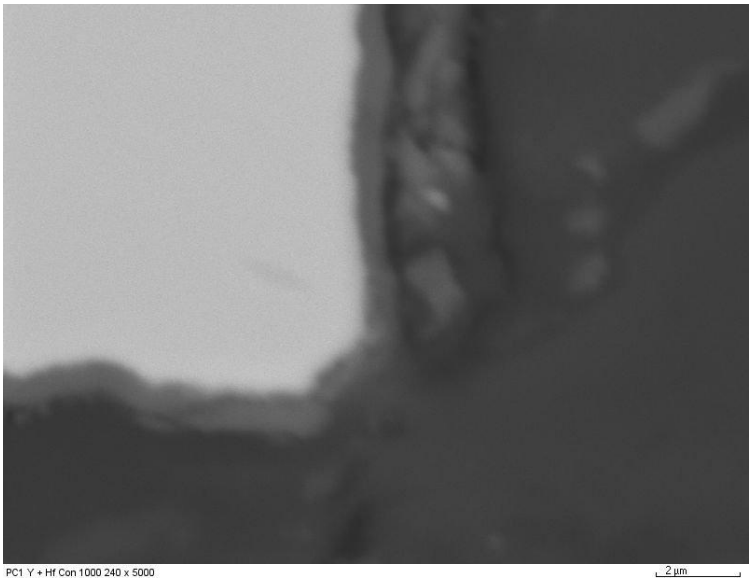

Figure 6-58 Back scattered SEM micrograph of Fe_3Al-(Y+Hf) after isothermal air oxidation at 1000ºC for 240h

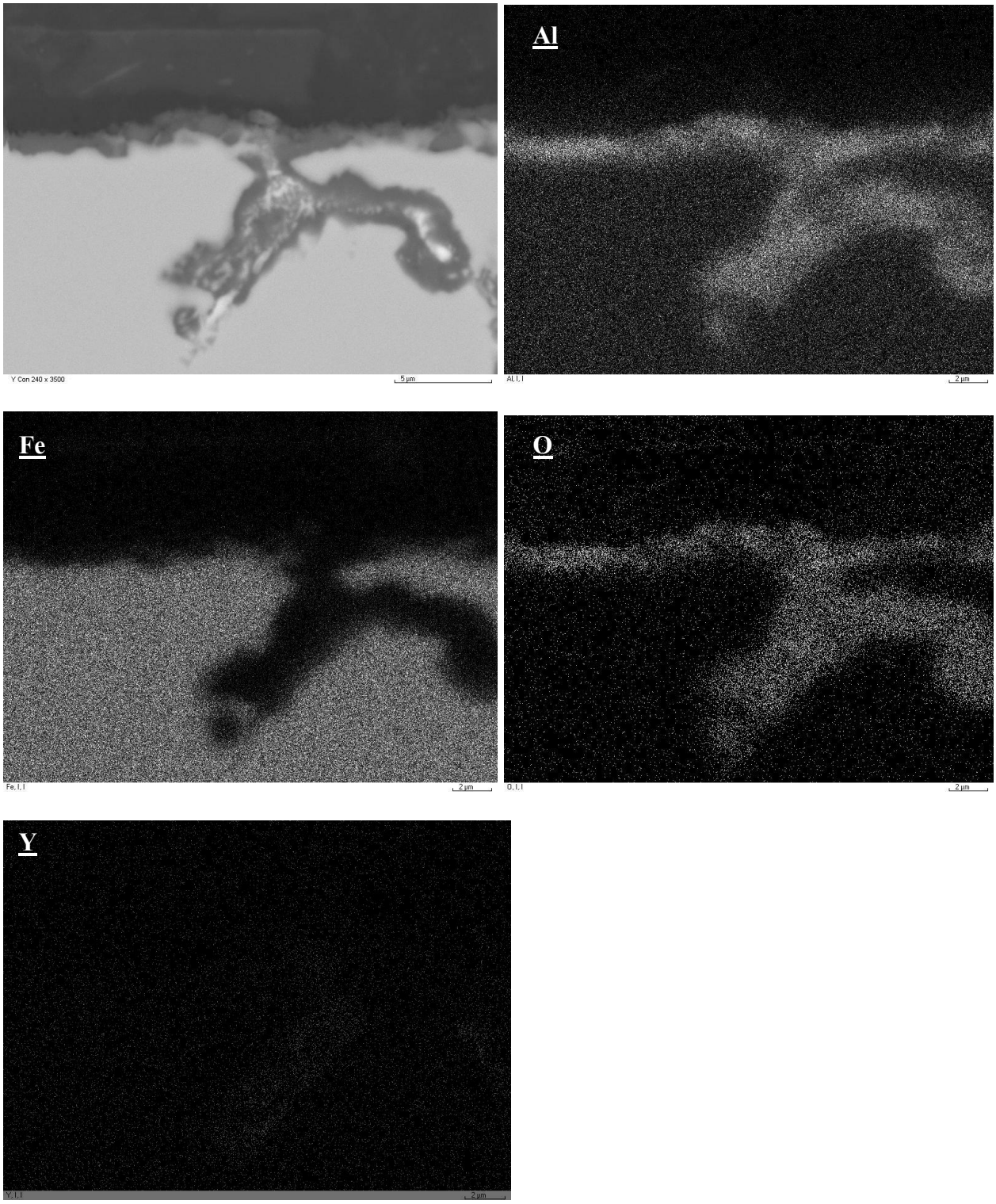

Figure 6-59 Back scattered SEM micrographs and Digimaps of Fe_3Al-Y intermetallic alloy after isothermal air oxidation at 1000ºC for 240h

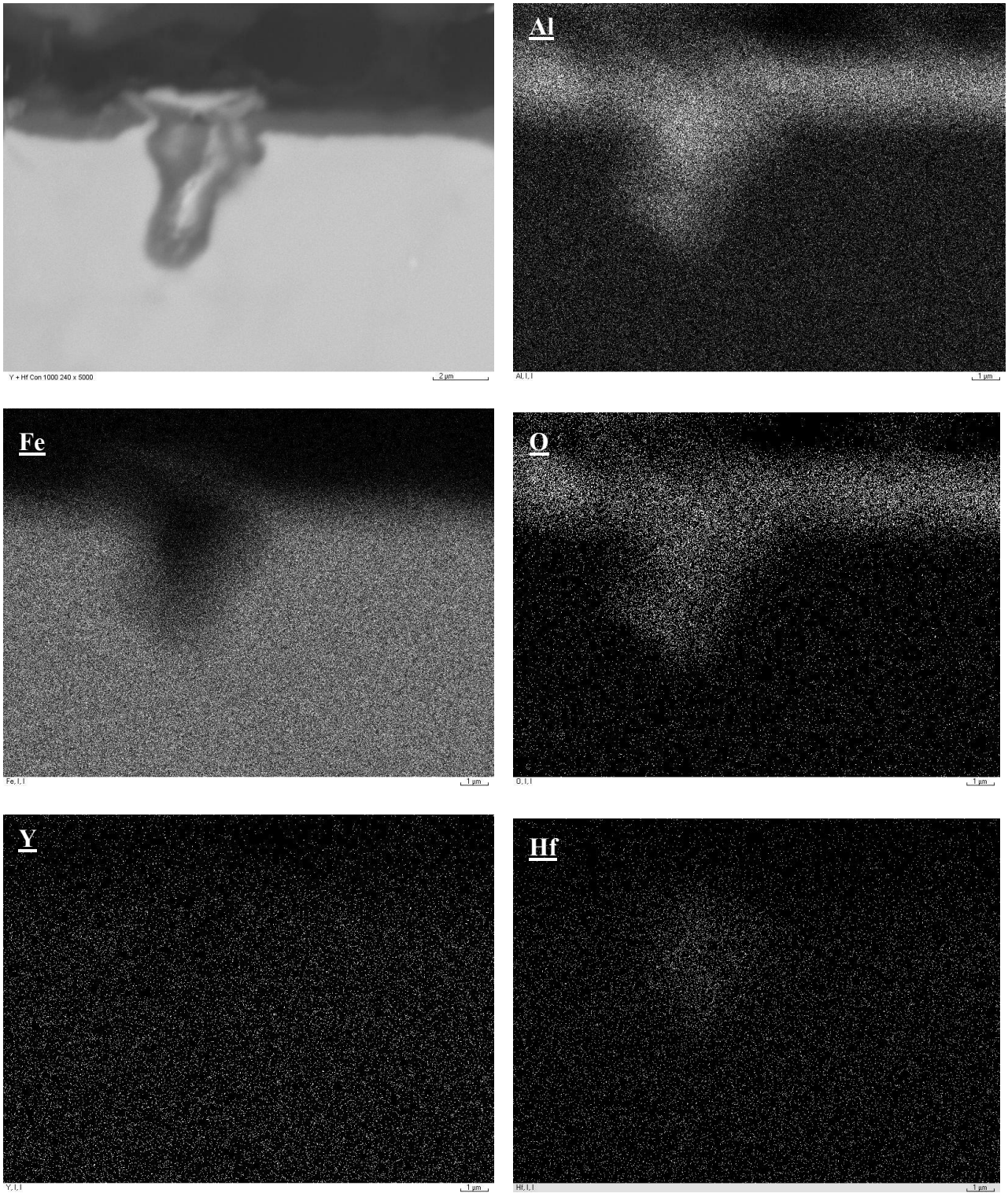

Figure 6-60 Back scattered SEM micrographs and Digimaps of Fe_3Al-(Y+Hf) intermetallic alloy after isothermal air oxidation at 1000ºC for 240h

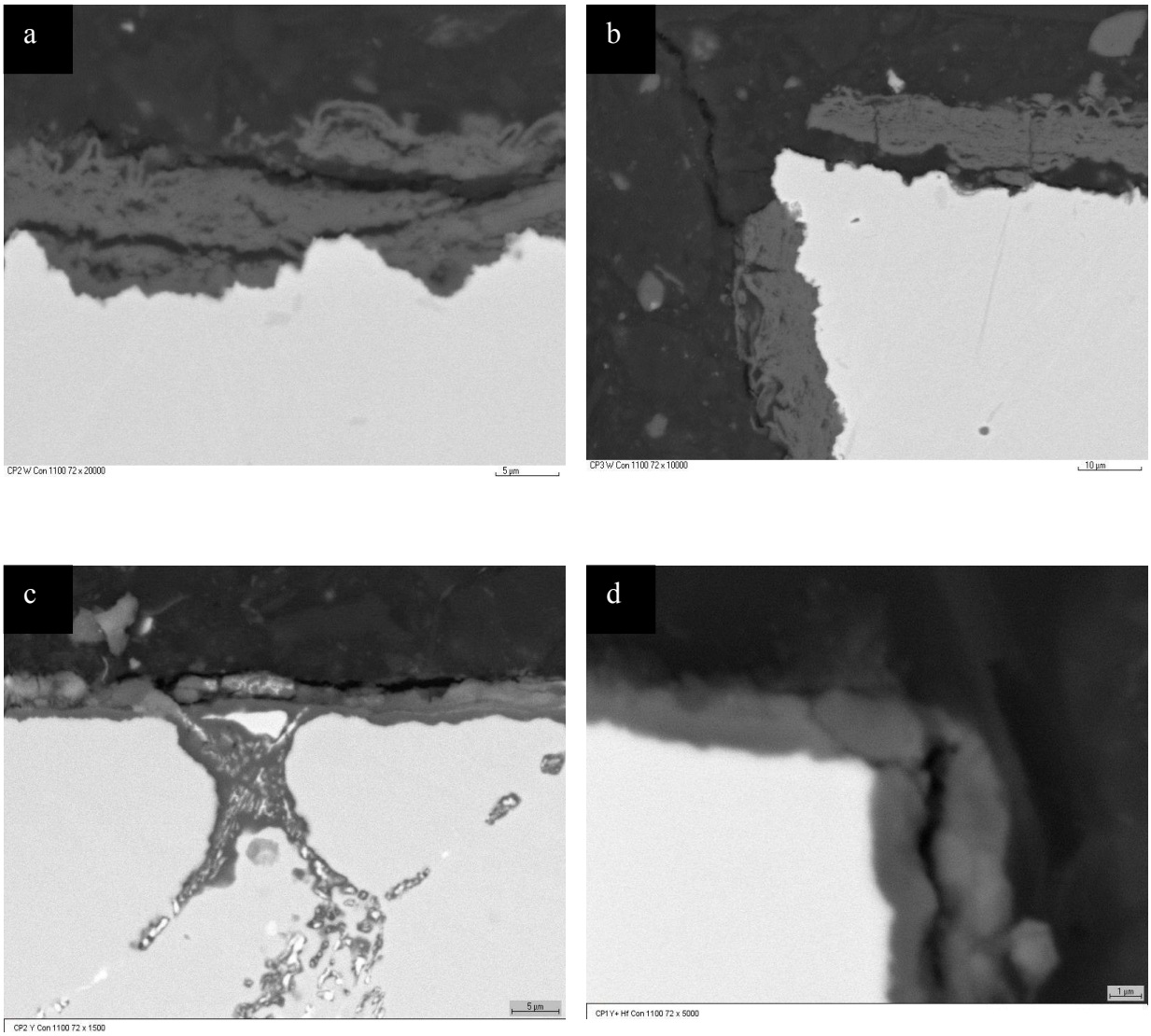

Figure 6-61 SEM micrographs of (**a** and **b**) Fe_3Al, (**c**) Fe_3Al-Y and (**d**) Fe_3Al-(Y+Hf) after isothermal air oxidation at 1100ºC for 72h

(**a**)

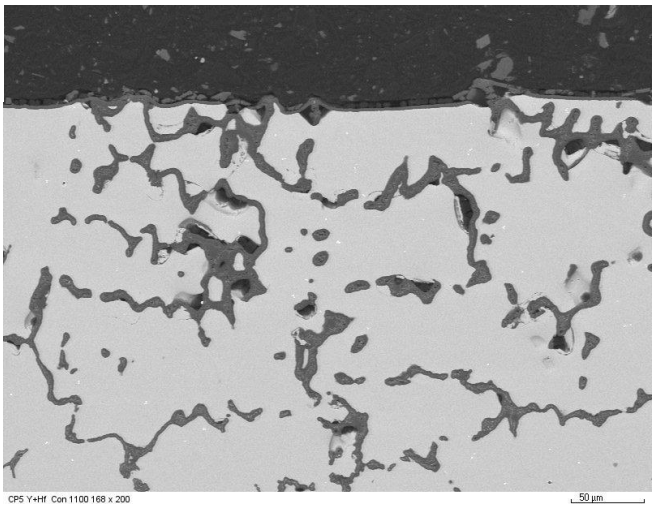

(**b**)

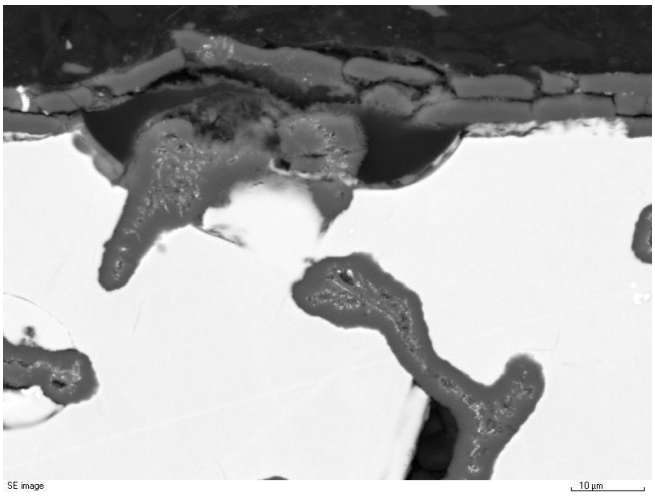

(**c**)

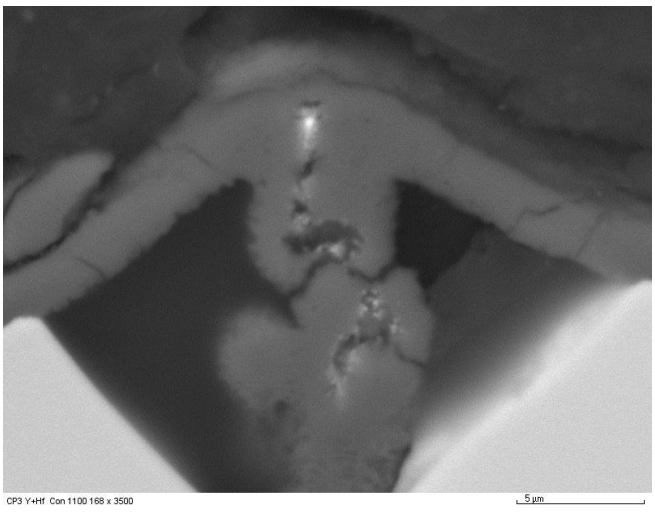

Figure 6-62 SEM micrographs of Fe_3Al-(Y+Hf) after isothermal air oxidation at 1100ºC for 168h

of cavities and voids formed (**Figure 6-62**(**b**)). These voids caused severe damage to the external oxide scale during cooling as shown in **Figure 6-62**(**c**). However, the scale formed on Fe_3Al-Y at 1100ºC after 168h, showed single external scale (almost flat and free from voids – **Figure 6-63**(**a**)) and the scale tends to spall after cooling especially at the oxide ridges and sample corners, **Figures 6-63**(**b**) and (**c**) respectively.

Thus it appears that the oxidation process of Fe_3Al alloys is complex. The single and combined effects of Y and Hf on the isothermal oxidation behaviour of Fe_3Al are complicated and it is a strongly influenced by the experimental conditions such as exposure time and temperature in particular. Obviously, various degrees of scale spallation took place during cooling of the oxide scales formed not only for undoped alloy but also the scales of RE-containing materials. The phenomena of scale adherence and spallation is more clear when the materials is subjected to a number of thermal cycling as will be summarised in **Section 6.4.3**.

(**a**)

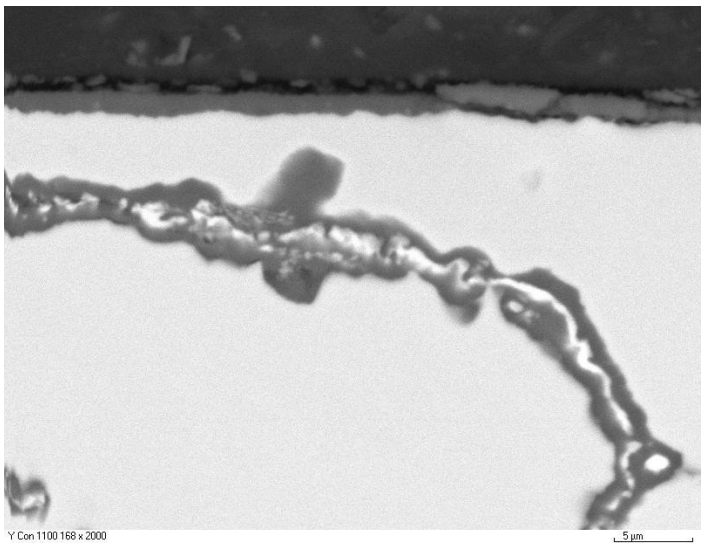

(**b**)

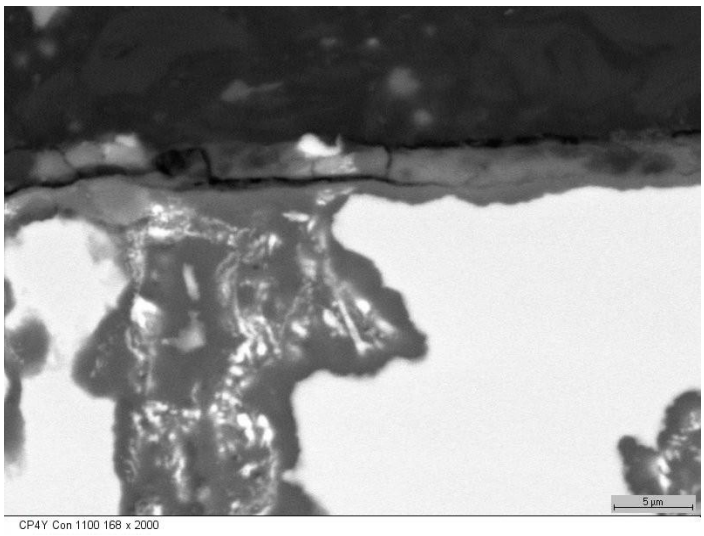

(**c**)

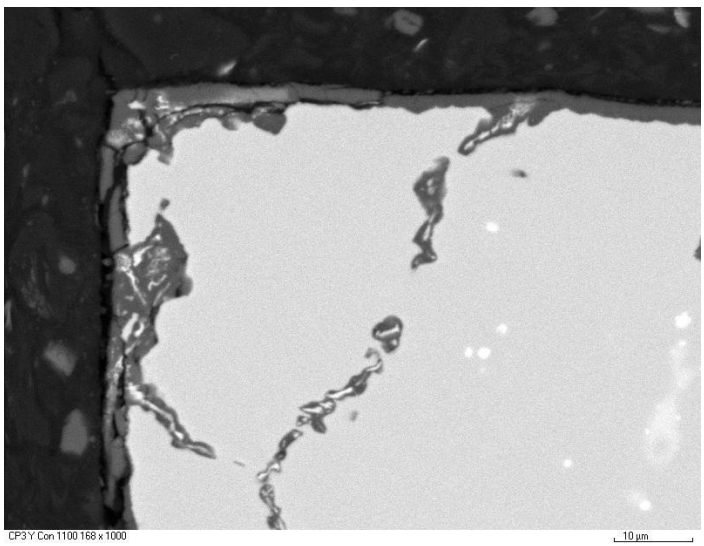

Figure 6-63 SEM micrographs of Fe_3Al-Y after isothermal air oxidation at 1100ºC for 168h

6.4.3 Cyclic Air Oxidation Behaviour of Fe_3Al Intermetallic Alloys

Thermal cycling conditions seem to be more severe and realistic than isothermal conditions in many high temperature applications. Thus a considerable part of the current research programme was undertaken to examine the REE on the cyclic oxidation behaviour of Fe_3Al intermetallics and to compare with the isothermal oxidation results at a fixed temperature.

Mass changes after cyclic oxidation of Fe_3Al intermetallic alloys

Figures 6-64 to **6-66** show the oxidation behaviour of the four Fe_3Al intermetallic alloys under thermal cycling conditions at 900, 1000 and 1100ºC for up to 240 one-hour cycles. The cyclic oxidation rate constants of the Fe_3Al experimental materials are summarised in **Table 6-5**. From **Table 6-5**, cyclic oxidation behaviour of the materials under investigation seems to be more complicated than that under isothermal conditions described in **Section 6.4.2**. For example, at 900°C, similar to the isothermal oxidation conditions, the reaction rate constant of the Y-doped alloy is one order of magnitude higher than that of other materials – including the undoped Fe_3Al. Also, at 900°C, the weight gain of Fe_3Al-Y dramatically increased with the increase of cycles (one-hour cycles), while in the other materials, the changes of their weight gain from initial stage of oxidation to the prolonged stage (up to 240 cycles) were very similar (**Figures 6-64**). The experimental materials (except the Y-doped alloy) at 900°C showed similar weight gain data up to 240 cycles at 900°C, however their scale properties at this temperature were different. Unlike the isothermal oxidation of Fe_3Al alloys (refer to **Figures 6-45** to **6-47**), the Y-doped Fe_3Al alloy under thermal cycling conditions showed lower oxidation rates after long-term exposure at 1000 and 1100ºC.

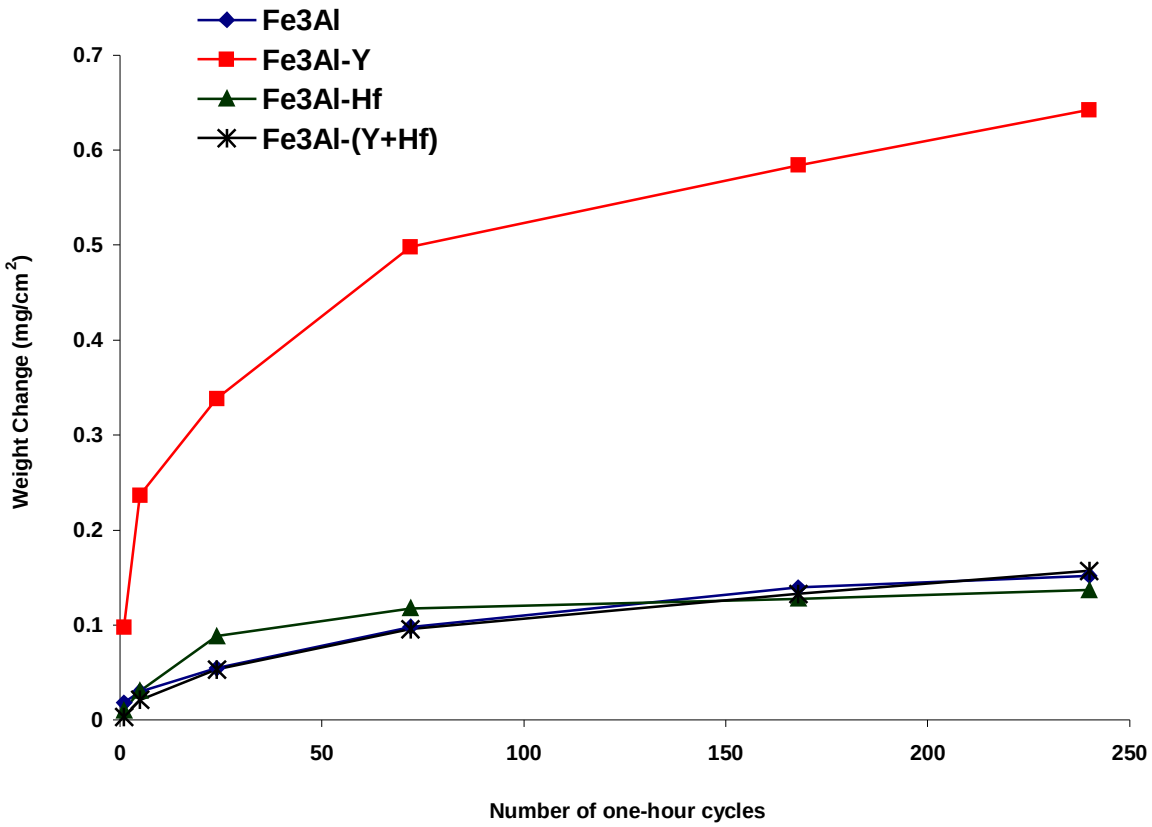

Figure 6-64 Weight gains versus exposure time for the Fe_3Al intermetallic alloys after cyclic air oxidation at 900ºC for up to 240 one-hour cycles

Material	**Kp** ($g^2/cm^4/s^{-1}$)		
	at **900ºC**	at **1000ºC**	at **1100ºC**
Fe_3Al	2.75×10^{-14}	4.12×10^{-12}	9.63×10^{-11}
Fe_3Al-Y	4.55×10^{-13}	1.14×10^{-12}	1.51×10^{-11}
Fe_3Al-Hf	2.02×10^{-14}	8.93×10^{-12}	1.61×10^{-10}
Fe_3Al-(Y+Hf)	2.85×10^{-14}	1.72×10^{-13}	6.42×10^{-11}

Table 6-5 Cyclic air oxidation rate constants ($g^2/cm^4/s$) of Fe_3Al intermetallic alloys at 900, 1000 and 1100ºC for up to 240 one-hour cycles

At 1000°C (**Figures 6-65)**, the cyclic air oxidation behaviour of the Fe_3Al alloys varied from the initial stage to the prolonged exposure time (or cycles). After the first 24 one-hour cycles at 1000ºC, Fe_3Al-Y showed the highest weight gain among the experimental Fe_3Al materials. Although the cyclic oxidation rate constant of the experimental alloys [except Fe_3Al-(Y+Hf)] are of the same order of magnitude at 1000ºC (see **Table 6-5**). However, it is clear from **Figure 6-65**, the weight gain for Fe_3Al-Hf under cyclic oxidation at 1000°C showed almost linear relationship with the increase of thermal cycles. Other Fe_3Al materials showed parabolic relationships with the increase of cycles (exposure time). The oxidation rate constant of Fe_3Al-(Y+Hf) at 1000°C under cyclic conditions is one order of magnitude less than that of other materials (refer to **Table 6-5**). Comparison of the kinetic data of Fe_3Al-Y, Fe_3Al-Hf and Fe_3Al-(Y+Hf) in cyclic conditions at 1000°C reveals the beneficial – rather than detrimental – effect of Y to the kinetic behaviour of Fe_3Al alloys during cyclic oxidation.

At 1100°C, it is clear that Y-containing alloys [Fe_3Al-(Y) and Fe_3Al-(Y+Hf)] show better cyclic oxidation behaviour by one order of magnitude less than that of undoped and Hf-doped Fe_3Al materials. However, the weight gain of the four experimental materials behaves similarly under cyclic oxidation conditions at 1100°C for up to 24 one-hour cycles, beyond that the divergence in the weight gain data of the alloys becomes significantly different, **Figure 6-66**. The weight change (with the spalled scale) of Fe_3Al-Y after 24h exposure did not alter significantly (quasi-parabolic – protective – behaviour) with the increase of exposure time at 1100°C, while other materials did show significant weight gain as the number of cycles increased. The cyclic oxidation kinetics of Hf-doped alloy at 1000°C and 1100°C are very similar. At these two temperatures the Hf-doped alloy recorded the highest weight gain among the Fe_3Al alloys and a linear relationship between its weight change and the number of cycles was recorded, **Figure 6-66**.

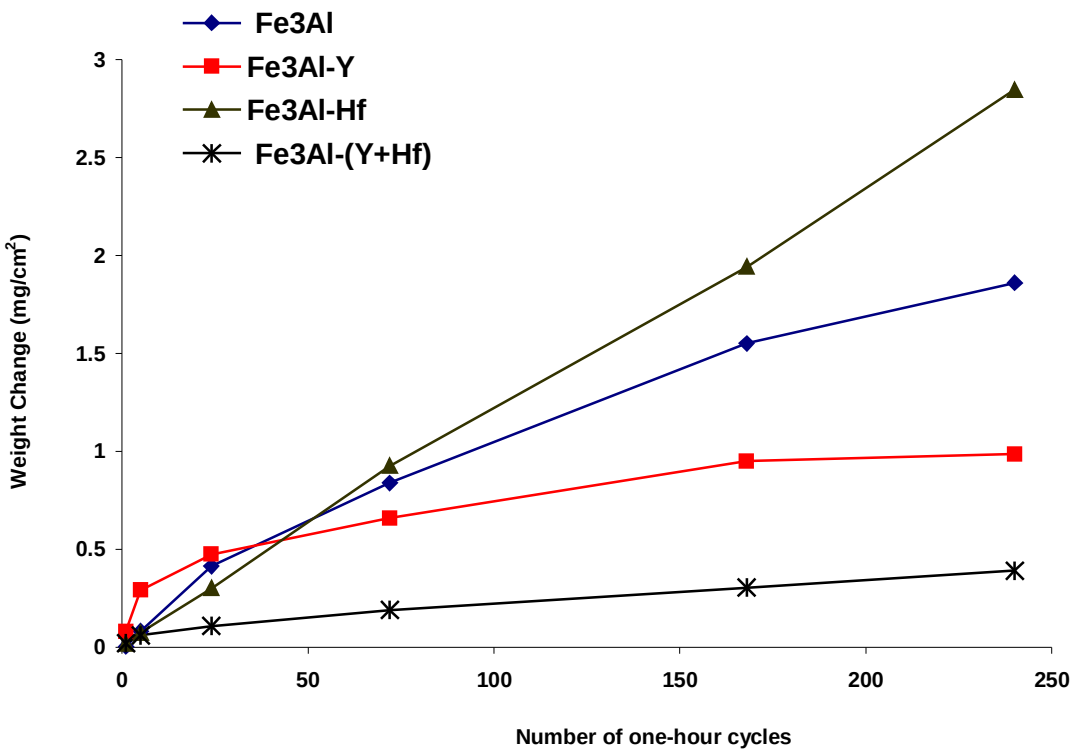

Figure 6-65 Weight gains versus exposure time for the Fe_3Al intermetallic alloys after cyclic air oxidation at 1000ºC for up to 240 one-hour cycles

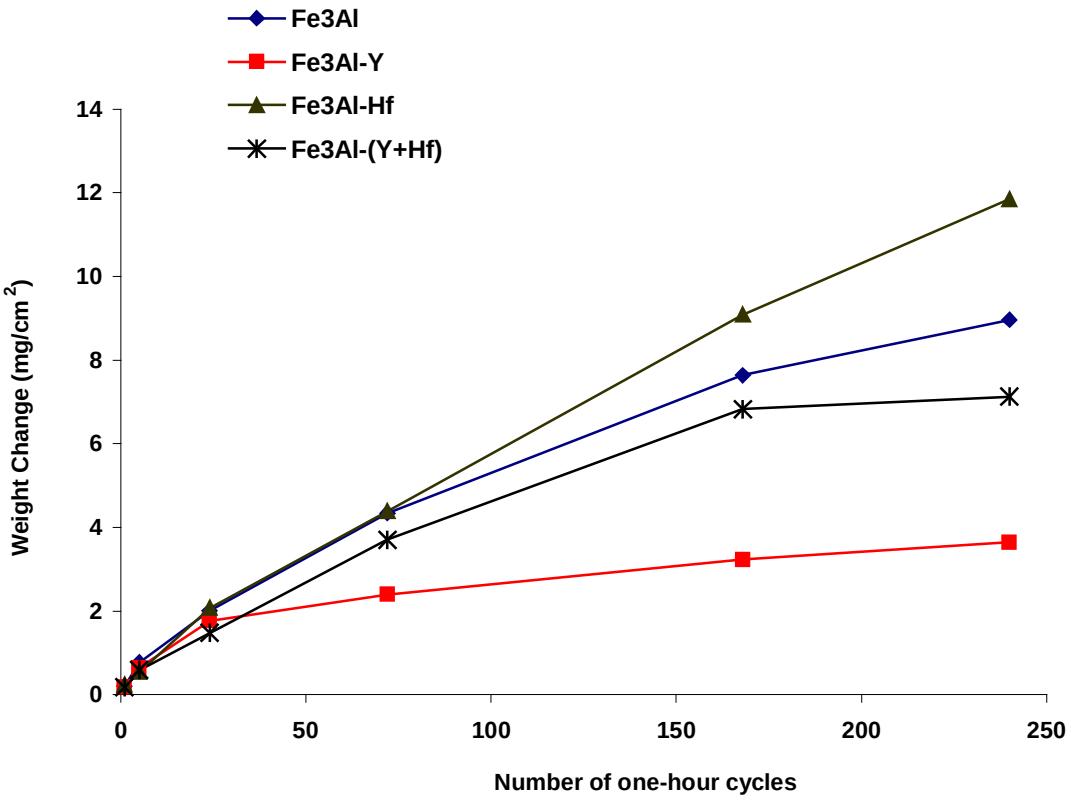

Figure 6-66 Weight gains versus exposure time for the Fe_3Al intermetallic alloys after cyclic air oxidation at 1100ºC for up to 240 one-hour cycles

Scale morphology and composition after cyclic air oxidation of Fe_3Al intermetallic alloys

The microscopic results of the cyclic oxidation are different from those at isothermal conditions for the Fe_3Al intermetallics. Also, the phenomenon of intergranular oxidation is limited under cycling conditions, while the material wastages due to internal oxidation under thermal cycling oxidation were clearly observed. The degree of internal oxidation under cycling condition varies for the same material as the temperature increased. Generally, the scale characteristics of the Y-doped material under cyclic oxidation are different to those in other Fe_3Al alloys. At 900°C the scale formed on undoped Fe_3Al under cycling (240 one-hour cycles) conditions is characterised by convoluted surface – **Figure 6-67**(**a**) – if compared to that formed on other Fe_3Al alloys. Also the scales of Y-containing materials [Fe_3Al-Y and Fe_3Al-(Y+Hf)] are characterised by rough surface morphologies (cigar-like shape – **Figures 6-67**(**b**) and (**c**)) if compared with those of Hf-doped Fe_3Al alloys (**Figure 6-67**(**d**)) after 240 one-hour cycles at 900°C.

At 1000°C and under cycling conditions, the most noticeable effect of the RE to the kinetics and scale morphologies of Fe_3Al intermetallics can be seen. At the early oxidation period (e.g. 5 one-hour cycles) at 1000°C, the scale formed on Fe_3Al without RE is porous but still in contact with the substrate (**Figures 6-68**(**a**)). After 72 one-hour exposure cycles, the oxide of the undoped Fe_3Al alloy severely spalled from the undoped substrate as shown in **Figure 6-68**(**b**). The morphology of the oxide scale formed on the surface of Fe_3Al-Y at 1000°C is found to be different to the scale of undoped Fe_3Al alloy. The scale of Fe_3Al-Y after 5 one-hour cycles at 1000°C is very adherent to the substrate (**Figures 6-69**(**a**) and (**b**)) and most of the scale remains in contact with the alloy. Increasing the number of cycles (240 cycles), the scale thickness especially, at the oxide grain boundaries – **Figures 6-69**(**c**)

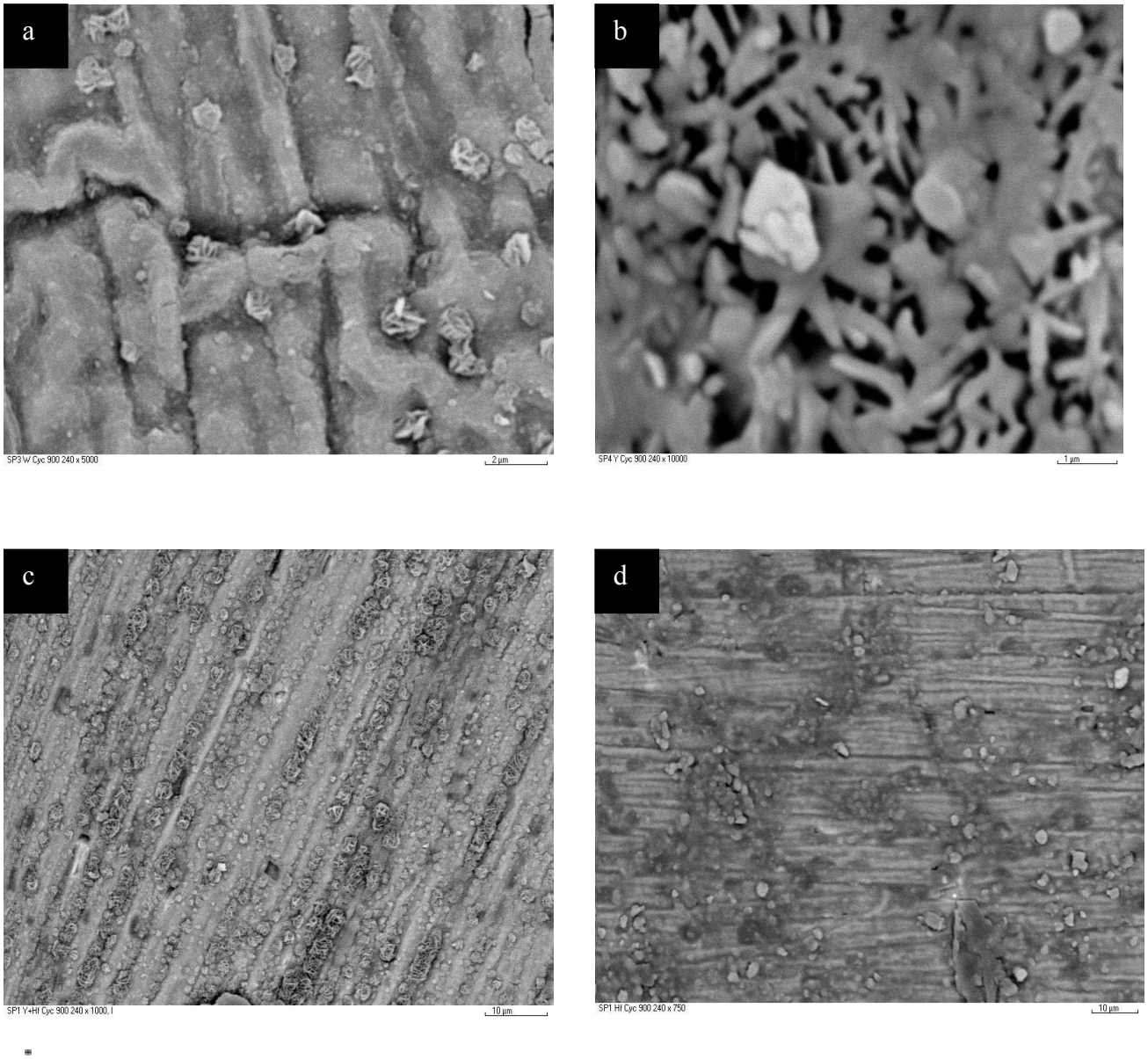

Figure 6-67 Back scattered SEM micrographs of (**a**) Fe_3Al, (**b**) Fe_3Al-Y, (**c**) Fe_3Al-(Y+Hf) and (**d**) Fe_3Al-Hf intermetallic alloys after cyclic air oxidation at 900ºC for 240h

(**a**)

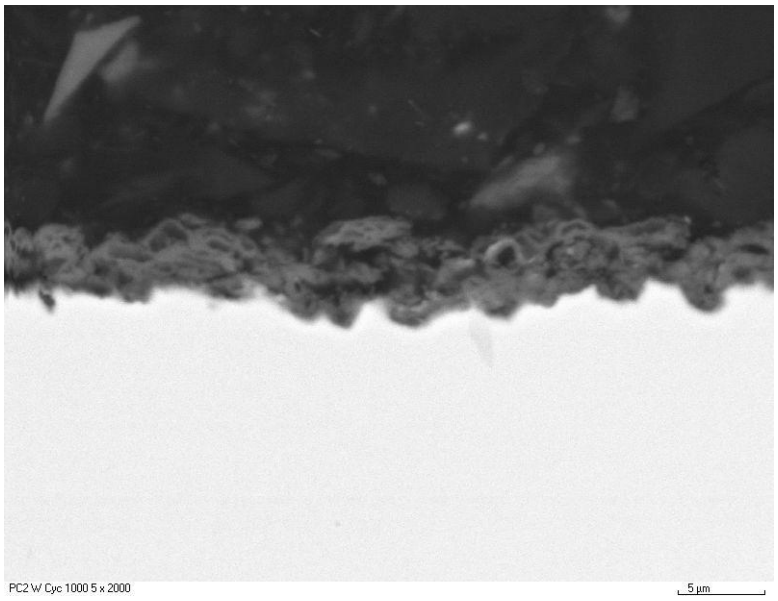

(**b**)

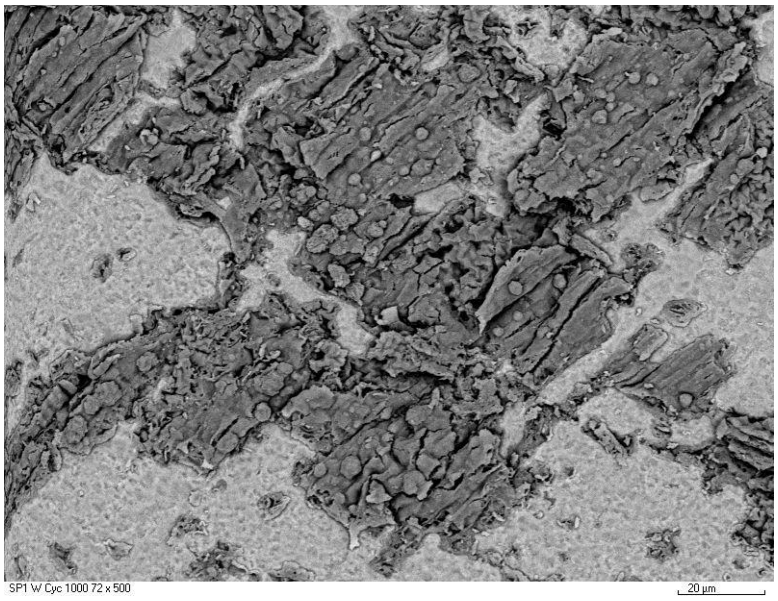

Figure 6-68 Back scattered SEM micrographs of Fe_3Al intermetallic alloy after cyclic air oxidation at 1000ºC (**a**) for 5h and (**b**) for 72h

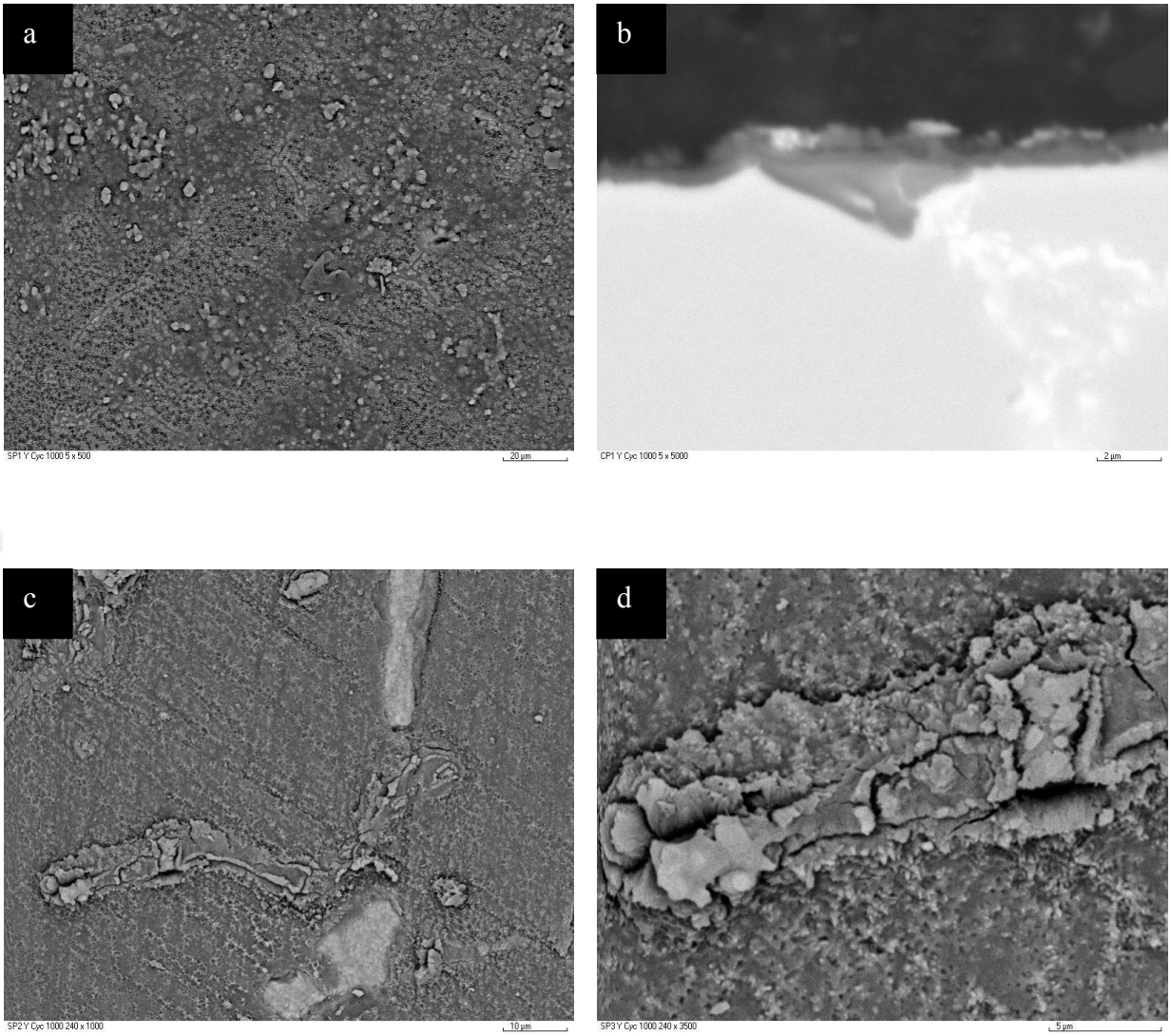

Figure 6-69 Back scattered SEM micrographs of Fe_3Al-Yintermetallic alloy after cyclic air oxidation at 1000ºC (**a** and **b**) for 5h, (**c** and **d**) for 240h

and (**d**)) – of Fe_3Al-Y alloy increased and eventually the oxide ridges cracked and small areas of the oxide had spalled. Generally, the scales on the Fe_3Al-Y were less convoluted than those formed on the undoped Fe_3Al. Under cycling conditions at 1000°C, the scales formed on Fe_3Al-Hf were relatively non-protective and showed formation of oxide pegs even after just 5 one-hour cycles (**Figures 6-70**(**a**)). The depth and width of the oxide pegs increased rapidly with increase of exposure time (168 cycles) as shown in **Figures 6-70**(**b**) and the scales became relatively thick. Surprisingly, although the scale of Hf doped Fe_3Al alloy was thick, most of the scale remained in contact with the substrate. The intermetallic alloy doped with both Y and Hf [Fe_3Al-(Y+Hf)] at 1000°C showed the best response among the Fe_3Al experimental materials in terms of the scale adhesion under cycling conditions. The scale of Fe_3Al-(Y+Hf) after 5 one-hour cycles was very thin, almost flat and adherent to the substrate and no sign of intergranular or internal oxidation was observed (**Figure 6-70**(**c**). After 240 one-hour cycles, the scale of Fe_3Al-(Y+Hf) became thicker and very convoluted (**Figure 6-70**(**d**)). Higher magnification showed that the convoluted scale of Fe_3Al-(Y+Hf) alloy seriously cracked along the oxide ridges during cooling (**Figure 6-70**(**e**)).

At 1100°C, the scale of undoped and Hf-doped Fe_3Al became thick and spall easily from their substrates especially after long exposure time (cycles). For example, after the first 5 one-hour cycles, the scale of the undoped Fe_3Al alloys was relatively thick and multi-layered **Figures 6-71**(**a**). As the number of cycles increased, the scale of the undoped Fe_3Al material suffered severe spallation and the substrate surface also became highly convoluted (**Figure 6-71**(**b**)). The external scale of Y- and Hf-containing materials remains very thin for the first 5 one-hour cycles, consisting of single layer. Increasing the exposure time to 72 cycles, the external scales of Y and Y+Hf alloys were non-protective (**Figure 6-72**(**a**)

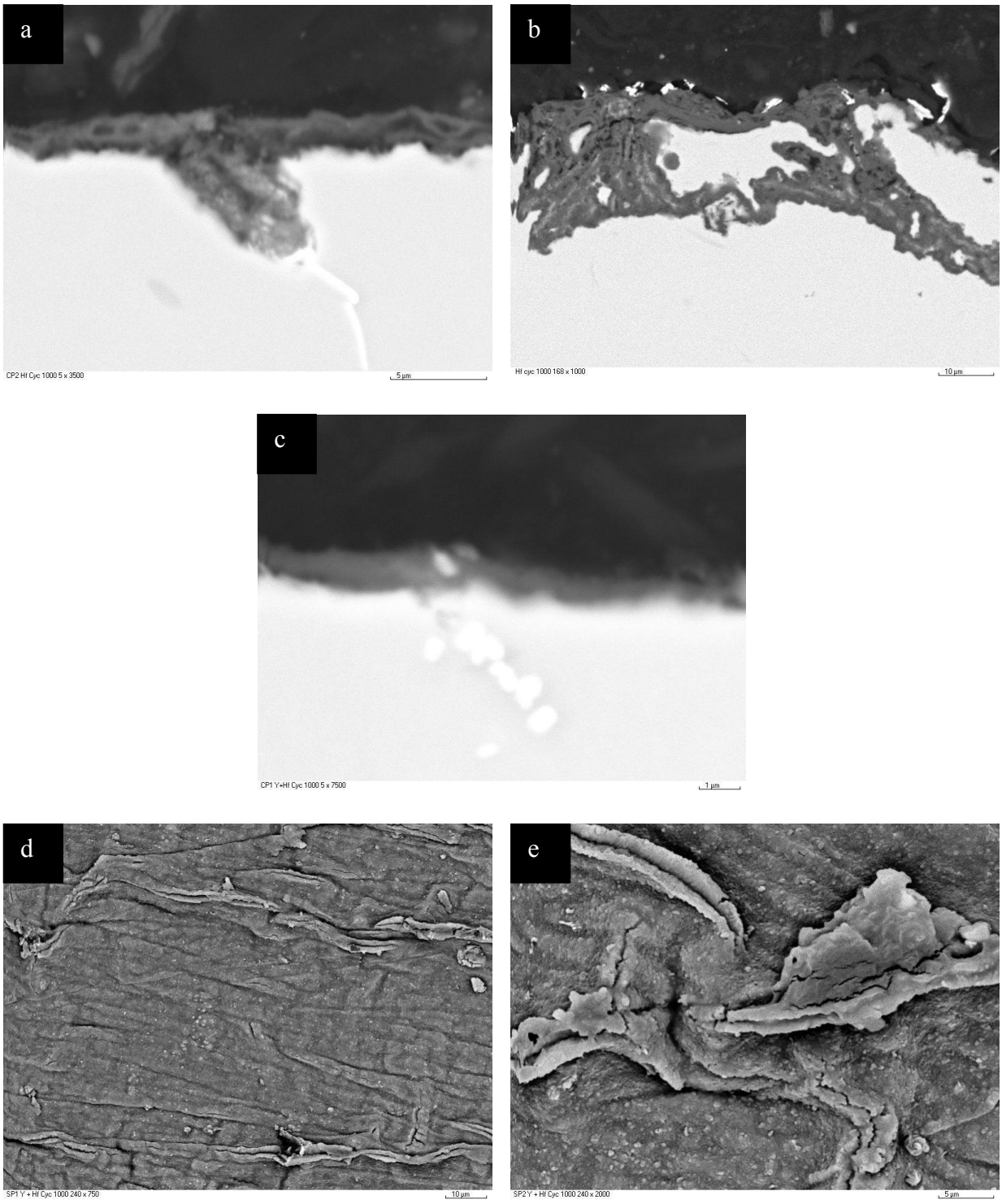

Figure 6-70 Back scattered SEM micrographs after cyclic air oxidation at 1000ºC of (**a**) Fe_3Al-Hf for 5h, (**b**) Fe_3Al-Hf for 168h, (**c**) Fe_3Al-(Y+Hf) for 5h, and (**d** and **e**) Fe_3Al-(Y+Hf) for 240h

(**a**)

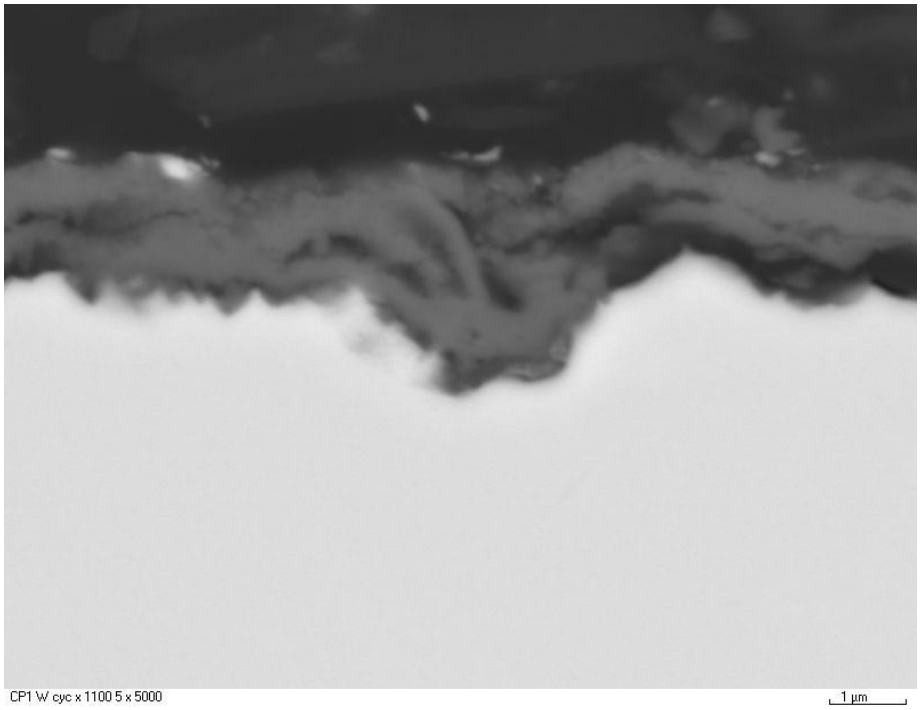

(**b**)

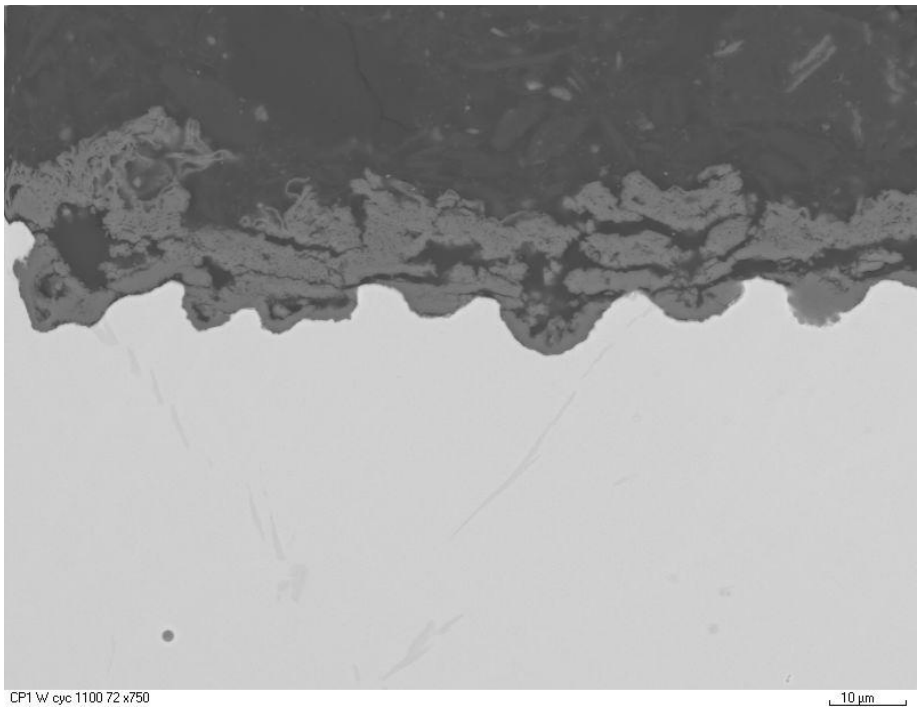

Figure 6-71 Back scattered SEM micrographs of Fe_3Al intermetallic alloy after cyclic air oxidation at 1000ºC (**a**) for 5h and (**b**) for 72h

and (**b**)) and the scale severely spalled. Careful examination to the external scale of the Fe_3Al-Y revealed that spallation of the scale starts at the interface of the intergranular and external scales (at the oxide ridges – **Figure 6-72**(**c**)). Under same cycling conditions (after 72 cycles at 1100ºC), the scale of Hf-doped Fe_3Al materials was very thick, full of cavities and showed large oxide pegs (**Figure 6-72**(**d**)) especially in places where Hf oxide is expected to exist. After further increase of the number of cycles to 240 one-hour cycles at 1100ºC, the scales of all Fe_3Al alloys became non-protective and spalled easily from their substrates. **Figure 6-73**(**a**) showed severe material losses of undoped Fe_3Al alloy, also the alloy with Hf suffered very deep oxide penetration (oxide pegs – **Figure 6-73**(**b**)). However, the scale of Y-containing alloys [Fe_3Al-Y and Fe_3Al-(Y+Hf)], showed sever intergranular attack (**Figure 6-73**(**c**) and (**d**)) as well as massive damage to their external scales (**Figure 6-73**(**e**) and (**f**)) respectively.

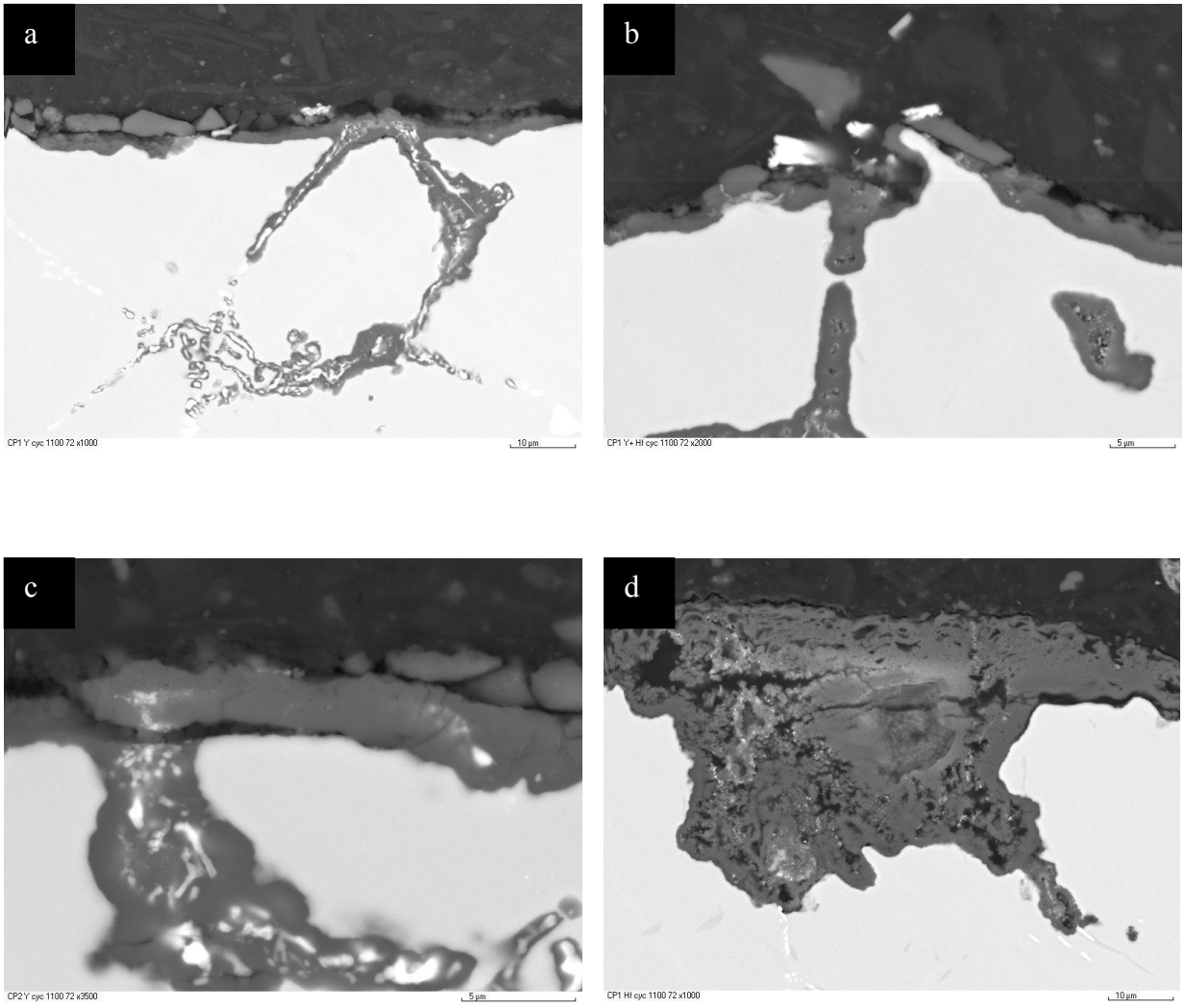

Figure 6-72 Back scattered SEM micrographs of (**a** and **c**) Fe_3Al-Y, (**b**) Fe_3Al-(Y+Hf) and (**d**) Fe_3Al-Hf intermetallic alloys after cyclic air oxidation at 1100ºC for 72h

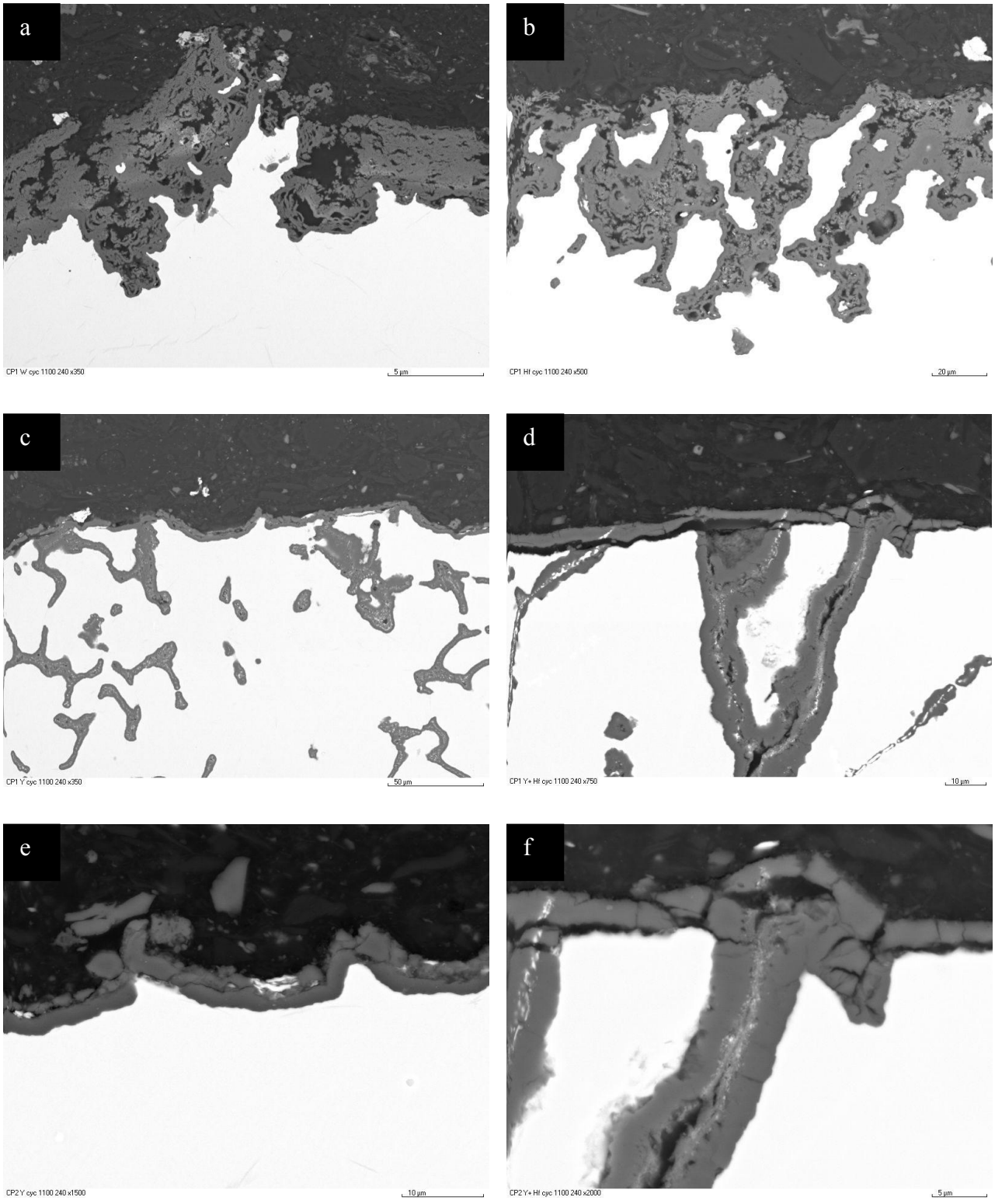

Figure 6-73 Back scattered SEM micrographs of Fe_3Al intermetallic alloys after cyclic air oxidation at 1100ºC for 240h

CHAPTER SEVEN

DISCUSSION OF RESULTS

CHAPTER SEVEN

7.0 DISCUSSION OF RESULTS

7.1 Oxidation of Ti-46.7Al-1.9W-0.5Si Intermetallic Alloy

7.1.1 Introduction

From the results presented in **Chapter 6**, oxidation of Ti-46.7Al-1.9W-0.5Si alloy in air led to titanium nitride formation beneath the scale, whilst under the same exposure conditions in Ar-20%O_2 (free of other impurities), different scale morphologies – no nitridation – and kinetic data were obtained. The differences are attributed to the nitrogen effect(s). A few observations in the literature indicated that the nitridation could have beneficial effect with regard to protective Al_2O_3 formation at the scale/alloy interface. However, others (refer to **Section 3.2.3**) concluded it accelerates the oxidation rate of TiAl alloys. With the vast number of the corrosion studies on titanium aluminides, no publication could be found in the open literature in which a model has been proposed even for the effects of nitrogen on the oxidation behaviour of titanium aluminides and γ-TiAl in particular. The nitrogen effects are not yet clearly understood. However, in the present investigation, detrimental effects of nitrogen on the oxidation behaviour of Ti-46.7Al-1.9W-0.5Si alloy were clearly noticed in both scale properties and kinetics of Ti-46.7Al-1.9W-0.5Si alloy oxidation as will be discussed and modelled in the following section.

After exposure of Ti-Al alloy of high aluminium content in oxygen-containing environments (free from other impurities – including nitrogen) at high temperature, it is natural at a first glance to predict the formation of a protective alumina layer. However, protective alumina was not observed in many studies. Very little published work has been done regarding the effect of oxygen partial pressure on the oxidation behaviour of Ti-Al

systems. However, large disagreement between authors (refer to **Section 3.2.3** was reported on the mechanism of scale formation in relation to the partial pressures of oxygen in the reactive atmosphere. Failure of Ti-Al alloys to form protective Al_2O_3 was attributed to the similarity in the affinity of Ti and Al for oxygen. The situation is far more complex than given by the simple thermodynamic relations between the reacting species of the alloy with the surrounding atmosphere. In the present work, scaling processes in Ti-46.7Al-1.9W-0.5Si alloy at various oxygen partial pressures have been studied not only as a function of oxygen partial pressure but also in an environment of (Ar-20%O_2), where nitrogen was eliminated keeping oxygen partial pressure in the reactive atmosphere same as in air, bearing in mind high purity of Ar-O_2 gas mixtures have been used.

7.1.2 Effect of Nitrogen

In order to predict and understand the scaling process of the materials under investigation, it is considered necessary to carry out some basic thermodynamic calculations using available thermodynamic data. In this study, the minimum activities of Ti and Al required to form TiO_2 and A_2O_3 can be calculated at the known oxygen partial pressure (0.2 x 10^5 Pa) and experimental temperatures (750, 850 and 950^{o}C). The standard free energies of formation for TiO_2 and Al_2O_3 [**296**] are described as follows (J/mole):

$$\Delta G^{o}_{T,TiO_2} = -910000 + 173T \quad \text{.....(30)}$$

$$\Delta G^{o}_{T,Al_2O_3} = -1676000 + 320T \quad \text{.....(31)}$$

where T is the experimental temperature in Kelvin. Our calculations for the Ti-46.7Al-1.9W-0.5Si alloy indicated that the Ti activity in the alloy should be slightly higher than the Al activity at the three temperatures (750, 850 and 950ºC) as summarised in **Table 7.1**.

Therefore, it is concluded that TiO_2 should be the favoured product when the alloy was exposed to both air and Ar-20%O_2 atmospheres.

	750°C	**850°C**	**950°C**
$\mathbf{a}_{Ti}$	$1.23x10^{-34}$	$8.01x10^{-31}$	$1.23x10^{-27}$
$\mathbf{a}_{Al}$	$1.86x10^{-37}$	$2.55x10^{-33}$	$7.38x10^{-30}$

Table 7.1 The minimum activities of Ti and Al to form TiO_2 and Al_2O_3 in 0.2 atmosphere of oxygen partial pressure at 750, 850 and 950°C.

A layer of discontinuous TiO_2 at the early stages of oxidation was observed in this study. This can be attributed to the nature of the two-phase microstructure, which implies that the activities of Ti and Al preventing TiO_2 to form in certain areas. When the Ti-46.7Al-1.9W-0.5Si alloy is exposed to air at the experimental temperatures favouring the formation of TiO_2, that is, the following reaction occurs:

$$Ti_{(s)} + O_{2\,(g)} \rightarrow TiO_{2\,(s)} \quad \text{.....(32)}$$

The formation of TiO_2 would change the balance of activities of Ti and Al and oxygen partial pressure between TiO_2 and the substrate. The reduced activity of Ti and the decreased partial pressure of oxygen at this interface, the formation of Al_2O_3 became possible, i.e.

$$2Al_{(s)} + 3/2\ O_{2\,(g)} \rightarrow Al_2O_{3\,(s)} \quad \text{.....(33)}$$

The development of an Al_2O_3 layer leads to the formation of a Ti-enriched zone beneath the Al_2O_3 layer. At the same time nitrogen migrates through the Al_2O_3 thin layer

to the Ti-enriched zone from the external atmosphere (air), which creates a favourable situation for the following reaction to take place:

$$Ti_{(s)} + 1/2\ N_{2\,(g)} \rightarrow TiN_{(s)} \quad \text{.....(34)}$$

Thus a TiN layer develops beneath the Al_2O_3 layer. In the mean time oxygen species also diffuse inward to the interface between the Al_2O_3 layer and TiN layer and there builds up the oxygen partial pressure. When the oxygen partial pressure reaches a certain level, TiN becomes unstable at the Al_2O_3/TiN interface and decomposes, i.e.

$$TiN_{(s)} + 1/2\ O_{2\,(g)} \rightarrow TiO_{2\,(s)} + 1/2\ N_{2\,(g)} \quad \text{.....(35)}$$

Nitrogen is released and migrates inwards via the TiN layer. The nitrogen partial pressure gradually increases at the TiN/substrate interface and the nitrogen species meets titanium from the substrate and **reaction** (**34**) takes place again. This gives rise to the formation of a titanium-depleted zone beneath the TiN layer, which is demonstrated by the existence of a $TiAl_2$ band beneath the TiN layer. The oxidation mechanisms of Ti-46.7Al-1.9W-0.5Si alloy in air are schematically described in **Figure 7-1**. It is apparent that the thickness of the TiO_2 layer increases with exposure time. So does the thickness of the TiN layer as nitrogen migrates inwards from the external environment. However it is not clear why AlN did not develop between the TiN and $TiAl_2$ band, as the affinities of Al and Ti for nitrogen are very close [**296**]. This is probably due to the faster self-diffusion of Ti in the TiAl substrate than that of Al especially at lower temperatures (< 1000ºC – see **Table 7-2**). Thus, TiN became the kinetically favoured product.

T (°C)	D_{Ti} (m^2/s)	D_{Al} (m^2/s)
900	1.18×10^{-17}	2.40×10^{-18}
1000	8.87×10^{-17}	3.52×10^{-17}
1100	2.17×10^{-16}	1.69×10^{-16}

Table 7.2 Titanium and aluminium self-diffusion coefficients (**D**) in TiAl at various temperatures [**123**]

In the Ar-20%O_2 atmosphere – the same oxygen partial pressure as in air ($pO_2 \sim 0.2 \times 10^5$ Pa) – also favoured TiO_2 formation on the surface of Ti-46.7Al-1.9W-0.5Si alloy when it is exposed to the environment. Similarly as in air, the formation of TiO_2 leads to changes in the activities of Ti and Al and oxygen partial pressure between TiO_2 and the substrate. Then an Al_2O_3 layer develops. Also, a Ti-enriched zone is created between the Al_2O_3 layer and substrate. Some of titanium further diffuses outwards through the Al_2O_3 layer to the specimen surface and reacts with oxygen in the atmosphere forming TiO_2. At the same time, oxygen diffuses inwards to the Al_2O_3/substrate interface. When the oxygen partial pressure reaches a certain level, **reaction** (**32**) occurs and a TiO_2 layer develops. The formation of the TiO_2 layer creates a circumstance where Al_2O_3 becomes the favourable corrosion product from the reaction of ingressing oxygen and Al_2O_3 and TiO_2 layers. The formation of the second Al_2O_3 layer again would deplete Al in the substrate and create a Ti_3Al band. The oxidation mechanisms of Ti-46.7Al-1.9W-0.5Si alloy in the Ar-O_2 environments are schematically illustrated in **Figure 7-2**.

The experimental results show that the oxidation rate of Ti-46.7Al-1.9W-0.5Si alloy is higher in air than in Ar-20%O_2 environment at all three experimental temperatures. For example, the oxidation parabolic rate constant in air at 950°C ($Kp = 3.7 \times 10^{-12}$ $g^2/cm^4/s$) is one order of magnitude higher than in Ar-20%O_2 ($Kp = 3.8 \times 10^{-13}$ $g^2/cm^4/s$). It is apparent that the continuous layer of Al_2O_3 may be the control step for the whole scaling

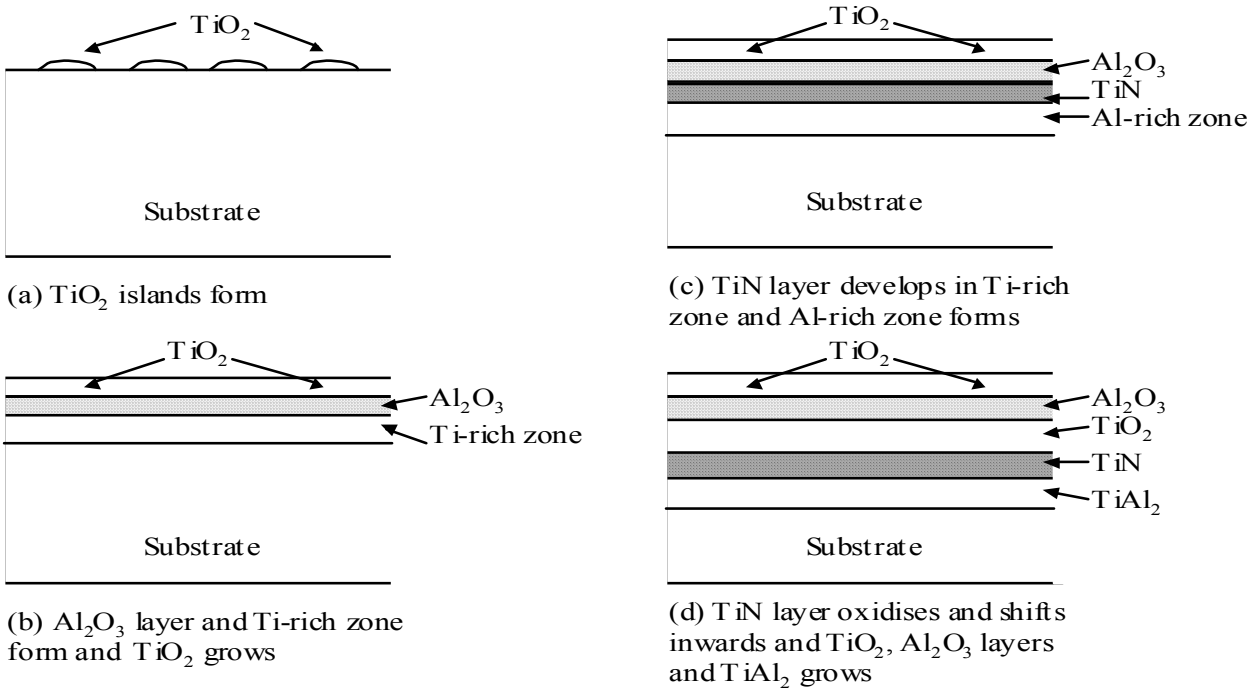

Figure 7-1 Stages of Ti-46.7Al-1.9W-0.5Si alloy oxidation in air atmosphere

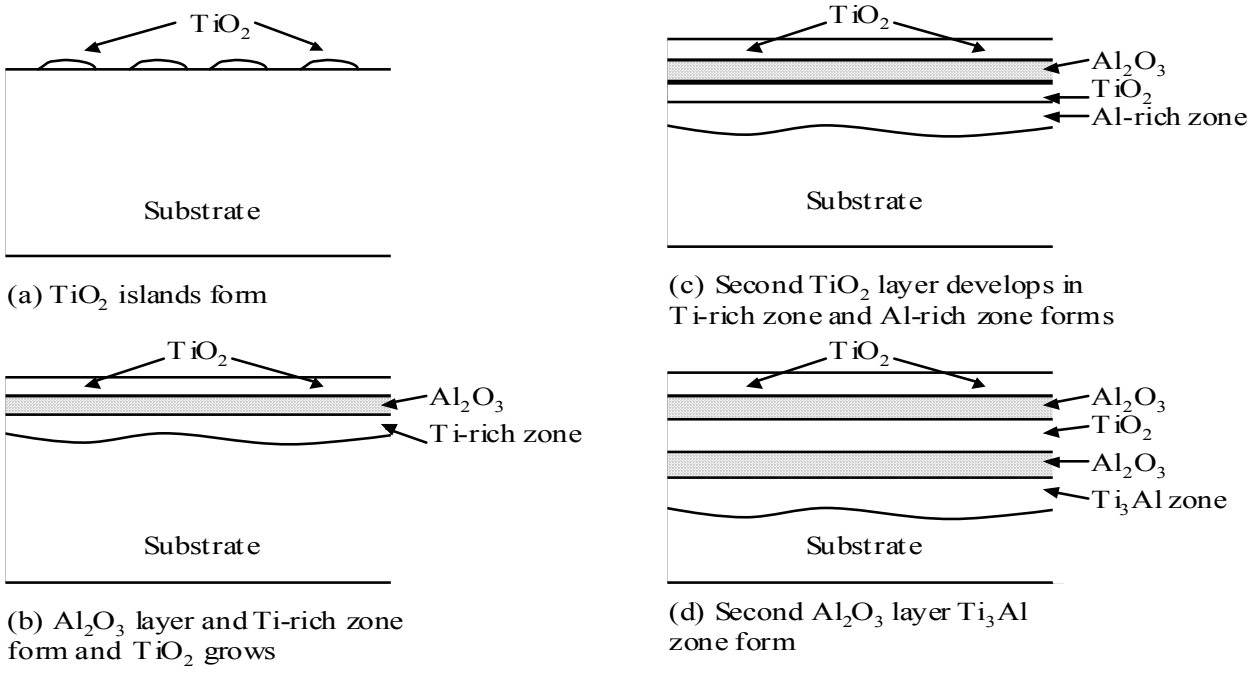

Figure 7-2 Stages of Ti-46.7Al-1.9W-0.5Si alloy oxidation in Ar-O_2 atmospheres

processes in both air and Ar-20%O_2. The thickness of the Al_2O_3 layer played an important role. It is noticed that two continuous layers of Al_2O_3 developed on the alloy in Ar-20%O_2, whilst only one Al_2O_3 layer was formed in air. The thickness of all Al_2O_3 layers was similar. Thus the total thickness for the two Al_2O_3 layers in Ar-20%O_2 is nearly doubled compared to that in air. According to Fick's first law of diffusion:

$$J = -D\left(\frac{\partial c}{\partial x}\right) \quad \text{.....(36)}$$

where, J is the flux of reactant species, D is the diffusion coefficient, c is the concentration or partial pressure and x is the thickness of oxide layer. At a certain moment of diffusion, **equation** (**36**) becomes:

$$J = -D\frac{c}{x} \quad \text{.....(37)}$$

This indicates that the flux J, is inversely proportional to the thickness of the barrier oxide layer. As the Al_2O_3 layer is the key step of the whole scaling process – an increase in thickness of Al_2O_3 "barrier" would lead to a decrease in the oxidation rate. The formation of the two-layers of Al_2O_3 would also bring about another advantage, that is, the reduction of the growth and thermal stresses during the cooling cycle. The weight gains of the Ti-46.7Al-1.9W-0.5Si alloy in air are actually contributed from the formation of the oxides (TiO_2 and Al_2O_3) and nitride (TiN). It is assumed that the inward diffusion of oxygen and nitrogen are not mutually influenced. Thus the formation of TiN in air simply contributes to the total weight gains.

It is found that spallation of the oxide scale by the wedging process above the TiN layer occurred during the cooling period after air oxidation. This must be caused by thermal stresses generated in the scale by the mismatch of thermal expansion coefficients between the TiN and TiO_2 layers. According to Evans [**241**], the critical temperature drop ΔT_c to initiate spallation is:

$$\Delta T_c = \left(\frac{\gamma_F}{xE_{OX}(\Delta\alpha)^2(1-\upsilon_{OX})} \right)^2 \quad \text{.....(38)}$$

where γ_F is the fracture energy per unit area of interface, x is the thickness of oxide layer, $\Delta\alpha$ is the difference of thermal expansion coefficients and υ_{OX} is the Poisson's ratio of the oxide. In the present situation this derivation has been considered in relation to Evans fracture of the oxide/nitride interface. However, as wedging spallation happened, it is also necessary to consider the development of shear cracks through the oxide layer since these needs first to be present before wedging can proceed. Evans [**241**] also gave the critical temperature drop ΔT_s to produce shear cracks in a four-side array of side length λ as:

$$\Delta T_s = \left(\frac{4\gamma_o}{(1-\upsilon_{ox})(E_{ox}\lambda(\Delta\alpha)^2} \right)^{1/2} \quad \text{.....(39)}$$

where γ_o is the surface energy of the oxide. In both cases, the critical temperature drops are strongly related to the mismatch of the thermal expansion coefficients ($\Delta\alpha$). The ΔT_c is proportional to the reciprocal of $\Delta\alpha$, and particularly, ΔT_s is inversely proportional to $(\Delta\alpha)^2$. The relevant data of thermal expansion coefficients for the oxides and TiN are given in **Table 7.3**. It is apparent that the mismatch of thermal expansion coefficients between TiN and TiO_2 (in the case of air oxidation) are much more severe than those between TiO_2 and Al_2O_3 (in the case of Ar-20%O_2 oxidation).

	TiN	**TiO_2**	**Al_2O_3**	**TiAl**	**$TiAl_3$**
α x 10^{-6} (1/T)	9.35	7.14	8.5	11.43	10.65

Table 7.3 Data for linear thermal expansion coefficients of various compounds [**241**]

Therefore the critical temperature drops in air oxidation would be much smaller than those in the Ar-20%O_2 atmosphere. It was difficult to calculate the exact values of ΔT_c and ΔT_s

owing to the lack of the relevant data. Nevertheless these descriptions do help to explain qualitatively why spallation of an oxide scale by the wedging process happens in air oxidation. In addition, severe segregation of vacancies and the formation of large voids are occurred at the TiO_2/TiN interface, as illustrated in **Figures 6-10**. These voids would reduce the cohesion between TiO_2 and TiN and obviously this would enhance spallation by the wedging process as demonstrated in **Figure 6-19**(**a**).

7.1.3 Effect of Oxygen Partial Pressure

In general the scale microstructures and the kinetics of scale formation in all the three different partial pressures of oxygen (0.05, 0.2 and 0.8) x 10^5 Pa are different. Comparison of the present oxidation results of the Ti-46.7Al-1.9W-0.5Si alloy in different oxygen partial pressures revealed the differences in the scale properties (see **Figures 6-34** and **6-35**) and kinetics (refer to **Figures 6-20** to **6-22**) at the three atmospheres. Such differences can be understood, to some extent, by considering the defect structures in the scale, which are influenced by the oxygen partial pressures in the reactive atmospheres. Previous studies on the TiO_2 and Al_2O_3 defect structures and the solubility of these phases in each other and the effect of oxygen partial pressure has been reported (refer to **Section 3.2.3**). These studies concluded that the transport processes in TiO_2 are more rapid than in Al_2O_3 due to the defect structure of TiO_2. Also, the solubility of Al_2O_3 and TiO_2 decreased as the partial pressure of oxygen increased in the environment. These findings are consistent with the obtained results in this study and will be used for the interpretation of our experimental observations.

For illustration, the cross-sectional morphology (**Figure 7-3**) of the scale formed on Ti-46.7Al-1.9W-0.5Si alloy at 950ºC after 240h exposure in Ar-5%O_2, Ar-20%O_2 and Ar-80%O_2 is employed to explain the effect of oxygen partial pressure on the oxidation

behaviour of Ti-46.7Al-1.9W-0.5Si alloy. After oxidation of Ti-46.7Al-1.9W-0.5Si alloy at 950ºC in all Ar-O_2 atmospheres proceeds, a multi-layered scale of alternating TiO_2 and Al_2O_3 is formed. The composition of the inner layer of the scale was different at various oxygen partial pressures in the oxidising atmosphere as illustrated in **Figure 7-3**. In Ar-5%O_2, the inner layer consisted predominantly of TiO_2 with some Al_2O_3 (**Figure 7-3**(**a**)). As the oxygen content increased in the reactive atmosphere (Ar-20%O_2), the Al_2O_3 content in the inner layer of the scale increased at the expenses of TiO_2 (**Figure 7-3**(**b**)). Further increase of oxygen in the Ar-O_2 gas mixture (Ar-80%O_2), led to the formation of oxide scale consisting of mostly Al_2O_3 with discontinuous TiO_2 (**Figure 7-3**(**c**)). The gradual increase of Al_2O_3 in the scale with the increase of oxygen partial pressure in the reactive atmosphere is due to the following reasons: (i) the lower solubility of Al_2O_3 in TiO_2 at higher oxygen partial pressures in the reactive atmosphere, (ii) lower defect structure in Al_2O_3 if compared to that in TiO_2. The consequences of the Al_2O_3 formation in the scale at higher oxygen partial pressures is that minimum possible flux of oxygen vacancies in the scale significantly lower than that at lower oxygen partial pressures. In fact, the process of Al_2O_3 barrier formation at various oxygen contents in the environment has been reported by Becker *et. al.* [**8**] and the present experimental observations is consistent with their schematic model (refer to **Figure 3-9** and see **Figure 7-3**). Furthermore, the process of Al_2O_3 dissociation reported in the same study of Becker *et. al.* [**8**] explain the existence of porosity at the outer part of the inner layer at low oxygen content in the atmosphere (e.g. Ar-5%O_2 – **Figure 7-3**(**a**)). The dissociation of Al_2O_3 – at higher oxygen partial pressures (Ar-20%O_2 and Ar-80%O_2) in the scale probably changes the defect concentration in TiO_2.

(**a**)

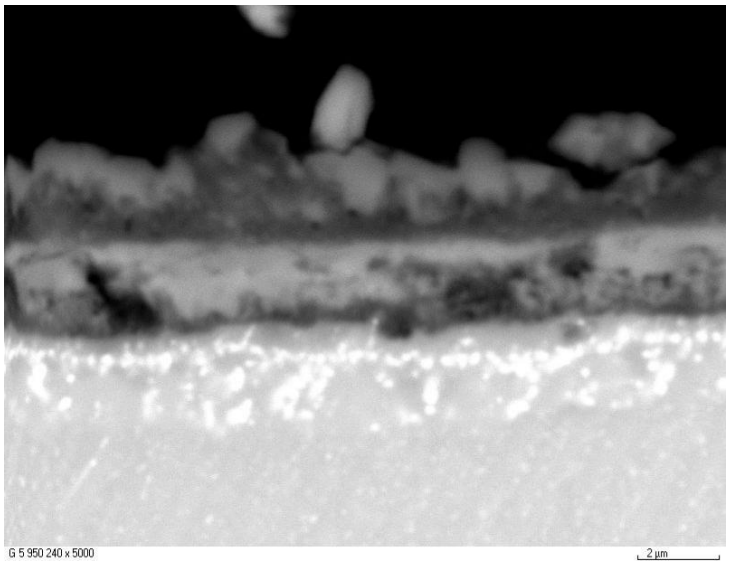

(**b**)

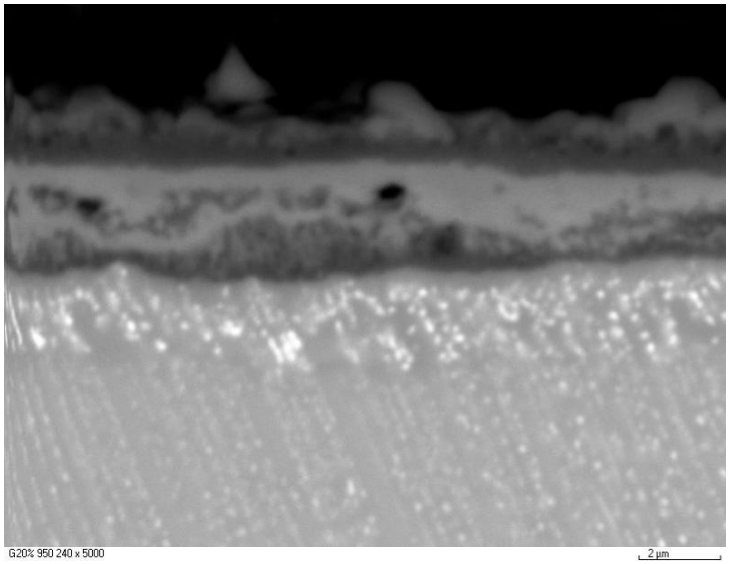

(**c**)

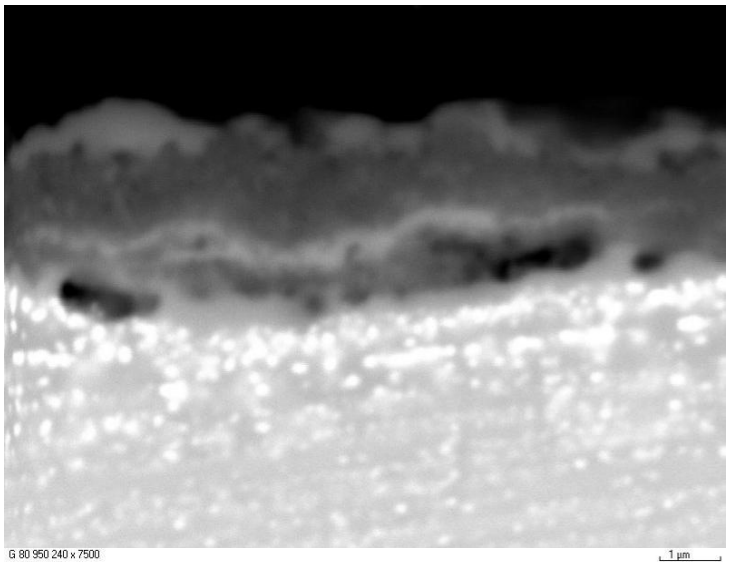

Figure 7-3 SEM micrographs of Ti-46.7Al-1.9W-0.5Si alloy after oxidation at 950ºC for 240h in (**a**) Ar-5%O_2, (**b**) Ar-20%O_2 and (**c**) Ar-80%O_2

7.1.4 Comments on the role of W and Si on the Oxidation of Ti-46.7Al-1.9W-0.5Si Alloy

The as received Ti-46.7Al-1.9W-0.5Si alloy showed the presence of WSi_2 (refer to **Figure 6-2**). However, the distribution of this compound was not uniform in the alloy. From the amounts of W and Si, it can be concluded that the formation of WSi_2 could leave some free W in the alloy probably as solid solutions in some of the phases. Following oxidation W-enrichment at the alloy/scale interface was observed. It is speculated that W probably played an indirect role in the processes of oxidation by influencing (i) the activity of Ti and Al, (ii) the diffusion of Al.

7.2 Sulphidation/Oxidation of Coated and Un-coated Ti- 46.7Al-1.9W-0.5Si Intermetallic Alloy in $H_2/H_2S/H_2O$ Gas Mixture

7.2.1 Introduction

The present results indicate that the uncoated Ti-46.7Al-1.9W-0.5Si alloy performed reasonably well (Kp ~ 6 x 10^{-11} $g^2/cm^4/s$) in the environment of low oxygen and high sulphur partial pressures at 850^{o}C. The employment of single and double layer coatings further improved the high temperature sulphidation/oxidation corrosion resistance of the alloy. The interpretation of these results can be understood in terms of the mechanisms and theories relating to the processes of scale development in these coated and uncoated samples.

7.2.2 Scaling of Ti-46.7Al-1.9W-0.5Si Intermetallic Alloy in $H_2/H_2S/H_2O$ Gas Mixture

The parabolic rate reaction (Kp ~ 6 x 10^{-11} $g^2/cm^4/s$) of uncoated Ti-46.7Al-1.9W-0.5Si alloy in the environment of $H_2/H_2S/H_2O$ with pS_2 ~ 6.8 x 10^{-1} Pa and pO_2 1.2 x10^{-15} Pa at 850^{o}C indicate that the corrosion process was controlled by diffusion of the substrate

elements and of oxygen and sulphur species from the atmosphere. The scaling kinetics of the various layers also followed a parabolic rate law; the parabolic rate constants for TiO_2 and TiS layer were $6x10^{-16}$ and $3x10^{-16}$ m^2/s respectively. When the Ti-46.7Al-1.9W-0.5Si alloy exposed to the environment of $H_2/H_2S/H_2O$ at 850°C, **reactions** (**32**) and (**33**) was also likely to occur. For both reactions, the values of standard free energies of formation (ΔG_T^o, Joule/mole) for TiO_2 and Al_2O_3 with temperature (T in Kelvin) can be obtained from **equations** (**30**) and (**31**) respectively.

Also,

$$\Delta G_{32}^o = -RT \ln K_{32} = -RT \ln \frac{a_{TiO_2}}{a_{Ti}.pO_2} \quad \text{..... (40)}$$

$$\Delta G_{33}^o = -RT \ln K_{33} = -RT \ln \frac{a_{Al_2O_3}}{(a_{Al})^2.(pO_2)^{3/2}} \quad \text{.....(41)}$$

where K_{32} and K_{33} are the equilibrium constants for **reactions** (**32**) and (**33**) respectively and R is the gas constant. In the present situation ascribing unit activities to Al_2O_3 and TiO_2, our thermodynamic calculations reveal that the minimum activities of Al and Ti required to form Al_2O_3 and TiO_2 in the environment used (i.e. $pO_2 \sim 1.2 \times 10^{-15}$ Pa) are 2.1×10^{-16} and 4.3×10^{-14} respectively. However, the actual activities of Al and Ti in this alloy are around 7.0×10^{-3} and 1.4×10^{-1}. These results indicate the difficulty, using solely thermodynamic grounds, to decide which oxide formed preferentially on exposure of the alloy to the environment. However, in the present situation the observed formation of TiO_2 at the initial stages of exposure, it is suggested, was decided by the kinetic factors. The temperature dependence of self-diffusivities of Ti and Al are [**297**]:

$$D_{Ti}\ (m^2/s) = 1.5x10^{-6} \exp\ [-250\ (kJ/mol)/RT] \quad \text{..... (42)}$$

$$D_{Al}\ (m^2/s) = 2.1x10^{-2} \exp\ [-360\ (kJ/mol)/RT] \quad \ldots\ldots\ldots\ldots\ldots\ldots\ldots\ldots\ (43)$$

The calculated values for D_{Ti} and D_{Al} are ~ 3.5 x 10^{-18} (m^2/s) and 3.8 x 10^{-19} (m^2/s) at 850°C giving the value of D_{Al} ten times smaller than that of D_{Ti}. Thus, when the Ti-46.7Al-1.9W-0.5Si alloy was exposed to the sulphidising/oxidising environment at 850°C, it was more favourable for TiO_2 to form as Ti diffused faster than Al. The development of TiO_2 led to the depletion of Ti beneath the TiO_2 layer, which promoted the formation of the Al_2O_3 layer by the ingress of oxygen species through the TiO_2 layer. Meanwhile, sulphur species also diffused inward through the layers of TiO_2 and Al_2O_3 and reacted with Ti to form TiS.

It is to be noted here that the scaling processes involved did not allow the development of tungsten sulphide and/or oxide. The lack of WS_2 and WO_2 formation can be explained on the following theoretical basis. The formation of WSi_2 using all Si in the alloy would indicate 0.5 at%Si reacting with 0.25 at%W allowing ~1.65 at%W to remain in the alloy. When W reacts with sulphur and oxygen species, the following reactions may take place:

$$W\ (s) + S_2\ (g) = WS_2\ (s) \quad \ldots\ldots\ldots\ldots\ldots\ldots\ldots\ldots\ (44)$$

$$W\ (s) + O_2\ (g) = WO_2\ (s) \quad \ldots\ldots\ldots\ldots\ldots\ldots\ldots\ldots\ (45)$$

The values of standard free energies (ΔG_T^o, Joule/mole) with temperature (T in Kelvin) can be obtained from the following equations [**296**]:

$$\Delta G_{44,T}^o = -260{,}900 + 96T \quad \ldots\ldots\ldots\ldots\ldots\ldots\ldots\ldots\ (46)$$

$$\Delta G_{45,T}^o = -579{,}484 + 153T \quad \ldots\ldots\ldots\ldots\ldots\ldots\ldots\ldots\ (47)$$

or

$$\Delta G^{o}_{44,T} = -RT \ln K_{44} = -RT \ln \frac{a_{WS_2}}{a_W . pS_2} \quad \text{..... (48)}$$

$$\Delta G^{o}_{45,T} = -RT \ln K_{45} = -RT \ln \frac{a_{WO_2}}{a_W . pO_2} \quad \text{..... (49)}$$

where K_{44} and K_{45} are the equilibrium constants for **reactions** (**44**) and (**45**) respectively. Assuming unity for the activities of both WS_2 and WO_2, then the minimum W activities required to form WS_2 and WO_2 in the atmosphere ($pS_2 \sim 6.8 \times 10^{-1}$ Pa and $pO_2 \sim 1.2 \times 10^{-15}$ Pa) and at reaction temperature (850°C) employed in this project were about 10^{-2} and 7.3 respectively. Therefore the formation WO_2 can be excluded under the employed experimental conditions as the minimum W activity for the formation of WO_2 was greater than unity. It is believed that the sulphur partial pressure beneath the coating was even lower than 6.8×10^{-1} Pa, so that the minimum activity of W required to develop WS_2 would be higher than 10^{-2}. It should also be noticed that the W content was only 1.9at% in the alloy and the presence of WSi_2 would further lower the W activity. Thus the effective W activity would be lower than the value of 10^{-2}, making it difficult for WS_2 to form in the current situation. Therefore when Ti beneath the layers of TiO_2 and Al_2O_3 reacted with sulphur species, W remained in a metallic form. This is verified by the presence of pure W in the TiS layer as confirmed by XRD analysis (refer to **Figure 6-39**(**b**) and (**c**)). The formation of the $TiAl_3$ band resulted from Al-enrichment beneath the TiS layer following faster outward diffusion of Ti. It is apparent that high Al concentration existed closer to the TiS layer and higher Ti concentration closer to the substrate. Thus it would be reasonable for a band of $TiAl_2$ to exist between the $TiAl_3$ layer and TiAl substrate.

7.2.3 Protection of Ti-46.7Al-1.9W-0.5Si Intermetallic Alloy in $H_2/H_2S/H_2O$ Gas Mixture Using Single and Double Layered Coatings

It is suggested that the protectivity of uncoated Ti-46.7Al-1.9W-0.5Si intermetallic alloy against sulphidising/oxidising attack was conferred by the formation of Al_2O_3 and $TiAl_3$ layers. The significant improvement of sulphidation resistance exhibited by the coated samples is indicated by the low weight gain. The coatings remained adherent and compact in general up to an exposure time of 240h. However some coatings suffered localised degradation characterised by the formation of nodular corrosion products. The development of cracks in the AlTiN coating probably from pre-existing defects within the coating or at the coating/substrate interface. These cracks within the coating acted as a rapid diffusion path for the reactant species during the isothermal exposure.

Thus on exposure of the coated Ti-46.7Al-1.9W-0.5Si alloy to the sulphidising/oxidising environment, an Al_2O_3 layer would be formed on the surface of the coating. In the mean time, the cracks would also be formed within the coating caused by thermal stress. The cracks would act as rapid diffusion paths for the ingress of oxygen and sulphur and outward migration of substrate elements. The experimental results confirmed the localised nodular attack. The compositions and phases of these nodules were similar to those formed on uncoated samples, as illustrated in **Figures 6-40** and **6-42**. The nodular shape of the corrosion products stemmed from the diffusion of the reactant species occurring through the cracks. CrN and NbN layers not only acted as diffusion barriers but also were effective in reducing the thermal stresses produced by mismatch between the AlTiN coating and substrate. It was apparent that a similar formation of the cracks also occurred within the double layer coatings producing the nodular corrosion products although the number of nodules formed was less than that on the single (AlTiN) layer coating.

In the case of NbN and AlTiN double layer coating, NbS_2 would form by the inward diffusion of sulphur through the cracks beneath the AlTiN coating. The formed NbS_2 was still an effective diffusion barrier as there is low defect concentrations or defect mobility in this sulphide [**42**]. However for the CrN and AlTiN system, the formed Cr_2S_3 would not be able to effectively stop diffusion of the reactant species [**42**] as it has much higher deviations from stoichiometry, and thereby contain significantly higher defect concentrations than NbS_2. The differential performance of the CrN and NbN diffusion barriers is reflected in the kinetic data (**Figure 6-37**). However, all double layer coatings had superior corrosion resistance to the uncoated specimens.

7.3 Isothermal and Cyclic Air Oxidation of Fe_3Al Intermetallic Alloys

7.3.1 Introduction

The objective of this section is to discuss the effects of adding Y and/or Hf on the oxidation resistance of Fe_3Al alloy under isothermal and cyclic conditions in air. The first part (**Section 7.3.2**) discusses the REE on the scale formation and the variation of scale thickness in both single and combined addition of Y and Hf after isothermal air oxidation of Fe_3Al alloys. The second part (**Section 7.3.3**) discusses the oxide adherence of Fe_3Al alloys (with and without REs) under thermal cycling conditions. The aim of the cycling process is to examine the REE on the degree of adherence between the substrate and the scale. Due to lack of information in the literature, it was found necessary in many instances, to correlate and to compare the isothermal oxidation and the cyclic oxidation results for the same type of alloy. The REE under thermal cycling conditions seems to be more complicated than isothermal exposure due to various reasons as discussed throughout this section.

7.3.2 Effect of Reactive Elements (Y and/or Hf) on Al_2O_3 Oxide Growth after Isothermal Oxidation

No clear interpretation of the REE in this study can be obtained based only on the observed variation of the reaction rate constants of the alloys at a temperature, **Tables 6-4** and **6-5**. For example, the Fe_3Al alloy with Y addition showed the highest oxidation rate constant. However, the external scale thickness of Y-containing alloys [Fe_3Al-Y and Fe_3Al-(Y+Hf)] was found to be about ten times less than that of undoped alloy especially at high temperatures (see **Figures 6-51**(**a**) and **6-57**(**a**). Also the scale adhesion significantly improved by the addition of Y and/or Hf (**Figures 6-54**, and **6-58**. This inconsistency in weight gain, scale thickness and adhesion can be attributed to the formation of intergranular (at the alloy grain boundaries) oxide, which adversely affected the oxidation rates of the alloys. This intergranular attack caused the formation of oxide ridges affecting the external scale adhesion, **Figure 6-62**.

The RE affecting scale characteristics of the doped Fe_3Al alloys were more distinguishable at higher temperature (> 900ºC). At lower temperature (e.g. 900ºC), the comparable weight gains of the doped and undoped alloys failed to indicate clearly the effects of RE. Additionally, at lower temperatures the formation of some transient θ-Al_2O_3 as evidenced by the formation of blade-like morphologies (**Figure 6-48**(**a**), probably masked the RE effect due to its faster growth rate. At 1000°C, little or no transient alumina phases would be expected to form and there were much clearer effects of the RE on the oxidation behaviour of Fe_3Al alloys. The formation of iron oxide at 1000°C was rapidly suppressed due to the faster diffusion of aluminium and oxygen facilitating the development of α-Al_2O_3. Trace peaks of spinel from iron and aluminium oxide at the early exposure time (e.g. 5h) at 1000°C was detected, **Figure 6-52**(**a**). However, after longer exposure time (e.g. 72h), Al_2O_3 was the only oxide detected, **Figure 6-52**(**b**). As the

exposure temperature increased to 1100°C, faster diffusion of aluminium and oxygen ensured more rapid formation of Al_2O_3 even at short exposure time (e.g. 5h).

At present no agreement in the literature regarding the oxidation mechanism of Al_2O_3 The oxidation mechanism of alumina-forming alloys has been characterised by ^{18}O tracer and inert marker experiments. Pint, *et al* [**261**] and Young, *et al* [**257**] in ^{18}O tracer experiments attributed Al_2O_3 scale growth to the outward diffusion of aluminium. However, it is difficult to obtain clear conclusion from most of the inert marker experiments reported in the literature regarding the mechanism of Al_2O_3 growth. For example Young *et al* [**257**] expressed strong doubt on the validity of the marker-type experiments and the marker was found buried within the scale. From our oxidation results, the formation of convoluted scales of the undoped Fe_3Al (**Figure 6-51** (**a**), indicate both the inward diffusion of oxygen and outward diffusion of aluminium to form Al_2O_3. However, the flat surface of the Y-contaning materials scale after oxidation suggested the Al_2O_3 scale (**Figure 6-57**) growth was mainly by the inward diffusion of oxygen. It should be pointed out that the scale corrugation and flatness of the Al_2O_3 scale for the same materials (doped or undoped) are also influenced by the experimental conditions especially the exposure temperature

The segregation of RE (especially Y) at the alloy grain boundaries (**Figure 6-59**), is believed to have acted as oxygen getter leading to aluminium oxidation. The scale thickness of the Y-containing alloys was also modified probably by segregation of the RE to the oxide/substrate interface and also through the oxide grain boundaries. The segregation process of the RE to the alloy/scale interface limited the outward diffusion of Al cations. This reduction in cation diffusion played an important role in the scale growth mechanism and thus reduced the scale thickness. The oxide ridges (e.g **Figures 6-57(c**) and **6-62(a**)) on Y-containing alloys were also observed which is indication of aluminium outward – towards the alloy/scale interface – diffusion through the alloy grain boundaries.

These oxide ridges cracked during cooling – **Figures 6-61(c)** and **6-62(b)** (more clear in cycling conditions). The depth and the width of the alloy intergranular attack increased with increasing exposure time and temperature due to faster diffusion of aluminium and more segregation of Y to the alloy grain boundaries. As oxidation proceeded for Y-containing Fe_3Al alloy, the continuous movement of oxide at the alloy/oxide interface inevitably resulted in either fracture or partial detachment (**Figure 6-63**) of the oxide from the alloy surface during cooling. The later was most likely to occur especially at the oxide ridges and thus led to the development of cavities between the external oxide and alloy interface, **Figure 6-62**. The development of the cavities or voids at the scale/substrate interface has previously been observed for various undoped Al_2O_3-forming alloys [**298, 299**] after prolonged exposure – as found in the present case – and accounted for the vacancy condensation. These studies were carried out in disordered FeCrAl alloy and not in ordered intermetallics. However, in the study of Golightly *et al.*[**253**] vacancy condensation was considered unlikely to be the case and cavities were observed at the very early stage of oxidation (after 1 minute) at 1200°C. In the present study, the excessive formation of interfacial voids in Fe_3Al scales is believed to be due to the diffusion characteristics of the ordered Fe_3Al matrix (unlike FeCrAl alloys), which may have been inherently more susceptible to the formation of the Kirkendall-type voids at the oxidation front. After longer-term exposure (240h) at 1100°C, the Al_2O_3 of Y-containing alloys was no longer effective in protecting the alloys. Careful examination to the cross-sectioned scale of Y-containing alloys revealed that cracks at the area of the oxide ridges (**Figure 6-62** and **6-63**) facilitated breakdown of the flat oxide from the substrate during cooling.

The increased scale thickness of the Hf doped alloy (**Figure 6-54**) may be attributed to the scale-embedded HfO_2 stringers acting as short-circuit paths for oxygen transport. This transport mechanism would lead to the observed preferential localised scale thickening in the neighbourhood of the possible HfO_2 particles as indicated by EDX results, **Figure 6-**

56. The formation of oxide pegs of Fe_3Al-Hf led to the development of a highly irregular alloy/scale interface. Smialek *el al.* [**252**] also observed scale spallation on Fe-40%Al with Hf and Zr alloy additions. They concluded that the inability of these RE additions to prevent scale spallation was related to the large differences in the coefficient of thermal expansion between α-Al_2O_3 and iron-aluminides than other alumina-formers. The present results suggest that, rather than the occurrence of excessive damage during cooling, the observed scale spallation on undoped Fe_3Al and Hf-doped alloys was a result of scale buckling (**Figure 6-51**), yet there was some improvement of scale adherence for the Hf-doped alloys (**Figure 6-51**(**b**) if compared to undoped Fe_3Al alloy, **Figure 6-51**(**a**).

In the present study, the use of 0.25 wt%Hf in the Fe_3Al alloys appeared to be "over-doping" if compared to 0.15 wt%Y in the experimental alloys. Excessive amounts of RE in the alloy may result in detrimental effects to the corrosion behaviour of the alloy. For example, higher Y_2O_3 contents in ODS FeCrAl have been observed to accelerate the alloy oxidation [**247, 300**]. Thus in the present study, the lower Hf concentration (e.g. 0.1 at%), could have been well effective in improving scale growth and better integrity of the scale. For the case of 0.15 at%Y addition in our study, it appeared to be just above the optimum level probably due to its low solubility in the alloys. However, addition of 0.15 at%Y to Fe_3Al did improve the scale adhesion to a great extent. This improvement, was attributed by (e.g. Smeggil et al [**284**]) to gettering of sulphur and decreasing the growth stresses as a result of Y segregation through the oxide grain boundaries and alloy/scale interface respectively. However, excessive amounts of Y segregate and enriched the alloy grain boundaries with oxygen and thus facilitating the formation of Al_2O_3 along the grain boundaries (intergranular oxidation), which contributed high weight gains for the Y-containing Fe_3Al alloys.

7.3.3 Effect of Reactive Elements (Y and/or Hf) on Al_2O_3 Oxide Adherence Under Cycling Conditions

The analysis using SEM of the surface and cross-sectioned morphologies of Fe_3Al alloys showed significant differences in scale adherence to the substrate under cycling conditions. Generally, the scale of the RE-doped alloys under cycling conditions was thin and more adherent to the substrate at all temperatures. However, the scale of undoped Fe_3Al material was generally less protective and showed different morphologies under thermal cycling if compared to those under isothermal conditions. One major difference between the isothermal and the cyclic oxidation was the increased oxidation rate under cycling, which was associated with increased oxide thickness and formation of voids and cracks within the scale and also at the alloy/scale interface especially at higher temperatures.

Under thermal cycling conditions, the scale of Fe_3Al alloy without RE was cavity-filled and poorly adherent to the substrate, **Figure 6-71**. There are several mechanisms by which stresses can develop within the scale and/or at the scale/alloy interface, such stresses are due to oxide growth or during thermal cycling. Interfacial voids also play an important role in the stress development within the scale.

For the present experimental Fe_3Al alloy with only 0.25at%Hf under cycling conditions, a moderate oxide adherence to the substrate was observed although a considerable thick scale with a number of robust Al_2O_3 pegs was readily apparent at the oxide/alloy interface of Fe_3Al-Hf alloy, **Figure 6-70**(**a** and **b**). The development of a peg-like morphology of Hf doped Fe_3Al alloys supported Stott's [**240, 298**] idea that the interlocking between the scale and the alloy through the growth of a profusion of oxide intrusions, or "pegs", is the most pertinent factor in the adhesion of thick scales "by pinning". However, it is not clear weather the remarkable cohesion between the oxide intrusions and the alloy is purely mechanical or involves chemical bonding as well. The

mixed alloy/scale region would accommodate the mismatch in the specific volumes and thermal expansion coefficients of the scale and the substrate. It improves the fracture toughness of this composite system due to: (a) the obvious limited crack propagation path, (b) large interfacial contact area associated with the dendritic, lateral peg growth (see **Figure 6-72**(**d**)).

When yttrium rather than hafnium was utilised in the present study as an "active" element, very thin, and excellent adherence of the scale with the substrate was observed with almost flat surfaces especially at low exposure and no sign of oxide pegs was observed, **Figure 6-69**(**b**). However, oxidation of the Y-containing alloys at the alloy grain boundaries (intergranular oxidation) was clearly noticed also under cycling conditions (**Figure 6-72**(**a**) and **(b**)). One major difference between the isothermal and cycling oxidation for Y-doped alloy is attributed to the reproducibility (after external scale spallation under cycling conditions) of thin Al_2O_3, which limited the ingress of oxygen through the grain boundaries. Another possibility is that after a number of cycles and due to the small amount of Y in the alloy, there were not enough Y to segregate to the alloy grain boundaries (e.g. **Figure 6-72**(**a**). During longer-term testing especially under cyclic conditions at high temperature (1100ºC), the relatively flat scale of Y-containing alloys would fail as a result of the growth of voids, which would limit contact between the scale and the substrate. When the void fraction would reach a critical level, the cooling stresses could be sufficient to spall the scale. The scale of the RE doped alloys would also be subjected to thermal stresses, which leading to the cracking of the external scale. Due to the high aluminium content of the alloys (21 at%Al), and also the oxygen diffusion through the preformed cracks, oxides (after internal oxidation) reformed and pushed outwards the external scale. With further increase of cycles, the number of cavities – between the internal and the external scales – for all Fe_3Al alloys (**Figure 6-73**) increased and eventually the external scale completely or partially delaminated from the system.

Comparison of our oxidation results of Y-doped and undoped Fe_3Al alloys clearly showed detrimental effect of sulphur – possibly present with small quantities in our experimental alloys – to the scale adherence of undoped Fe_3Al alloy at the scale/substrate interface. This effect is suppressed by the presence of 0.15 at%Y in the Y-containing intermetallics. Funkenbush *et al* [**282**] and Smialek [**301**] found that the scale adhesion was poor when Y was added as Y-sulphide. Also in the same study [**301**], when yttrium was added to a sulphur-containing alloy at levels sufficient to tie up both indigenous sulphur and a sulphur resulting from the deposition of Y_2S_3, adherent scale returned. Surprisingly, the presence of 0.25 at%Hf with just 0.15 at% of Y in Fe_3Al alloy [Fe_3Al-(Y+Hf)] did not alter significantly the external scale morphology of the alloy and the scale remained thin, with no oxide pegs at the alloy/scale interface (**Figure 6-73**(**d** and **e**)). The dominant effect of Y on the Fe_3Al-(Y+Hf) oxidation behaviour is still not clear and needs further investigation.

CHAPTER EIGHT

CONCLUSIONS AND SUGGESTIONS FOR THE FUTURE WORK

CHAPTER EIGHT

8.0 CONCLUSIONS AND SUGGESTIONS FOR THE FUTURE WORK

This chapter summarises the main conclusions from the carried out work and also some suggestions for the future work are included.

8.1 Conclusions

8.1.1 Oxidation of Ti-46.7Al-1.9W-0.5Si Intermetallic Alloy

1. The Ti-46.7Al-1.9W-0.5Si alloy displayed parabolic kinetics of oxidation in air and Ar-20%O_2 at 750ºC - 950ºC although the rate of oxidation was relatively slower in Ar-20%O_2.
2. In both air and Ar-20%O_2, multi-layered scales developed. The scales on Ti-46.7Al-1.9W-0.5Si alloy developed in air were comprised of $TiO_2/Al_2O_3/TiO_2/TiN/TiAl_2$/substrate whilst a multi-layered scale $TiO_2/Al_2O_3/TiO_2/Al_2O_3/Ti_3Al$/substrate was generated in Ar-20%O_2.
3. During cooling, spallation of oxide layers by a wedging processes occurred in air oxidation due to the large mismatch of thermal expansion coefficients between the TiO_2 and TiN. However, the scales formed in Ar-O_2 remained adherent and uneven after long exposure time.
4. The observed reduction of the Ti-46.7Al-1.9W-0.5Si alloy scale thickness in Ar-80%O_2 (pO_2 = 0.8 x 10^5 Pa) with the likely reduction in the rate of diffusion of the reacting species (oxygen, aluminium and titanium) throughout the scale were associated to:
    i. the increased tendency of the formation of relatively pure Al_2O_3 – rather than multi-layered scale of TiO_2 and Al_2O_3 (in at Ar-5%O_2 – pO_2 = 0.05 x 10^5 Pa);

ii. the low defect structure of the formed Al_2O_3 compared to that of TiO_2;

iii. the low solubility of Al_2O_3 in TiO_2 at higher oxygen pressures.

5. While the diffusion of Ti and Al in the long-ordered Ti-46.7Al-1.9W-0.5Si alloy was not investigated in this study, however, the mechanism of scale growth is strongly believed to be controlled by diffusion of the reacting species.

8.1.2 Sulphidation/Oxidation of Coated and Uncoated Ti-46.7Al-1.9W-0.5Si Intermetallic Alloy

1. The high temperature corrosion behaviour of uncoated Ti-46.7Al-1.9W-0.5Si alloy at 850°C in an environment of $H_2/H_2S/H_2O$ ($pO_2 \sim 1.2 \times 10^{-15}$ Pa and $pS_2 \sim 6.8 \times 10^{-1}$ Pa) followed a parabolic reaction law with the Kp value of 6×10^{-11} $g^2/cm^4/s$.
2. A multi-layered scale formed on the uncoated Ti-46.7Al-1.9W-0.5Si alloy consisted of $TiO_2/Al_2O_3/TiS+W/TiAl_3/TiAl_2$ from the gas/scale interface to the surface of the substrate.
3. Employment of AlTiN coating greatly increased the sulphidation/oxidation resistance of Ti-46.7Al-1.9W-0.5Si alloy, particularly at the early stages of exposure. However the mismatch of thermal expansion coefficients between the coating and the substrate led to the development of cracks in the coating, which became diffusion paths for the reaction species – substrate elements, oxygen and sulphur – brought about the formation of the nodular corrosion products. The morphologies, composition and phases in the nodules were similar to the scales formed on the uncoated samples.
4. The involvement of diffusion barrier coatings of NbN and CrN with AlTiN further enhanced the corrosion resistance of Ti-46.7Al-1.9W-0.5Si alloy. The benefits of double layer coatings lasted even after 240h exposure at 850ºC. The degradation mechanism of the double layer coatings showed a similar pattern to that of the single AlTiN layer

coating. The formation of nodular corrosion products due to localised attack did not undermine the overall integrity of the coatings.

5. For the single layer CrN coating, the protection stemming from the formation of a Cr_2S_3 was limited and the integrity of the Cr_2S_3 was undermined by the outward diffusion of the substrate elements. In the case of the double layer coatings of CrN and NbN, the formation of NbS_2, that has a low defect concentration, prevented the outward migration of the substrate elements, and hence increased the high temperature corrosion resistance of the alloy.

8.1.3 Isothermal and Cyclic Air Oxidation of Fe_3Al Intermetallic Alloys

1. Without RE (Y and/or Hf) additions, the Al_2O_3 scales developed on Fe_3Al alloys became convoluted and grew by a mixed diffusion mode of aluminium and oxygen transport. With the addition of a RE (especially yittrium), aluminium diffusion was reduced and the scale became almost flat and it grew mainly by the inward transport of oxygen. This was observed at the three temperatures (900, 1000 and 1100°C).
2. No aluminium nitride was detected in the scales of Fe_3Al alloys within the range of exposure temperatures studied.
3. The reduction in the transport of aluminium in RE-doped Fe_3Al alloys, which reduced the Fe_3Al alloy rate of oxidation, was probably caused by the segregation of the RE to the scale/alloy interface.
4. Intergranular oxidation of the Y-containing Fe_3Al alloys can be explained by the segregation of Y (not Hf) to the alloys grain boundaries.
5. Excessive Hf content in Fe_3Al alloy was detrimental to the oxide growth process. The formation of Hf-rich oxide particles facilitated inward scale growth, leading to the

formation of localised oxide thickening “pegs” and eventual formation of less protective oxide especially under thermal cycling.

8.2 Suggestions for Future Work

A series of further investigations is needed for a better understanding of the corrosion mechanisms and for the development of better corrosion resistant Ti-Al and Fe-Al intermetallic alloys. Such investigations should include the following:

1. The effects of reactive gas composition (conclusively oxygen and sulphur) especially at the very early stage of corrosion of Ti-Al alloys, which would result in either different corrosion products or different rates of growth of the same product. This could be useful for:
   a) allowing a better understanding of the high temperatures oxidation/sulphidation mechanism of Ti-Al systems;
   b) providing a strong basis to investigate the effects of surface modification such as pre-oxidation (preferably in pure oxygen) or pre-sulphidation (at high sulphur pressure) on the prolonged high temperature corrosion behaviour of Ti-Al alloys.
   c) allowing also a better understanding of the solubility of different gas components (especially oxygen) in titanium and Ti-Al alloys at high temperatures.
2. Diffusion studies are essential in order to achieve more fundamental understanding of the scale growth mechanism of Ti-Al systems. Of special importance is to calculate precisely the diffusion coefficients of Ti and Al at various temperatures.
3. Studies of the solid solubility between oxide phases existing in the Ti-Al-O phase diagram, and their oxygen pressure dependence could provide information on the transport processes in TiO_2 and Al_2O_3 oxide phases. Studies of the influence of oxygen

solubility on the activities of Ti and Al at different phases (α and/or γ) present in the alloy would be appropriate.

4. Phase diagrams, which can explain other nitrogen effects on the corrosion behaviour of Ti-Al systems, are required. For example AlN could not be detected within the temperature range 750 to 950°C for Ti-46.7Al-1.9W-0.5Si alloy and between 900 - 1100ºC for Fe_3Al alloys in this study, however TiN was formed after Ti-46.7Al-1.9W-0.5Si alloy oxidation in air even at 750°C.
5. The effects of ternary addition to Ti-Al alloy are important: For example, small additions of Nb or Si to Ti-Al alloys were found to have significant effect on their oxidation behaviour at high temperatures. However, the combined effects of Nb and Si need to be fully investigated. The influence of various concentrations of a third element addition to Ti-Al would lead to better design of Ti-Al alloys.
6. Studies of the ion implanted RE in Fe_3Al would further elucidate the role of the elements in changing the scale adhesion.

References

References

1. J. V. Cathcart, in Proceeding of High Temperature Alloys, edited by Z. A. Foroulis and F. S. Pettit, The Electrochemical Society, 1976, p 99

2. N. Birks, G. H. Meier and F. S. Pettit, J. of Metals, 28 (1987)

3. S. Mrowec, Werk. Korr, 31, 371 (1980)

4. D. B. Rao and H. G. Nelson, in Proceeding of High Temperature Alloys, edited by Z. A. Foroulis and F. S. Pettit, The Electrochemical Society, 1976, p 464

5. K. Natesan and O. K. Chopra, in Proceeding of High Temperature Alloys, edited by Z. A. Foroulis and F. S. Pettit, The Electrochemical Society, 1976, p 493

6. N. S. Choudhury, H. C. Graham, J. W. Hinze in Proceeding of High Temperature Alloys, edited by Z. A. Foroulis and F. S. Pettit, The Electrochemical Society, 1976, p 99

7. G. H. Meier, F. H. Pettit and S. Hu, High Temperature Corrosion (Les Embiez, France, 1992, Proc. J. Phys. IV 3, 395 (1993)

8. S. Becker, A. Rahmel, M. Schorr, and M. Schurtz, Oxid. of Met. 38, 425, 1992

9. J. Rakowski, D. Manccau, F. S. Pettit, and G. H. Merier, Proc. 2nd Int. Conf. Microscopy of Oxidation, S. B. Newcomb and M. J. Bennett, eds (Institute of Metals, London), p 476.

10. N. Zheng, W. J. Quadakkers, A. Gil and H. Nickel; 1995

11. Cooper A R, PhD Thesis (CNAA), Newcastle Polytechnic, 1989

12. F. H. Stott, F. M. F. Chang and C. A. Stirling, in Conf. Proc. Of Met. Soc. AIME/Met. Soc. Division ASM Symp. On High Temperature Corrosion in Energy Systems, ed. M. F. Rothman, Michigan 1994

13. H. B. Bomberger et al, Titanium Technology (Dayton, OH, TDA, 1985) pp 13-17

14. N. G. Tupper, J. K. Elbaum and H. M. Burte, JOM, 30, (1978), pp 7-13

15. F. H. Froes, Space Age Metals Tecnology (Covina, CA: SAMPE, 1988), pp 1-19

16. H. A. Lipstitt, Advanced High Temperature Alloys (Metals Park, OH: ASM, 1986), pp 157-164

17. M. Khobaib and F. W. Vahldiek, Op. Cit. 3, pp 262-270

18. J. Subrahmanyam, J. Materials Science, 23 (1988), pp 1906-1910

19. C. H. Xu, W. Gao, H. Gong, Intermetallics 7 (1999) 1128-1140

20. Devan J. H. In Grobstein J, editors, Oxidation of High Temperature Intermetallics.

Warrendale (PA): TMS, 1989, P 107

21. Guy-HREN, Elements of Physical Metallurgy, Third Edition, Published by Addison-Wesely, 1974

22. N. Birks, G. H. Meier. Introduction to High Temperature Oxidation of Metals, published by Edward Arnold, 1983

23. P. Kofstad, High Temperature Corrosion, Elsevier Applied Science Publisher Ltd., 1988

24. J. Benard, Elsevier Applied Science Publisher Ltd , Oxidation of Metals and Alloys, 1971

25. K. Fueki and J. B. Wagner, (1965), J. Eelectrochemical Soc. V. 112 p 384-388

26. G. J. Yurek, (1987), in Corrosion Mechanisms, F. Mansfield ed., Marcel Dekker Inc., New York, NY, P. 397-446

27. K. N. Strafford, in Institution of Metallurgists Conference on Environmental Degradation of High Temperature Materials, Isle of Man (1980)

28. S. Mrowec, Defects and Diffusion in Solids, Elsevier Scientific Publishing Company, 1980

29. S. Mrowec and K. Przybylski, Oxid. Met., 23 (3/4), 107 (1985)

30. G. C. Wood, Oxid.of Met., 2 (1), 11 (1970)

31. P. Kofstad, High Temperature Oxidation of Metals, J. Wiley, 1966

32. P. Shewmon, Diffusion in solids, 2nd Eddition, The minerals, Metals and Materials Society, Pennsylvania 1989

33. J. M. Blakely, Surface Diffusion, Progr. Mater. Soci., 10, 1963

34. P. Kofstad, Nonstoichiometry, Diffusion and Electrical Conductivity in Binary Metal Oxides (Wiley-Interscience, 1972, pp 137

35. K. S. Forland, Acta Chimica Scandinavica 20, 2573 (1966)

36. G. Neumann, in Defect and Diffusion forum, Editors F. J. Kedves and D. L. Beke, SCI. Tech. Publications, p 43

37. F. Morin, G. Beranger and P. Lacombe, Oxidation of Metals **4/1**, (1972), 51

38. C. Wagner, Z. Electrochem. Soc., 103, 1956, 627

39. J. L. Meijering and Druyversteyn, M. J., Philips Res. Rep., 2 (1947), 81, 260

40. C. R. Austin, Trans. Amer. Soc. Metals, 24, (1936).

41. G. C. Wood and F. H. Stott, Materials Science and Technology, **3**, 1987, p 519

42. K. N. Strafford and P. K. Datta, Mater. Sci. Techn., 5, 765 (1989)

43. N. B. Pilling and R. E. Bedworth, J. Inst. Met. 29 (1923) 529

44. D. P. Whittle, Oxidation of Metals, **4/3**, (1972), 171

45. D. L. Douglass, Oxidation of Metals, **1/1**, (1969), 127

46. J. Stringer, Corrosion Sci., 10, 1970, 513

47. D. Griffin, A. Daadbin, P. K. Datta, Surface&Coating Techn., **126** (2000), 142-151

48. J. K. Wright, R. L. Williamson, R. M. Cannon, Mater. Sci. Eng. A238 (1997) 411

49. G. Schumacher, F. Dett., M. Schutze, U. Hornauer, E. Richter, E. Wieser, W. Moller: Intermetallics 7 (1999) 1113-1120

50. E. P. George and C. T. Liu; in Symp. of High Tempetature Ordered Intermetallic Alloys VI, 1994, Massachusetts, USA, pp 1131-1145

51. G. H. Meier, Materials and Corrosion, 1996, 47, 595-618

52. S. Taniguchi: Materials and Corrosion, 1997, 48, 1-9

53. Lang, M. Schutz. Oxidation of Metals, 1996, 46; 255-285

54. F. Dettenwagner, E. Sch., M. Ruhle, G. H. Meier: Oxidation of Metals, 1988; 50: 269-307

55. R. U. Vaidya, Y. S. Park, G. T. Gray, D. P. Butt: Oxidation of Metals 1998, 50, 215-240

56. M. F. Stroosnijder, H. J. Schmutzler, VAC. Haanappel, JD Sund,; Materials and Corrosion 1997, 48, p. 40-47

57. M. Kumagai, K. Shibuc, MS Kim, M. Yonemitsu. Intermetallics, 1996; 4, 557-566

58. M. Hald, M. Schutze; Materials Science and Engineering, 1997, A259, 240, 847-858

59. G. Schumacher, C. Lang, M. Schutze, U. Hornauer, E. Richer, E. Wieser, W. Moller: Materials and Corrosion, 1999; 50: 162-165

60. T. Hanamura, Y. Ikemastu, H. Morikawa, M. Tanino, J. Takamura. Proc. of JIMIS-6, 1991, 179-183

.

61. G. Schumacher, F. Dett., M. Schtze, A. Iberl, D. Reil: In Preparation for Materials and Corrosion, The Minerals, Metals and Materials Society, 1982, p 76

62. W. B. Retallick, M. P. Brady, D. L. Humphrey; Intermetallics, 1998: 6: 335-337

63. H. L. Du, P. K. Datta, D. B. Lewis and J. S. Burnell-Gray: Corrosion Science, 1994, Vol. 36 (4), 631-642

64. H. L. Du, P. K. Datta, D. B. Lewis and J. S. Burnell-Gray and D. Jenkinson; 10th Irish Materials Forum Conf., Coleraine, 1994: In Key Engineering Materials, 1995, Vol. 99-100, 151-158

65. 63. H. L. Du, P. K. Datta, D. B. Lewis and J. S. Burnell-Gray: Oxidation of Metals, 1996, Vol. 45, (5/6), 507-527

66. H. L. Du, P. K. Datta, D. B. Lewis and J. S. Burnell-Gray: Materials Science and Engineering (A), 1996, Vol. 205, 199-208

67. P. K. Datta, J. S. Burnell-Gray, H. L. Du, A. Dowson and M. Jacob: Conf. Proc. CIMTEC 98, Florence, Italy, 1998

68. H. J. Schmutzler, N. Zheng, W. J. Quadakkers and M. F. Stroosnijder; Surface and Coatings Technology 83 (1996) 212-217

69. M. Yamaguchi, H. Inul, K. Kishida, M. Matsumuro and Y. Shiral; in Symp. of High Temperature Ordered Intermetallic Alloys VI, 1994, Massachustts, USA pp 3-16, Edited by J. Horton *et al*; Materials Research Society

70. E. Fischer, J. of Phase Equilibria. Vol. 18, 4, 1997, 338-343

71. Lee, Byeong-Joo; Saunders, Nigel. Zeitschrift fuer Metallkunde, Vol. 88, 2, 1997, 152-161

72. F. Zang, S. L. Chen, Y. A. Chang and U. R. Kattner: Intermetallics, 5 (1997), 471-482

73. P. Markku, K. Jorma: Zeitschrift fuer Metallkunde Vol. 83, 1, 1992, 17-20

74. J. B. McAndrew and H. D. Kessler; Trans. Met. Soc., A. I. M. E., 206-1348, 1956

75. C. S. Giggins and F. S. Pettit, J. Electrochem., Soc., 118, 1782 (1971)

76. W. C. Tripp and H. C. Graham, J. Electrochem. Soc., 118, 1195, 1971

77. K. N. Strafford and J. M. Towell; Oxidation of Metals, 10, 41, 1976

78. S. Anderson, B. Gollen, V. Kuylenstierna and A. Magneli, Acta Chem. Scand., 11, 1641 (1957)

79. L. Krishan, Luthra. Oxidation of Metals, 36, 5/6, 1991, p. 475-490

80. V. V. Samokhval, P. A. Poleshchuk and A. A. Vecher, Russian J. of Phys. Chem., 45, 1174-1175

81. I. Barin; Thermochemical Data of Pure Substances (VCH Publishers, New York, 1989)

82. L. Kaufman, Coupled Phase Diagrams and Thermchem. Data for Transition Metals

Binary Systems VI, CALPHAD, 3, 45-76 (1979)

83. G. H. Meier and D. Appalonia: Oxidation of High Temperatures Intermetallics, Edited by T. Grobstein and J. Daychak: The Minerals, Metals and Materials Soc., 1989, pp 185-193

84. C. Wagner, Z. Electrochem., 61, 772 (1959)

85. F. Gesmund and F. Viani: Oxidation of Metals, 25, 269 (1986)

86. E. U. Lee and J. Waldman. Scripta Metall., 22, 1389

87. R. Strafford and S. Poize: In High Temperature Corrosion, R. A. Rapp, Ed. NACE, 1983, p. 591

88. J. Subrahmanyam and J. Annapura; Oxidation of Metals, 26, 275, 1986

89. G. Wesch and A. I. Kahveci: Oxidation of High Temperatures Intermetallics, Edited by T. Grobstien and J. Doychak: The Minerals, Metals and Materials Society, 1989

90. H. A. Lipsitt, MRS Symp. Proc., Vol. 39 (1985) 351

91. H. A. Lipsitt, D. Shechtman and R. Schafrik, Metall. Trans. A, Vol. 6A (1975) 1991

92. H. A. Lipsitt, D. Schechtman and R. Schafrik: Metall. Trans. A, Vol 11A (1980) 1369

93. P. L. Martin, M. Mendiratta and H. A. Lipsitt,: Metall. Trans. A, Vol. 14A (1983) 2170-2174

94. W. J. S. Yang, Metall. Trans. A, Vol. 13A (1982) 324

95. R. J. Kerans, Metall. Trans., Vol. 15A (1984) 1721

96. T. Kawabata, T. Kahaf and O. Izumi, Acta Metall., Vol. 33 (1985) 1355

97. P. Kofstad, K. Hauffa and H. Kjollesdal (1958): Acta Chem. Scand., Vol. 12 (1958) 239

98. K. Hauffe; Oxidation of Metals, Plenum Press, 1965, 217-223

99. S. Taniguchi, T. Shibata and S. Itoh: Materials Transactions, JIM, Vol. 32, Nos. 2 (1991), p. 151 to 156

100. K. Kasahara, K. Hashimoto, H. Doi and T. Tsujimoto: J. Japan Inst. Met., 53, 1989, 58

101. Y. Umakoshi, M. Yamaguchi, T. Sakagami and T. Yamane; J. Mat. Sci. 24 (1989), 1599

102. E. Kobayashi, M. Yoshihora and R. Tanaka: J. Japan Inst. Met., 53 (1989), 251

103. J. D. Kuenzly and D. L. Douglass; Oxidation of Met., 8, 1974, 227

104. S. Taniguchi and T. Shibata: Oxidation of Metals, 25 (1986), 201

105. S. Taniguchi: Trans. ISIJ, 25 (1985) 3

106. J. S. Fish and D. J. Duquette; J. De Physics, Vol. 3, 1993, p. 411

107. T. Yoshioka, A. Takayuki, T. Narita, T. Toshio; Corrosion Eng., Vol. 48, 4, 1999, 214-219

108. T. Yoshioka, A. Takayuki, T. Narita, T. Toshio; Corrosion Eng., Vol. 45, 12, 1996, 712-716

109. T. Yoshioka, A. Takayuki, T. Narita, T. Toshio; Corrosion Eng., Vol. 48, 4, 1999, 220-225

110. T. Yoshioka and T. Narita: In Advances in Surface Eng. Vol.1 Edited by P. K. Datta and J. S. Burnell-Gray, Royal Society of Chemistry 1997, p. 67-75

111. T. Izumi, T. S. Hayashi and T. Narita, Intermetallics, 2000, 891-901

112. T. Yoshioka, T. Narita: Report to the 123rd Committee on High Temperature Metals and Alloys, Japan Soc. for Promotion of Science, 1994; 35, 221, 1996; 37:317

113. T. Yoshioka, T. Zairyo-to-Kankyo, 1996; 45, 712

114. T. Yoshioka, T. Narita, Z. Kankyo, 1999; 48: 214

115. T. Yoshioka, T. Narita, Z. Kankyo, 1999; 48: 220

116. T. Yoshioka, T. Narita. Corrosion Eng. 1996; 45: 749

117. T. Narita, T. Izumu, M. Yatagai, T. Yoshioka. Intermetallics, 2000; 8: 371

118. K. Hashimoto, H. Doi, T. Tsujimoto, Mater. Trans. JIM, 1996, 27:94

119. T. Izumi, S. Hayashi, M. Fujine and T. Narita: In Proc. of the Int. Symp. on High Temperature Corrosion and Protection; Hokkaido, Japan, 2000, p. 535, Edited by T. Narita, T. Maruyama and S. Taniguchi, Science Reviews

120. T. Izumi, T. Yoshioka, S. Hayashi and T. Narita: Intermetallics, 9 (2001) 547-558

121. X. Y. Li, Y. C. Zhu, K. Fujita, N. Iwamoto, Y. Matsunaga, K. Nakagawa, S. Taniguchi: Surface and Coating Techn., 136 (2001) 276-280

122. S. Taniguchi, Bulletin of Japan Inst. Metals, 31 (1992) 497

123 C. Herzig, T. Przeorski, Y. Mishin. Intermetallics 7 (1999) 389-404

124. M. Koppers, C. Herzig, M. Friesel, Y. Mishin: Acta Mater. 1997, 45, 4181

125. U. Gerold, C. Herzig; Defect and Diffusion Forum, 1997; 437: 143-147

126. J. Rusing, C. Herzig; Scripta Metall. Mater., 1995, 33, 561

127. J. Rusing, C. Herzig; Intermetallics, 1996, 4, 647

128. W. Sprengel, W. Oikawa, H. Nakajima; Intermetallics, 1996; 4; 185

129. S. Kroll, H. Mehrer, N. Stolwijk, C. Herzig, R. Rosenkranz. Frommeyer, G. Z. Metallkd, 1992, 83, 591

130. S. Frangini, A. Mignone, F. DeRiccadis: J. of Materials Science 29 (1994) 714-720

131. S. A. Kekare, P. B. Aswath: J. of Materials Science 32 (1997) 2485-2499

132. V. Shemet, H. Hoven and W. J. Quadakkers. Intermetallics 5 (1997) 311-320

133. H. Al-Badairy and G. J. Tatlock; in the 4th Int. Conf. on the Microscopy of Oxidation, Edited by G. Tatlock and S. Newcomb, p. 133

134. V. Shemet, A. K. Tyagi, J. Penkalla, L. Singheiser, J. S. Becker and W. J. Quadakkers. In Proc. of the 4th Int. Conf. on the Microscopy of Oxidation; Edited by G. Tatlock and S. Newcomb, 1999, p. 41

135. M. Nombela, V. Kolarik, M. Grob, H. Fietzek and N. Eisenreich: In Proc. of the 4th Int. Conf. on the Microscopy of Oxidation, Edited by G. Tatlock and S. Newcomb, 1999, p. 49

136. V. A. C. Haanappel, J. D. Sunderkotter, M. F. Stroosnijder. Intermetallics 7 (1999) 529-541

137. J. Geng, G. Gantner, P. Oelhafen, P. K. Datta; Applied Surf.ace Sci., 158 (2000) 64-74

138. M. Yoshihara and Y. W. Kim: In the Proc. of Int. Symp. on High Temperatures Corrosion and Protection, Edited by T. Narita, T. Maruyama and S. Taniguchi, 2000, p. 529

139. S. Hayashi and T. Narita: In Proc. of the Int. Symp. on High Temperature Corrosion and Protection, Edited by T. Narita and T. Maruyama and S. Taniguchi, 2002, p. 79

140. S. K. Varma, A. Chan and R. N. Mahapatra: Oxid. of Metals, Vol. 55, 5/6, 2001, p. 423

141. H. Jiang, M. Hirohasi, H. Imanari and Y. Lu. Scripta Materialia 45 (2001) 253-259

142. W. Gao, Z. Li and D. Zhang: Oxidation of Metals, Vol. 57, ½ (2002), p. 99

143. J. D. Sunderkotter, H. J. Schmutzler, V. A. C. Haanappel, R. Hofman, W. Glatzy, H. Clemens and M. F. Stroosnijder; Intermetallics 5 (1997) 525-534

144. L. D. Yu, S. Thongtem, T. Vilaitong, M. J. McNallan. Surface and Coating Technology 128-129 (2000) 410-417

145. S. Taniguchi, T. Fujioka, M. Nakujima, T. Shibata, M. Yoshihara and Can Zhu: Int. Proc. of the Int. Symp. on High Temperature Corrosion and Protection, Edited by T. Narita,

T. Maruyama and S. Taniguchi; Science Reviews. 2000, p. 495

146. V. A. C. Haanappel, M. F. Stroosnijder; Surface and Coating Technology 105 (1998) 147-154

147. M. F. Stroosnijder: Surface and Coating Technology, 100-101, 1998, 196-201

148. Z. Tang, F. Wang and W. Wu; Materials Science and Engineering A 276 (2000) 70-75

149. B. S. Yilbm, A. Z. Sahin, Z. Ahmad and B. J. Abdul-Aleem. Corrosion Science, Vol. 37, Nos 10, pp 1627-1636, 1995

150. A. Joshi, H. S. Hu, Surface and Coating Technology 76-77 (1995) 499-507

151. C. Leyens, M. Peters, W. A. Kaysser. Surface and Coatings Technology, 94-95 (1997) 34-40

152. B. Navinsek, P. Panjan. Surface and Coating Technology 74-75 (1995) 919-926

153. P. K. Datta, H. Chu, J. S. Gray and K. N. Strafford: Conf. Proc. Surface Engineering Practice; Adelaide, Australia, 1991

154. P. K. Datta, K. N. Strafford, H. L. Du, B Lewis and J. S. Gray,: Proc. 1st Int. Conf. Heat-Resistant Materials; Wisconsin, USA, 1991, p. 323-332

155. S. Taniguchi, Y. Tachikawa and T. Shibata: Materials Science and Engineering A232 (1997) 47-54

156. R. Kremer and W. Auer. Materials and Corrosion, 48, 35-39 (1997)

157. S. Taniguchi, N. Hongawara and T. Shibata: Materials Science and Engineering A307 (2001) 107-112

158. K. N. Strafford, P. K. Datta: Corrosion Science, Vol. 35, Nos 8 p. 1053-1063, 1993

159. K. N. Strafford, Metall. Rev., 14, 153 (1969)

160. K. N. Strafford: High Temperatures Technology, 1, 307 (1983)

161. K. N. Strafford: in High Temperatures Alloys; Their Exploitable Potential (eds. J. B. Marrott et al), p. 53 Elsevier, Applied Science, London 1987

162. K. N. Strafford, A. F. Hampeon and D. Jenkinson; in High Temperatures Alloys; Their Exploiable Potential (eds. J. B. Marriott et al) p. 165 Elsevier, Applied Sci., London, 1987

163. K. N. Strafford, G. R. Winstanley and J. M. Harrison, Werkstoffe Korros, 25, 487,1974

164. K. N. Strafford and R. Mansfold: Oxidation of Metals, 1, 221 (1969)

165. K. N. Strafford and A. F. Hampton, J. Less Common Met. 25, 305 (1971)

166. F. Gesmudo and F. J. Viani, J. Electrochem. Soc. 128, 470 (1981)

167. W. Kai, M. T. Chang and C. Y. Bai; Oxidation of Metals 56, No 8, ¾, 2001

168. H. L. Du, P. K. Datta and S. K. Hwang, Materials Science Forum, Vols. 251-254 (1997) pp 219-226

169. H. L. Du, P. K. Datta, A. L. Dowson and M. H. Jacobs, Surface and Coatings Technology 78 (1996) 111-120

170. M. F. Stroosnijder, J. D. Sunderkotter, V. A. C. Chang, C. T. Liu (Eds), Design Fundamentals of Composites, Intermetallics and Metal-Ceramics Systems, TMS, Warrendale PA, 1996, p. 287-293

171. K. Kasahars, Y. Ikeda, T. Kimura and T. Tsujimoto: J. of the Japan Institute of Metals, Vol. 60, 10, 1996, p. 907-913

172. H. GyoJung, C. Hyeok Oh and K. Young Kim. In Proc. of the Int. Symp. on High Temperatures Corrosion and Protection, Eds; T. Narita, T. Maruyama and S. Taniguchi, Science Reviews 2000, p 509-513

173. M. N. Mungole, R. Balas, A. Ghosh: Intermetallics, 8 (2000) 717-729

174. Y. Shida and H. Anada; Corrosion Science, Vol. 35, 5-8, 1993, p. 945-953

175. P. Perez, J. A. Jimenez, G. Frommeyer, P. Adera: Materials Science and Engineering A 284 (2000) 138-147

176. B. Y. Huang, Y. H. He, J. N. Wang. Intermetallics, 7 (1999) 881-888

177. M. Yoshihara and K. Miura,: Intermetallics, 3 (1995) 357-363

178. S. Taniguchi and T. Shibada: Intermetallics, 4 (1996) 585-593

179. Y. Shida and H. Anada; Oxidation of Metals, Vol. 45, Nos ½, 1996, p. 197-219

180. K. Maki, M. Shioda, M. Sayashi, T. Shimizu and S. Isobe. Materials Science and Engineering A153 (1992) 591-596

181. Y. Shida and H. Anada; J. of the Japan Inst. of Metals, Vol. 58, 7, 1994, p. 754-762

182. J. S. Wu, L. T. Zhang, F. Wang, K. Jiang and G. H. Qiu; Intermetallics 8 (2000) 19-28

183. M. Kumagai, K. Shibue, M. Soon Kim and M. Yonemitsu: Intermetallics, 4 (1996) 557-566

184. D. J. Larson, C. T. Liu and M. K. Miller. Intermetallics 5 (1997) 497-500

185. A. Elex., J. Inst. Metals, 84, 1955/56, 1

186. H. Champin and C. Coddet. J. Less Common Metals, 69, 1980, 163

187. A. M. Chaz and C. Coddet, J. Less Common Metals. 157, 1990, 55-70

188. A. M. Chaze and C. Coddet. Oxidation of Metals, 27, ½, 1987, 1

189. A. M. Chaze and C. Coddet. Oxidation of Metals, 28, ½, 1987, 61

190. A. M. Chaze and C. Coddet. Materials Science, 22, 1987, 1206

191. W. Kinner and W. Knorr, Tech. Met. Krupp. 14, 1956, 99

192. W. Kinner and W. Knorr, Z. Metallk, 47, 1956, 594

193. R. A. Perkins and K. T. Chiang: Oxidation of High Temperature Intermetallics, Eds; T. Grobstein, 1989

194. X. Y. Li, S. Taniguchi, Y. C. Zhu, K. Fujita, N. Iwamoto, Y. Matsunaga and K. Nakagwa; Intermetallics 9 (2001) 443-449

195. T. S. Chen and C. J. Rosa; Oxidation of Metals, 14, 1980, 147

196. T. Hanamura, et al; Proc. Conf. of Intermetallic compounds-Structure and Mechanichal Properties, Japan, 1991, 179

197. I. Gurappa and A. K. Gogia; Proc. of the 5th National Conversion on Corrosion, New Delhi, 1999, p. 210-219

198. H. Kawaura, K. Nishino and T. Saito. J. of the Japan Inst. of Metals, Vol. 63, 12, 1999, p. 1584-1590

199 B. Zhao, J. Wu, J. Sun, B. Tu and F. Wang. Intermetallics 9 (2001) 697-703

200. S. J. Bull and A. M. Jones; Surface and Coatings Technology 78 (1996) 173-184

201. J. H. Wood and E. Goldman; in C. T. Sims, N. S. Stolloff and W. C. Hagel (Eds), Superalloys II, Wiley, New York, 1987, Chapter 13, p. 359

202. T. F. Manley, MSc Thesis, Naval Postgraduate School, Monterey, CAADA 164506, 1985

203. P. Deb, D. H. Boone and T. F. Manely: J. Vac. Sci. Techn.A, 5 (1987) 3366

204. J. Shen, Z. Teng, Z. Jiang, I. Zhou, T. Li; J. Univ. Sci. and Techn., Beijing S13, 1991, 624

205 A. Takei, A. Ishida, 7th APCCC, Inter. Acad. Publ. China A (1991) 718

206. T. Simizu, T. Likubu, S. Isobe, Mater. Science and Engineering A 153 (1992) 602

207. Z. Tang, F. Wang and W. Wu; Surface Coating and Techn. 99 (1998) 248

208. R. L. McCarron, J. C. Schaeffer, G. H. Meier, D. Berztiss, R. A. Perkins, J. Culliman: In F. H. Froes, I. Caplan (Eds) Titanium 92 TMS, Warrendale, PA, 1993, p. 1971

209. M. P. Brady, W J. Brindley, J L. Smialek, I E. Locci, J Organomet. Chem. 48 (1996) 40

210. Z. Tang, F. Wang and W. Wu; Oxidation of Metals, 48 (1997) 511

211. F. Wang, H. Lou, W. Wu: Oxidation of Metals 43 (1995) 395

212. Z. Tang, F. Wang and W. Wu; Trans. Non-ferrous Met. Soc. China, 7 (1997) 103

213. S. Taniguch, T. Shibada, T. Yamada, X. Liu, S. Zou, ISU, Int. 33 (1993) 869

214. S. Taniguchi, T. Shibada, K. Takeuchi: Materials Trans. JIM 32 (1991) 299

215. Z. Tang, F. Wang and W. Wu,; China J. of Mat. Research 11 (1997) 507

216. P. K. Datta, H. L. Du, J. S. Burnell-Gray and K. N. Strafford: Key in 2nd Australian Int. Conf. Surface Eng.; Practice and Prospects. Adelaide, Australia 1994, Conf. Proc. K71-K85

217. D. Mclntyre, I. E. Greene, G. Hakansson, J. E. Sundgren and W. D. Munz, J. Appl. Phys. 67 (1990) 1542

218. O. Knotek, W. D. Munz and T. Leyendecker, J. Vac. Scie. Techn. A 5 (1987) 2173

219. W. Munz, J. Vac. Sci. Techn. A, 1986, 2717

220. H. A. Jehn, S. Hofmann and W. D. Munz: Thin Solid Films, 153, 1987, 45

221. O. Knotek and A. Barimassi: Thin Solid Films, 174 (1989) 51

222. T. Hurkmans, D. B. Lewis, J. S. Brooks and W. D. Munz: Surface Coating and Techn.; 86-87 (1996) 192

223. U. Hornauer, E. Richer, W. Matz, H. Reuther, A. Mucklich, E. Wieser, W. Moller, G. Schumacher and M. Schutze. Surface and Coating Techn. 128-129 (2000) 418-422

224. G. Shumacher, F. Dett. and M. Schutze; in Proc. of 4th Int. Conf. of Microscopy of Oxidation, (Eds., G. Tatlock and S. Newcomb, Science Reviews, 1999, pp 53-58

225. X. Y. Li. S. Taniguchi, Y. C. Zhu, K. Fujita, N. Iwamoto, Y. Matsunaga and K. Nakagwa; Nuclear Instruments and Methods in Physics Research (2001), p 342

226. X. Y. Li. S. Taniguchi, Y. C. Zhu, K. Fujita, N. Iwamoto, Y. Matsunaga and K. Nakagwa; Materials Science and Engineering A 316 (2001) 224-230

227. X. Y. Li, T. H. Zhang, B. K. Ma, Y. G. Zhang, C. Q. Chen; Nuclear Instruments and Methods in Physics Research B 169 (2000) 37-42

228. U. Hornauer, E. Richer, E. Wieser, Nuclear Instruments Methods B 148 (1999) 858-

862

229. M. Schutze and M. Hald, Materials Science and Eng., A 239-240 (1997) 847-858

230. U. Hornauer, R. Gunzel, H. Reuther, E. Richter, E. Wieser, W. Moller, G. Schumacher, F. Dett. And M. Schutze: Surface and Coating Technology 125 (2000) 89-93

231. X. Y. Li, et al, ICAM 97/E-MRS Strasbourg, France, 1997

232. X. Y. Li, et al, Int. Symp. on the Structure of Intermetallics, Pennsylvania, USA, 1997, p. 353-360

233. C. Bocheng. M Sc Thesis, Beijing Univ. of Aeronautics and Astronutics, Beijing, 1999.

234. D. M. Dimiduk, D. B. Mirccle, Y. M. Kim, M. G. Mendiratta. Iron and Steel Inst. Japan, 1989, p 432

235. Loo Van, G. D. Rieck: Acta Metallurgica, 1973; 21, 73

236. H. Hindam, J. J. Hechler and D. P. Whitte. In the Int. Congress on Metallic Corrosion, Toranto, Canada, 1984, p. 353-359

237. M. Schutze, S. Ito, W. Przybilla, H. Echsler and C. Bruns: In Proc. of the Int. Symp. on High Temperatures Corrosion and Protection, Eds; T. Narita, T. Marwyama and S. Taniguchi, Science Review, 2000, p. 19-30

238. B. A. Pint, P. F. Tortorelli and I. G. Wright. Oxidation of Metals. Vol 58, Nos ½, 2002, pp 73-101

239. H. E. Evans: Materials at High Temperatures, 1994, Vol. 12, Nos. 2-3, p. 219-227

240. F. H. Stott: Materials Science and Technology, 1988, Vol. 4, pp 431-438

241. H. E. Evans: Int. Materials Reviews, Vol. 40, 1, 1995, p. 1-40

242. B. A. Pint, K. L. More, I. G. Wright and P. F. Tortorelli. In Proc. Of the 4th Inter. Conf. On the Microscopy of Oxidation. (Eds; G. Tatlock and S. Newcomb) Science Reviews, 1999, pp. 165-171

243. J. G. Smeggil; Materials Science and Engineering 87 (1987) 261-265

244. S. Mrowec, A. Gil and A. Jedlinski, Werkstoffe und Korrosion, Vol. 38, 10, 1987, p. 563-574

245. Y. Niu, F. Gesmundo, R. Yan and W. Wu; Corrosion Science, 41 (1999) 989-1012

246. I. Kim, W. D. Cho and J. C. Choi; in Value-Added Metallurgy. Edited by W. D. Cho and H. Y. Sohn. The Minerals, Metals and Materials Society, 1998, p. 71-84

247. B. A. Pint. Materials Science Forum. Vols. 251-254 (1997) pp 397-404

248. B. A. Pint, A. J. Garratt-Reed and L. W. Hobbs. Materials at High Temperatures 1995,Vol 13 No. 1, pp 3-16

249. C. H. Xu, W. Gao and S. Li. Corrosion Science 43 (2001) 671-688

250. C. H. Xu, W. Gao. Corrosion Science and Protection Technology, 1996, pp 26-37

251. A. UI-Hamid. Oxidation of Metals, Vol, 58, Nos. ½, 2002, pp 23-40

252. J. L. Smialek, J. Doychak and D. J. Gaydosh; in the Proc. of Oxidation of High Temperatures Intermetallics, Eds: T. Grobstein and J. Doychak. The Minerals, Metals and Materials Society, 1989, p. 83-95

253. F. A. Golightly, F. H. Stott and G. C. Wood, (1976): Oxidation of Metals Vol. 10, p. 163-187

254. M. J. Bennett, H. Romary and J. B. Price (1991): In Heat Resistant Materials, K. Natesan and D. J. Tillack, Eds, ASM Int. Materials Park, OH, p. 95-103

255. H. M. Hindam and W. W. Smeltzer: Oxidation of Metals, 1980, Vol. 14, p. 337-349

256. J. Doychak, J. L. Smialek and C. A. Barrett, 1988; in Oxidation of High Temperatures Intermetallics, Eds; T. Grobstein and J. Doychak. TMS, Warrendale, PA, p 41-56

257. E. W. A. Young, H. E. Bishop and J. H. W. de Wit, (1986): Surface Interface Analysis, Vol. (9), p. 163-168

258. E. W. A. Young and J. H. W. de Wit, (1986): Oxidation of Metals Vol. (26), p. 351-361

259. J. H. DeVan; in Oxidation of High Temperatures Intermetallics, Edited by T. Grobstein and J. Doychak. The Minerals, Metals and Materials Society, 1989, p. 107-115

260. P. F. Tortorelli and J. H. DeVan: Materials Science and Eng. A153 (1992) 573-577

261. B. A. Pint, J. R. Martin and L. W. Hobbs. Solid State Ionics, Vol. (78), 1-2, 1995, pp 99-107

262. N. Babu, R. Bala and A. Ghosh: Corrosion Science 43 (2001) 2239-2254

263. M. A. Montealegre, J. L. Gouzalez-Carrasco and M. A. Munoz-Morris, Intermetallics 9 (487-492)

264. H. J. Grabke: Intermetallics, 7, 1999, 1153-1158

265. K. Przybylski and S. Mrowec, 1984; in Proc. of the 9th Int. Congress on Metall. Corrosion, Toranto, Vol. 1, National Research Council, Ottawa, Canada, p. 47-52

266. T. T. Huang, R. Richter, Y. L. Chang and E. Pfender, (1985), Met. Trans., Vol. 16A, p 2051-2059

267. P. F. Tortorelli and J. R. Kaiser, 1991, Electrochem. Society, Vol. (91-92), p. 924-925

268. D. R. Sigler, 1989, Oxidation of Metals, Vol. (32) p. 337-355

269. I. M. Allam, D. P. Whittle and J. Stringer, 1978; Oxidation of Metals, Vol. 10, p. 35-66

270. J. D. Kuenzly and D. L. Douglass, (1974), Oxidation of Metals, Vol. 8, p. 139-178

271. A. Kumar and D. L. Douglass (1974), Oxidation of Metals, Vol.(8), p.139-178

272. J. A. Spraque and G. R. Johnston, 1983; in Proc. of the 41st Annual Meeting of ElectroMicroscopy Soc. Of Amer., G. W. Bailey ed., San Francisco Press, San Fracisco CA p. 216-217

273. J. Jedlinski and S. Mrowec (1987); Mater.Science and Engineering Vol. 87, p. 281-287

274. J. C. Piria, C. Roques-Carmes, J. Chaumont and H. Bernas, 1980; Corrosion Science, Vol. 20, p. 947-962

275. J. S. Benjamin, 1970, Metall. Trans. Vol. 1, p. 2943-2951

276. J. L. Smilek, J. Doychak and D. J. Gaydosh. Oxidation of High Temperatures Intermetallics, Edited by T. Grubstein and J. Doychak; The Mineral, Metals and Materials Society, 1989, p. 83-95

277. K. Ishil and S. Taniguchi, Oxidation of Metals Vol. 34, Nos 5/6, 2000, p. 491-508

278. J. Doakin, V. Prunier, G. C. Wood and F. H. Stott. Materials Science Forum, Vol. 251-254, 1997, p. 41-48

279. M. E. Whitte: Corrosion Science, Vol. 17, p. 879-891

280. C. M. Cotell, G. J. Yurek, R. Hussey, D. Mitchell and M. I. Graham, 1987, J. Electrochem. Soc., Vol. (134), p. 1871

281. K. Przybylski and G. J. Yurek, 1989, Materials Science Forum, Trans. Tech. Publ. Ltd. Aedermannsdorf, Switzerland, p. 1-45

282. A. W. Funkenbush, J. G. Smeggil and N. S. Bornstein, 1985, Metall. Trans. Vol.(16A), p. 1164

283. J. L. Smialek, 1987; Metall. Trans. Vol. 18A, p. 164-166

284. J. G. Smeggil, A. W. Funkenbusch and N. S. Bornstien, 1986; Metall. Trans., Vol. 17A, p. 923-932

285. B. A. Pint, A. Jain and L. W. Hoobs, 1991, Mater. Res. Soc. Symp. Proc. Vol. (213), p 981-986

286. T. A. Ramanarayanan, M. Raghavan and R. Petkovic-Luton, (1983); in Proc. JIMIS-3, High Temperature Corrosion Transactions Supplement, Japan Inst. Met., Toko, Japan, Vol.

24, p. 199-206

287. G, C. Wood and J. Boustead, (1986), Corrosion Science, Vol. 8, p. 719-723

288. T. A. Ramanarayanan, M. Raghavan and R. Petkovic-Luton, (1984); J. Electrochm. Soc., Vol. 131, p. 923-931

289. E. J. Felten, 1961: J. Electrochem. Soc. Vol. (108), p. 490-495

290. R. Pendse and J. Stringer, 1985: Oxidation of Metals, Vol. 23, p. 1-16

291. J. G. Smeggil, E. L. Paradis, A. J. Shuskus and N.S. Bornstein, 1985, J. Vac. Sci. and Techn. A, Vol. 3, p. 2569-2573

292. J. Stringer, 1966, Mat. Rev., Vol. 11, p. 113

293. E. Tsuzi, 1980, Met. Trans. Vol. 11A, p 1965-1972

294. E. P. Katz, B. A. Pint and G. J. Yurek, 1987, Metall. Trans. Vol. 11A, p. 1980-1993

295. F. S. Pettit, 1967 Trans. of Metal Soc., AIME Vol. 239, p. 1296-1305

296. O. Kubaschewski, E. Evans and C. B. Alcock, Metallurgical Thermochemistry (Pergamen Press, 1967)

297. Defects and Diffusion in Metal-Annual Retrospective II, Edited by D. J. Fisher, John Wiley&Sons, 1999

298. B. A. Pint and L. W. Hobbs, Oxidation of Metals 41 (1994) 75

299. B. A. Pint and L. W. Hobbs, J. Electrochem. Soc., 144 (1994) 2443

300. B. A. Pint and P. F. Tortorelli and I. G. Wright, Materials and Corrosion 47, 663-674

301. J. L. Smialek, 1987, NASA report, Clevelend, OH

302. B. A. Pint and K. B. Alexander J. Electrochem. Soc., 145, No. 6 1819 (1998)

303. A. Strawbridge and R. A. Rapp, J. Electrochem. Soc., 141, 1405 (1994)

304. Technical Report from Ion Bond Ltd (UK), 2002

Appendix A

Appendix A

Ion Bond Coating Procedure

- The polished (up to 1200 SiC grit) samples were cleaned using an ultrasonically agitated cleaning line, this consists of a serious of aqueous alkaline detergent baths, towns water rinse stage, de-ionised water rinse stages and hot air drying.
- The coating system was evacuated to a pressure of 2.0 E-5 mT (milli-Tar) during this time the samples were radiant heated for 20 minutes with a heater set point of 480°C.
- A vacuum integrity test was then carried out by closing-off the pumping system and monitoring the change in vacuum level. A final pressure of less than 2E-4 mT after 60 seconds is regarded as a pass.
- The first stage of the in-situ cleaning process was then commenced; this involved the creation of DC gas plasma using a high negative bias (final level – 1000V) in the presence of first hydrogen, then a mixed hydrogen/argon environment with a system pressure in the range of 100 to 150 mT.
- The next stage is high-energy metal ion bombardment using ions derived from the coating source. During this phase a bias of -1000V is applied to the samples and an arc source ignited. Energetic ions released from the source are accelerated by the bias and bombard the samples. The temperature of the samples rises rapidly during this stage and the process is halted when the samples reach 380°C. this is repeated twice more before proceeding to the coating stage and no gas is admitted during this step.

- For the coating phase, the bias level is reduced to the required level for the coating process typically –50 to –250V and gas is admitted into the coating system. In all cases the flow of gas was adjusted such that the pressure within the coating system was 15mT. The samples positioned directly in front of the coating source and the conditions held constant. The temperature of the samples during the coating process was between 370° and 430°C in all cases. The following table shows the conditions which were used during the coating stage:

Conditions of Ionbond coating procedure [**304**]

Coating	**Arc current**	**Substrate bias**	**Coating time**
NbN	90A	-150V	47Ah
CrN	80A	-150V	47Ah

Appendix B

Appendix B

Sample surface area calculations

The specimen surface areas were precisely calculated using the following equations:

- For Fe_3Al samples

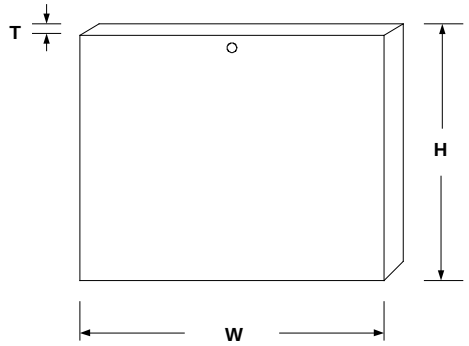

$$SA = 2(H * W) + 2(W * T) + 2(H * T)$$

- For coated and uncoated γ-TiAl samples

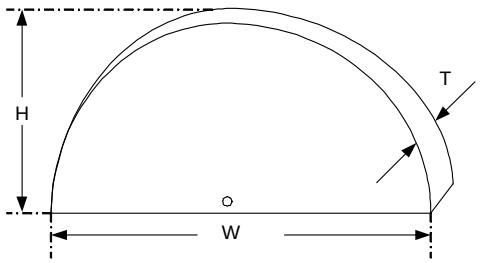

$$SA = 2\left[\frac{H}{6W}\left[3(H)^2 + 4(W)^2\right]\right] + (W * T) + \left[(\pi) * \left(\frac{W}{2}\right) * T\right]$$

where SA is the sample surface area, H is the sample height, W is the sample width and T is the sample thickness. The small hole surface area in the samples was neglected.

Appendix C

Appendix C

Calculations of Sulphur and Oxygen Partial Pressures

q Calculation of Sulphur Partial Pressure

From the reaction:

$$2H_2S_{(g)} \rightleftharpoons 2H_{2(g)} + S_{2(g)} \quad \text{(i)}$$

The value of the standard free energy change (ΔG°_T, cal/mole) with temperature (T in Kelvin) for the reaction can be obtained from the following equation:

$$\Delta G^\circ_T = A + BT \log T + CT \quad \text{(ii)}$$

where, A = 40210, B = -7.25 and C = 1.21 which were provided by Kubaschewski, Evans and Alcock [**297**]. Then equation (ii) becomes:

$$\Delta G^\circ_T = 40210 - 7.25\ T \log T + 1.21\ T \quad \text{(iii)}$$

on the other hand, ΔG°_T can also be expressed by Van't Hoff's reaction as

$$\Delta G^\circ_T = - RT \ln Kp \quad \text{(iv)}$$

where R is the gas constant (1.987 cal.degree/mole), Kp is the equilibrium constant.

From equations (iii) and (iv), the relationship between ΔG°_T and Kp can be established, that is:

$$\ln Kp = - \Delta G^\circ_T / RT$$

or

$$\log Kp = - \Delta G^\circ_T / 4.575\ T \quad \text{(v)}$$

by substituting for $\Delta G^{o}{}_{T}$ from (iii)

$$\text{Kp} = anti\log\left\langle \frac{\left(-40210 - 7.25T\log T - 1.21T\right)}{4.575T} \right\rangle \qquad \text{(vi)}$$

Applying the law of Mass Action for equation (i), the equilibrium constant can be expressed by the following relationship:

$$\text{Kp} = \frac{(pH_2)^2(pS_2)}{(pH_2S)^2} \qquad \text{(vii)}$$

or

$$\text{pS}_2 = \frac{Kp(pH_2S)^2}{(pH_2)^2}$$

or

$$\text{pS}_2 = Kp\left(\frac{pH_2S}{pH_2}\right)^2 \qquad \text{(viii)}$$

By combination of equations (vi) and (viii), the sulphur partial pressure (pS_2), in atm, can be calculated at any temperature (T). For a 10%H_2S/90%H_2 gas mixture at 850ºC (1123K), the sulphur partial pressure is given by

$$\text{pS}_2 = \left\langle anti\log\left[\frac{-40210 + 7.25T\log T - 1.2T}{4.575T}\right]\right\rangle\left(\frac{pH_2S}{pH_2}\right)^2$$

= antilog [(40210 - 7.25 x 1123 log 1123 + 1.21 x 1123)/(4.575 x 1123)] x $(10/90)^2$

= 6.8 x 10^{-6} atm

= 6.8 x 10^{-1} Pa

q **Calculation of Oxygen Partial Pressure**

For the reaction

$$H_2O_{(aq)} \text{ D } H_{2\,(g)} + \tfrac{1}{2}\, O_{2\,(g)} \qquad \text{(a)}$$

The value of the standard free energy change is given by the relationship [**297**]:

$$\Delta G^{o}{}_{T} = 57250 - 4.48\ T \log T + 2.21\ T \qquad \text{(b)}$$

and it can be expressed by

$$\Delta G^{o}{}_{T} = -4.575\ T \log Kp \qquad \text{(c)}$$

and

$$Kp = \frac{(pH_2)(pO_2)^{\frac{1}{2}}}{(pH_2O)} \qquad \text{(d)}$$

From equations (b), (c) and (d) and assuming pH_2 to equal 1 atm in the system, then the oxygen partial pressure is given at 850ºC by the following relationship:

$$pO_2 = 4.3 \times 10^{-20} (pH_2O)^2 \qquad \text{(e)}$$

From the vapour pressure/temperature relationship of H_2O:

$$\log (pH_2O) = -2900/t + 22.613 - 4.65 \log t \qquad \text{(f)}$$

where t is the temperature of water in Kelvin

pH_2O is the saturated water vapour pressure at t in mm of Hg

It is possible to achieve a value for pH_2O in mm Hg.

Dividing by 760 will give a value of pH_2O in atm and therefore, at any water temperature (t) and any furnace temperature (T), the oxygen partial pressure, pO_2 can be determined.

At 23ºC (296K) and at T = 850ºC, the oxygen partial pressure, pO_2, can be calculated:

$$pO_2 = 4.3 \times 10^{-20} \times (-2900/296 + 22.613 - 4.65 \times \log 296)^2$$

$$= 9.12 \times 10^{-18} \text{ mm Hg}$$

$$= 1.2 \times 10^{-20} \text{ atm}$$

$$= 1.2 \times 10^{-15} \text{ Pa}$$